Ongoing Temporal Dynamics of Broadband EEG During Movement Intention for BCI

Maitreyee Wairagkar

Biomedical Engineering, School of Biological Sciences
University of Reading

This dissertation is submitted for the degree of
Doctor of Philosophy

February 2019

This thesis is dedicated to my four grandparents for their constant inspiration, encouragement and inquisitive spirit. Three of whom became a fond memory.

Declaration

I confirm that this is my own work and the use of all material from other sources has been properly and fully acknowledged.

<div align="right">

Maitreyee Wairagkar

February 2019

</div>

Acknowledgements

First I would like to express my sincere gratitude to my supervisors Prof Slawomir J Nasuto and Dr Yoshikatsu Hayashi for their excellent guidance, continuous support and motivation throughout my PhD. Slawek and Yoshi, I would like to thank you for encouraging me, helping me to grow as a researcher, and challenging to me at every step to do more. Thank you for your insightful comments and critical analysis of my work which helped me to broaden my research horizon.

Slawek, thank you for giving me an opportunity to do a summer project in BCI in my second year undergrads. I immediately knew that I wanted to do research in this area and continue working on it through my PhD and beyond. Thanks for your mentorship throughout all these years, the extended meetings and intriguing discussions. I truly appreciate and value everything I have learned from you. Yoshi, thank you for introducing me to the temporal dynamics in EEG in my final year undergrads, researching it has ultimately become this thesis.

I am also grateful to Profs Rachel McCrindle, William Harwin and William Holderbaum for giving me the opportunity to work on different research projects, collaborate with multidisciplinary teams and grow as a researcher. I would like to thank all the academics in our department for their teaching, support and encouragement throughout my undergrads and PhD. I would like to thank Prof Kevin Warwick, my undergrad mentor for inspiring me to pursue Cybernetics. I would like to thank the University of Reading for funding my research.

It was fantastic to have the opportunity to work with everyone in the Brain Embodiment Lab. It was great sharing the lab and interacting with all of you. I enjoyed working on collaborative projects, demos and doing science outreach to share the fascinating research we do in our lab.

I would like to thank my mother and father for promoting the love for science since the early days which inspired me to pursue a PhD. Thank you for guiding me, supporting me at every stage, taking a keen interest in my work and sharing my vision. I am also very grateful to my family and friends for their constant support and encouragement.

Abstract

Brain Computer Interface (BCI) empowers individuals with severe movement impairing conditions to interact with the computers directly by their thoughts, without the involvement of any motor pathways. Motor-based BCIs can offer intuitive control by merely intending to move. Hence, to develop effective motor-based non-invasive BCIs, it is essential to understand the mechanisms of neural processes involved in motor command generation in electroencephalography (EEG).

The EEG consists of complex narrowband oscillatory and broadband arrhythmic processes. However, there is more focus on the oscillations in different frequency bands for studying motor command generation in the literature. The narrowband processes such as event-related (de)synchronisation (ERD/S) and movement-related cortical potential (MRCP) are commonly used for movement detection. Analysis of these narrowband EEG components disregards the information existing in the rest of the frequencies and their dynamics. Hence, this thesis investigates various facets of previously unexplored temporal dynamics of neuronal processes in the broadband arrhythmic EEG to fill the gap in the knowledge of motor command generation on a single trial basis in the BCI framework.

The temporal dynamics of the broadband EEG were characterised by the decay of its autocorrelation. The autocorrelation decayed according to the power-law resulting in the long-range temporal correlations (LRTC). The instantaneous ongoing changes in the broadband LRTC were uniquely quantified by the Hurst exponent on very short EEG sliding windows. There was an increase in the temporal dependencies in the EEG leading to slower decay of autocorrelation during the movement and significant increase in the LRTC ($p<0.05$). Different types of temporal dependencies in the broadband EEG were comprehensively examined further by modelling the long and short-range correlations together using autoregressive fractionally integrated moving average model (ARFIMA). The short-range correlations also changed significantly ($p<0.05$) during the movement. These ongoing changes in the dynamics of the broadband EEG were able to predict the movement 1 s before its onset with accuracy higher than ERD and MRCP. The LRTCs were robust across participants and did not require determination of participant specific parameters such as most responsive spectral or spatial components.

The oscillatory ERD, motor-related cortical potentials (MRCP) and the arrhythmic broadband LRTC are independent processes providing complementary information about the movement. These novel neural correlates based on the temporal dynamics of broadband EEG help in obtaining a deeper understanding of the neuronal processes involved in voluntary movement and may help in assessing the criticality in the neuronal mechanisms which is often associated with the LRTC. The broadband LRTCs can be used to develop robust BCIs based on the actual temporal dynamics of neuronal processes occurring during movement intention.

Table of contents

List of figures

List of tables

Abbreviations

Acronyms / Abbreviations

AAR   Adaptive Autoregressive

ACF   Autocorrelation Function

AIC   Akaike Information Criteria

AR   Autoregressive

ARFIMA Autoregressive Fractionally Integrated Moving Average

ARIMA Autoregressive Integrated Moving Average

ARIMAX Autoregressive Integrated Moving Average with Explanatory Variable

BCI   Brain Computer Interface

BIC   Bayesian Information Criteria

BP   Bereitschaftspotential

CAR Common Average Reference

CSP Common Spatial patterns

DFA Detrended Fluctuation Analysis

E/I   Excitation/Inhibition balance

ECG Electrocardiography

ECoG Electrocorticography

EEG Electroencephalography

ERD   Electroencephalography

EMD   Empirical Mode Decomposition

EMG   Electromyography

EOG   Electroocculography

ERD   Event-Related Desynchronisation

ERP   Event-Related Potential

ERS   Event-Related Synchronisation

FES   Functional Electrical Stimulation

fMRI Functional Magnetic Resonance Imaging

ICA   Independent Component Analysis

iid   Independently and Identically Distributed

LDA   Linear Discriminant Analysis

LFP   Local Field Potential

LRD   Long-Range Dependence

LRP   Lateralised Readiness Potential

LRTC Long-Range Temporal Correlation

MA   Moving Average

MEA   Microelectrode Array

MEG   Magnetoencephalography

ML-DFA Maximum Likelihood Detrended Fluctuation Analysis

MLE   Maximum Likelihood Estimation

MRCP Motor-Related Cortical Potential

PACF Partial Autocorrelation Function

PCA   Principal Component Analysis

PC   Principal Component

PSD   Power Spectral Density

R/S   Rescaled Range Analysis

RMS   Root Mean Square

SNR   Signal-to-Noise Ratio

SOC   Self-Organised Criticality

SRD   Short-Range Dependence

SSVEP   Steady State Visually Evoked Potential

SVM   Support Vector Machine

TMS   Transcranial Magnetic Stimulation

Chapter 1

Introduction

1.1 Background

1.1.1 Neurophysiology

The human brain is the most complex organ in the body that is responsible for control and coordination of all the mental and physical tasks. The brain operates by processing a large amount of information obtained from the surroundings via the sensory organs and from different parts of the body to achieve these tasks. The fundamental units of information processing are neurons. The neurons are connected to other neurons via synapses forming complex networks in which the information is propagated via action potentials [1]. An action potential is a rapid change in the membrane electrical potential that travels along the axon to the axon terminal [1]. The action potentials (also known as the firing of a neuron) can happen in rapid temporal successions forming spike trains [2]. Studying the properties of these neuronal firings or spike trains can provide an insight into the neuronal processes happening during different tasks and thus functioning of the brain [2, 3].

The neuronal activity can be recorded at different levels with invasive and non-invasive techniques providing different electrophysiological signals of different resolutions. Spike trains from the individual neurons can be measured by fine-tipped microelectrodes [4]. The microelectrode arrays (MEA) which can be implanted into the brain can record activity from a few hundred neurons simultaneously [5]. Local field potential (LFP) is an aggregate activity of neurons from a small volume of nervous tissue [6] which can be recorded using microelectrodes that are bigger than the ones used for single-unit recordings. On a coarser spatial scale, electrocorticography (ECoG) can measure aggregate signals from the surface of the cortex by placing electrodes on it [7, 8]. These techniques of recording neuronal activity are invasive. The non-invasive techniques record the electrophysiological signals from the

scalp. The electroencephalography (EEG) measures the aggregate activity of a relatively large number of neurons by placing electrodes on the scalp [9]. The electrodes are placed on the positions defined by the international 10-20 system [10] as shown in Fig 1.1. EEG has very low spatial resolution and is contaminated by the noise and artefacts induced by the interference of the layers between the electrodes and the cortex such as skin on the scalp, hair, skull, dura mater etc. [11]. The spatial resolution gradually improves as the recording becomes more invasive in ECoG, LFPs and MEA. Another surface level recording technique is magnetoencephalography (MEG) which has similar properties to EEG [12]. All these electrophysiological signals have a high temporal resolution as they can measure neuronal processes taking place over milliseconds. The non-invasive technique of functional magnetic resonance imaging (fMRI) has a higher spatial resolution but low temporal resolution [13, 14]. This thesis focuses on EEG activity.
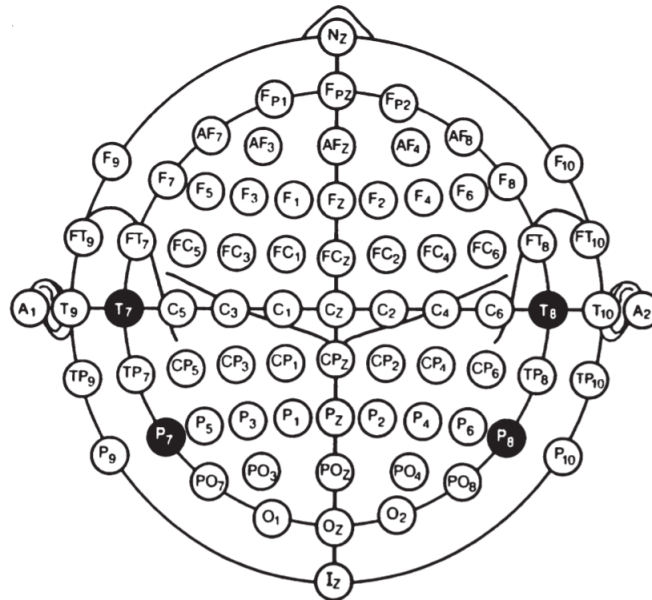
Fig. 1.1 **Schematic of 10-20 international system of EEG electrode placement [10].**

1.1.2   Components of EEG

The EEG can be described in terms of its oscillatory rhythmic components, slow potentials evoked due to an event and arrhythmic broadband components.

1.1.2.1   Spectral characteristics of EEG

The most common approach of extracting information from EEG is to study its spectral characteristics. The EEG is composed of different oscillations or brain rhythms that are represented in different frequency bands [15, 16]. The different rhythms in EEG are delta (< 4 Hz), theta (4 - 7 Hz), alpha (8 - 13 Hz), beta (14 - 30 Hz) and gamma (> 30 Hz) [17, 18]. There is also mu rhythm (8 - 13 Hz) that overlaps with the frequencies of alpha rhythm but is present over the sensorimotor cortex. The frequency bands of these rhythms are defined loosely and may change from individual to individual. These oscillations have been shown to correspond to different neurological processes obtained over specific cortical regions [17]. The delta rhythm is found in adults during slow-wave sleep and during certain attention tasks [19–21]. The theta rhythm is found during drowsiness and idling in adults and is associated with inhibition of a response or action [22, 17]. The alpha rhythm is observed during wakeful rest, relaxed states and when eyes are closed [22]. It is disrupted during attentiveness, and due to external stimulus [17, 22]. Alpha is often considered as the most prominent oscillation in EEG and shows a peak in the spectrum of EEG which has a $1/f$ shape [23], and hence it is analysed widely. The $1/f$ spectrum of EEG is shown in Fig 1.2. The beta rhythm is associated with cognition, problem-solving and motor planning [17]. The mu rhythm is also related to voluntary movement planning, intention, execution and imagination [9, 24]. The gamma rhythm is involved in sensory perception involving multiple senses and in short term memory tasks [20]. The properties and occurrence of these rhythms change during pathological conditions. Throughout this thesis, the terms rhythms, oscillations, frequency bands and spectral bands are used interchangeably, because, in practice, the oscillations are extracted from EEG by filtering between the canonical bands mentioned above.

The spectral characteristics of EEG are mostly studied using Fourier analysis. The band power of different frequency bands is obtained from its power spectral density (PSD) and time-frequency analysis. The Hilbert transform is also used to obtain the instantaneous phase of the frequency band and its analytic envelope.

1.1.2.2   Event related-potential

The event-related potential (ERP) is a measured brain response to sensory, cognitive, or motor event [25]. The ERP causes changes in electro-potential amplitude in response to the stimuli. The ERP is time-locked to an event [26]. The ERP waveforms have positive and negative potential deflections which are named after their positive or negative polarity with letters P, N and the latency of its occurrence in milliseconds after an event, for example, P200, P300 and N100 [27]. The ERPs are usually derived by averaging over several time-locked
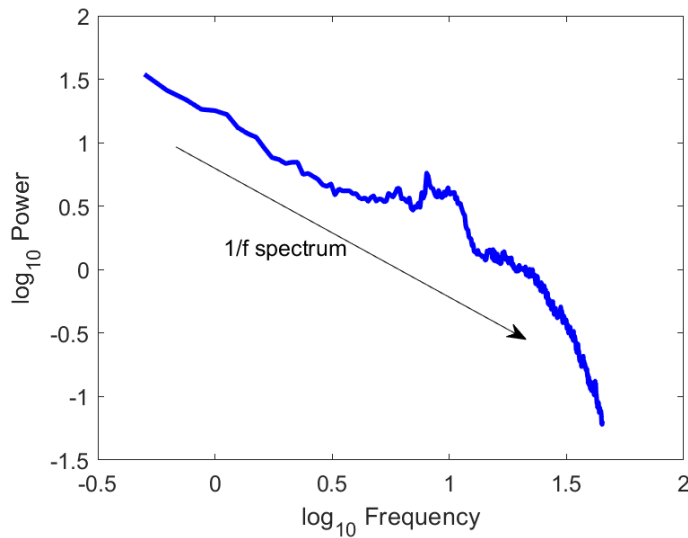
Fig. 1.2 **1/f spectrum of EEG.** The spectrum of EEG is shown in log-log scale. The spectrum has a $1/f$ shape with a peak in alpha band frequencies around 8-13 Hz. This $1/f$ spectrum shows power-law relationship between the frequencies and their power.

EEG trials recorded by repeating the same event and are difficult to observe over single trials. Nevertheless, ERP is a widely used measure of assessing differences in the response of EEG during different events [28].

1.1.2.3 Temporal dependencies in EEG

Another way of extracting information from EEG is to study the temporal dependencies in EEG [29]. The temporal dependencies can be evaluated by studying the decay of autocorrelation of independent EEG channels. The autocorrelation decay signifies how the present samples of EEG relate to the past samples and characterising this relationship can provide insight into the fundamental properties of EEG time series [30]. The temporal dependencies in EEG can be evaluated using various time series analysis techniques and by fitting parametric models such as autoregressive (AR), moving average (MA) and their variants [31].

A time series can contain long-range and short-range dependencies (LRD/SRD) [32]. The autocorrelation of the LRD process decays slower than exponential and autocorrelation of SRD decays exponentially or faster. The EEG is known to have a specific kind of long-range dependence known as long-range temporal correlations (LRTC) in which the autocorrelation decays according to the power-law [29]. The LRTC provides information about the underlying nature of EEG and how the information is persisted over time. The

LRTC has been observed in several different brain processes like neuronal firing [33], neuronal avalanches [34, 35], LFP [34], ECoG and EEG [36]. It is said that the LRTC helps the brain in optimising information storage and processing and adapting quickly to the processing demands [37]. The LRTC signifies the scale-free structure of EEG over several timescales.

The LRTC in EEG is observed in the amplitude fluctuations of individual oscillations as well as in the arrhythmic broadband EEG. The presence of LRTC gives EEG spectrum its distinct $1/f$ shape with a peak in the alpha band. The LRTC in EEG changes during different events [38], physiological conditions [39–42] and neurofeedback [43] or due to external stimulus [38]. Thus, the temporal dependencies in EEG can determine the temporal dynamics of EEG and help in extracting additional information from it. Further details of EEG temporal dependencies are included in chapter 2.

1.1.3   Characterisation of voluntary movement from EEG

One of the primary functions of the brain is motor control. Voluntary movement is one of the fundamental life processes because it allows humans to navigate the world, interact with it and communicate. Hence there is a broad interest in understanding the brain mechanisms related to movement intention, preparation and execution. Several complex neuronal processes are involved in motor command generation [44]. While certain components of movement like motor control, balance, coordination and its fine calibration are controlled by subcortical structures such as cerebellum, basal ganglia, pedunculopontine nucleus, red nucleus, nucleus [45–47], the movement intention, planning of a specific movement and motor command generation and execution are done by the motor cortex [48]. Hence EEG from sensorimotor cortex is examined commonly to decode the movement-related information. The motor homunculus in the motor cortex shows the locations on the motor cortex in charge of the movement of different parts of the body [49]. A cortical motor and sensory homunculus is shown in Fig 1.3 [50]. A large area is allocated for the motor control of the hands and feet (which are controlled by the contralateral hemispheres of the brain), and hence EEG related to these general areas is easier to obtain. Roughly, EEG channels C3 and C4 according to the international 10-20 system capture the areas responsible for the right and left hand movement respectively and Cz captures the areas responsible for the movement of the feet. This thesis focuses on studying the neuronal processes in EEG for hand movements.

There are two commonly used neural correlates to identify movement from EEG: event-related (de)synchronisation (ERD/S) which are the changes in the spectral characteristics of EEG [26] and motor-related cortical potentials (MRCP) which are the event-related potentials evoked in response to movement intention [51]. The ERD is the attenuation of the amplitude
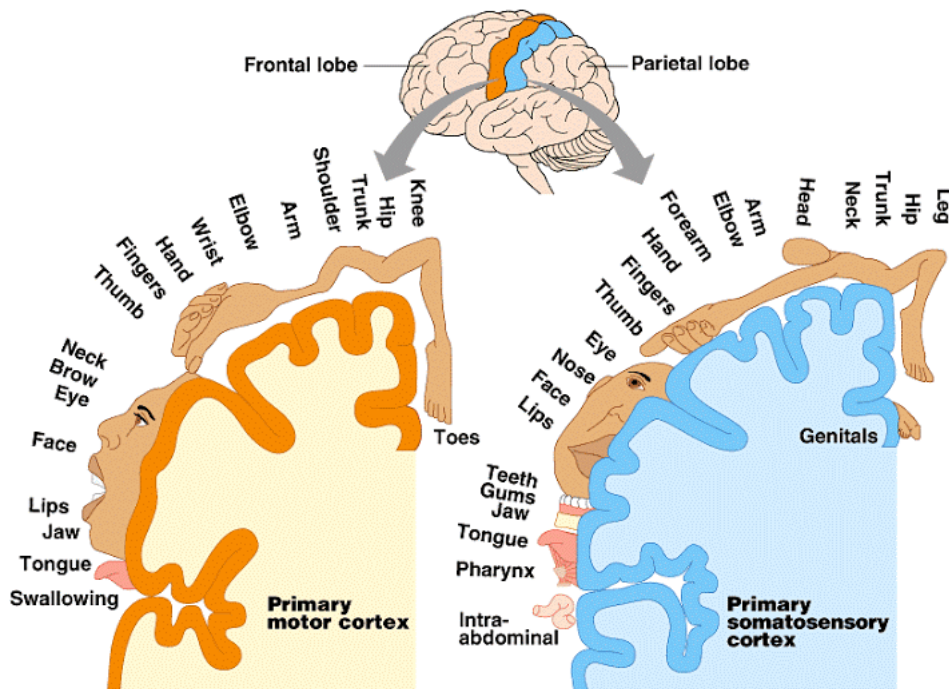
Fig. 1.3 **Cortical homunculus [50].** The cortical homunculus shows the areas and proportions of human brain dedicated to the motor and sensory functions of different parts of the body. It can be seen that a large area is dedicated to the motor function of hands and fingers.

of the mu band power during movement [26], and ERS is the increase in the beta band power after the movement [52]. Since mu band overlaps with the alpha band in frequency, mu and alpha band are used interchangeably throughout the thesis, but both refer to the 8-13 Hz frequency band over the sensorimotor area. The MRCP leads to increase in the slow negative cortical potentials during movement [53]. The details of these processes are given in chapter 2.

1.1.4   Brain computer interface (BCI)

Brain computer interface (BCI) provides a direct interface for communication with a computer and external devices without utilising motor pathways in the body [44]. The BCI provides a new mode of communication to individuals paralysed due to spinal cord injury, stroke and other severe motor disabilities, and enables them to perform simple tasks by utilising their capability of producing tailored thoughts. Recently, BCIs have gained prominence in motor rehabilitation making it more active by engaging the patient [54–57]. The applications of BCI for healthy participants are for entertainment and brain training via neurofeedback for meditation, relaxation and concentration. The BCI can also be used as a research tool to

study different neuronal processes. The BCI is controlled by the neuronal activity recorded using invasive or non-invasive techniques.

BCI can be driven by various paradigms such as steady state visually evoked potentials (SSVEP) [42], Event Related Potentials (ERP) [58], e.g. P300 as well as cognitive processes arising from motor-related paradigms such as motor intention and imagery [59]. SSVEP and evoked potentials employ visual and attention processes, and they require an external stimulus to evoke a detectable response. There has been an increasing interest in exploring the neural correlates of movement for driving BCI as they enable a very intuitive control by producing a voluntary movement intention at will without the requirement of any external stimulus [60]. However, to use motor intention for practical BCI, it is essential to study the underlying neural mechanisms of voluntary movement generation. Voluntary movement detection is done on a single trial basis using ERD/S and MRCP. Further details of BCI are given in chapter 2. This thesis focuses on understanding the fundamentals of movement intention generation in the brain by studying the temporal dynamics of EEG for applications in BCI.

1.2 Research questions

The rhythmic (oscillations) and arrhythmic processes coexist in EEG [23, 61]. However, in the literature, there is more focus on the rhythmic components such as the alpha rhythm. The neuronal processes are widely explored by extracting individual oscillations. This approach limits the amount of information that can be obtained from EEG because it disregards the arrhythmic broadband component. The broadband arrhythmic processes in EEG which have a $1/f$ spectrum used to be considered as background noise, however, recent research has shown that this arrhythmic process plays a functional role [23]. This indicates that the broadband EEG can contain additional information about the event/state being studied and should be analysed along with the oscillatory components to get a complete picture. However, the temporal dynamics of the broadband processes in EEG are not widely investigated.

The temporal dynamics in EEG can be examined by characterising the short and long-range dependencies present in it. In cases where the temporal dependencies are investigated [29, 36], their properties are considered invariant in a particular state. The ongoing changes in the broadband temporal dependencies have not been investigated before. Characterising these temporal dependencies on the ongoing basis may reveal new properties of the neuronal processes. This can be especially useful in the cases where the event to be studied is short such as voluntary movement and not a state persisting over long timescales. The

changes in the temporal dynamics of short events can go unnoticed on larger timescales if not characterised on the short timescales on an ongoing basis.

The long-range dependency, LRTC, in EEG suggests the presence of scale-free dynamics in neuronal processes [40]. The LRTC is often evaluated from the fluctuations in the amplitude of individual oscillations, mainly the alpha oscillation [29, 62, 40]. In this case, even though the scale-free LRTC properties are being examined, they are still limited to the temporal dynamics of individual oscillations. The LRTC in the broadband EEG temporal dynamics must be evaluated to observe how these LRTCs differ from the LRTCs in individual oscillations.

The focus of this thesis is to characterise the neuronal processes during movement intention and obtain more in-depth insight into the motor command generation such that these neuronal processes could be used in BCI. However, the movement-based BCIs primarily use the oscillatory ERD/S components and MRCP, both of which are narrowband processes. The ERD/S only consider the relative power-change in the alpha or beta bands during movement and neglect the changes occurring in the rest of the frequencies and also disregard the temporal dynamics of EEG. Moreover, the ERD/S requires the selection of most responsive frequency bands and spatial locations which differ from individual to individual. Thus, the BCI developed using ERD/S have to be fine-tuned to an individual user. The MRCP characterises merely the changes in the slow negative potentials during movement intention and does not account for the changes in the dynamics of the faster fluctuations in EEG. The MRCP is also challenging to obtain on a single trial basis which is required for the BCI application because of its small amplitude which can get buried in the high amplitude components. The ERD/S and MRCP do not provide any information about the changes in the temporal dependencies in EEG and its broadband dynamics.

This thesis has hypothesised that the ongoing changes in the temporal dependencies of the broadband EEG which have not been studied before may contain complementary information about the voluntary movement. This can help in movement detection, give a better understanding of the underlying scale-free processes involved in the motor command generation and also can be applied in BCI by providing access to the information that is not represented by the ERD/S and MRCP. Besides being inclusive of all the available information in the broadband EEG, another advantage of broadband is that it does not require fine-tuning of parameters such as the most responsive frequency band for detecting movement. The changes in the ongoing broadband temporal dependencies during movement have not been identified before. The broadband temporal dependencies have not been obtained on an ongoing single trial basis during movement. Hence, there is a vast scope for exploring and

identifying the properties of the temporal dependencies in the broadband EEG and enhancing the current understanding of the processes contributing to the motor command generation.

1.3 Aims

The aims of this thesis are:

1. To characterise the ongoing dynamics of the temporal dependencies (LRTC and SRD) of the broadband EEG on a single trial basis.

2. To assess whether the temporal dynamics of the broadband EEG provide information about voluntary movement.

3. To model this broadband LRTC and SRD and show that the scale-free arrhythmic broadband EEG processes contribute to motor command generation.

4. To differentiate between the movement EEG trials and the resting state trials and detect voluntary motion intention using the LRTC and SRD before the onset of the movement.

5. To determine whether the broadband temporal dynamics are independent and complementary to the ERD/S.

6. To determine whether the broadband temporal dynamics are independent and complementary to the MRCP.

7. To explore the suitability of broadband temporal dynamics for application in BCI.

1.4 Thesis structure

The four main chapters 3 to 6 of this thesis are written in the form of manuscripts which are either published, submitted or being submitted to the academic peer-reviewed journals. The papers in chapters 3 and 4 are published in *PLOS ONE* and *Brain Informatics and Health, Lecture Notes in Computer Science*, respectively. The manuscript in chapter 5 has been submitted to *Scientific Reports* and the manuscript in chapter 6 will be submitted to *Frontiers in Neuroscience* . The papers are written according to the guidelines and requirements of the respective journals, and hence there may be variations in the structure and format of the papers. The EEG data recorded for the voluntary movement intention detection which are used in all the four papers have also been published in the *University of Reading Dataset Archive*. The EEG experiments and all the work in the four papers including the analysis and

writing have been conducted by the author of this thesis Maitreyee Wairagkar, who is also the first author of these papers. The other authors, Slawomir Nasuto and Yoshikatsu Hayashi, have supervised this research.

Chapter 2 reviews the literature related to the commonly used spectral approaches and slow-cortical potentials for movement intention detection. It also discusses the temporal dependencies in EEG and the methods for its assessment. The models for describing temporal dynamics in EEG are reviewed. This chapter also describes the methods for movement-based BCI. The relevant literature review is also included in the individual chapters.

Chapter 3 explores the changes in the temporal dynamics of EEG in different frequency bands and broadband during movement intention by studying the decay of autocorrelation. This chapter thoroughly compares the performance for temporal autocorrelation decay dynamics with the ERD in different EEG bands for movement intention detection for application in BCI. This chapter also seeks to establish the complementarity between these two EEG processes.

Chapter 4 compares the broadband EEG autocorrelation decay based movement intention detection with MRCP and establishes their complementarity. It also compares their classification accuracy and time of movement prediction.

Chapter 5 formally identifies the LRTC in broadband EEG on a single trial basis. It investigates the changes in the fast dynamics of the broadband LRTC on short timescales during movement intention. This chapter compares the novel broadband LRTC with the widely recognised LRTC in the fluctuations of the alpha band which cannot be obtained on a single trial and hence cannot detect movement intention from the ongoing EEG. The feasibility of using broadband LRTC to identify movement intention in real time is shown by measuring the accuracy and prediction times of movement.

Chapter 6 models this LRTC using autoregressive fractionally integrated moving average model (ARFIMA). The ARFIMA models the LRTC as well as the remainder SRD after taking out LRTC in the broadband EEG simultaneously on single trials. The changes occurring in the SRD during movement are also studied. The complementarity of spectral changes and broadband LRTC dynamics during movement are confirmed. Thus, the broadband temporal dependencies are established as the independent neuronal processes providing additional movement related information which is shown by the improvement in the movement detection accuracy and prediction timings.

Finally, chapter 7 states and discusses the novel findings of this thesis. The mechanisms of broadband LRTC are discussed. The broader impact of this novel approach of obtaining ongoing broadband temporal dynamics on wider areas is discussed, followed by the future research direction and individual contributions of the author to the four papers.

Chapter 2

Literature Review

2.1 Voluntary movement detection from EEG

The spectral and temporal changes occur in EEG during voluntary movement generation. The voluntary movement intention, execution and imagery can be detected from EEG using spectral and temporal components of EEG. There is increasing interest in single trial techniques of movement intention detection for application in BCI.

2.1.1 Event-related (de)synchronisation (ERD/S)

Different events such as voluntary movement can block or desynchronise brain activity in different frequency bands such as alpha band [26]. This results in reduction of amplitude of the ongoing EEG in that frequency band. The changes occurring because of the desynchronisation are time-locked to the event but are not phase-locked. Hence such changes cannot be identified simply by linear method of averaging over several EEG trials that is commonly used to detect ERP. Spectral analysis is done to extract the power of a frequency band of interest to observe the desynchronisation. The power of a frequency band reduces due to desynchronisation. These changes are called event-related desynchronisation (ERD) [63, 64]. An event can also cause increased synchronisation in specific EEG frequency bands leading to increase in the power of that frequency band. Such changes are called event-related synchronisation (ERS) [52]. Thus, different events can cause frequency-specific changes in EEG leading to increase or decrease in the power of the frequency band of interest.

2.1.1.1 Overview of ERD/S

The ERD/S is the most commonly used neural correlate of movement [26, 65]. The ERD and ERS occur during voluntary movement intention, execution and imagery. The ERD during movement is represented by the attenuation of mainly the mu band power relative to the baseline power [63]. The ERS, also known as beta rebound, is represented by the increase in the band power of mainly beta band. ERD and ERS both can be seen in alpha and beta band. The ERD starts before movement onset and continues during movement execution which is then followed by ERS. The ERD and ERS are only defined on a specific frequency band which must be specified while referring to ERD and ERS. The ERD and ERS are the changes in the band power relative to a baseline measured during resting few seconds prior to movement [66]. The most responsive frequencies in the mu and beta bands over which ERD/S is observed are individual specific [26]. ERD/S can detect movement intention and imagery with high accuracy [67, 68].
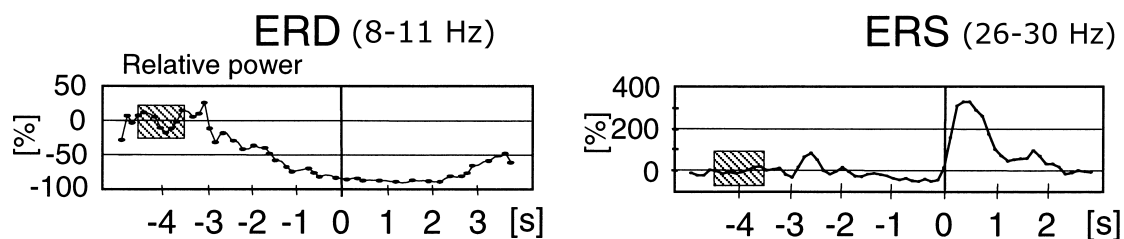
Fig. 2.1 **Event Related Desynchronisation and Synchronisation.** The ERD between 8-11 Hz decreases before and during the movement. The ERS between 26-30 Hz increases after movement onset. The movement onset is at 0 s. The shaded boxes are the baseline relative to which ERD and ERS are measured. This figure is from Pfurtscheller et al.[26].

2.1.1.2 Neuronal mechanisms of ERD/S

ERD and ERS are caused due to a decrease and an increase in synchrony of the underlying neuronal populations respectively [26]. ERD/S phenomena are caused due to changes in the factors controlling the oscillatory behaviour in the neural networks. The characteristics of oscillations in EEG are determined by the intrinsic membrane properties of the neurons and the dynamics of synaptic processes such as modulations in the influence from neurotransmitter systems [69] as well as by the properties of neural networks forming thalamo-cortical and cortico-cortical feedback loops over variable distances. The main circuits of the thalamus and cortex are responsible for the occurrence and modulation of alpha oscillations [70]. Oscillations are also observed in different frequency bands with different levels of synchrony.

These oscillations have a functional role in the workings of neural networks particularly in acting as gating function and formation of assemblies of neurons that represent the stimulus patterns.

The oscillations in low frequency bands such as alpha are caused by the recruitment of neurons in larger cortical areas and the oscillations in the higher frequency bands such as beta are more localised and spatially restricted. ERD/S are observed due to changes in the local interactions between principal neurons and interneurons that control the frequency components (oscillations) of the ongoing EEG [26]. Further details of the mechanisms behind production and synchronisation of brain oscillations can be found in the fundamental works by Pfurtscheller et al. [26], Lopes da Silva et al. [70], and Singer et al. [69].

2.1.1.3   Techniques to characterise ERD/S

Several different techniques are used to compute the relative change in the mu and beta band powers to quantify ERD/S. Most common methods of quantification of ERD/S are spectral domain methods using power spectral density (PSD) and time-frequency analysis; and time domain methods for computing band power [53, 71, 72, 26]. The temporal techniques such as band power estimation by filtering EEG in the specific frequency band and then obtaining the average of its squared samples is widely used [26, 73]. Inter-trial variance method can also be used to determine ERD which is based on subtraction of mean of subsequent samples from all the trials to improve the variance [74, 75]. The spectral methods include spectral perturbations that uses short-time Fourier transform [76, 77], simply a Fourier transform [78], peak trace method which compute the maximum power in mu band [79, 80], wavelet transform based methods [78] and temporal-spectral evolution method [81]. Hilbert transform has also been used to estimate the ERD from the band power computed from its analytic signal [78]. The Hilbert-Huang transform or the empirical mode decomposition (EMD) can be used for computing ERD [82, 83]. In spite of different methods of characterising ERD/S, the underlying principle of decrease and increase in the spectral power respectively remains constant.

Another temporal approach of estimating spectral properties of EEG in mu band is using autoregressive (AR) models [84–89]. The parameters of the autoregressive models can be used to characterise changes in the selected frequency band. Since EEG is non-stationary, a variation of AR models adaptive autoregressive models (AAR) was developed. Adaptive autoregressive modelling approach allows model parameters to adapt because of non-stationarity. The changing parameters of adaptive autoregressive model are often tracked using Kalman filter.

Since the ERD/S is relative change in the spectral power, usually the analysis using above techniques is done on short 1 or 2 s EEG sliding windows to see the changing spectral power over the time. The current ERD/S is quantified as the percent change in the current band power as compared to the baseline band power. Details of this sliding window approach for estimating ERD are described in chapters 3 and 6. A comprehensive review of movement detection using sensorimotor rhythms from EEG is given in Yuan et al. [90] and He et al. [90, 44].

Throughout this thesis, ERD has been computed using bandpower method [26]. Firstly, EEG trials are band-pass filtered in 8-13 Hz frequency band. Filtered trials are then squared and averaged. The mean of corresponding samples in all trials is subtracted from each sample. This gives the bandpower of an EEG trial. Then to compute ERD, which is the relative change in the bandpower, a baseline is determined from EEG when there is no movement intention. This baseline is then subtracted from the mean of a sliding EEG windows. ERD percentage is obtained for each sliding window using equation (2.1).

$$ERD(i) = \left(\frac{A(i) - R}{R} \right) \times 100 \tag{2.1}$$

where R is the baseline obtained from the mean of EEG 1.5 s to 2 s prior to movement onset and $A(i)$ is the mean of (i^{th}) sliding window in the single trial of EEG.

2.1.1.4 Temporal progression of ERD/S

The ERD occurs during movement starting about 2 s before its onset [26]. The ERD is maximum at the movement onset [53] and returns to its baseline level after movement execution. The ERS occurs after the movement execution. The ERS has maximum strength at 1 s after the end of movement execution [26, 53], after which it gradually restores to the baseline level. It is recommended that there should be a gap of about 6 to 10 s between each movements to detect ERD/S clearly [26, 86].

2.1.1.5 Spatial localisation of ERD/S

ERD is localised to sensorimotor area of the cortex around the region on homunculus corresponding to the part of the body (e.g hand or feet) involved in movement. ERD starts about 2 s before movement onset over the contralateral Rolandic region [26, 91, 92]. It becomes bilaterally symmetrical just before the movement execution. While the ERD for hand movement can be identified from the contralateral hand areas (C3 or C4), the ERD for feet movement is observed around the central area (Cz) [67]. The ERD in the alpha band

obtained from EEG is spatially diffused as compared to the ERD in alpha and beta bands obtained using ECoG. It has been shown in the ECoG that the topography of beta ERD is more specific than that of alpha ERD [26]. During hand movement, there is beta ERD in the contralateral hand area in the sensorimotor cortex and beta ERS in the ipsilateral hand area. The beta ERS is dominant over the contralateral primary sensorimotor area and has a maximum amplitude around 1 s after the end of movement execution [26, 53].

This localisation of ERD/S can change under different pathological conditions such a stroke. Meng et al. [88] observed greater ERD on the ipsilateral sensorimotor area especially in the beta band of the stroke patients which is different from the healthy participants. This could be a result of brain plasticity.

2.1.1.6   Movement-related information from ERD/S

Sensorimotor rhythms and other frequency rhythms can not only detect movement imagination, intention and execution but also provide information about the nature of the movement such as its direction, speed and intention. He et al. [44] showed that intent of velocity of movement, its acceleration and force can be estimated from sensorimotor rhythms. Movement-related parameters can be decoded from the low-pass filtered components roughly corresponding to delta band [93–95]. The study by Demandt et al. [72] used delta band to classify different directional reaching movements by studying its movement end-related potentials. The speed of the movement has been decoded from alpha and beta bands [96, 97]. Yong et al. [98] identified motor imagery of different types such as grasping movement and elbow movement. The beta rebound reflects the active inhibition of neuronal networks after termination of a motor program, such as motor planning, motor execution, or motor imagery which can be used to identify termination of the motor task, yet another property of the movement [99].

Individual finger movements, gestures or trajectory of movement can be identified from the broadband gamma band features [85, 100, 101]. The gamma band of EEG tends to be noisy due to smaller bandwidth of EEG and hence detecting movement type is difficult from EEG, but it can be achieved using ECoG which can provide less noisy gamma band with higher frequencies. Liao et al. [102] were able to identify single finger movement using broadband EEG as well.

2.1.1.7   Limitations of ERD/S

While the ERD/S has been so far the most widely used index for motor intention, imagery and execution detection, it has certain limitations. Estimating strong ERD/S requires selecting the

most responsive frequency band which differs from individual to individual [26]. Selecting canonical alpha band between 8-13 Hz and beta band between 14 - 30 Hz may lead to weaker ERD/S detection. Moreover, alpha and beta rhythms may have different constituent frequencies in different individuals [103]. The most optimum spatial locations also need to be identified for detecting strong ERD/S which are again individual specific [104]. Spatial filtering techniques such as common spatial patterns (CSP) on individual participants can be used to enhance ERD/S strength [105]. The ERD/S is a narrow band process and it does not account for the movement-related information that might be present in the rest of the EEG.

2.1.1.8   Factors affecting motor intention detecting from ERD

The strength of ERD/S depends on the learning in the participants. The most common paradigm of ERD experiments is neurofeedback where the level of ERD is displayed to the participants on the screen [86]. Such a neurofeedback paradigm facilitates the learning in participants who are then able to produce stronger ERD and consequently more accurate movement detection from EEG. The learning may take several EEG experimental sessions.

2.1.1.9   Application of ERD features in BCI

The most common and widely researched BCI paradigm is based on ERD/S. Several different techniques for ERD/S evaluation are used as mentioned in the previous subsections. The ERD based BCI can detect movements on single trial basis. The ERD based BCIs have also showed high classification accuracies. Often hybrid approaches combining different features and advance classifiers are used to enhance the BCI performance. Some of the studies were able to achieve accuracies as high as 92%, 87.5% [106], 88.2% [107] and modest accuracies of 69.4% [108] and 72.7% and 56.4% [109]. Thus there was a high variability in the BCI performance using ERD. Multiple classes can also be classified using ERD based paradigms due to the lateralisation and spatial localisation of ERD [110].

2.1.2   Movement-Related Cortical Potential (MRCP)

2.1.2.1   Overview of MRCP

MRCP is a slow negative potential arising during movement intention. The MRCP is a non-oscillatory component of EEG. The MRCP is associated with the planning of voluntary movements [111] and occurs during movement intention, prior to its execution [112, 100, 89]. The MRCP is composed of eight components occurring before and after the movement [51]. The earliest component is called early Bereitschaftspotential (BP1) also called readiness

potential. It is followed by negative slope or BP2, P-50 and N-10 (also known as motor potential) before the movement where P stands for positive and N stands for negative potential and the numbers following them are their latencies in milliseconds with respect to the movement onset. After the movement onset, there are components N+50, P+90, N+160, P+300 generally known as movement-monitoring potential. The early BP has smaller amplitude of 2-3 μV, BP2 had larger amplitude of 8-10 μV [53]. The MRCP changes during neurological conditions [111]. The MRCP and its components are shown in Fig 2.2 [113].
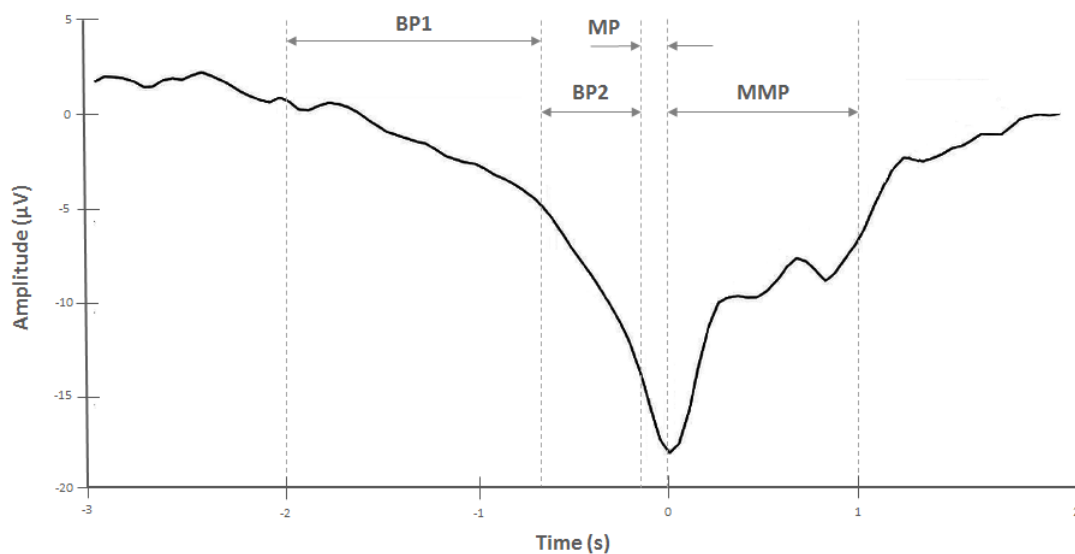
Fig. 2.2 **Components of MRCP.** MRCP shows increase in slow negative potential before movement. Movement onset is at 0 s. Different components of MRCP are BP1, BP2, Motor Potential (MP) and Movement-Monitoring Potential (MMP). This figure is adapted from Shakeel et al.[113].

2.1.2.2   Neuronal mechanisms of MRCP

The MRCPs are event-related potentials occurring due to movement intention and preparation. They are slow shifts in the cortical DC potentials. The MRCPs are time-locked to the movement and can be commonly detected by averaging over several trials. The generator sources of MRCP are said to be the bilateral sensorimotor area and lateral precentral gyrus [51]. The late component of MRCP is steeper and becomes contralateral.

2.1.2.3   Techniques to characterise MRCP

The MRCP has very small amplitude as compared to alpha oscillations and hence can be detected by averaging over several trials. Typically, EEG is first filtered from 0.1 Hz up to

maximum 3 Hz [114, 92]. Various spatial filters such as common spatial patterns can also be used to enhance the MRCPs by reducing the signal-to-noise ratio (SNR). The single trial analysis of MRCP is possible [112].The asymmetric distribution of the late BP associated with unilateral hand movement is derived by subtracting the potential recorded at C4 from that at C3 for both the left-hand movement and the right-hand movement separately. It is called the lateralized readiness potential (LRP) [115].

2.1.2.4 Temporal progression of MRCP

The MRCPs are divided into different components based on the timing of their occurrence in relation to the movement. The early component BP1 that starts 2 to 1.7 s before the movement onset is a slow negative slope which reaches maximum over the central-medial region [51]. This is followed by BP2, also known as late BP, starting from around 400 to 300 ms before movement onset and has a steeper negative slope. BP2 is lateralised over primary motor area. The onset of MRCP with respect to the movement onset significantly differs among different types of movement and in different individuals.

2.1.2.5 Spatial localisation of MRCP

The early component BP1 of the MRCP is observed over central-medial (supplementary motor) area [53] and is widely and symmetrically distributed on both hemispheres [51]. The late component BP2 has lateralisation over primary motor area [53] and is present on the contralateral region for hand movement (around C1 and C2) and central region (around Cz) for feet movement. The asymmetric distribution of the late BP associated with unilateral hand movement is called the LRP [115]. In healthy individuals, upper limb movements typically present a maximal late BP over the contralateral central areas of the cortex [51, 71].

2.1.2.6 Movement-related information from MRCP

MRCP detects movement intention. Movement intention is composed of an early plan to move [116] and represents a high-level state which specifies the goals of movements rather than the exact muscle activations required for its execution. Identifying movement intention before its onset facilitates prediction of its timing [117, 100, 114] and the desired target [112]. The study done by Lew et al. [112] identified the direction of self-paced movements using MRCP.

2.1.2.7   Limitations of MRCP

MRCP is often used for decoding intention of movement but it does not contain information about the handedness of the movement. The MRCPs have very small amplitude which makes their detection difficult from the high frequency and high amplitude components of EEG. This also make MRCPs challenging to be characterised on single trial basis. In several cases MRCP are detected by averaging over several trial which helps in eliminating the high amplitude noise [53]. The MRCP can also show individual specific brain patterns and spatial locations [71] which may require additional individual specific tuning [100]. The MRCP which is a slow negative potential, has low frequency making it a narrowband process which does not incorporate information from the other frequency components in EEG.

2.1.2.8   Factors affecting motor intention detecting from MRCP

The magnitude and time course of BP recorded in the self-paced condition are influenced by various factors such as level of intention, preparatory state, movement selection as to freely selected versus fixed, learning and skill acquisition, pace of movement repetition, praxis movement, perceived effort, force exerted, speed and precision of movement, discreteness and complexity of movement, and pathological lesions of various brain structures [51].

2.1.2.9   Application of ERD features in MRCP

The MRCP can be used in EEG for movement intention detection for application in BCI. The MRCP can be found in single trials [112, 114]. The classification accuracies obtained from MRCP were in the range of 76% [112], $66.9 \pm 26.4\%$ [91], 75% to 40% [92] and $68 \pm 10\%$ [118]. The classification accuracies had high standard deviation indicating that the movement detection performance of MRCP based BCI is variable. It was also possible to predict the movement before its onset.

2.2   Temporal changes in EEG

EEG is composed of complex temporal neuronal processes. Some of the underlying properties of the temporal dynamics of EEG are discussed in this section.

2.2.1   Autocorrelation of EEG

The autocorrelation function characterises the temporal dependencies in EEG. It indicates how the current EEG signal is related to its past at varying times. The autocorrelation captures

the temporal dynamics in EEG and can help in studying the changes in the dynamics and temporal dependencies in EEG. The autocorrelation can help in characterising the nature of the temporal processes in EEG and can give information about their periodicity. For example, the white noise process does not have any correlations in its samples and hence it drops to zero very quickly. For the signals with more temporal dependencies, the autocorrelation decays slowly. Thus, the decay of autocorrelation can be used to study the dynamical changes occurring in EEG. The autocorrelation of EEG in different frequency bands and broadband is investigated in chapters 3 and 4 in details.

In this thesis, the autocorrelation has been computed using equation (2.2).

$$R(\Delta) = \frac{\sum\limits_{t=0}^{N-\Delta} (s(t) - \bar{s})(s(t+\Delta) - \bar{s})}{\sum\limits_{t=0}^{N} (s(t) - \bar{s})^2} \tag{2.2}$$

where, $s = s(0), s(1), s(2), ..., s(N)$ is a discrete EEG signal with N samples, $R(\Delta)$ is the autocorrelation of s at a lag Δ and $\bar{s}$ is the mean of signal s. At $\Delta = 0$, the signal is perfectly correlated ($R(0) = 1$). At an infinite time lag, the signal components are completely uncorrelated ($R(\infty) = 0$). How the signal becomes uncorrelated over time can be described by the trend of autocorrelation decay. EEG and its autocorrelation is shown in Fig 2.3.

2.2.2   Power-law in neuronal processes

Power-laws are ubiquitously present in nature. The power-law can be useful for describing properties of an entity for which averages such as mean and median are poor descriptors. Such entities do not have a characteristic scale and hence are scale-free. The power-law is a relationship between two entities such that on a log-log scale, a relative change in one entity results in proportional relative change in another entity. The power-law between x and y can be described by equation (2.3).

$$y(x) = Cx^{-\alpha} \tag{2.3}$$

where, α is called the scaling exponent of the power-law and C>0 is a constant.

The most interesting property of the power-law is scale invariance. Scale invariance indicates that similar properties are observed over a wide range of scales. All power-laws with the same scaling exponents are essentially scaled versions of each others. The common examples of power-law is fractals. The fractals are scale-free and are self-similar over large number of scales. The power-laws emerge from complex underlying dynamical processes
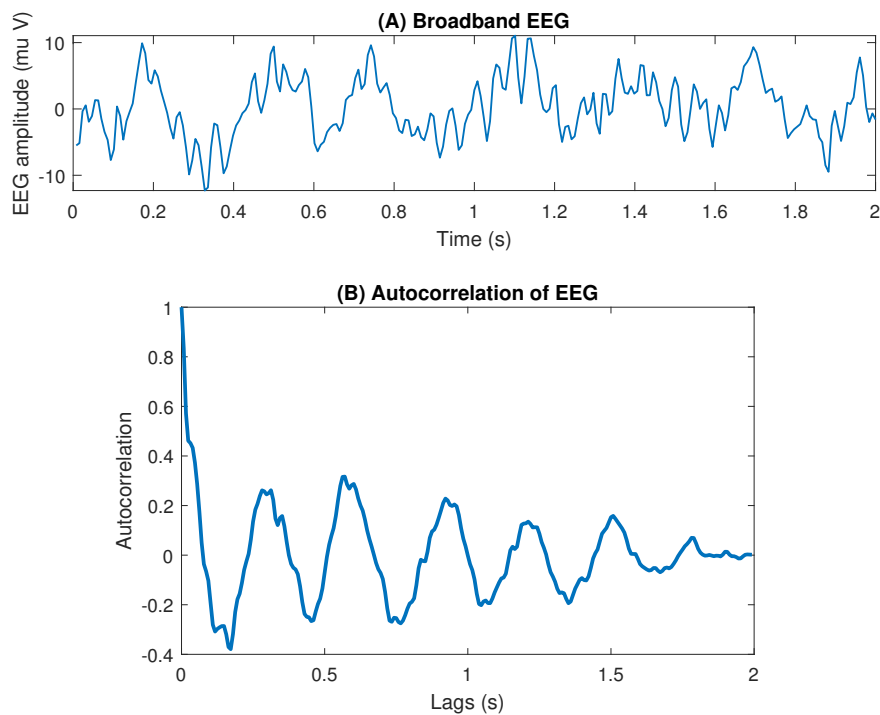
Fig. 2.3 **EEG and its autocorrelation.** (A) 2 s window of broadband EEG between 0.5-45 Hz (B) Normalised autocorrelation of 2 s EEG window.

and give insight into the mechanism of the entity being studied. The power-law is observed in critical systems which is discussed in the subsequent sections.

When the two quantities with power-law relationship are plotted on log-log scale, they show a linear relationship. This log-log linear relationship is commonly used to identify the presence of power-law. However, determining power-law is inherently difficult. It has been argued that the linear relationship is a necessary but not sufficient condition for power-law [119]. Common method of determining this linear relationship using linear regression resulting in small R^2 value is not accurate (see section 2.4.4 for details on R^2 estimation). It has been suggested [119] that if the fit of linear model is the best after comparing it with log-linear or other such models, then it can be said that the power-law is present, though not with absolute certainty.

In self-similar processes such as fractals, power-law holds true in all the dimensions. However, in other processes, the power-law may hold only in one of the dimension where the properties in that dimension are similar over different scales. Such processes are said to have self-affinity rather than self-similarity [39]. One such self-affine process is the time series with power-law in the time dimension.

Power-law is observed in several different spatial and temporal neuronal processes in the brain. Neuronal networks in the brain also show power-law scaling in the connections of its nodes. Power-law scaling is observed in neural avalanches which are the bursts of firing and in neuronal recordings. To understand the dynamics of these processes, it is important to study the power-law. This thesis focuses on temporal neuronal processes, especially EEG which shows power-law scaling in its autocorrelation and spectrum.

2.2.3   Long-range dependence (LRD) and short-range dependence (SRD)

The nature of autocorrelation decay reveals the temporal dependencies in the time series. If the autocorrelation decays slower than exponential, then the time series is said to have long-range dependence (LRD). If the autocorrelation decays exponentially or faster than exponential, then the time series is said to have short-range dependence (SRD) [120]. In SRD process, the coupling between the samples at different time decreases fast as the time between the two samples increases. In SRD the autocorrelation drops to zero after certain lags or decays exponentially. In the LRD process, the coupling in the two samples is stronger and autocorrelation decays slower than exponential or according to the power-law. The LRD processes with power-law decay can be self-similar or self-affine. The LRD and SRD processes in EEG are explored further in chapters 5 and 6. Fig 2.4 shows the autocorrelation and spectrum of SRD process and LRD process [32]. The autocorrelation of SRD process decays exponentially and autocorrelation of the LRD process decays slowly (according to the power-law). The log-log spectrum of SRD process is non-linear and that of LRD is linear following $1/f$ shape. Further details of these characteristics of SRD and LRD processes are included in the subsequent sections.

2.2.4   Long-range temporal correlation (LRTC)

The long-range temporal correlation is a specific case of the LRD when the autocorrelation decays according to the power-law as shown in equation (2.4)

$$\rho_{xx}(\tau) \sim C\tau^{-\alpha} \tag{2.4}$$

where there is asymptotic equivalence between the autocorrelation ρ_{xx} at the lag τ and its power-law which has a scaling exponent of α. This translates to a linear relationship in log-log scale. The autocorrelation of LRTC processes is finite even at large lags because of the power-law statistics and its sum diverges on the contrary to the SRD where the autocorrelation eventually becomes zero [120].
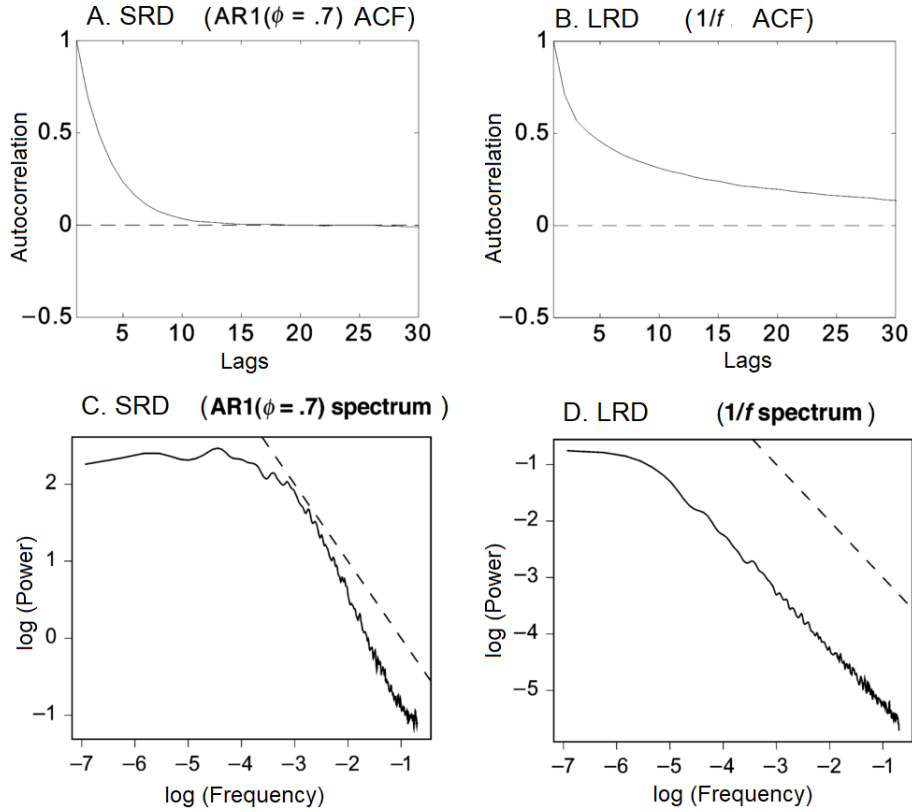
Fig. 2.4 **Autocorrelation and spectrum of short-range dependence and long-range dependence.** (A) Autocorrelation of SRD process generated by autoregressive process of order 1 (more details on this in the next sections). (B) Autocorrelation of LRD process generated by $1/f$ process. (C) Log-log spectrum of the above SRD process. (D) Log-log spectrum of the above LRD process. This figure is adapted from Wagenmakers et al. [32].

The time series showing LRTC according to equation (2.4) also shows power-law relationship in the spectral domain which is obtained by taking Fourier transform of the above equation leading to the relation given in equation (2.5). Thus the LRTC process with power-law decay of its autocorrelation also shows power-law in its spectrum G_{xx}. The spectrum of LRTC process has a linear relationship between their frequencies and their amplitudes in the log-log scale giving rise to $1/f$ spectrum. EEG is known to have $1/f$ spectrum with a prominent peak around 10 Hz corresponding to alpha rhythm.

$$G_{xx}(f) \sim Bf^{-\beta} \qquad (2.5)$$

where, G_{xx} is the spectrum, f is the frequency, β is scaling exponent of the power-law and B is a constant.

The autocorrelation and spectral scaling exponents α and β are related by $\beta = 1 - \alpha$. Estimating these scaling exponent is difficult and hence in practice, the LRTC is quantified by Hurst exponent (H) which can be obtained using several methods, one of which is described in the following sections. The Hurst exponent is related to the α and β by $H = \frac{2-\alpha}{2}$ and $H = \frac{1+\beta}{2}$. The LRTC in the autocorrelation and spectrum of EEG is shown in chapters 5 and 6.

2.2.4.1   Hurst exponent

The values of Hurst exponent determine the nature of temporal dependencies present in the underlying time series as follows.

- If $0 < H < 0.5$, then the time series is anti-correlated. This means that the large value tends to be followed by a small value in a time series.

- If $H = 0.5$, then the time series is a white noise or random noise that does not have any correlations. In the case of white noise, the autocorrelation function (ACF) is zero at any lags other than lag 0, and the corresponding spectrum is flat which makes the scaling exponent $\beta = 0$ and from the relation given above, the H becomes 0.5.

- If $0.5 < H < 1$ then the time series is said to have LRTC and have persistent correlations. In this case, a large value tends to follow a large value and small value tends to follow a small value in a time series. There is a positive correlation between the samples that are close together.

- If $H = 1$ then the time series is long-range correlated and has a $1/f$ spectrum. Such a time series is called pink noise. There the scaling exponent i.e. the slope of the spectrum scaling exponent is $\beta = 1$

- If $H = 1.5$ then the time series is integrated white noise process also known as Brownian noise. There is a strong correlation and a value of a particular sample is completely dependent on its previous sample. Such a time series is obtained from a cumulative sum of the white noise. In this case, the scaling exponent is scaling exponent $\beta = 2$.

The LRTC process is hence between white noise which is random and has no correlations and Brownian noise which has strong trends emerging from correlation.

2.2.4.2   Detrended fluctuation analysis (DFA)

The Hurst exponent can be estimated by a temporal method developed by Hurst called rescaled range analysis [121]. Peng et al. [122] proposed an adaptation of rescaled range

analysis called detrended fluctuation analysis (DFA) for identifying Hurst exponent of non-stationary time series. Since then, the DFA technique has become one of the most widely used technique of estimating Hurst exponent of time series. The method for DFA has been described in detail in chapter 5 and 6. The DFA describes LRTC in the time series by finding a power-law relationship between the RMS fluctuations at different time scales. Firstly it creates an integrated series by cumulatively summing the time series. Then at each timescale, the series is segmented into the non-overlapping boxes of length equal to the timescale. Each box is detrended with a linear or polynomial function to extract the fluctuations at that timescale. The RSM of the fluctuations in all the boxes is computed at each timescale. The detrending step removes any correlations that are resulting from these trends at different timescales. Hence this technique is suitable for non-stationary time series to determine real long-range correlations and not the artifactual correlations caused by the trends. The RMS fluctuations at each timescales are plotted in log-log scale and if these RMS fluctuations show a linear relationship (i.e. power-law relationship), then the scaling exponent or the Hurst exponent can be estimated from the slope of the linear fit to the fluctuations. If the DFA scaling exponent is between 0.5-1, then the time series is said to have LRTC [123].

Sometimes, a DFA fluctuation plot has different linear relationships over different timescales. These linear trends are separated by the crossover points, the points at which the slope of the fluctuations in different timescales change. Such time series can be defined by different scaling exponent for different range of scales separated by the crossover points. Such time series with multiple scaling exponents are known to be multifractal [124, 125]. Multifractal time series have more complex dynamics that differ over different timescales.

The DFA scaling exponent is valid and represents Hurst exponent only if the relationship between RMS fluctuations at different timescales is linear (power-law) on log-log scale. However, assessing this linear relationship is difficult [119, 126]. It is mostly assumed that the relationship between the fluctuations is linear when scaling exponent is computed using DFA, however this assumption must be tested by assessing the fit of the linear model to the fluctuations. A common method of assessing the goodness of fit for DFA is simple R^2 measure which is widely used [29, 38]. However, R^2 is an insensitive measure of goodness of fit because it can give high value even when the relationship between the points is not linear but they closely surround the fitted line. It does not take into account whether the points are distributed randomly around the fitted line. To assess the random distribution of the points around the fitted line, Wald-Wolfowitz runs test was used [127]. Botcharova et al. [120, 128, 126] proposed a new method called maximum likelihood DFA which fits numerous models such as linear, polynomials of different orders, logarithmic, exponential and root models to the RMS fluctuations and identify the best fitting model. If the best

fitting model was linear, then it can be said that the DFA scaling exponent is valid. The models can be compared using Akaike Information Criterion (AIC) [129] and Bayesian Information Criterion (BIC) [130] that compare maximum likelihood of the models. The model comparing approach to identify possible power-law has also been suggested by Clauset et al. [119]. However, it cannot be said with certainty that the fluctuations show a power-law because there can be some non-compared model that can fit better.

The DFA exponent is highly dependent on the box size. Too few samples in an individual box will give inaccurate estimates of RMS fluctuations after detrending. The minimum box size commonly used is 10 [131]. The maximum box size is chosen such that the time series is divided in at least 4 boxes to get correct estimation of overall RMS fluctuations. More discussion about this is given in the study by Botcharova et al. [120].

2.2.4.3   LRTC in EEG during movement

The LRTC is commonly observed in several neuronal processes such as neuronal firings [33], neuronal avalanches [34, 35], intra-cranial recordings such as LFPs [34] and ECoG, and non-invasive scalp recordings of EEG and MEG [34, 36] in both periodic and aperiodic processes. The LRTCs have been observed in the alpha, beta, theta oscillation amplitudes [132], alpha oscillation phase [128], broadband phase synchrony [37] avalanches [34, 35] and energy profile [133].

It was first proposed by Linkenkaer-Hensen [29] that the individual oscillations in EEG (and MEG) show LRTCs in their amplitude fluctuations, which means that the fluctuations in the amplitudes of individual oscillations are similar across different time scales. LRTCs in EEG are commonly extracted from the fluctuations of individual oscillations [36, 40, 125, 134, 135]. Further details of LRTCs in EEG are discussed in chapters 5 and 6.

The LRTC is considered as an invariant property of healthy brain in the resting state. It was found that there are changes in the LRTC in different neurological disorders [42, 41, 40, 39, 133]. The strength of LRTC is reduced due such disorders and the LRTC can be restored to their baseline level with certain medications for the neurological conditions. Zhigalov et al. [135] found that the neurofeedback can increase the LRTC. This suggests that the closed-loop interactions can modulate the LRTC. The external stimulus or an event also induce changes in the LRTC [38, 126, 135].

The amplitude fluctuations of sensorimotor oscillations are modulated due to somatosensory stimuli [38]. Though the modulated oscillations still showed LRTC, their magnitude is attenuated and the DFA scaling exponents decrease. Linkenkaer-Hansen et al. [38] observed that the LRTC in oscillations around 10 Hz and 20 Hz decreased after periodic repeated median nerve stimulation. Botcharova et al. [126] showed that the LRTC in the alpha and

beta oscillations decreased during repeated finger movement. The reason for this might be that the neural activity is reorganised by the sensorimotor stimuli and is likely to disrupt the functional connectivity leading to attenuation of temporal correlations [38]. Botcharova et al. [126] hypothesised that the movement produces a phase relationships in the oscillations that is similar to Gaussian white noise which ultimately disrupts the long-range correlations.

Though the common hypothesis is that the movement-related event disrupts the LRTCs, there are several gaps in the understanding of the effects of movement on the LRTC. It is not known whether a single movement would cause the same effect on the LRTCs over larger time scales because the above studies examined the effect of the repeated movements. The effect of movement on the temporal correlations in the arrhythmic broadband EEG is not known as the LRTCs are canonically obtained from individual oscillations. Also, the timescales considered for oscillations LRTC are long. Finger tap movement being a very short event lasting for about a second, it is vital to study its effect on short timescales. All these questions are investigated in details in chapters 5 and 6.

2.2.5 Parametric models for EEG

EEG time series can be modelled using several different types of models. One of the most common families of models used for EEG is stochastic parametric models such as autoregressive and moving average models and their variants. While AR and MA models are suitable for stationary time series with SRD, their integrated variant autoregressive integrated moving average (ARIMA) model is used for non-stationary time series. EEG has LRTC which can be modelled using a generalisation of ARIMA called autoregressive fractionally integrated moving average model (ARFIMA). The scale-invariant arrhythmic broadband EEG can be considered as a stochastic process and hence can be modelled by a stochastic parametric model such as ARFIMA. ARIMA can model the LRD as well as the SRD in the time series. How ARFIMA can model LRTC is described in the following sections [32].

2.2.5.1 White noise

The time series without any correlations is called white noise. The samples in white noise are independently identically distributed (iid). The white noise can be represented by equation (2.6).

$$X_t = \varepsilon_t \tag{2.6}$$

where ε_t also known as innovation is randomly drawn from a Gaussian distribution [32]. The white noise is a stationary process. The power spectrum of white noise is flat with slope of 0 in log-log scale as shown in section 2.2.4.1.

2.2.5.2   Random walk process

The random walk process is an integrated white noise. It is a running sum or cumulative sum of the independent samples. Random walk is given by equation (2.7) and (2.8). The power spectrum of a random walk in log-log scale is a straight line with slope -2 (see 2.2.4.1).

$$X_t = \sum_{i=0}^{t} \varepsilon_i \tag{2.7}$$

$$X_t = X_{t-1} + \varepsilon_t \tag{2.8}$$

The random walk process is non-stationary because its variance increases over time. The current value of the random walk can be defined entirely by the value of its previous sample and current innovation. Taking difference between successive samples gives the random white noise process. This procedure is called differencing. Differencing a random walk changes its slope from -2 to 0 making it a white noise and integrating a white noise changes its slope from 0 to -2.

2.2.5.3   Autoregressive (AR) model

In AR processes, the current value depends only partly on the previous value unlike random walk as given in equation (2.9).

$$X_t = \phi X_{t-1} + \varepsilon_t \tag{2.9}$$

where ϕ is magnitude of the difference. Such a process has order 1 and is called AR(1) because the currently value is partly dependent only on the previous value. The $\phi \in (-1, 1)$ keeps the values of the samples within certain bounds preventing drifting to very high or low values. The ACF of AR(1) follows an exponential function indicating that it is an SRD process. The log-log power spectrum of AR(1) is not a straight line, but it is a curve. For AR(1), more power is present in the lower frequency which flattens the power spectrum in these low frequencies. Thus, AR(1) power spectrum has a slope of 0 in lower frequencies and -2 in higher frequencies [32].

The AR process can have higher order such that the current value is dependent on certain number (p) of past values. The AR(p) process is given by equation (2.10).

$$X_t = \phi_1 X_{t-1} + ... + \phi_p X_{t-p} + \varepsilon_t \tag{2.10}$$

AR models of several different orders are used to model EEG oscillations. High order AR models usually between 8 to 16 [136, 137, 84, 138] are required for EEG. AR models can model oscillations but cannot give good estimation of broadband EEG because the broadband EEG is non-stationary and AR model is suitable for stationary processes. Moreover, EEG contains LRTC but the AR models can only capture SRD in the time series. Hence, AR models alone cannot model EEG accurately. Further discussion on AR models is included in chapter 6.

The modification of AR models for non-stationary data is adaptive autoregressive models [139, 140] whose parameters are estimated with Kalman filter. Adaptive autoregressive model adaptively changes the order of model to estimate EEG.

2.2.5.4 Moving average (MA) model

The current value of the sample in MA process depends on the current random innovation and the previous random innovation. The equation (2.11) shows the MA(1) process. Higher order MA(q) process is shown in equation (2.12) in which the current value is dependent on the current innovation and q previous innovations. The power spectrum of MA(1) is similar to that of white noise with a very steep slope at highest frequencies.

$$X_t = \varepsilon_t + \theta \varepsilon_{t-1} \tag{2.11}$$

$$X_t = \varepsilon_t + \theta_1 \varepsilon_{t-1} + ... + \theta_q \varepsilon_{t-q} \tag{2.12}$$

The values of innovations earlier than ε_{t-p} do not have any effect on the current value and are completely unrelated to X_t. Hence MA processes can be used as filters to remove noise and smooth the time series.

Both AR and MA are linear combinations of the random innovations. The AR model absorbs innovations ε into x_t such that any previous ε_t will have an impact on all the future values of X_{t+k}. On the other hand, as stated previously, the current value of MA process is a finite combination of the q previous random innovations. The future values will not be impacted by the innovations previous than the last q innovation values. The invertible MA(1) process (with $\theta \in (-1,1)$) can be represented by an infinite order AR process and vice versa.

2.2.5.5 Autoregressive moving average (ARMA) model

The ARMA(p,q) model is a combinition of pth order AR model and q^{th} order MA model as given by the equation (2.13).

$$X_t = \sum_{i=1}^{p} \phi_i X_{t-i} + \varepsilon_t + \sum_{i=1}^{q} \theta_i \varepsilon_{t-i} \tag{2.13}$$

ARMA models have also been used to model EEG.

2.2.5.6   Autoregressive integrated moving average (ARIMA) model

The ARIMA(p,d,q) model is a generalisation of ARMA(p,q). The ARFIMA model incorporates non-stationarity in its integration parameter d as given in the equation (2.14). The time series is differenced d times to make it stationary after which, the AR and MA parameters are estimated.

$$\left(1 - \sum_{i=1}^{p} \phi_i B^i\right)(1-B)^d X_t = \left(1 + \sum_{i=1}^{q} \theta_i B^i\right)\varepsilon_t \tag{2.14}$$

where B is the backshift operator such that $BX_t = X_{t-1}$ and $B^n X_t = X_{t-n}$. ARFIMA models are also used for modelling EEG where EEG is usually differenced once and then the AR and MA parameters are estimated.

2.2.5.7   Autoregressive fractionally integrated moving average (ARFIMA) model for LRTC

While ARIMA(p,d,q) can model non-stationary time series, it is not suitable for LRTC process. The white noise can be modelled with ARIMA(0,0,0) with $d = 0$ and log-log power spectrum slope of 0. The random walk can be modelled by ARIMA(0,1,0) with $d = 1$ and log-log power spectrum slope of -2. The process with LRTC has a log-log power spectrum with a slope of approximately -1. The LRTC processes lies between random walk and white noise and hence would need a fractional value for d between 0 and 1 because as mentioned in section 2.2.5.2, differencing once changes the slope of power spectrum from -2 to 0. Hence the fractional differencing with a fractional value of d can model the LRTC part of the time series and the residual stationary SRD could be modelled using AR and MA parameters of ARFIMA(p,d,q) with the equation 2.14. Generally for LRTC, the slope of the power spectrum is between -0.5 and -1.5. An ARIMA model would require an infinite number of parameters to accurately model LRTC process of infinite length [32].

The process of fractional difference is given in chapter 6. For $0 < d < 0.5$, the ARFIMA process is stationary and for $d > 0.5$, the ARFIMA process is non-stationary. The d is estimated from the Hurst exponent using $d = H - 0.5$. Further details of ARFIMA modelling are comprehensively given in Wagenmakers et al. [32]. Though ARFIMA can model LRTC

and SRD simultaneously, it is a mathematical model that is very descriptive and it does not give any information about the underlying physiological processes. ARFIMA model has been used to generate LRTC process to test different signal analysis approaches [126, 120, 127] but it is not used commonly to model broadband EEG that contains LRTCs as described in this thesis.

2.2.6   Self-organised criticality in neuronal processes

The concept of criticality originated from physics to describe systems that have critical points, i.e. the points of phase transition for example, a liquid turning to a gaseous state [120]. Such critical points depends on tuning of external parameters such as temperature in this case. However, the critical behaviour that is observed in the dynamical systems is fundamentally different from the critical point. The dynamical systems with criticality have these critical points as an attractor and the system evolves towards this critical state without any external force or requirement of tuning of external parameters. Such a system is said to have self-organised criticality (SOC), which was first described in the seminal work by Bak et al. [141]. The systems with SOC are on the brink of stability and instability, hence are poised at criticality, ready to respond to external stimuli. The main property of the SOC is the scale-invariance in spatial and temporal domain. Bak et al. [141] proposed that the SOC is the underlying mechanism behind the ubiquitously present $1/f$ noise and self-similarity in the fractal structures in the nature and no fine-tuning is necessary to produce these phenomena in the nature. Hence, power-law which represents scale-invariance is considered as a property of SOC. Bak et al. also proposed that SOC is the mechanism giving rise complex systems [142]

As described in previous sections, the brain shows power-law dynamics and $1/f$ noise in several neuronal processes. This has led to a *critical brain hypothesis* that the brain operates at criticality. Since there are no external factors that control the development of neural networks and processes in the brain, it is hypothesised that the brain has SOC because it evolves to criticality by itself. The brain is said to be at a critical state ready to process any external stimuli efficiently. The criticality can help in optimising information transfer, storage capacity and adapting to different cognitive demands [37, 62]. The criticality in the brain could also help in rapid transitions in the functional connectivity [143]. The LRTCs in the neuronal processes are considered as markers of criticality [29, 36, 135, 62, 128, 144–146]. A comprehensive background on LRTC and criticality in neuronal processes is given in the study by Botcharova et al. [120].

There are no known characteristics or methods that can guarantee the detection of criticality. The criticality is always hypothesised based on the observation of power-law statistics. However, not all critical systems show power-law dynamics and not all power-laws

lead to criticality [128]. Several different mechanisms can give rise to criticality in the brain, one of which is said to be the balance between the excitation and inhibition [62, 43, 147]. Poil et al. [62] propose that excitation/inhibition balance cause critical dynamics in the form of avalanches and LRTCs in different oscillations.

2.3 Movement based BCI

Movement intention and movement imagery are some of the most popular BCI paradigms because they allow intuitive control of the BCI application. This thesis is focused on extracting neural correlates of movement intention for application in BCI. This section gives an overview of EEG based BCI development procedure and its applications.

2.3.1 BCI procedure

2.3.1.1 Preprocessing and artefacts removal

EEG is often contaminated by various artefacts. An artefact is a signal recorded by EEG which does not have its source in the brain, causing disturbances in recording the brain signal and has a high negative impact on BCI control. The artefacts usually have higher amplitudes and hence the minute characteristics of EEG are hidden underneath. The aim of artefact removal is to eliminate the artefacts to reveal the underlying EEG. EEG artefacts can be classified into two categories according to their sources: artefacts arising due to external sources and artefacts arising due to internal sources. External artefacts are caused by electrical interference of electronic devices in the surrounding and 50 Hz power line noise. Their effect can be reduced by using EEG recording apparatus that tolerant to external electrical interference as well as using notch filter to filter out 50 Hz component. Internal sources of artefacts are electrooculography (EOG) signals caused due to eye movement and blinking, electromyography (EMG) signals caused due to movement of facial muscles and jaw movement, and electrocardiography (ECG) signals. It is difficult to avoid artefacts caused by internal sources since most of them are due to involuntary movements like eye blinks. Various manual as well as automated techniques are developed to remove artefacts from contaminated EEG.

Manual artefacts rejection: The simplest method of artefacts removal is manual identification of trials with artefacts and rejection of these trials [148] process leads to huge loss of data. The simplest manual method of managing artefacts is to avoid them, which can be

achieved with shorter trials and frequent breaks. Manual artefacts rejection cannot be used for online BCI application.

Blind source separation using Independent component analysis (ICA): Blind source separation can be used to extract independent source signals and separate artefacts sources and EEG sources. This can be achieved by using independent component analysis (ICA) [149]. ICA assumes that the acquired EEG on any one channel is the linear mixture of temporally independent signals from different sources and channels and hence it estimates an unmixing matrix which gives independent EEG sources. Artefactual sources are either identified manually or automatically by setting certain criteria. ICA is one of the most commonly used technique for artefacts removal [149]. Schlogl et al. [150] used EOG channels recorded simultaneously with EEG to remove the EOG sources for EEG using regression. The classifiers such as support vector machine (SMV) were used for identifying trials with and without artefacts [151]. The principal component analysis (PCA) was also used in many studies [152] but performed poorly in comparison to ICA. In this thesis, ICA has been used to identify sources with artefacts which were eliminated and uncontaminated EEG was reconstructed.

Other artefacts removal methods: Wavelet transform is widely used for EOG artefacts removal automatically without manual intervention. Wavelet transform sets the threshold limit for EEG trials with artefacts by comparing with the baseline without any artefacts and Haar wavelets can be used to identify regions of EEG contaminated with artefact [153]. Other methods of artefacts removal include regression, template matching, neural networks and hybrid techniques [154].

Online artefacts removal: The methods described above for artefacts removal are used offline, however for application of these techniques for BCI requires online artefacts removal methods. Moreover, these online artefacts removal techniques must have minimum latency for BCI output to feel intuitive. There are several online artefact removal techniques [155, 156].

2.3.1.2   Feature extraction

Various types of temporal, spectral, time-frequency and spatial features can be extracted from EEG for controlling a motor based BCI [157]. The most significant features that represent the required information in EEG accurately are extracted. A single feature can represent the task appropriately or a vector of features may be required to define the information content in EEG. The features are selected such that they maximise the distinction between two classes.

The autocorrelation of EEG, power spectrum, band power, instantaneous phase, wavelets are some of the commonly used analysis techniques. Features can be extracted by fitting AR, MA or adaptive autoregressive models to EEG [138, 84, 136]. The functional networks can also be evaluated from different channels of EEG using different connectivity measures such as synchronisation, cross-correlation, coherence and phase difference. EEG has low spatial resolution and is affected by volume conduction. To enhance the quality of signals, spatial filters can be used. Various spatial techniques for feature extraction such as principal component analysis, independent component analysis, common spatial patterns, Laplacian filtering [158] are commonly used. The common spatial patterns technique is common for movement detection [159]. Referencing EEG with different montages such as latitudinal and longitudinal bipolar montage and common average referencing [158] can be used.

The two most common correlate of movement are ERD/S and MRCP as discussed earlier. Majority of the research studies use ERD/S and MRCP and their variants as features for movement based BCI. These features have to be extracted on single trial basis for application in BCI.

2.3.1.3 Classification

Various types of classifiers are used for classifying features. Neural network based classifiers prove to be more useful and accurate for classification due to their ability to learn the pattern. If features are easily separable, then simple classifier can perform the classification task accurately. However if the features are not very separable, then more advanced classifier is required to obtain good accuracies. Linear discriminant analysis (LDA) is one of the most commonly used classifier [160, 161]. The LDA can classify multiple classes at a the same time. The LDA is simple to construct and gives very good results. However, because of its linear nature, LDA does not classify non-linear data accurately.

Support Vector Machine (SVM) can classify non-linearly separable data as well as inseparable data unlike LDA [157]. SVM aims towards forming optimum boundary between the two classes by finding support vectors from both the classes and maximises the distance between the boundary and the support vectors. The SVM maps the points in the higher dimensional hyper-plane to extract the classifying hyper-surface which helps in classifying non-separable low-dimensional data. SVM is complex to execute and may be computationally demanding for online BCI.

Classifiers such as Bayesian classifiers, particle swarm, optimisation Elman Neural Network [162], logistic regression, decision trees, k-nearest neighbour [163] and many more can be used in BCI. If the feature vector has high dimension, dimensionality reduction could be done using principal component analysis to find the most classifiable features.

2.3.1.4   Applications of movement based BCI

BCI provides a mode of interaction with different objects directly by brain without using any motor pathways. This is useful for patients with motor disorders to communicate with their environment. BCI can also be used for movement rehabilitation. Traditional rehabilitation involves therapist passively moving patients arms/legs for exercises, while this rehabilitation therapy has been in use for long, it does not give movement ownership to the patient. The patient is not actively engaged in the movement being performed. Rehabilitation could be more useful if the patient is actively engaged in the movement that is executed and if the patient has the ownership of their movement. Rehabilitation BCI can provide this movement ownership and active engagement to the patient [54–56, 164]. The patient can produce a desired movement intention and the BCI would identify the movement and send a corresponding command to for example, a robotic rehabilitation device. This would give a sense of movement ownership to the patient since, patient was the one who initiated the movement. This would help in a faster recovery and motor relearning.

Several BCI studies have been done for rehabilitation based BCI. One of the rehabilitation technique is BCI controlled functional electrical stimulation (FES). The BCI based on motor imagery of arm has been used to trigger functional electrical stimulation to perform wrist movements for upper limb rehabilitation in chronic stroke patients [88]. The performance of the patients was reported to improved over the time. Other similar BCI-functional electrical stimulation rehabilitation studies used spatial, spectral and temporal patterns simultaneously to detect motor imagery [165, 166]. The study [166] also reported a significant increase in the EMG amplitude of the targeted muscles after 20 min of functional electrical stimulation rehabilitation session using motor imagery BCI as compared to rehabilitation using just passive FES.This supports the fact that active engagement improves the rehabilitation outcome. Hybrid approaches mimicking the hierarchy in human nervous system has also been used for developing functional electrical stimulation-BCI for paralysed patients [167].

Another advantage of FES based rehabilitation BCI is that functional electrical stimulation provides a direct feedback to the patients which in turn helps in producing better ERD [168]. Rehabilitation exercise based on BCI mediated neurofeedback mechanisms that enabled a better engagement of motor areas and thus it can promote neuroplasticity in the affected brain regions [169]. Study conducted by Pfurtscheller et al. [170] has achieved the restoration of hand grasp function in a tetraplegic patient. The functional electrical stimulation was triggered by β bursts due to foot motor imagery. Using switching between different grasping sequence, the patient was able to grasp a glass with the paralysed arm.

Other major group of rehabilitation BCIs use robotic rehabilitation using robotic arm or similar mechanical devices. These BCIs again used motor imagery to drive the robotic

device [171]. Comparison studies have been perform to compare the performance of robotic BCI rehabilitation vs passive robotic rehabilitation. Robotic rehabilitation techniques have been reported to show more improvement in patients [172, 57, 173]. The appendix A describes a demo of a temporal dynamics BCI to control virtual reality and soft robotics rehab system [174].

Rehabilitation BCIs are not only used for arms or legs rehabilitation but also for rehabilitation of walking [175]. Even if the walking is largely controlled by spinal cord, brain is very important in monitoring locomotion patterns and coordination between upper and lower limbs. Exoskeleton driven by BCI was used for walking rehabilitation. In another research, BCI controlled walking simulator was developed [176] in conjunction to lower extremity functional electrical stimulation for rehabilitation.

All the rehabilitation BCIs used ERD produced by motor imagery. However, all the constraints for good ERD detection like selection of optimum channel, optimum frequency band also followed. The training requirements for producing usable ERD could also play a role in usability of these rehabilitation BCIs. Moreover ERD does not ensure movement prediction. For creating a system which seems natural to the user, the delay between the movement imagery produced and the feedback provided by functional electrical stimulation and robotic device must be minimum. Hence there is a need of a robust predictive BCI.

2.3.2   Challenges in the current BCI systems

The BCIs show great potential in the applications for people with motor disabilities, rehabilitation and even entertainment and gaming. However, there are several reasons why BCIs are still used in research facilities and not by the general targeted audience. Invasive BCIs have many challenges and issues, the major one being the need of high-risk brain surgery and prolonged insertion of implant in the body. EEG based BCIs are non-invasive, cheap and easy to use, but they have different challenges. The major hurdle in EEG based BCIs is the poor quality brain signals recorded by the sensor electrodes placed on the scalp with low signal to noise ratio. There are several factors limiting the widespread non-research use of BCI.

Who can use BCI: Not all the people can use BCI. No universal BCI that could be used by everyone has been developed yet [177], around 20% of the participants cannot use it. Researchers have tried to mitigate this problem by improving the signal processing algorithms, participant training, novel tasks/paradigms and instructions. In spite of these efforts, not everyone can use BCI with same proficiency and produce detectable patterns of brain activity.

For example, in the study [178], 93% of participants were able to use BCI with accuracy above the chance level.

BCI system design and performance: There could be much inconsistency in the BCI system in session-to-session basis and subject-to-subject basis [179]. It is difficult to identify the signal in baseline state when the user is idle, this leads to false detection. EEG signals are non-stationary and hence adaptation of the processing algorithms is necessary. Also, BCI must be capable of handling continuous stream of data rather than operating on trial by trial basis. The hybrid approaches have been used to overcome some of these difficulties to a some extent [180]. The comparisons across different studies is also very difficult because different groups use different measures of performance. The performance can also vary depending on number of trials or their size [177].

Offline or online: Many studies in the literature have showed good results with machine learning and pattern recognition algorithms. However, getting same level of results online has been a challenge [181]. However, for practical use of BCI, it has to be a real-time system that can identify the user's intent and send appropriate command at the same time. High information transfer rates are very difficult to achieve because as EEG epoch length is reduce, it becomes harder to reliably detect the BCI command [182].

Training requirement: The training is often required by the participants to operate BCI. The participants often tend to improve their performance with training and practice [183]. The train requirement is often accompanied with the calibration of the system [184].

Poor quality of EEG: EEG has poor signal to noise ratio which could be difficult to adjust [185]. The spectrum of EEG shows $1/f$ distribution which results in high-frequency EEG buried in noise. Because of this, higher frequencies in EEG are not accessible for use in signal processing. Due to volume conduction, the electrodes on the surface record the data from multiple sources and it becomes difficult to identify the sources, especially in real time.

All these limitations affect the usability of BCIs. The main issue being reliable detection of command due to all the factors mentioned above. This thesis aims to identify neuronal processes that can facilitate a robust movement intention detection on single trial basis and aid in solving at least some of the BCI challenges.

2.4 Fundamentals of EEG analysis: Methods

This section outlines the fundamental methods used for EEG analysis and classification throughout the thesis.

2.4.1 Linear Discriminant Analysis (LDA) Classifier

Linear classifiers are most commonly used in BCI because they are easy to interpret and also easy to train [186]. The computations required for identifying the classification boundary (hyperplane) are also straightforward. Linear Discriminant Analysis classifier is widely used for binary classification of two classes in BCI. LDA uses supervised learning to determine classification boundary from several samples of training data. LDA has been used for classification of motor intention vs resting state throughout this thesis.

LDA uses a discriminant function for classifying two classes. Fig 2.5 adapted from Hong et al. [187] shows the schematic representation of LDA. LDA identifies a discriminant function $g(\mathbf{x})$ for input feature vector $\mathbf{x}$ and according to the sign of the value of $g(\mathbf{x})$, assigns the class labels +1 or -1 to the input sample. For a new sample $\mathbf{x}$, class 1 is assigned if $g(\mathbf{x}) > 0$, otherwise class 2 is assigned.
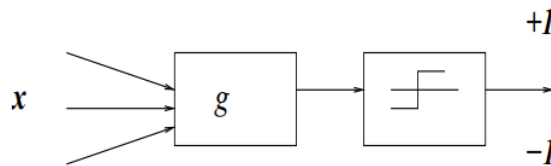
Fig. 2.5 **Schematic of Linear Discriminant Analysis classifier [187].**

A discriminant function is a a linear combination of the components of vector $\mathbf{x}$. The discriminant function $g(\mathbf{x})$ is given in equation (2.15).

$$g(\mathbf{x}) = \mathbf{w}^T \mathbf{x} + w_0 \tag{2.15}$$

where $\mathbf{x}$ is a feature vector, $\mathbf{w}$ is a weight vector and w_0 is the threshold weight. The equation $g(\mathbf{x}) = 0$ determines the decision boundary that separates the input feature vectors belonging to two classes [187]. In case of LDA, discriminant function $g(\mathbf{x})$ is linear. The weight vector $\mathbf{w}$ is normal to $g(\mathbf{x})$.

There are several ways of determining linear discriminant function $g(\mathbf{x})$ given a set of training feature vectors. For two-class classification, equation (2.15) is set to value of +1 or -1 such that $\mathbf{w}^T \mathbf{x} + w_0 = 1$ or $\mathbf{w}^T \mathbf{x} + w_0 = -1$ depending on the class label of training data.

A set of several such equations is obtained from the training set with multiple samples of $\mathbf{x}$ belonging to class 1 and 2. The value of the weight vector $\mathbf{w}$ is then estimated by solving these equations. Often there is no exact solution to these equations, and hence, the value of $\mathbf{w}$ is determined by minimising the error between the both sides of equations using methods such as least squares estimate [187]. The least squared method is form of regression that minimises the sum of squares of errors iteratively.

2.4.1.1   Cross-validation

Cross-validation is often used to evaluate the performance of a classifier [188]. A common cross-validation technique is k-fold cross-validation where the available data samples are divided into k bins and $k-1$ bins are used as training set and 1 bin is used as testing set. The classification is repeated by setting each bin as a testing set. This ensures that all the samples in the available dataset have been used as training set as well as testing. The estimate of classifier accuracy is the overall number of correct classifications divided by the total number of samples in the dataset [189]. Thus, when the sample size is sufficiently large and representative, the cross-validation predicts a true performance of the classifier for unseen data or generalisation capacity [190].

It is common to use 5-fold cross-validation or 10-fold cross-validation where the data are divided into 5 and 10 sections respectively. Throughout this thesis, a 10x10 fold cross-validation scheme has been employed to evaluate the performance of the LDA classifiers to identify movement intention. In a 10x10 fold cross-validation, a 10-fold cross-validation is done 10 times to obtain more generalised average performance of the classifier. A 10-fold cross validation in this thesis was done as follows:

1. Features obtained from all EEG trials which are to be used for classification are first randomly shuffled.

2. Randomly shuffled features are divided into 10 equal bins.

3. 9 bins (90% data) are used as training set for the classifier and 1 bin (10% data) is used as unseen testing set and classification accuracy is determined.

4. The classification is performed by considering each of the 10 bins as testing set and the remainder of the 9 bins as the training set.

5. Average classification accuracy of all the 10-folds is computed.

The above process is repeated 10 times and average classification accuracy is computed. This ensures that a large number of possible combinations of samples are used for training the classifier and testing it leading to a good estimate of its true performance.

2.4.2 Principal Component Analysis

Principal Component Analysis (PCA) is a statistical technique used to interpret high dimensional datasets [191]. PCA transforms the correlated features of the samples in dataset into linearly uncorrelated features. It identifies the features that contain maximum variability of the data and hence is widely used as a technique for dimensionality reduction [191]. The aim of PCA is to reduce the dimensionality of the data whilst preserving the most of the information content (variability) in the data. PCA finds new variables using orthogonal transformation that are linear functions of the features in the original dataset, that maximise variance and that are uncorrelated with each other. These new uncorrelated variables are called principal components. Principal components are obtained by solving an eigenvalue/eigenvector problem. The first principal component captures maximum variance, the second principal component has lower variance than the first and so on. Usually for dimensionality reduction, only the topmost principal components that account for 95% of the variability of the data are retained and used in further analysis. Thus, with PCA dimensionality reduction, most of the important information in the data is preserved and new features (PCs) that are uncorrelated to each other can contain maximum variability in the data are obtained. These principal components help in identifying important distinct patterns in the dataset that are not accessible from the original features [192]. Following method is used to perform PCA. For a detailed method, refer to a tutorial on PCA created by Smith [192].

1. Consider a dataset with n features.

2. First, mean is subtracted from each of the n features in the dataset. This creates a dataset with zero mean.

3. A covariance matrix of size $n \times n$ is computed.

4. From the covariance matrix, n eigenvalues and eigenvectors are computed.

5. The eigenvector with the highest eigenvalue is the first principal component of the dataset. It contains the most important relationships between the data dimensions.

6. The n eigenvectors are ordered according to their eigenvalues in the descending order (from highest to the lowest). This gives n principal components in order of significance.

7. To reduce the dimensionality of the data, only p top most significant principal components are retained. Thus, the new dataset has a reduced dimension of p, i.e. it has p features. The p is selected such that it accounts for 95% variance of the data.

The above procedure has been used to reduce dimensionality of the features obtained from EEG to identify movement intention in this thesis in chapter 6. There are several features that can be extracted from EEG and PCA is a common technique used for dimensionality reduction in EEG [193]. PCA is also used to obtain features for BCI from EEG [194].

2.4.3   Model selection using Akaike's Information Criterion and Bayesian Information Criterion

EEG is often characterised using various types of models to understand its dynamics better and model the patterns in systematically as well as predict the patterns. In chapters 5 and 6 of this thesis, ARMA and ARFIMA models have been used to characterise the temporal dynamics of EEG. The Akaike's Information Criterion (AIC) and Bayesian Information Criterion (BIC) are the statistical techniques used to assess the quality of statistical models to assist in model selection. AIC and BIC are used to quantify the goodness of fit of the model and select the better fitting model for the given data. When multiple models are to be compared with each other, AIC and BIC estimate the quality of each model relative to the rest of the models and thus helping in model selection.

AIC estimates the quality of the model by assessing the trade-off between the goodness of fit of the model and the simplicity of the model (number of model parameters) [129]. This balance between the goodness of fit and complexity of the model helps in avoiding overfitting and underfitting models being selected. AIC is computed using equation (2.16).

$$AIC = 2k - 2ln(\hat{L}) \tag{2.16}$$

where k is the number of estimated parameters of the model which is indication of its complexity and $\hat{L}$ is the maximum value of the likelihood function for the model which is indication of its goodness of fit. The most suitable model is the one which has the lowest AIC value. AIC rewards goodness of fit quantified by likelihood function, but also penalises for increased complexity of the model quantified by the number of parameters. This penalty tries to avoid overfitting because increasing the number of parameters improves the goodness of the fit [129].

BIC is similar to AIC, and also penalises for number of parameters in a model to avoid overfitting [130]. The penalty for increased complexity is higher in BCI than AIC. BIC penalises free parameters more strongly. BIC is computed using equation (2.17).

$$BIC = ln(n)k - 2ln(\hat{L}) \tag{2.17}$$

where k is the number of estimated parameters of the model which is indication of its complexity and $\hat{L}$ is the maximum value of the likelihood function for the model which is indication of its goodness of fit and n is the sample size of the data on which the model is fitted. The most suitable model is the one which has the lowest BIC value.

2.4.4 Goodness of fit using R^2

R^2 also known as a coefficient of determinant is a statistics that quantifies goodness of fit of a regression model. R^2 measures a percentage of variance in the dependent variable that is predicted from the independent variables in regression [195, 196]. R^2 measures how well the predictions from regression approximate the real data points. R^2 ranges between 0 and 1 where R^2 of 1 indicates that the predicted values from regression are accurate and perfectly fit the original data and lower values of R^2 indicates that the predictions from the regression are further away from the true values. Thus, R^2 provides a measure of how well the data are replicated by the model and gives indication of the spread (variance) of the predicted data points from the original data points [195, 196].

R^2 is calculated as variance explained by the model (residual sum of squares) divided by the total variance (total sum of squares). Consider a dataset with n values as $y_1, ..., y_n$ and let the corresponding predicted or modelled values with regression be $f_1, ..., f_n$, then the R^2 of the predictions of the regression can be determined using equation (2.18).

$$R^2 = 1 - \frac{\sum_{i=1}^{n}(y_i - f_i)^2}{\sum_{i=1}^{n}(y_i - \bar{y})^2} \tag{2.18}$$

where $\bar{y}$ is mean of dataset $y_1, ..., y_n$. R^2 measure has been used in chapters 5 and 6 as a goodness of fit of regression model.

Chapter 3

Exploration of Neural Correlates of Movement Intention based on Characterisation of Temporal Dependencies in Electroencephalography

Maitreyee Wairagkar, Yoshikatsu Hayashi, Slawomir J Nasuto

Abstract

Brain computer interfaces (BCIs) provide a direct communication channel by using brain signals, enabling patients with motor impairments to interact with external devices. Motion intention detection is useful for intuitive movement-based BCI as movement is the fundamental mode of interaction with the environment. The aim of this paper is to investigate the temporal dynamics of brain processes using electroencephalography (EEG) to explore novel neural correlates of motion intention. We investigate the changes in temporal dependencies

of EEG by characterising the decay of autocorrelation during asynchronous voluntary finger tapping movement. The evolution of the autocorrelation function is characterised by its relaxation time, which is used as a robust marker for motion intention. We observed that there was reorganisation of temporal dependencies in EEG during motion intention. The autocorrelation decayed slower during movement intention and faster during the resting state. There was an increase in temporal dependence during movement intention. The relaxation time of the autocorrelation function showed significant ($p < 0.05$) discrimination between movement and resting state with the mean sensitivity of $78.37 \pm 8.83\%$. The relaxation time provides movement related information that is complementary to the well-known event-related desynchronisation (ERD) by characterising the broad band EEG dynamics which is frequency independent in contrast to ERD. It can also detect motion intention on average 0.51 s before the actual movement onset. We have thoroughly compared autocorrelation relaxation time features with ERD in four frequency bands. The relaxation time may therefore, complement the well-known features used in motion-based BCI leading to more robust and intuitive BCI solutions. The results obtained suggest that changes in autocorrelation decay may involve reorganisation of temporal dependencies of brain activity over longer duration during motion intention. This opens the possibilities of investigating further the temporal dynamics of fundamental neural processes underpinning motion intention.

3.1   Introduction

Brain computer interfaces (BCIs) that use electroencephalography (EEG) are being increasingly used in research due to their non-invasive nature and their potential in therapeutic applications such as motor rehabilitation [54–56, 164]. BCIs allow users to control computers, robots or other devices directly via their brain activity and hence, could potentially enable patients with spinal cord injuries or other motor disabilities to interact with devices by producing tailored mental activity. BCI is commonly driven by paradigms involving evoked activity, such as steady state visually evoked potentials (SSVEP) [42, 197], event-related potentials (ERP) [198], as well as motor-related paradigms e.g. motor imagery [59]. SSVEP and ERP employ visual and attention processes, and they always require an external stimulus to evoke a detectable response. On the other hand, neural correlates of movement enable intuitive control of BCIs by producing movement intention at will without requiring any external stimuli [60, 44]. Typically, changes in power at specific EEG frequency bands are used for detecting movement intention. However, this disregards the movement related information present in the rest of EEG spectrum and in the time domain, as EEG signal is essentially non-stationary. In this paper, we explore movement related information which is

not reflected in the band power changes, by studying the evolution of temporal dependencies in EEG during motion intention.

The detection of voluntary movement intention, execution and imagery from EEG is typically achieved by widely used neural correlates of movement namely event-related (de)synchronisation (ERD/S) and motor-related cortical potential (MRCP) [44, 26, 65, 53, 91]. ERD and ERS corresponding to attenuation and increase predominantly in μ and β power respectively [26], are commonly used for detecting movement intention and imagery [65]. Based on this, most features for detecting movement related tasks [60] are extracted from the spectral domain of EEG. Power spectral density (PSD) and time-frequency analysis being by far the most common methods of evaluating ERD [53, 91, 72]. Even though ERD/S can detect motor imagery with high accuracy [67, 68], these spectral features have to be tuned to individuals as most responsive frequency bands are different for each individual. Often, different spatial filters or other optimization techniques are used to enhance the spectral features [68, 199, 159, 184]. MRCP is a slow negative cortical potential observed in low frequencies [53] from approximately 2 s prior to human voluntary movement [51]. MRCP has a very small amplitude ($8\text{-}10\mu V$) compared to spontaneous EEG activity ($100\mu V$) [53] which makes its detection difficult. A common method of detecting MRCP is to average several EEG trials of voluntary movements [53]. ERD/S and MRCP have been used to distinguish between different types of movements involving different joints [200, 98, 102]. It is also possible to determine the end of movement planning, execution and imagery from the increase in β power also known as β rebound [99] and increase in γ power [72].

In addition to movement execution information, movement prediction is important for hybrid rehabilitation systems combining BCI and robotic assistance as it can compensate for the delay between the detection of the motion intention and the onset of motion assistance. Enabling the coordination of motion assistance with a subject's motion intention can generate the ownership of the movement [201, 88] and improve the efficiency of a BCI-driven robotic rehabilitation systems [202]. ERD and MRCP can also be used for voluntary movement prediction before its actual onset. ERD power spectral density features in the μ and β bands were shown to predict movement on average 0.62±0.25 s before actual movement onset [53], while a narrow frequency band of 0.01-1 Hz gave a good movement prediction from -0.5 s using MRCPs for reaching movement [112, 100]. For a unilateral hand movement, ERD occurs 2 s before movement onset in the contralateral hand area of the sensorimotor region and becomes bilaterally symmetrical just before movement execution. ERD is followed by contralateral ERS within 1 s of movement offset. ERD is also observed contralaterally during motor imagery [26]. In contrast, early component of MRCP starts 2 s before movement onset, bilaterally distributed around midline-central region. The late MRCP component

has larger amplitude and is observed 400ms before movement onset over the contralateral central region [51]. Combination of ERD and MRCP features provides complementary neurophysiological information about movement and improve the detection rate of movement intention [71, 71].

Various signal processing and statistical analysis techniques are increasingly being explored to improve the movement intention detection accuracy and decrease the latency between movement intention and its detection [114, 157, 203], however, the underlying principles of ERD/S and MRCP remain the same. The ERD and MRCP can detect movement intention only in specific narrow frequency bands. ERD also requires tuning of the most discriminative frequency band for each participant. Also, ERD and MRCP, though successfully employed to detect movement intention, do not completely describe all aspects of motor command generation, dynamical properties of brain activities, and changes in temporal dependencies. These characteristics of brain activities focus only on a selected frequency band. Thus, we explored a complementary process that will enable us to detect motion intention from a wider frequency band and which can be used in conjunction to ERD and MRCP to obtain a deeper insight into EEG dynamics during voluntary movement.

The aim of this paper is to identify novel neural correlates of movement based on changes in the dynamics of EEG by characterising its temporal dependencies, such that they provide movement intention related information that is complementary to ERD and MRCP. Hayashi et al. [204] identified a specific change in EEG autocorrelation during movement, which could be used as a marker of movement intention, however there were no further studies investigating the reorganisation of the autocorrelation structure during movement. Extending this line of investigation, we computed the autocorrelation function of EEG signals recorded during asynchronous finger tapping to evaluate the effect of the voluntary movement on EEG dynamics. The changes in relaxation time of autocorrelation were observed during movement intention, and were then used as a novel time domain characteristic to classify movement intention from single trials. In this paper, we detected the motion intention before actual movement onset from the relaxation time of autocorrelation, and found that the autocorrelation relaxation time increases before and during voluntary movement, i.e. autocorrelation decays slowly during this period compared to the resting state. Thus, we obtained a neural correlate of motion intention based on characterisation of the temporal dependencies in EEG.

The paper is organised as follows: in the Methods section, we provide details of EEG experimental paradigm, EEG pre-processing, procedure for characterising motion intention from single trials using ERD and the novel autocorrelation relaxation time and classification of movement intention. In the Results section, we present the relaxation times of EEG

autocorrelation in four frequency bands and compare them with ERD in the corresponding bands. We compared their classification sensitivities, timing of movement intention detection and spatial locations of the most responsive channel. This is followed by the Discussion section and the Conclusion.

3.2 Methods

3.2.1 Ethics Statement

Fourteen healthy participants (8 female, age 26 ± 4 years, 12 right handed) with no prior experience in EEG experiments and BCIs, normal or corrected to normal vision, no motor or communication impairing conditions and not receiving any medication for such conditions participated in the study. Ethical approval for EEG experiment was obtained from the ethics committee of the School of Systems Engineering, University of Reading, UK. Participants were provided with an information sheet detailing the purpose of the study, procedure of the experiment and the nature of the data collected. Informed written consent was obtained from all the participants before beginning the experiment.

3.2.2 Experimental paradigm

A simple self-paced, asynchronous index finger tapping task was chosen to study the brain activities related to the motor intention.

In order to record the onset of a finger tap, a bespoke microcontroller based tapping device was developed (Fig 3.1A) using an 8-bit Microchip PICDEM2 Plus demo board (Microchip Technology Inc., Arizona, USA). The tapping circuit consists of a finger cap covered with a conductive metal strip and a conductive plate placed on the tapping board and was connected to the pins on the I/O port of the Microchip board for peripheral devices. The participant was required to place the index fingers of both their hands in the corresponding finger caps of the tapping device as shown in Fig 3.1B, and perform the finger tap when instructed. The microcontroller sent a continuous 5 V output to the tapper circuit and the analogue input from the right and left tapper was received on the input pins. This analogue input of 0-5 V was converted to a digital signal in the range of 0 to 1023 by using the Microchip board's inbuilt 10-bit analogue-to-digital converter. Thresholding was then applied to convert this signal into a binary stream (1 when there was no tap, and 0 when there was a finger tap) for each hand, which was then sent to the computer via a universal asynchronous receiver-transmitter (UART) to a serial port. This binary stream captured the onset and duration of each finger tap.

These additional two channels of binary tapping signals, one for each hand were recorded at a sampling frequency of 1000 Hz.
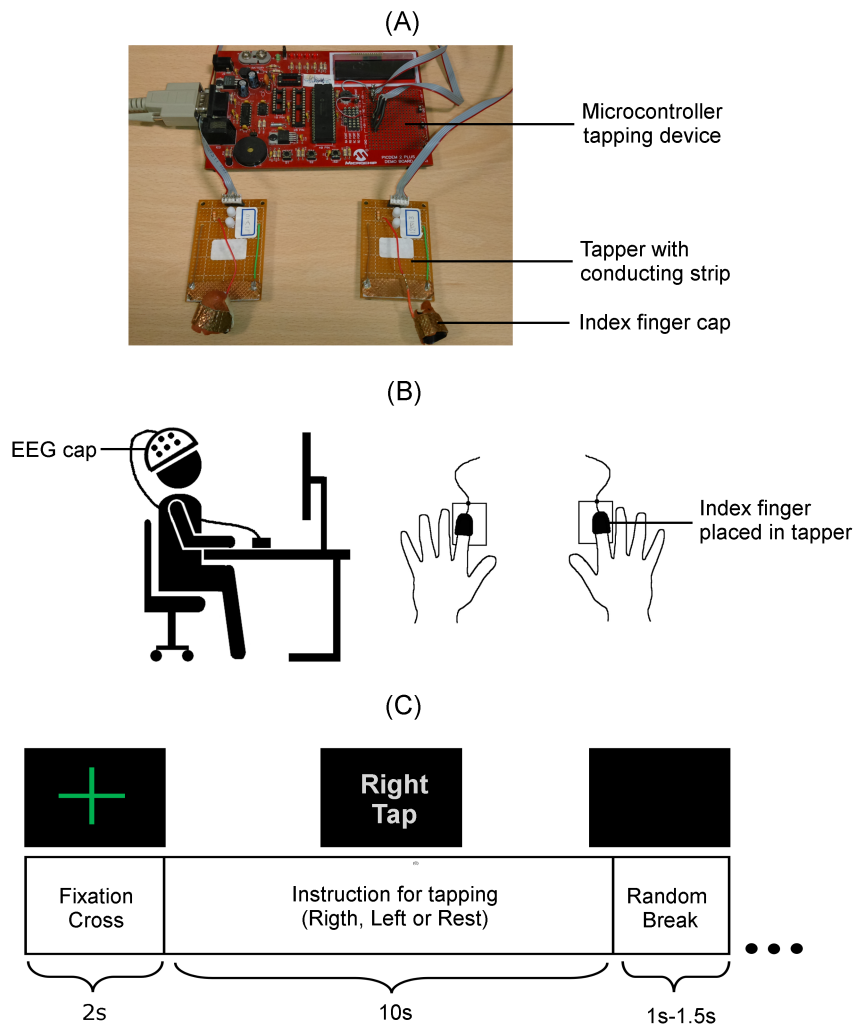
Fig. 3.1 **Experimental setup, devices and EEG trial structure.** (A) Microcontroller tapping device to record right and left index finger taps, which were co-registered with EEG to mark the tap onset. (B) Illustration of EEG experimental setup and index fingers placed in the tapping device. (C) Structure of single EEG trial.

In addition to the motor execution, motor imagery EEG trials were also recorded to assess whether the novel techniques for identifying motor intention could also detect self-paced motor imagery. Motor imagery trials for single right and left finger tap imagery were recorded using the same protocol as the actual finger tap trials. Self-paced single motor imagery is often very difficult to detect and hence it would be interesting to explore the possibility of their detection with the novel method developed in this study.

The experimental paradigm was developed in MATLAB Simulink R2014a (The Math-Works, Inc., Natick, Massachusetts, United States) using the BioSig toolbox [205]. The structure of a single trial is illustrated in Fig 3.1C. The experimental procedure was as follows:

1. Participants placed their index fingers in the tapping device as shown in Fig 3.1B.

2. A fixation cross was displayed for 2 s on the screen.

3. This was followed by an instruction displayed in random order for a single right or left finger tap, imagined single right or left finger tap or the resting state.

4. Participants were given a 10s window to perform the instructed task at a random time of their choice and were instructed to avoid tapping immediately after the display of the instruction to avoid cue effects. During the resting state, participants stayed still without thinking of anything in particular.

5. Each trial was followed by a random break of 1-1.5 s.

EEG was recorded using a Deymed TruScan 32 EEG amplifier (Deymed Diagnostic s.r.o., Hronov, Czech Republic) and EASYCAP EEG cap with Ag/AgCl ring electrolyte gel based electrodes (EASYCAP GmbH, Herrsching, Germany) with 1.5 mm touchproof safety sockets. Nineteen EEG channels according to the international 10-20 system were recorded using a referential montage with reference on FCz and ground on AFz. The cap was placed on the participant's head such that Cz was located exactly on the central point between nasion and inion and right and left ear which was measured with a tape. The Deymed digital amplifier is battery operated to reduce artefacts and outside noise and has an inbuilt impedance monitoring system. The impedances of all the electrodes were kept below 7 $k\Omega$. EEG was sampled at 1024 Hz to obtain sufficiently high temporal resolution. No filtering was done on EEG during recording. 40 trials per condition were recorded for each participant to obtain sufficient statistical power while minimising experiment time to avoid fatigue in the participants.

Sample size of 40 trials per class was determined by performing power analysis. We estimated the sample size to obtain significance of 5% ($\alpha = 0.05$) and 95% power. We used the power analysis method of comparison of means of two classes for two tailed hypothesis testing [206] using the equation (3.1).

$$n = \frac{2 \times \sigma^2 \times (Z_{1-\alpha/2} + Z_{1-\beta})^2}{\mu_d^2} \tag{3.1}$$

50

Exploration of Neural Correlates of Movement Intention based on Characterisation of
Temporal Dependencies in Electroencephalography

where n is the sample size, σ is the pooled standard deviation of the two groups, μ_d is
the mean difference between the samples of the two groups, $Z_{1-\alpha/2}$ is the normal standard
deviation for significance α and $Z_{1-\beta}$ is the normal standard deviation for statistical power
$1-\beta$. In our case $\alpha = 0.05$ (5% significance) which makes $Z_{1-\alpha/2} = 1.96$ and $1-\beta =$
0.95 (95% power) which makes $Z_{1-\beta} = 1.64$. Standard deviation of the novel features to
be investigated in this study and the mean difference between resting state and movement
intention is unknown. However, we assume a generous pooled standard deviation $\sigma =$
40% which is much larger than the previous studies on traditional features of ERD and
MRCP [92, 112, 53] and detect much smaller difference between rest and movement intention
of $\mu_d = 30\%$ than the previous studies. Plugging in the above values in equation (3.1), we
obtained sample size of $n = 36.7$. Rounding it up to 40 EEG trials per class, we can obtain
95% statistical power for identifying movement intention from the resting state. Also, as a
rule of thumb, the number of samples per class should be at least 10 times the number of
features for training a classifier [207] which means with 40 EEG trials, we can have up to 4
features for successfully training a classifier.

EEG and finger tapping signals were recorded and co-registered together with the stimulus
markers on the computer using the tools for brain-computer interaction (TOBI) SignalServer
2.0 which is a program for signal acquisition, co-registration and transmission that uses a
standardised TOBI interface A protocol [208]. This co-registered signal was saved using the
BioSig toolbox. This ensured that onset of the movement was accurately marked on EEG
time series. EEG data is available from http://dx.doi.org/10.17864/1947.117 [209].

3.2.3 Pre-processing and artefact removal

The offline EEG analysis was performed to identify the neural correlates of voluntary
movement intention. All EEG analysis and statistical analysis was done in MATLAB. EEG
signals were filtered using a fourth order zero-phase non-causal Butterworth filter to avoid
phase distortions in the filtered signal. The DC offset was removed by high-pass filtering
with a 0.5Hz cut-off frequency. A notch filter at 50 Hz was used to remove the power line
noise. High frequency noise was eliminated by low-pass filtering with a cut-off frequency at
60 Hz. Baseline noise caused by the drift in EEG was removed by subtracting the mean of
the signal, making it a zero mean, before artefacts removal and extraction of individual trials.

EEG was visually inspected for large spikes and irregular artefacts [210], neither of
which were observed in the data. Following this, artefacts removal was performed using inde-
pendent component analysis (ICA) [149]. The independent components with artefacts were
identified and eliminated manually using EEGLAB toolbox for MATLAB [211], which uses
an automated version of infomax ICA algorithm [212]. The reconstructed uncontaminated

signal was visually inspected for any residual large artefacts and any undesirable trials were eliminated. EEGLAB was only used for artefacts removal using ICA.

All channels were re-referenced using a longitudinal bipolar montage, which enhances the signal by eliminating similarities in adjacent channels leading to magnification of the features associated with that region and suppression of the common noise between the channels [213]. Bipolar montage is a simple and fast spatial filter [213] commonly used for BCIs to reduce the number of channels [214–216], improve the signal-to-noise ratio by reducing the background noise in EEG and significantly improve the classification results [217, 218]. Nine EEG channels surrounding the motor cortex (F3, Fz, F4, C3, Cz, C4, P3, Pz and P4) were used to obtain six bipolar channels, viz. F3-C3, Fz-Cz, F4-C4, C3-P3, Cz-Pz and C4-P4. Time locked trials of length 6 s were obtained by extracting 3s before and 3s after the onset of the finger tap. These trials were divided into 1 s sliding windows from time (t-1 s) to t which were shifted by 100 ms for further EEG analysis. Thus, each feature at time t was obtained on a window from (t-1 s) to t. The baseline was removed from each trial to make it a zero mean.

3.2.4   Characterising grand average and single trial ERD

To confirm that the recorded EEG data had captured the movement related information during finger tapping, the grand average ERD was estimated using event-related spectral perturbation [219] and the band power method [26].

Spectral perturbation of EEG was obtained via a short-time Fourier transform along the length of a 6 s trial. To observe ERD, the average spectrogram of the resting state trials was subtracted from the average spectrogram of the movement trials. Data from all participants were visually inspected for the presence of ERD. The grand average spectrogram was obtained by averaging results across all the participants.

ERD was also identified using the band power method [26] by, firstly, band-pass filtering in a selected frequency band, and subsequently squaring and averaging the trials. The mean of corresponding samples in all trials was subtracted from each sample. For further smoothing and minimising the effects of spurious peaks or outliers on the band power, the mean of the upper and lower envelopes of data was used to compute ERD. This smoothing step was partly inspired by the techniques described in Clochon et al. and Bastiaansen et al. [220, 221] where they use amplitude envelope of EEG to get the band power. The mean of 1.5 s to 2 s prior to movement onset was used as a baseline (R). This baseline was then subtracted from the mean of a 1 s window (A) shifted by 100ms over the trial. ERD percentage was obtained for each window (i) using equation (3.2). The grand average of ERD for six channels was obtained by averaging the corresponding ERDs of all the participants.

$$ERD(i) = \left(\frac{A(i) - R}{R} \right) \times 100 \qquad (3.2)$$

Single trial ERD was obtained as above, but on individual trials. The upper envelope of the squared EEG amplitude of each trial was used to get the baseline (R) and mean of each window (A). equation (3.2) was used to get percent ERD for each trial.

3.2.5 Characterising autocorrelation relaxation time of single trial EEG by fitting exponential curve

The autocorrelation function captures the changing EEG dynamics and shows how the temporal dependencies change over time during voluntary movement [204, 222]. The decay trend of the autocorrelation provides an insight into how the signal is related to its past. Hence, the autocorrelation decay of EEG was studied during finger tapping to investigate the influence of motion intention on temporal dependencies by estimating the relaxation time of autocorrelation.

The autocorrelation of each trial was obtained to study the time development of the relaxation process of the brain activity before, during and after the finger tapping movement. The decay trend of autocorrelation was used as a measure of reorganisation of brain dynamics. Let $s = s(0), s(1), s(2), ..., s(N)$ be a discrete EEG signal with N samples. Then, the autocorrelation of s at a lag Δ is defined by equation (3.3), where $\bar{s}$ represents the mean of signal s.

$$R(\Delta) = \frac{\sum\limits_{t=0}^{N-\Delta} (s(t) - \bar{s})(s(t+\Delta) - \bar{s})}{\sum\limits_{t=0}^{N} (s(t) - \bar{s})^2} \qquad (3.3)$$

At $\Delta = 0$, the signal is perfectly correlated $(R(0) = 1)$. At an infinite time lag, the signal components are completely uncorrelated $(R(\infty) = 0)$. How the signal becomes uncorrelated over time can be described by the trend of autocorrelation decay. We assumed that the relaxation process of the brain signals can be understood in terms of the models using the damped mass-spring system, the dynamics of which can be thought of in terms of a relaxation process and an oscillatory process and can be represented by the general form $Ae^{-\frac{t}{\tau}}cos(\omega t - \phi)$. Hence, we have obtained the first order approximation of the autocorrelation relaxation

process by assuming an exponential decay model for the upper envelope of the autocorrelation function. By using this approximation, the autocorrelation decay is asymptotically equal to the exponential decay represented by equation (3.4) over the length of a signal with N samples, where $C > 0$. Even if the autocorrelation decay is not exactly exponential, but follows a different trend, the exponential decay model may still quantify how fast or slow the autocorrelation decays.

$$R(\Delta) \sim Ce^{-\frac{t}{\tau}} \tag{3.4}$$

Normalised autocorrelation was performed on a single trial basis using equation (3.3). Each 6 s EEG trial was divided into 1 s windows shifted by 100ms. EEG processing steps are shown in Fig 3.2.

Based on the approximation of the autocorrelation decay using the exponential function, the relaxation process of autocorrelation was obtained by fitting the exponential curve (equation (3.4)) to the autocorrelation. The decay constant τ corresponds to the relaxation time and is used as a feature for movement intention detection (see Fig 3.2B). The exponential curve given by equation (3.4) was fitted to the local maxima of half of the total positive lags of the autocorrelation of each 1 s EEG windows. Here, $C = 1$, because the autocorrelation was normalized. How fast or slow the autocorrelation decays with respect to the movement intention was studied by observing the τ values over the period of the trial as shown in Fig 3.2C. Time progression of τ values during right and left finger tapping trials were compared with corresponding τ values of the resting state trials and were used for classification of movement (see Fig 3.2D).

3.2.6 Comparison of autocorrelation relaxation time with ERD in multiple frequency bands

We have represented movement intention with two features viz. autocorrelation relaxation time and ERD. To examine if the changes in the relaxation time of autocorrelation during movement were more prominent in specific frequency bands, single trial autocorrelation analysis was performed independently on three non-overlapping frequency bands: 0.5-8 Hz (lower frequencies), 8-13 Hz (middle frequencies, μ band), 13-30 Hz (higher frequencies), along with the wide frequency band of 0.5-30 Hz covering the entire spectrum.

These broader frequency bands were chosen to analyse the changes occurring in the wider frequencies during movement, and because the most responsive frequency band for ERD differs from individual to individual [26, 223]. Wider frequency bands contain all the

information from the individual specific responsive frequency bands while mitigating the inter-participant variability and increase robustness of the results. This gave a fair mode of comparison of the two distinct features representing movement intention. The new single trial autocorrelation relaxation time feature was compared with the corresponding single trial ERD feature obtained in the four frequency bands described above.

3.2.6.1   Classification of movement intention

Classification was done using a binary linear discriminant analysis (LDA) classifier for autocorrelation relaxation time and ERD features for right tap vs. resting state and left tap vs. resting state independently for each participant. LDA analysis was done on each of the six bipolar channels independently. A separate LDA classifier was trained for each sliding window with all the corresponding features from windows in all the trials. Thus, for each LDA, there were 40 data samples with a single feature for each class. Sensitivity, also known as the true positive rate, was computed by dividing the number of trials correctly classified as tapping trials by the total number of tapping trials. A 10x10 fold cross-validation scheme was used to obtain the classification sensitivities at the time points given by the 1 s sliding windows with 90% of the data from corresponding windows from all the trials used as training data and 10% as testing data. The sensitivities of 6 s trials for each of the six channels were plotted for all the participants as illustrated in Fig 3.2D and 3.2G. The 95% confidence level for binary classification (tap or rest) was obtained from the binomial distribution with n = number of EEG trials available and $p = 0.05$.

3.2.7   Autocorrelation and ERD analysis of the imaginary single finger tap

We performed the autocorrelation decay analysis and ERD analysis on the motor imagery EEG trials for right and left hannd finger tap using the same procedure as the finger tap execution mentioned in the previous sections. Participants performed motor imagery of a single finger tap any a random time voluntarily within the 10 s window. This ensured that the motor imagery was asynchronous and self-paced. We wanted to determine whether self-paced motor imagery can be detected using single trial autocorrelation analysis on the sliding windows of EEG. We performed autocorrelation analysis on 0.5-30 Hz frequency band. We also performed the ERD analysis on the single trial basis on 8-13 Hz frequency band. We attempted to extract single distinct peak from the autocorrelation decay features of the single motor imagery similar to the example shown in Fig 3.2C. In the case of motor

imagery, there was no ground truth data representing motor imagery analogous to the actual finger tap movement captured by the microcontroller device.

3.3   Results

In this section, firstly, we report the movement related changes occurring in the ERD and relaxation time, and then compare both these features in terms of their classification sensitivity, timing of movement intention identification and spacial location of the most responsive feature. From these three measures, we have observed that relaxation time indeed provides information about movement intention that is distinct from ERD.

3.3.1   Grand average ERD

ERD was used to validate the recorded EEG data for presence of movement related features.

3.3.1.1   Event-related spectral perturbation

ERD was observed from the grand average EEG spectrograms over all participants corresponding to left tap and right tap as shown in Fig 3.3A and B. A relative decrease in μ power is observed around 10 Hz in all six channels.

3.3.1.2   Time progression of ERD

Time progression of the grand average ERD in the μ band of all the participants is plotted in Fig 3.3C. The plots for right (red) and left (blue) finger tapping drop below zero indicating the occurrence of ERD around motion onset (0s). The black plot represents resting state trials where no ERD is observed. ERD is seen more prominently in channels F3-C3, Fz-Cz and F4-C4. Channels C3-P3, Cz-Pz and C4-P4 show ERS after the onset of the movement.

Thus, ERD was present in EEG, validating EEG for motion intention.

3.3.2   Change in autocorrelation relaxation time related to motion intention

It was observed that there was a change in the decay of autocorrelation around the movement onset. The relaxation time τ increased starting prior to the onset of movement and persisted during the movement duration. This increase in τ around the onset of movement was observed in most single trials as shown in the example in Fig 3.2C. The τ values for resting state trials

did not show any such increase. The grand average τ for all the participants for right tap (red), left tap (blue) and resting state (black) for two channels is shown in Fig 3.4. Since most reactive channels were different in different participants, the aggregate build-up of τ was observed clearly only in C3-P3 and C4-P4 in the grand average. Relaxation time τ is large when the exponential curve decays slowly and small when the exponential curve decays fast. Thus, build up of τ prior to the onset of movement facilitates the prediction of movement before its actual occurrence.

The quality of fit of the exponential curve was assessed using the R^2 value of the fit. The average R^2 values for 0.5-8 Hz, 8-13 Hz, 13-30 Hz and 0.5-30 Hz were 0.89, 0.90 0.82 and 0.87 respectively, while the average range for R^2 values for all the frequency bands was 0.3 to 0.99. There was no difference in the R^2 values for exponential fitting in tap vs. no tap conditions. The τ features around the onset of the movement showed statistically significant differences between tap vs. rest conditions ($p < 0.05$, two sample t-test) for all the participants. Relaxation time of autocorrelation is hence, a robust way of characterising the changing dynamics of the brain activity during motion intention on a single trial basis.

3.3.3 Comparison of autocorrelation relaxation time and ERD in different frequency bands

The three measures obtained from LDA classifier viz. classification sensitivities, estimated timings of motion intention detection and spatial locations of most responsive bipolar channels were compared. The sensitivities were obtained from 1 s windows extracted from time (t-1 s) to t shifted by 100 ms.

3.3.3.1 Classification sensitivities of single trial autocorrelation relaxation time and ERD

The maximum sensitivities for all the participants for right/left tap vs. rest were statistically significant ($p < 0.05$) for autocorrelation relaxation time. Classification sensitivities for all the participants in different frequency bands varied with a small standard deviation (SD). The best results were obtained in the wide frequency band of 0.5-30 Hz for autocorrelation analysis. A peak sensitivity of 96.75% was achieved for participant number 6. The comparison of peak classification sensitivities for autocorrelation features for all the participants in all the frequency bands with the corresponding peak ERD classification sensitivities is shown in Fig 3.5.

Fig 3.6 shows the box plots for the classification results. It is observed from Fig 3.5 and Fig 3.6 that the sensitivities of autocorrelation and ERD are comparable and close to

each other with some participants showing higher sensitivities for autocorrelation than ERD in different frequency bands. Mean sensitivities in all the frequency bands are statistically significant ($p < 0.05$) for autocorrelation relaxation time and ERD features, although some participants do not show significant sensitivities for ERD features. Best autocorrelation sensitivities were obtained for the wide frequency band of 0.5-30Hz. Also, the SD of autocorrelation features is smaller than ERD in the 0.5-8Hz, 8-13 Hz and 13-30 Hz bands. These results show that the ERD performance varied in different frequency bands while the performance of autocorrelation features was consistent over different frequency bands.

Statistical tests on sensitivities of different frequency bands for all participants were performed using the non-parametric repeated measures Wilcoxon signed-rank test. Correction for six multiple comparisons between four frequency bands was done using the Holm-Bonferroni method [224] at a significance level of 0.05. The Holm-Bonferroni method was chosen because it is uniformly more powerful and less conservative than Bonferroni correction for multiple comparisons. Sensitivities of autocorrelation features were not significantly different in the four frequency bands. This shows that classification sensitivities for autocorrelation are consistent and independent of the frequency bands. In contrast, ERD sensitivities of different frequency bands were significantly different from the 8-13 Hz (μ) band ($p < 0.05$). ERD showed higher sensitivities in the μ band. Significant differences for ERD in different bands are shown in Fig 3.6B. We also performed Wilcoxon signed-rank test to compare the bands with best classification sensitivities for autocorrelation decay and ERD. We compared 0.5-30 Hz broadband autocorrelation decay sensitivities with the 8-13 Hz (μ) band ERD sensitivities. The 8-13 Hz band ERD sensitivities were significantly higher than 0.5-30 Hz broadband autocorrelation decay ($p < 0.05$).

Thus, autocorrelation relaxation time proved to be a robust frequency independent feature associated with motion intention. The classification sensitivities for all the four bands together for autocorrelation and ERD features were significantly different ($p < 10^{-7}$, Wilcoxon signed rank test). This demonstrates that autocorrelation relaxation time and ERD represent different information about movement intention.

3.3.3.2 Estimating timing of motion intention detection from autocorrelation relaxation time and ERD

The sensitivities of the relaxation time feature crossed the significance threshold (obtained using binomial distribution, $p < 0.05$) around the onset of the motion. In most of the participants, the sensitivities crossed the threshold before movement onset and then dropped back after the completion of the movement. This suggested that statistically significant classification was possible even before the actual onset of the movement for some trials. This

opened up the possibility for movement prediction using autocorrelation relaxation time. The time at which the classification sensitivity crossed the threshold was noted for each participant.

Fig 3.7 shows the comparison bar graphs for timings of the statistical crossing of the classification sensitivity for single trial autocorrelation and ERD features. It is observed from Fig 3.7 that prediction of movement is possible for most of the participants using autocorrelation analysis in all the frequency bands. In 0.5-8 Hz and 0.5-30 Hz bands for right and left hand tapping, many participants show movement intention detection as early as 1.5 s to 0.5 s prior to the onset of movement using autocorrelation relaxation time. ERD analysis shows earlier detection of movement intention in the 8-13 Hz band as compared to the other bands as expected, whereas timing of movement intention detection was not frequency band dependent in autocorrelation analysis.

We also performed Wilcoxon signed-rank test to compare the timings of the bands with best classification sensitivities for autocorrelation decay and ERD. We compared the timing of movement intention detection of 0.5-30 Hz broadband autocorrelation with the timing of 8-13 Hz (μ) band ERD. The timings of 8-13 Hz were significantly earlier than 0.5-30 Hz broadband autocorrelation decay ($p < 0.05$).

3.3.3.3 Spatial locations of most responsive bipolar channels for autocorrelation relaxation time and ERD

The bipolar channel that showed maximum classification sensitivity for each participant in each frequency band for autocorrelation relaxation and ERD feature was selected manually. Fig 3.8 shows the spatial locations of the most responsive channels for the classification of autocorrelation and ERD features. The sub-figures in Fig 3.8 depict the most responsive channel in different frequency bands. The width of a particular channel is directly proportional to the number of participants having that channel as the most responsive channel for classification. This is quantified by showing the number of participants having that channel as the most responsive channel beside the channel location.

The spatial locations of autocorrelation and ERD were different. Autocorrelation and ERD features have different most responsive channels suggesting that the spatial origin of the information about movement obtained from autocorrelation is different from the information obtained from ERD. The most responsive channels for ERD were obtained on the contralateral side, especially in the μ band (8-13 Hz) and β band (13-30 Hz). While typical ERD shows lateralisation in most cases [225], no lateralisation was observed in autocorrelation features. The most responsive channels for autocorrelation decay features differed from participant to participant. Autocorrelation did not show any distinct spatial pattern across different

frequency bands, however, for a given frequency band, most participants had same most discriminative channel for both right and left hand movement.

Thus, our study indicates that 1) autocorrelation relaxation time increases during movement intention; 2) the classification sensitivities, timings of motion intention detection and spatial locations of most responsive channels are different for the autocorrelation feature and ERD; 3) changes in autocorrelation relaxation time are independent of frequency band; 4) autocorrelation provides different and complementary movement intention related information to ERD.

3.3.4 Change in autocorrelation relaxation time and ERD in imaginary finger tap

The autocorrelation analysis on the motor imagery trials did not show any significant change in the autocorrelation decay throughout the trials. Unlike the movement execution trials, there was no build-up of autocorrelation decay. Hence, the self-paced imaginary single finger tap could not be detected using the novel feature of autocorrelation relaxation time. The right and left single motor imagery trials were indistinguishable from the resting state trials.

The ERD analysis on the motor imagery trials also did not show any significant decrease in the mu (8-13 Hz) band power. Thus, no ERD was observed during self-paced single imaginary finger tap and ERD could not be used as a feature to detect single motor imagery. The traditional method of ERD as well as the novel method of autocorrelation analysis failed to detect the self-paced single motor imagery.

3.4 Discussion

The aims of this paper are 1) to investigate reorganisation of the temporal dependencies in EEG in relation to motion intention and hence to put forward a novel neural correlate of voluntary movement preparation; 2) to determine if this new correlate provides complementary information about motion intention to ERD. This was achieved by studying the progression of changes in EEG autocorrelation structure of single trials with asynchronous finger tapping. The change in the decay of autocorrelation as a function of lag indicates changing temporal dependencies in the signal. We assessed the reorganisation of these dependencies using an exponential function. The trend of autocorrelation decay was characterised by relaxation time, τ, which was computed by fitting a decaying exponential curve to the autocorrelation. To confirm that the autocorrelation relaxation time provides complementary information to

ERD, the two single trial features were compared based on their classification sensitivities, timings and spatial locations.

The autocorrelation decayed fast during the resting state and slowly during motion intention and execution which suggests reorganisation of temporal dependencies prior to motion execution. When there is no movement, EEG autocorrelation decayed fast indicating fluctuating recruitment of neural populations over time. Slow decaying autocorrelation may occur when EEG becomes self-similar or periodic, characterised by the presence of temporal dependencies over longer periods. The increase in relaxation time was observed even in single trials as shown in the example in Fig 3.2C and hence, it can be used as yet another feature to detect motion intention. Although the mean R^2 value of exponential decay fit was high, it varied over a wide range of 0.3 to 0.99. Thus, there were still some trials and windows where the exponential decay was not a good fit, and perhaps these could be modelled better with a different decay trend like power-law.

Comparison of autocorrelation with ERD was performed because ERD is a well established phenomenon occurring during voluntary movement. However, ERD is highly frequency dependent and is only defined when a frequency band and a baseline are given [26]. ERD features in the μ band were significantly different from other frequency bands $(p < 0.05)$ which is also commonly reported in the literature [44, 65, 216]. Significant presence of ERD was also observed in the 0.5-8 Hz band which is not usually associated with movement ERD. However, ERD is not specific to movement and desynchronisation has been observed in a number of cognitive activities. Thus, presence of ERD in this frequency band could be due to the combination of factors such as influence of ERP components [74], desynchronisation occurring due to any task or attentional process [226], information encoding and memory [226, 227] or emotional intelligence [228]. Autocorrelation relaxation time on the other hand, was not frequency dependent and all the bands showed similar classification sensitivities which were tested using multiple comparisons with the Wilcoxon signed-rank test, with mean sensitivities in the narrow range of 77.11% to 79.24%, whereas, the mean ERD sensitivities varied over a wider range of 79.92% to 88.27% (see Fig 3.6). Autocorrelation analysis on broad band signal can identify movement intention without compromising the performance, unlike frequency specific ERD. Hence, we can conclude that some processes in the brain are represented by autocorrelation decay but not by ERD which fails to detect small changes in temporal dependencies. The wide band of 0.5-30 Hz showed better overall sensitivities (though not significantly better) indicating that identification of this change in temporal dependencies became easier with a wide frequency range. During motion intention, there might be a global reorganisation of these temporal dependencies in a wider spectrum

of brain activity. Thus, autocorrelation helps in gaining additional understanding of neural processes and opens a new avenue for further investigation of voluntary movement intention.

The autocorrelation relaxation decay can be used independently to detect motion intention with classification sensitivities comparable to the results reported in the literature using traditional MRCP and ERD, for example, 74.5 $\pm$ 13.8% in Ibanez et al. [229], 76% in Lew et al. [112, 100], 75% in Lopez et al. [200], 79$\pm$11% and 68$\pm$10% in Xu et al. [114]. All these methods are based on features extracted from different channels independently and show similar results. To improve these classification accuracies and obtain holistic understanding of the movement generation process, alternative approaches like connectivity analysis between different regions [230] may help in conjunction with the autocorrelation relaxation time, ERD and MRCP.

Autocorrelation analysis is capable of identifying movement intention as early as -1.5 s to -0.5 s in many participants (see Fig 3.7), particularly in the 0.5-8 Hz, 13-30 Hz and 0.5-30 Hz bands which can be used in future work to predict movement. This is comparable to the timings reported by [53] (-0.62 $\pm$ 0.25 s) using μ and β powers and -0.5 s [112, 100] using MRCP. There was no correlation between the motion intention onset time estimates obtained using autocorrelation relaxation and ERD features as seen from the bar graphs in Fig 3.7, which again suggests that both characteristics represent independent processes. This is further corroborated by the prominent spatial locations for the two features which were different in all the cases, with autocorrelation showing no lateralisation or spatial patterns as opposed to ERD, that was predominantly observed contralaterally in the μ and β bands as seen in Fig 3.8. Spatial locations of autocorrelation features were the same for right and left hand movement in many participants for a given frequency band. This may indicate that the change in autocorrelation decay purely characterises a fundamental correlate for voluntary movement intention and might not reflect on the handedness of the movement. Several cortical areas are involved in movement generation making it difficult to identify single specific spatial location [230]. Thus, autocorrelation decay features and ERD features have different spatial origins and represent two different movement related processes.

Even though the autocorrelation decay features are independent of frequency bands, they are not robust across different spatial locations. The spatial responsiveness of these features differ from individual to individual requiring manual selection of the most responsive channel for the movement intention detection. Further investigation is required to understand the spatial localisation of autocorrelation decay features in detail. This will then enable automated selection of characteristic spatial locations of autocorrelation features in the future.

The autocorrelation relaxation time is also complementary to small amplitude, low-frequency MRCP, because MRCPs are only observed clearly in lower frequencies [53], as

opposed to the wide band prevalence of the autocorrelation decay. This was also shown in our previous study detailed in Wairagkar et al. [231]. Thus, changes in relaxation time of autocorrelation represents a movement related process that is different from ERD and MRCP and possibly generated through a different neural mechanism, providing complementary information about movement intention related EEG temporal dynamics. Using autocorrelation in conjunction with ERD and MRCP correlates might lead to improved detection of motion intention. This will also help in assessing the complementarity of these features.

The autocorrelation analysis in our study was done on a single trial basis by characterising movement intention every 100ms from sliding windows of 1 s. The analysis was designed in such a way that it could be easily adapted for implementation in an online BCI for movement intention detection in the future by using any online artefacts removal technique such as [155]. In this study, we have used non-causal zero-phase filters for pre-processing the data, however, these non-causal filters cannot be used in an online BCI implementation. Hence, from this study, we do not know the effects of causal filtering on the autocorrelation-based features.

Our analysis shows that the phenomenon of an increase in the autocorrelation relaxation time is observed during voluntary movement intention, yet further research is necessary to investigate if it occurs only during voluntary movement generation reflecting the motor tasks or whether it can be observed during other tasks as well. The fact that the relaxation time increases prior to the onset of movement as seen from the prediction timings that vary among different participants, suggests that in this case, it is more likely to reflect the change in EEG dynamics during motor-related tasks rather than changes due to a general task. This is also supported by a recent study in Robinson et al. [232] that uses our autocorrelation decay features to discriminate the speed of hand movement characterising yet another aspect of a voluntary movement.

Although the autocorrelation analysis was able to successfully detect movement intention in actual finger tapping trails, it could not detect self-paced motor imagery of a single finger tap. The traditional method of ERD was also unable to detect self-paced single motor imagery. Detection of self-paced motor imagery is inherently difficult. To identify motor imagery using ERD, typically continuous movement or repeated movement is imagined and a feedback proportional to the level of ERD is displayed on the screen to help user improve their motor imagery strategy [67]. It may be the case that single motor imagery of a finger tap is not strong enough to cause a change in EEG dynamics similar to ERD and continuous or repeated motor imagery is required to cause measurable change in the autocorrelation decay. Another reason could be that the participants were not able to produce a proper kinesthetic single imaginary finger tap and there was no provision to check whether they actually performed the imagery. Learning to control ERD with motor imagery requires

training [233] and the current experimental protocol did not have a training session with feedback for the participants. This suggests that the current experimental paradigm is not suitable to study the effect of motor imagery on autocorrelation decay. A neurofeedback BCI paradigm based on repeated motor imagery which is typically used for ERD in the literature [86] might be more suitable. Also, there might be different mechanisms involved in motor imagery and motor intention and that autocorrelation decay only changes during motor intention but not during motor imagery. Hence, further investigation is required to study the changes in the temporal dynamics during motor imagery.

The apparent discrepancy between information about movement preparation, contained in the power spectrum-based ERD and our characterisation of autocorrelation relaxation trend, suggests some form of non-stationarity of the underlying processes. According to the studies reported in Zhigalov et al. and Dimitriadis et al. [135, 147], changes were observed in temporal dependencies in the brain activity in the 3-40 Hz frequency range with the most significant change in the α band during neurofeedback despite no changes in the power spectrum. Thus, they suggested that neuronal circuits were more capable of reorganising the temporal dynamics than the magnitudes of the brain activity. Our results also show similar reorganisation of EEG time series, indicating movement intention related modulation of temporal dependencies independent of changes in the power spectrum. The study in Zhigalov et al. [135] concentrated on long-range dependencies using detrended fluctuation analysis (DFA), a technique proposed for the characterisation of the non-stationary processes. Further studies have also reported long-range dependence in EEG [29, 234, 235]. This suggests an interesting possibility that, the processes we observed during motion preparation may be non-stationary and hence, in future work, it would be interesting to investigate the nature of long-range correlation structure during motion intention using other approaches [123], such as DFA [122].

3.5   Conclusion

In this paper, we have studied the changes in temporal dependencies in EEG related to voluntary movement intention. We have shown that a novel neural correlate of motion intention can be obtained in single trials from the modulations of EEG autocorrelation structure characterised by its relaxation time. Autocorrelation decayed slower during motion intention and execution as compared to a resting state. Thus, EEG became more self-similar during movement intention and execution due to this reorganisation of its temporal dynamics. Movement intention was detected using autocorrelation relaxation time on average 0.51 s

before its actual onset with the mean sensitivity of $78.37 \pm 8.83\%$ in the broad frequency band.

Information obtained from the autocorrelation relaxation time is different from ERD. It captures characteristics of movement intention that are not represented by ERD. The autocorrelation relaxation time is independent of frequency bands and represents a global change in the temporal dynamics of EEG in a wider spectrum. Thus, change in autocorrelation of EEG complements conventional ERD and MRCP processes and can be used in conjunction with the latter for improved movement intention detection in online BCI. This can again help in confirming their complementarity.

In future work, it would be interesting to explore further the impact of motion intention on long range temporal dependencies in EEG. Also, the proposed single trial neural correlate will be tested with online BCI for motion intention detection. It will also be interesting to investigate during which types of tasks does the autocorrelation relaxation time increase or whether it is specific to voluntary movement.
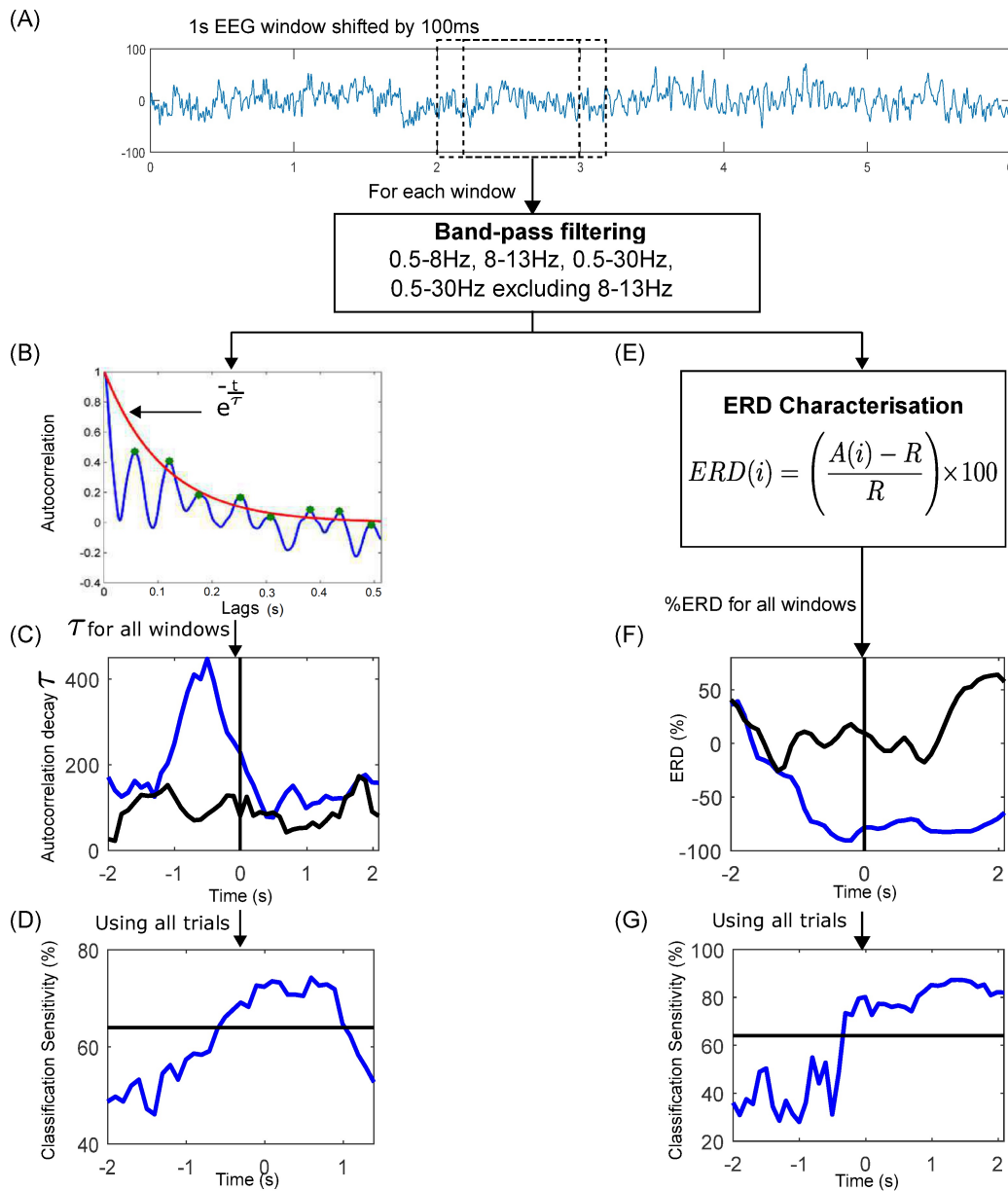
Fig. 3.2 **Autocorrelation relaxation time and ERD feature extraction and classification.** (A) 6 s EEG trial is divided into 1 s windows shifted by 100ms and band-pass filtering is performed for the four different frequency bands. (B) Exponential curve fitting representing the autocorrelation relaxation process on each window. The relaxation time τ was extracted as a feature. (C) Plot of all τ values in a single trial for tap (blue) and resting state (black) (vertical line marks the onset of finger tap at 0s). (D) Classification sensitivities for tap vs. resting state along the length of trial for autocorrelation feature. The horizontal line indicates the classification threshold with statistical significance ($p < 0.05$). (E) Computation of ERD(%) for each window. (F) Plot of all ERD values in a single trial for tap (blue) and resting state (black) (vertical line marks the onset of finger tap at 0s). (G) Classification sensitivities along the length of trial for tap vs. resting state ERD.
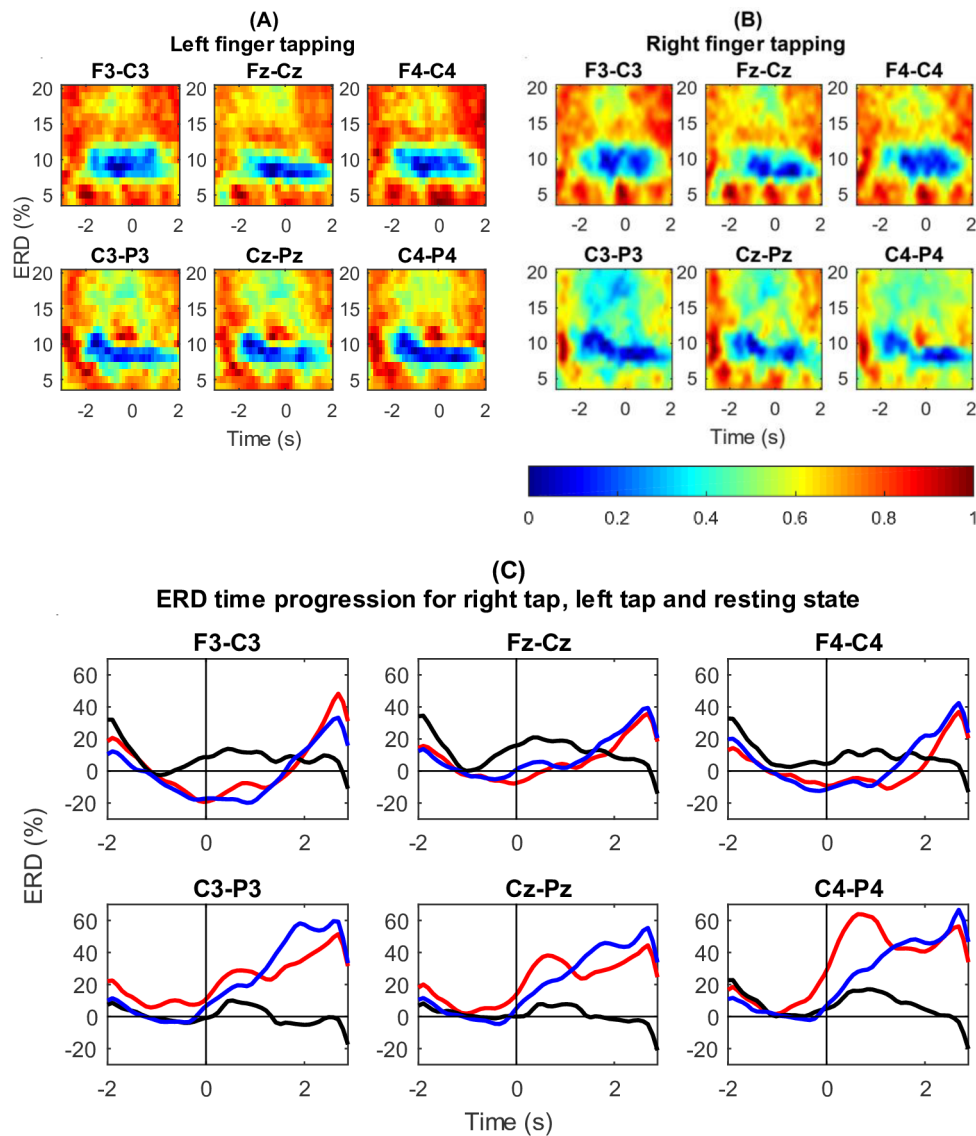
Fig. 3.3 **Grand average spectrograms and ERD time progression for six bipolar channels for all the participants.** (A) Left finger tapping grand average spectrogram in six bipolar channels (the onset of finger tap is at 0s). ERD is clearly seen around 10 Hz. (B) Right finger tapping grand average spectrogram in six bipolar channels (the onset of finger tap is at 0s). ERD is clearly seen around 10 Hz. (C) Grand average ERD time progression for right finger tapping (red), left finger tapping (blue) and resting state (black). Vertical line shows the onset of finger tap at 0s. ERD is seen in right and left hand finger tapping.
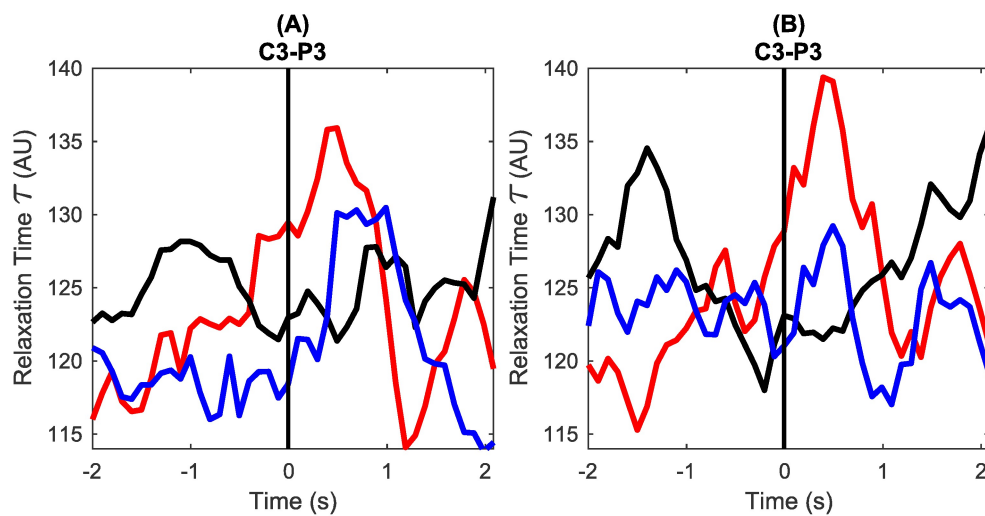
Fig. 3.4 **Grand average autocorrelation relaxation time** (τ) **for right finger tap, left finger tap and resting state for all participants.** (A) Plot of grand average τ in channels C3-P3 for right finger tapping (red), left finger tapping (blue) and resting state (black), in broad frequency band 0.5-30 Hz. The vertical line marks the onset of finger tap at 0s. (B) Plot of grand average τ in channel C4-P4 for right finger tapping (red), left finger tapping (blue) and resting state (black) in 0.5-30 Hz band. Clear increase is seen around the movement in right and left hand tapping conditions.
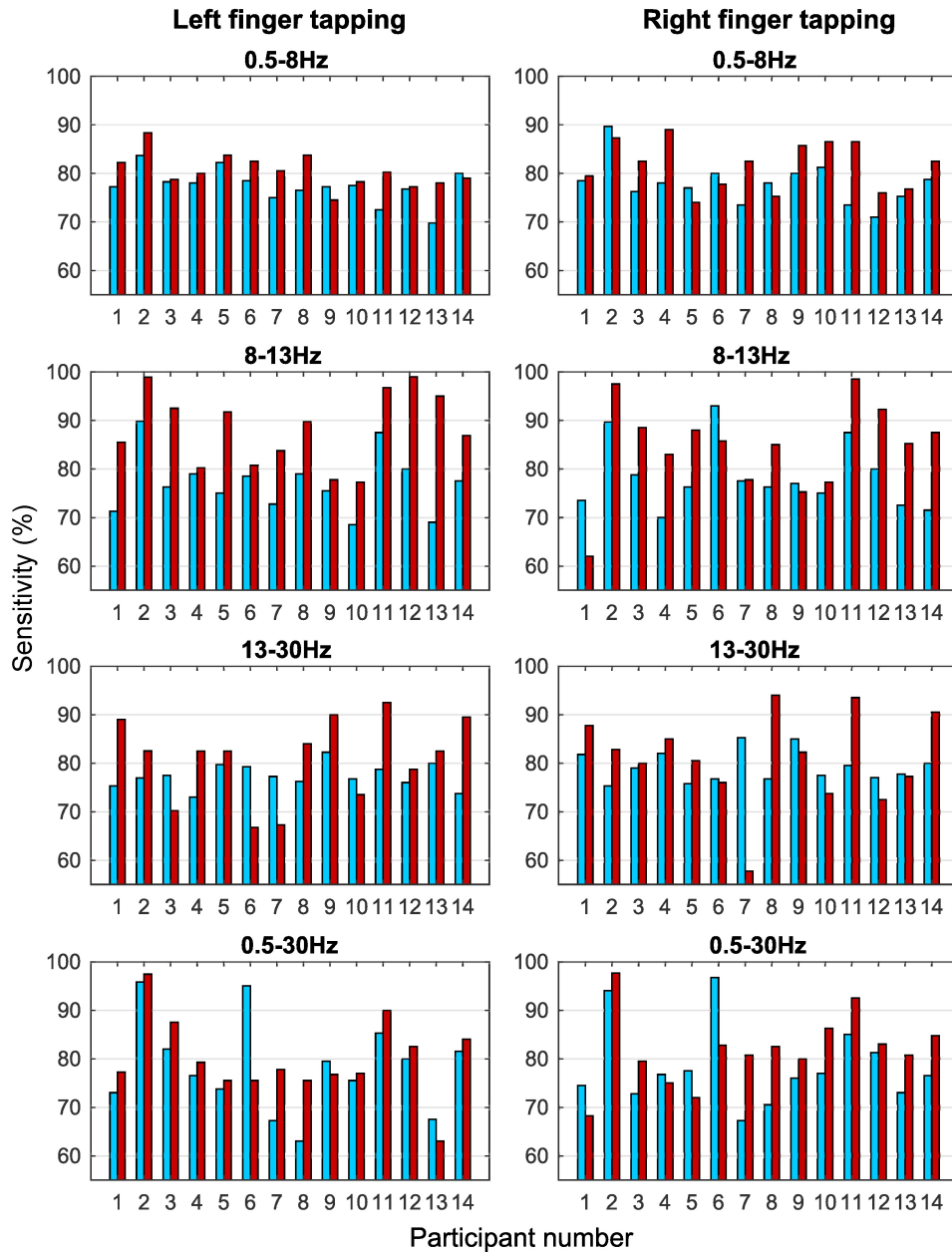
Fig. 3.5 The peak classification sensitivities for autocorrelation relaxation time and ERD. The comparison bar graphs of right tap vs. rest and left tap vs. rest peak classification sensitivities (%) for all the participants in the four different frequency bands for autocorrelation relaxation time (blue) and ERD (red) features. These sensitivities are obtained from one of the six bipolar channels that shows the highest classification sensitivity in each case.
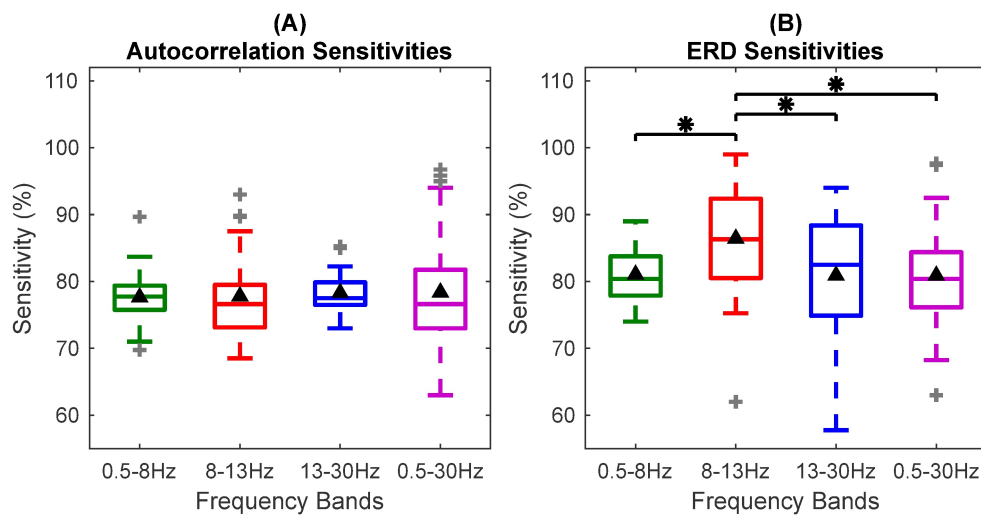
Fig. 3.6 **Box plot for comparison between classification sensitivities of autocorrelation relaxation time and ERD in four frequency bands.** (A) The box plot for classification sensitivities of autocorrelation features in the four different frequency bands. The horizontal line in the box shows the median and black triangle shows the mean sensitivity. No significant difference is observed in sensitivities of different frequency bands. (B) Box plot of classification sensitivities of ERD features in four frequency bands. The sensitivities in the μ band are significantly higher $p < 0.05$ than the sensitivities in the rest of the bands indicated by asterisks. These sensitivities are obtained from one of the six bipolar channels that shows the highest classification sensitivity in each case.
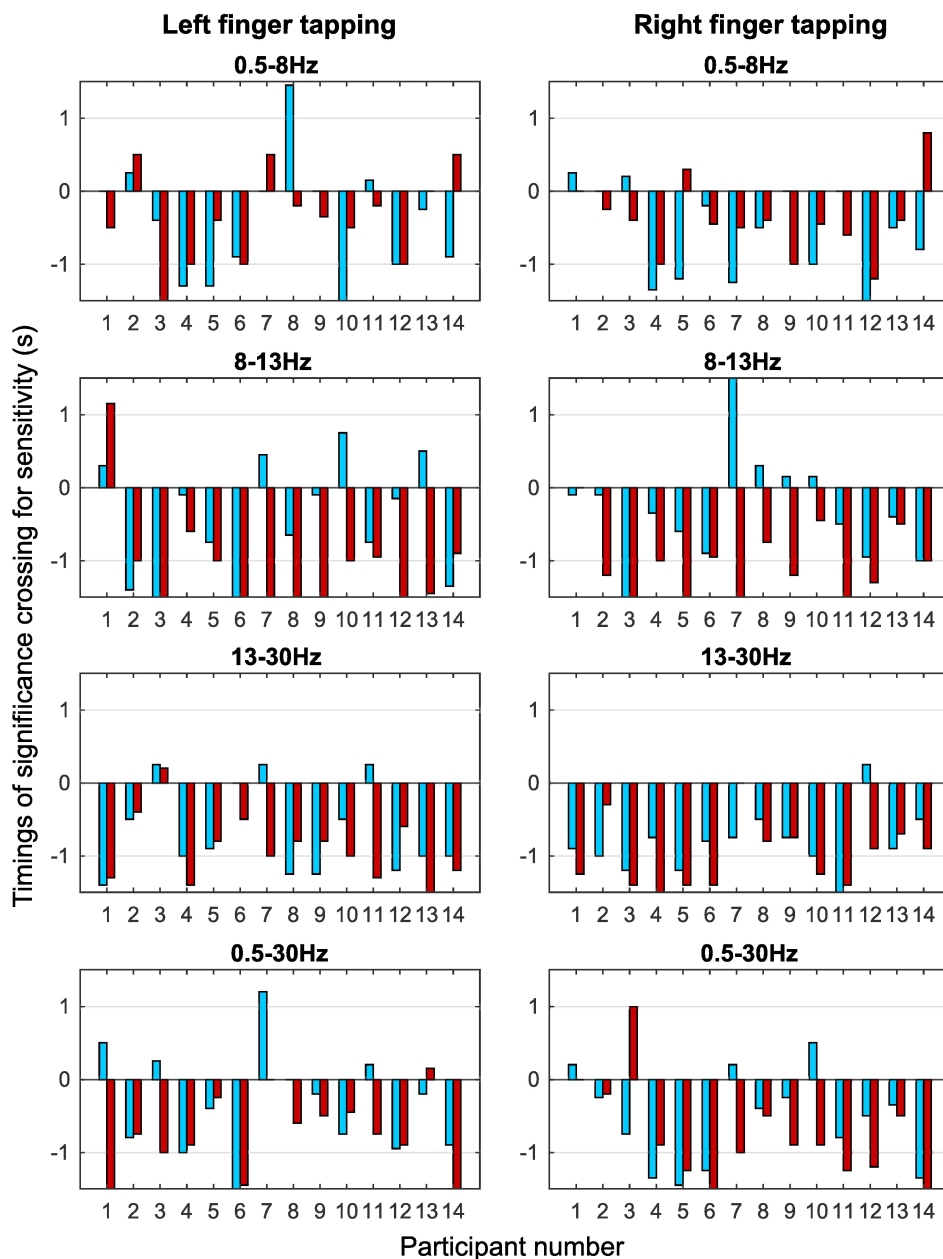
Fig. 3.7 **Timings for movement intention detection for autocorrelation relaxation time and ERD.** The bar graphs show the time at which the classification sensitivity crossed the significance threshold indicating the classification between tap and resting state is above the chance level in four frequency bands for autocorrelation relaxation (blue) and ERD (red) features. Autocorrelation features as well as ERD features show negative values for time of movement intention detection indicting the prediction of movement before its onset. The timings are obtained from one of the six bipolar channels that shows the highest classification sensitivity in each case.
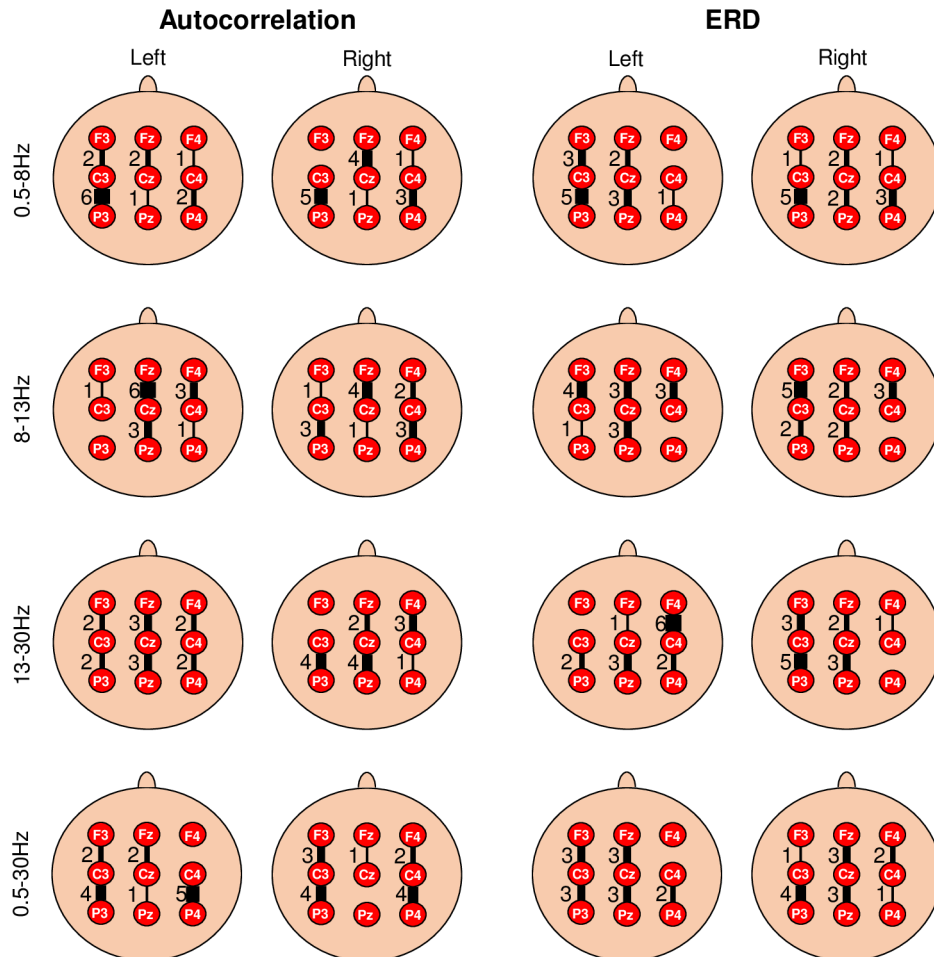
Fig. 3.8 **Spatial locations depicting most responsive channels for autocorrelation relaxation time and ERD.** Spatial distribution of most responsive channel for autocorrelation relaxation time and ERD is shown for right tap and left tap in four different frequency bands. The width of the channel is directly proportional to the number of participants having that channel as most responsive channel showing maximum classification sensitivity. Number of participants having that channel as most responsive channel is also shown beside the channel location.

Chapter 4

Movement Intention Detection from Autocorrelation of EEG for BCI

Maitreyee Wairagkar, Yoshikatsu Hayashi, Slawomir J Nasuto

Abstract

Movement intention detection is important for development of intuitive movement based Brain Computer Interfaces (BCI). Various complex oscillatory processes are involved in producing voluntary movement intention. In this paper, temporal dynamics of electroencephalography (EEG) associated with movement intention and execution were studied using autocorrelation. It was observed that the trend of decay of autocorrelation of EEG changes before and during the voluntary movement. A novel feature for movement intention detection was developed based on relaxation time of autocorrelation obtained by fitting exponential decay curve to the autocorrelation. This new single trial feature was used to classify voluntary finger tapping trials from resting state trials with peak accuracy of 76.7%. The performance of autocorrelation analysis was compared with Motor-Related Cortical Potentials (MRCP).

4.1 Introduction

Brain Computer Interface (BCI) provides a direct mode of interaction with computer and other external devices without utilising any motor pathways. Movement based BCI has a great potential for the use by patients with severe motor disabilities for operating robotic rehabilitation devices and for performing simple tasks intuitively. Thus, it is important to study underlying neural mechanisms of voluntary movement intention. This paper explores the fundamentals of movement intention by studying the temporal dynamics of EEG using novel feature.

Motor Related Cortical Potential (MRCP) and Event Related (De) synchronization (ERD/S) [26] are widely used movement correlates for movement detection from EEG. Although ERD can detect movement reliably [68, 67] , it relies on the most responsive frequency band that vary from individual to individual. It is challenging to compute accurate instantaneous frequency distributions without compromising the temporal resolution and inducing delays. MRCP is a slow negative potential occurring from about 2 s prior to the onset of the human voluntary movement [51], observed in frequencies lower than 1 Hz [53]. Amplitude of MRCP is extremely small (less than 8-10 μV)and hence, an average about 40-50 trials of repeated voluntary movements is used [53]. Single trial analysis is important for practical online BCI implementation. Although single trial variants of ERD [200] and MRCP [91, 114] have been developed, these traditional principles are best suited for analysing averaged EEG over several trials [26], [112]. This creates a need for a robust feature for movement detection that can solely be obtained from a single trial and is independent of any particular frequency band besides providing different information related to movement. In this paper, we have proposed a new process related to motor command generation in the brain that compliments the information that is obtained from conventional ERD and MCRP processes. The new autocorrelation relaxation time feature was successfully used for classifying movement and resting state trials. The performance of the new single trial movement feature was compared rigorously with MRCP.

4.2 Materials and methods

4.2.1 Experimental procedure

Fourteen healthy participants (7 males and 7 females, ages 26±4) participated in this EEG experiment. Ethical approval for EEG experimentation on humans was obtained from School of Systems Engineering, University of Reading, UK. Written consent was obtained from all

the participants. 12 participants were right handed and 2 were left handed. Participants did not have any previous experience of EEG experimentation.

This study was conducted to understand the neural correlates for detection of movement intention. A self-paced, asynchronous single finger tapping paradigm was developed to study EEG corresponding to motor command generation. Simple movement of index finger tapping was chosen as the task because it does not involve any complex hand gestures, directional reaching, grasping or trajectory planning.

EEG experimental paradigm was developed in Simulink using the tools provided by BioSig toolbox [205]. A customised tapping device was developed using a programmable micro-controller for recording the finger taps from both index fingers. One channel of binary finger tapping signal was recorded simultaneously with EEG for each hand. EEG and finger tapping signals were co-registered using tools provided by TOBI framework [208].

Participants were seated on a chair with palms placed on the table in front. Index fingers of both the hands were placed in finger caps of the tapping device. A fixation cross was displayed on the screen for 2 s at the beginning of each trial. It was followed by the instruction for right or left finger tap or resting state. A window of 10 s was given to perform the instructed task voluntarily at the time of the participant's choice. Each trial was followed by a random break of 1 s to 1.5 s. 40 trials for each of the three conditions (right tap, left tap and rest)were recorded. 19 EEG channels in accordance with 10-20 international system were recorded using TruScan Deymed EEG amplifier. Ground and reference electrodes were placed at the centre and all the impedances were kept below 7 kΩ.

4.2.2 EEG Pre-processing, artefacts removal and segmentation

EEG was prepared for further analysis by performing pre-processing and artefacts removal on all EEG channels. DC offset was removed by subtracting the mean of each channel from the signal. All EEG filtering was done using fourth order Butterworth filter. A notch filter at 50 Hz was used to remove the power line noise. EEG was low-pass filtered with the cut-off frequency of 60 Hz to eliminate high frequency noise.

Eye blinks and some movement artefacts were removed using Independent Component Analysis [236]. Independent components with artefacts were identified manually and were eliminated. EEG was segmented into time locked trials of length 6 s by extracting 3 s prior to the onset of finger tap and 3 s after the onset of the finger tap. Channels F3, Fz, F4, C3, Cz, C4, P3, Pz and P4 over sensorimotor cortex were used for movement intention analysis.

4.2.3   Analysis of movement-related cortical potentials

MRCPs are obtained from lower frequencies by averaging several trials of EEG [53]. EEG was filtered between 0.1 Hz to 0.5 Hz to obtain movement related slow cortical potentials. Grand average MRCP was computed by averaging the all the trials from all the participants for nine channels. MRCP was also obtained for single trial.

4.2.4   Movement intention analysis based on exponential decay of auto-correlation

Autocorrelation gives an estimation of how EEG is related to itself over time. Previous research shows that the autocorrelation changes during movement [204, 222]. Six virtual channels viz. F3-C3, Fz-Cz, F4-C4, C3-P3, Cz-Pz and C4-P4 were created using a longitudinal bipolar montage to enhance the movement related signal. EEG was band-pass filtered with cut-off frequencies 0.5 Hz and 30 Hz. Continuous autocorrelation was computed for each trial to determine the time development of the relaxation time of brain activity before, during and after the movement. Normalized autocorrelation was computed on 1 s window shifted by 100 ms from 6 s trial.

Let the single window of a signal be represented by $A(t)$, the autocorrelation of $A(t)$ is defined by $C(\Delta t) = \langle A(t)A(t - \Delta t) \rangle$, where $\langle ... \rangle$ represents the average over time. At zero lag, the signal is perfectly correlated, giving $C(0) = \langle A^2 \rangle$, and as lag approaches infinity, the signal becomes completely uncorrelated, giving $C(\infty) = \langle A \rangle^2$. The trend of relaxation process of autocorrelation could be described by $C(t) = \langle A^2 \rangle e^{\frac{-t}{\tau}}$. Here, τ (decay constant) represents the relaxation time of autocorrelation.When autocorrelation is normalised, $\langle A^2 \rangle = 1$.

To get the relaxation time of autocorrelation by capturing the exponentially decaying trend of autocorrelation, the exponential decay curve $y = Ke^{\frac{-t}{\tau}}$ was fitted to the local maxima points of positive lags of autocorrelation of each window in the trial (see Fig 4.1). The relaxation time τ was extracted as the feature at every 100 ms in the 6 s trial. The constant K was set to 1 as the autocorrelation was normalised. Changes in autocorrelation occurring during motor command generation were observed by studying the time progression of τ values.

4.2.5   Classification of movement and resting state trials

4.2.5.1   Classification of MRCP features.

MRCP for each 6 s trial was divided into 0.5 s windows by shifting it by 100 ms. Features for classification were obtained by averaging all the samples in each 0.5 s window. Feature from
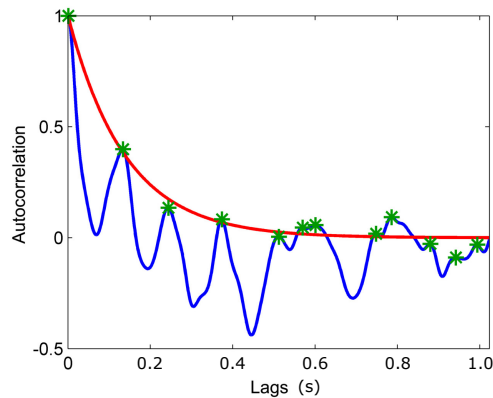
Fig. 4.1 Exponential curve fitting representing decay of autocorrelation (autocorrelation relaxation) for right finger tapping trial in F3-C3.

first 0.5 s window (-3 s to -2.5 s) was used as resting state feature for training the classifier. Linear discriminant analysis (LDA) classifier was trained for every window in the trial with two class corresponding features from all the trials. 10x10 cross-fold validation scheme was used for this binary classification and percent classification accuracy was obtained. The threshold for classifier outcome was obtained from 95% confidence level ($p < 0.05$) for binary classification. The best performing channel was selected manually for each participant.

4.2.5.2 Classification of autocorrelation decay features.

Autocorrelation decay features (τ) were obtained for three classes viz. right finger tap, left finger tap and resting state. Classification was performed on each 1 s window shifted by 100 ms in 6 s trial. LDA classifier was trained for each window with tap features and resting state features from the corresponding windows in all the trials. 10x10 fold cross-fold validation scheme was used for binary classification and percent classification accuracies were obtained. The classification accuracies for 6 s trials for all the six virtual channels were plotted for all the participants (see Fig 4.2).

4.3 Results

4.3.1 MRCP

4.3.1.1 Grand average of MRCP.

Grand average of MRCP is shown in the Fig 4.3 for right and left hand trials. Negative potential peaks just before the actual onset of the finger tap in most of the channels. Thus,
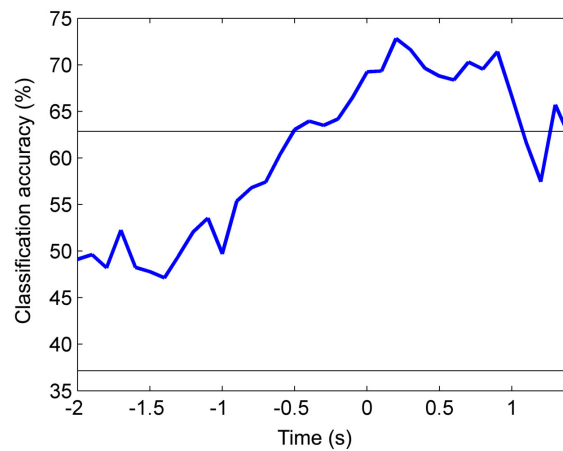
Fig. 4.2 Classification accuracies along the trial for left hand, participant 1 in virtual channel F3-C3. The horizontal line indicates statistical significance ($p < 0.05$).

movement could be predicted from the grand average MRCP before its actual occurrence. The peak of the MRCP has small amplitude as expected.

4.3.1.2 Single trial classification of MRCP

The classification accuracy crosses the threshold prior to the onset of movement indicating that movement could be predicted before its occurrence. Table. 4.1 shows the classification accuracies of MRCP for identifying movement intention.
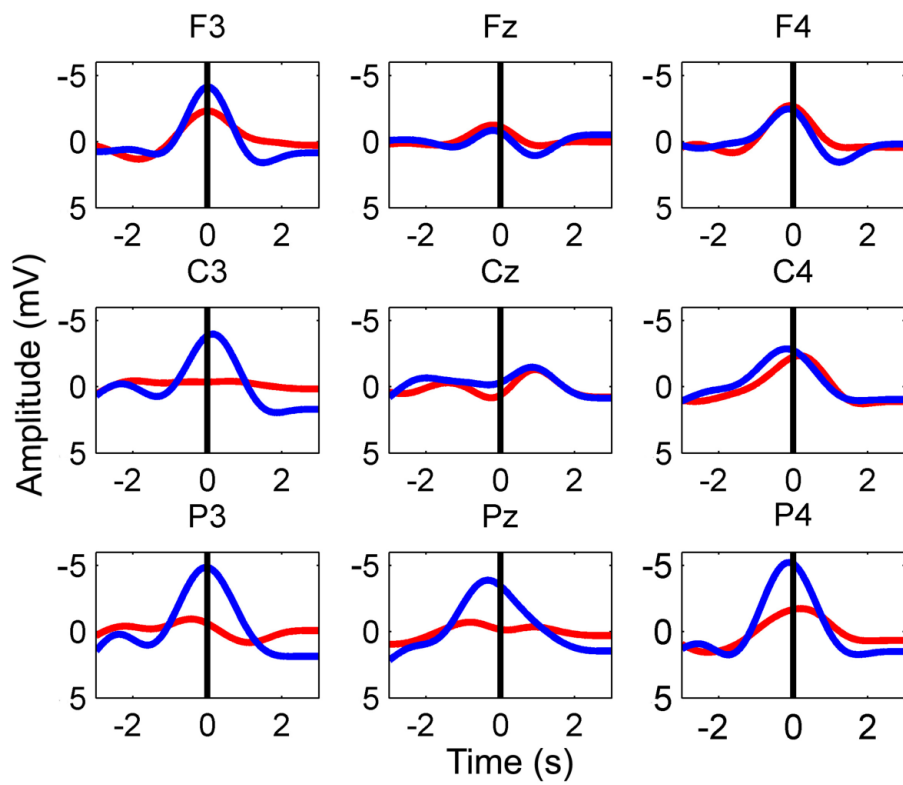
Fig. 4.3 Grand average of MRCP for nine channels. Red: right finger tapping, Blue: left finger tapping.

Table 4.1 Classification results for MRCP. Statistical significance ($p < 0.05$) is indicated in bold.

Participant ID	Right Finger Tapping			Left Finger Tapping		
	MRCP Classification Accuracy (%)	Channel	Time of threshold crossing (s)	MRCP Classification Accuracy (%)	Channel	Time of threshold crossing (s)
1	**70.25**	Pz	0.25	**68.63**	F3	-0.75
2	**64.08**	P3	0.30	**65.08**	P3	-0.80
3	**82.95**	C4	-1.60	**79.13**	P4	-1.60
4	**63.96**	P4	-1.35	**76.25**	P3	-1.75
5	**64.63**	F3	-0.90	**70.25**	F4	-0.50
6	**76.29**	P4	-0.90	**68.71**	F3	-0.20
7	**70.13**	F4	-0.95	**70.75**	Cz	-1.20
8	**66.25**	C4	-0.20	**77.50**	P4	-0.65
9	**66.25**	P3	-0.95	**64.63**	F4	-0.40
10	**70.38**	F3	-1.00	**67.75**	F3	-0.95
11	**64.50**	Cz	-1.20	59.88	C4	-
12	**67.13**	Fz	-1.10	**67.89**	Cz	0.60
13	**69.00**	C3	-1.95	**71.37**	P4	-0.90
14	**69.50**	F4	-0.25	**80.63**	C3	-0.25
Mean	68.95		-0.84	70.60		-0.72
SD	5.26		0.65	5.93		0.62
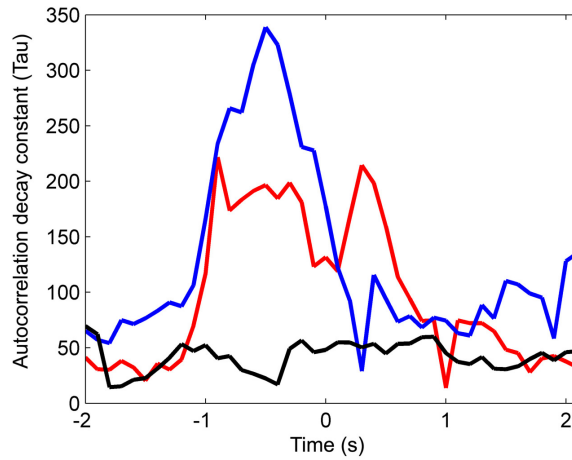
Fig. 4.4 Plot of changes in τ in virtual channel F3-C3 in a single trial for right finger tapping (red), left finger tapping (blue) and resting state (black) for participant 1.

4.3.2 Decay of autocorrelation related to the movement intention.

The trend of decay of autocorrelation which represents the relaxation time τ, changes during the voluntary movement. The τ value starts building-up prior to the onset of the motion. τ features in a single trial for right finger tap illustrated in Fig 4.4 clearly show the increase prior to the movement onset. There is no such build-up of τ values in the resting state trials. Two sample t-tests were performed on finger tapping trials and resting state trials on six bipolar channels (with ($p < 0.05$)) to confirm that the difference around movement onset was statistically significant. Autocorrelation decays slower during intention and execution of movement and it decays faster otherwise. Table. 4.2 shows single trial classification results.

Table 4.2 Classification results for autocorrelation analysis. Statistical significance ($p < 0.05$) is indicated in bold.

Participant ID	Right Finger Tapping			Left Finger Tapping		
	Autocorrelation Classification Accuracy (%)	Channel	Time of threshold crossing (s)	Autocorrelation Classification Accuracy (%)	Channel	Time of threshold crossing (s)
1	**71.00**	Cz-Pz	-0.20	**74.00**	C4-P4	-0.25
2	**76.70**	F4-C4	-0.25	**76.58**	F4-C4	-0.90
3	**65.75**	Fz-Cz	0.40	**66.63**	F4-C4	-0.60
4	**66.88**	F4-C4	-0.60	**69.00**	Fz-Cz	-0.55
5	**64.50**	F4-C4	-0.67	**65.38**	C3-P3	0.35
6	**69.57**	Cz-Pz	0.35	62.71	F4-C4	0.25
7	**69.25**	F3-C3	0.30	**72.50**	F3-C3	0.30
8	**66.13**	Cz-Pz	-0.20	63.00	F4-C4	0.10
9	**68.25**	F4-C4	-1.50	**65.38**	C3-P3	0.60
10	**64.38**	Cz-Pz	-0.75	58.88	Cz-Pz	-
11	**64.25**	F3-C3	0.35	**65.88**	F3-C3	0.10
12	**63.38**	C4-P4	0.75	**65.25**	C4-P4	-1.00
13	61.50	Fz-Cz	-	**65.38**	Fz-Cz	-1.00
14	**70.50**	C3-P3	0.40	**67.87**	C3-P3	-0.60
Mean	67.28		-0.12	67.03		-0.32
SD	3.92		0.63	4.71		0.57
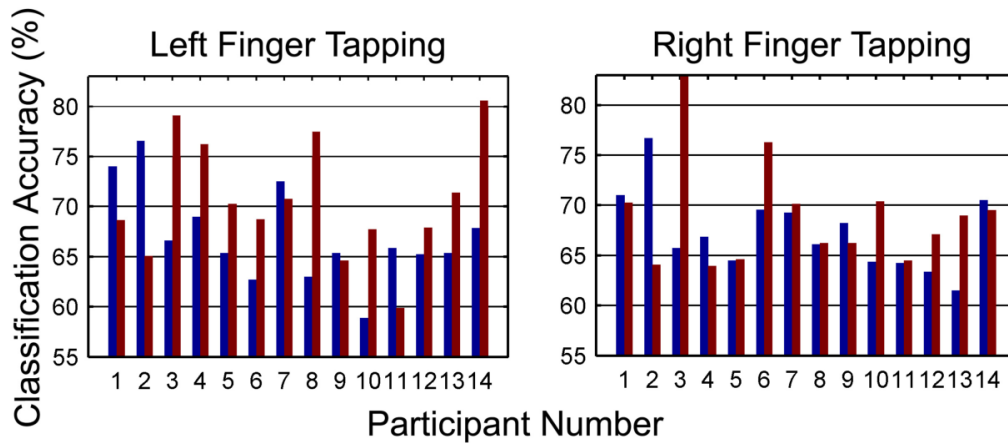
Fig. 4.5 Classification accuracies for autocorrelation and MRCP. Blue: Classification accuracies for Autocorrelation, Red: Classification accuracies for MRCP.

4.3.3 Comparison of autocorrelation and MRCP analysis

4.3.3.1 Classification accuracies of single trial autocorrelation and MRCP.

The classification accuracies of the newly proposed autocorrelation analysis method are very similar to the MRCP accuracies as shown in Fig 4.5. The mean accuracies of autocorrelation and MRCP for right and left finger tapping are comparable (67.28% and 68.95% for right and 67.03% and 70.60% for left respectively). MRCP has higher maximum classification accuracy than autocorrelation but also greater SD (see Table 4.1 and 4.2). We performed Wilcoxon signed rank test to compare the performance between autocorrelation decay classification accuracy and MRCP classification accuracy. There was no statistically significant difference between the classification accuracies of the two methods.

4.3.3.2 Timings for threshold crossing of classification accuracies and spatial locations for autocorrelation and MRCP.

Like MRCP, autocorrelation analysis could also predict the movement before its onset in most cases and can be used for detection of movement intention. The timings of movement prediction using autocorrelation analysis and MRCP are shown in Fig 4.6. However, MRCP can predict the movement earlier than autocorrelation decay feature. We performed Wilcoxon signed rank test to compare movement intention detection timings of autocorrelation and MRCP and found that MRCP detected movement significantly earlier than autocorrelation ($p < 0.05$). Spatial locations of autocorrelation and MRCP analysis are different. Lateralisation is not observed in both the cases. Different spatial locations suggests that the origin of the movement related information is distinct in both the cases.
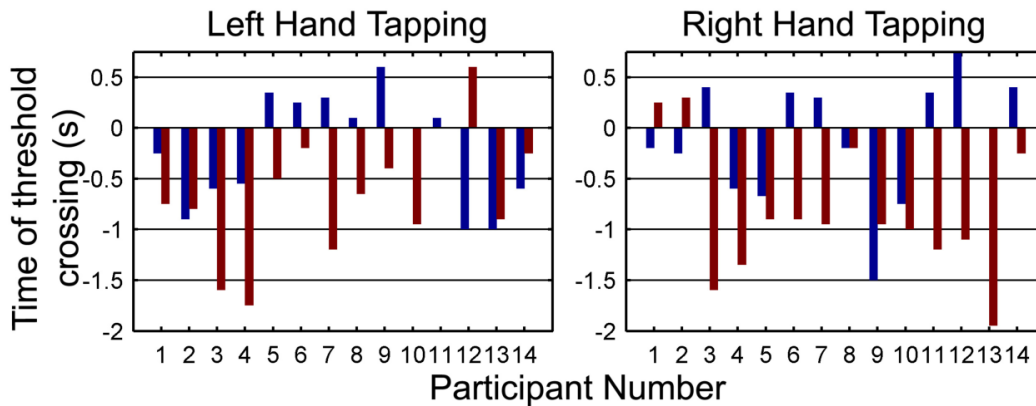
Fig. 4.6 Timings for threshold crossing for classification accuracies of autocorrelation and MRCP. Blue: Timings for autocorrelation, Red: Timings for MRCP.

4.4   Discussion and conclusion

The trend in decay of autocorrelation changes during the process of motor command generation. Autocorrelation decays slower during the preparation and execution of the voluntary movement than in the resting state. Decay constant τ, representing the relaxation time of autocorrelation, proves to be a robust feature related to the movement detection. The change in τ is observed in the single trial and, hence, it could be used for online BCI applications. In this paper, we have validated the new movement related process to complement traditional MRCP and ERD processes for movement prediction and detection.

Classification accuracies for autocorrelation (mean 67% with peak accuracy of 76.7%) are similar to the mean accuracies (69.95% and 70.60%) obtained from single trial MRCP analysis. Similar results were obtained with modified single trial ERD analysis (paper currently in preparation). These classification accuracies are also comparable to the other work done for movement prediction and detection using MRCP and ERD [200, 71, 114, 112, 100]. The accuracies obtained from the offline analysis using both the methods are not very high probably due to single finger tapping which involves fewer muscles. The results obtained from this task are purely based on movement intention and execution as opposed to other studies that used different full arm directional movements which can result to inclusion of cognitive information of trajectory planning and coordination.

This new feature is important because the information content on movement intention obtained from this feature is different from MRCP and ERD. This feature gives a third independent process related to movement in brain that complements MRCP and ERD. The advantage of this feature over ERD is that it does not require most responsive frequency band selection for individual and thus can be used more robustly. Unlike MRCP, this new

feature provides information from a wide frequency range without eliminating any potential movement related information from higher frequencies. Further work on this autocorrelation feature could be used for modelling the oscillatory processes during movement intention generation in brain and thus understand methodically what happens in brain when an individual intends to move.

The single feature of autocorrelation relaxation time is capable of identifying the intention of movement from single trial with equally good performance as MRCP. Thus, this autocorrelation decay feature could be adapted for online BCI applications. The SD of autocorrelation was very small as compared to the SDs of other ERD and MRCP studies [91, 114]. This is another indicator of the robustness and consistent performance of the autocorrelation. Thus, this paper introduces a new neural correlate of movement intention based on the temporal dynamics of EEG that is different from MRCP and ERD.

Chapter 5

Dynamics of Long-Range Temporal Correlations in Broadband EEG for Movement Prediction

Maitreyee Wairagkar, Yoshikatsu Hayashi, Slawomir J Nasuto

This chapter has been submitted to the journal Scientific Reports. This chapter continues the investigation of the fast arrhythmic broadband EEG temporal dynamics and formally identifies the long-range temporal correlations (LRTC) in the short timescales. This chapter shows that the instantaneous changes in the LRCT can be used to detect movement intention before its onset on single trials, and thus finds a novel neural correlate of movement intention.

Abstract

Brain activity is composed of oscillatory and arrhythmic components, however, there is more focus on oscillatory processes. Neuronal processes during movement intention are characterised by narrowband oscillatory event-related desynchronisation. However, the complex ongoing temporal dynamics of the arrhythmic broadband electroencephalography (EEG) remain unexplored. EEG is known to have long-range temporal correlations (LRTC) in the alpha oscillation fluctuations, but the temporal dependencies in the broadband EEG have not been investigated previously. We identified the presence of LRTC in the broadband EEG over short timescales. The broadband EEG facilitated detection of instantaneous changes in the scale-free dynamics during movement. The broadband LRTC increased significantly ($p < 0.05$) during movement. In contrast, the alpha oscillation LRTC, which

had to be computed on longer stitched EEG segments decreased significantly ($p < 0.05$) during movement consistently with the literature. This suggests the complementarity of underlying fast and slow neuronal scale-free dynamics during movement generation. The ongoing changes in the broadband LRTC could predict the movement 0.5 s before its onset with high accuracy of $75.88 \pm 6.4\%$ and hence can be used in BCI. We discovered a new complementary arrhythmic broadband temporal process capturing the ongoing fast dynamics that can unmask the novel properties of cognitive events.

5.1 Introduction

The brain activity during voluntary movement undergoes changes reflecting various complex processes. Two widely studied neural correlates of movement are the event-related (de)synchronization (ERD/S) [26] and movement-related cortical potential (MRCP) [53, 51]. The brain activity has a scale-free broadband arrhythmic component without a characteristic timescale or frequency which manifests as $1/f$ power spectrum [23]. The brain activity also has rhythmic components in the form of different oscillations with characteristic frequencies that show distinct peaks over this $1/f$ spectrum. Although broadband arrhythmic brain activity and oscillations coexist, there is more focus on studying the brain oscillations [23]. The oscillatory processes provide a common conceptual framework for understanding motor command generation via ERD/S obtained on specific narrowband sensorimotor oscillations [44, 90]. The broadband arrhythmic process was previously considered as background noise in the brain activity. However, recent reports suggest that the broadband activity has physiological and functional relevance [23], its dynamics change with task demand and cognitive state, and it has also been associated with the excitation/inhibition balance of the neuronal populations [61]. This has rekindled the interest to investigate the broadband activity during a motor task. We previously studied the temporal dynamics of the broadband electroencephalography (EEG) and found that the autocorrelation decayed slower during movement intention and execution than in the resting state leading to a discovery of the novel neural correlate of movement [237]. In this paper, we study the changes in the long-range temporal correlations (LRTC) in the broadband EEG to formalise the nature of this decay of autocorrelation.

Some of the neural activity has been reported to produce such long-range interactions leading to power-law scaling suggesting that these neuronal processes are similar across different scales [238, 239]. The power-law scaling has been observed in several cases of neuronal recordings such as neuronal firings [33], neuronal avalanches [34, 35], intracranial recordings such as LFPs [34] and ECoG, and non-invasive scalp recordings of EEG and

MEG [34, 36] in both oscillatory and non-oscillatory processes. On the surface level EEG and MEG activity, the power-law scaling is observed in the form of the $1/f$ power spectrum of non-oscillatory or arrhythmic scale-free neuronal activity. Spontaneous oscillatory neuronal processes also show LRTC in their amplitude envelope fluctuations [39, 29, 132, 36].The LRTCs are the result of power-law distribution in the autocorrelation of neural activity. The LRTCs have been observed in the alpha, beta, theta oscillation amplitudes [132], alpha oscillation phase [128], broadband phase synchrony [37] avalanches [34, 35] and energy profile [133, 34]. It is commonly postulated in the literature that the power-law behaviour and LRTCs occur because the brain operates at criticality [144, 62], thus optimising information storage capacity [37] and enabling quick adaptation to the cognitive processing demands.

In EEG, LRTCs have been traditionally identified in the amplitude envelope fluctuations of narrow frequency bands corresponding to different brain oscillations [29, 36]. The LRTCs have also been observed in the sensorimotor oscillations [38, 126]. The LRTCs in the alpha amplitude envelope fluctuations decrease due to the disruption caused in the long-memory process by an external stimulus [38, 135, 128]. Neurological conditions also affect LRTCs [133, 240, 241]. The LRTCs can be modulated using neurofeedback where LRTCs increase because of the closed loop stimulus [135, 240, 241]. The scale-free dynamics are also identified in behavioural data [35]. The LRTCs in neuronal activity and movement patterns are correlated [242, 33] and neural scale-free dynamics can predict the performance of motor tasks [243]. However, there have been no previous studies about LRTCs in broadband arrhythmic EEG during motor tasks.

The LRTCs are characterised in the amplitude envelope fluctuations of oscillations in brain activity. These oscillations are typically extracted using Fourier-based spectral methods. The recent work by Cole et al. [103] shows that the brain rhythms are non-stationary and not strictly restricted to selected narrow sinusoidal frequency bands; therefore a narrowband restriction of the analysis can disregard important features present in the entire power spectrum. Hence, the LRTCs computed from narrow frequency band amplitude envelope fluctuations may not give complete information present in these brain rhythms and there is a need for assessing LRTCs in the broadband arrhythmic brain activity as well.

The LRTCs in EEG can be assessed using spectral or temporal domain methods [244, 131]. In the spectral domain, the scaling exponent of LRTC is obtained by estimating the slope of $1/f$ power spectrum in a log-log scale. In the temporal domain, the scaling exponent of LRTC can be obtained by fitting the power-law directly to the autocorrelation, which is often difficult to achieve in practice [244]. Another most common way of characterising LRTC in temporal domain is using Hurst exponent. A consistent relationship between the Hurst exponent, scaling exponent from autocorrelation and scaling exponent from $1/f$ spectrum for

stationary time series is shown by Rangarajan and Ding [244]. The Hurst exponent indicates the presence of LRTC if it is between 0.5 and 1 [39]. The Detrended Fluctuation Analysis (DFA) [122] is the most common method for estimating Hurst exponent. DFA estimates the Hurst exponent from the slope of signal fluctuations at different timescales. The power spectrum analysis is not suitable for reliably identifying LRTC in non-stationary data [29]. The DFA is used for obtaining Hurst exponent from EEG because it facilitates the detection of LRTC embedded in non-stationary time series by avoiding the artefactual dependencies caused by non-stationarity and trends [39, 131, 122, 134, 29].

Our motivation for investigating the dynamics of the broadband EEG LRTCs is its implication for the brain computer interfaces (BCI). Movement is the fundamental mode of interaction with our environment, thus robust motor intention detection can facilitate the development of intuitive motor-based BCIs. Hence it is important to understand the underlying mechanisms of movement generation.

The LRTCs are considered an invariant property of brain dynamics spanning several scales and hence are not computed as a function of time. LRTC is traditionally estimated on an amplitude envelope of narrowband EEG oscillations which requires long EEG segments [29]. With this approach, we cannot observe the ongoing instantaneous changes in LRTC. Detecting movement from LRTC requires evaluating the changes in the dynamics of the LRTC continuous as a function of time. Berthouze et al. [238] have previously captured the changes in the LRTCs using Kalman filter, but the timescales over which the LRTCs were observed were still several seconds long. Here, we investigate the instantaneous changes occurring in the LRTCs using shorter timescales to study the fast brain dynamics. To our knowledge, the LRTCs in the broadband have not been observed before to study the mechanisms of motor command generation. Our analysis will help in understanding the functional role the broadband arrhythmic brain activity plays in motor command generation.

The ERD/S and MRCP are widely used as complementary neuronal processes' markers for movement detection from EEG. ERD/S quantifies the change in the band power of sensorimotor oscillations with reference to its baseline band power [26]. ERD/S does not take into account the information from other frequencies outside the selected oscillations. MRCP only characterises changes in the slow potentials during movement. Both ERD/S and MRCP do not consider the dynamical changes in the temporal dependencies in broadband arrhythmic scale-free neuronal processes. We propose that the changes in the broadband LRTC indicate yet another complementary neuronal process for voluntary movement generation.

Investigating the dynamics of the broadband EEG LRTCs can have applications in BCI. Continuous characterisation of LRTC can be used for detecting movement on a single-trial basis without the need of choosing participant specific parameters. Consistently, we obtained

high classification accuracies of movement using the LRTC index. In turn, the BCI-style of processing pipeline enables investigating the ongoing changes in the dynamics of broadband EEG via LRTC during movement. The aims of this paper are 1) to investigate the changes in the LRTC in broadband EEG during voluntary movement; 2) compare and contrast the broadband LRTC with the LRTC in the alpha oscillation amplitude envelope commonly observed in the literature during movement; 3) to detect movement intention by using LRTC on a single-trial basis as novel features for applications in BCI.

5.2 Methods

5.2.1 Participants

Fourteen healthy participants (8 female, age 26 ± 4 years, 12 right handed) with no prior experience in EEG experiments and BCI participated in the study. Ethical approval for EEG experiment was obtained from the ethics committee of the University of Reading, UK. Informed written consent was obtained from all the participants. The experiments were carried out in accordance with the guidelines set by the University of Reading.

5.2.2 Experimental paradigm

The details of the experimental paradigm and artefacts removal are given in Wairagkar el al. [237] EEG data is available from http://dx.doi.org/10.17864/1947.117 [209]. EEG was recorded for a single asynchronous index finger tapping task. An instruction was shown on the screen placed 1 m from the participant to perform a right finger tap, left finger tap or resting state (no tap) within a following 10 s window asynchronously at any random time. Fig 5.1 shows the structure of trial. Participants were instructed not to perform the task immediately after the instruction to avoid cue effects. Forty trials per condition were recorded with the sampling frequency of 1024 Hz which was downsampled to 128 Hz. The onset of finger tap was recorded using a microcontroller device and was co-registered with EEG. Artefacts were removed with independent component analysis [236] using EEGLAB toolbox [211, 212]. EEG was bandpass filtered between 0.5 Hz to 45 Hz. We extracted 6 s EEG trial (-3 s to +3 s of movement onset) from the channels C3, Cz and C4 over motor cortex according to the 10-20 international system. In this chapter, monopolar EEG channels C3, Cz and C4 are used instead of bipolar channels because the bipolar channels gave significantly lower classification accuracies than the monopolar channels using the method described in subsequent sections of this chapter. The results using bipolar EEG channels are included in Appendix B. The 6 s trials were divided into 2 s sliding Hanning

windows from time $(t-2 \text{ s})$ to t shifted by 100 ms. Each feature at time t was obtained on a window from $(t-2 \text{ s})$ to t. All the analysis was done offline in MATLAB (The MathWorks, Inc., Natick, Massachusetts, United States).
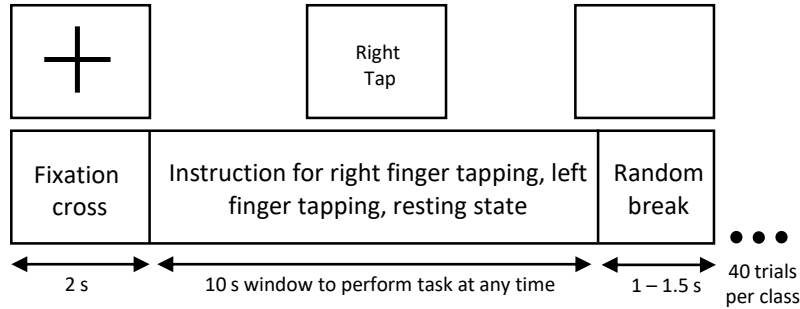
Fig. 5.1 **Structure of a single EEG trial.** Each trial started with a fixation cross followed by an instruction for right finger tap, left finger tap and resting state. 10 s window was given to the participants to perform the single finger tap at any time. This was followed by a random break. 40 trials per class were recorded.

5.2.3   Detrended Fluctuation Analysis (DFA) to identify LRTC in EEG

We hypothesised that the LRTCs in the broadband EEG change during movement intention and execution. We quantified the broadband LRTCs using Hurst exponent computed using DFA [122]. The DFA analysis calculates RMS fluctuations of integrated and detrended time series at different timescales as follows:

1. The time series x of length N is integrated according to equation (5.1) where $k = 1, ..., N$ and y is the integrated time series.

$$y(k) = \sum_{i=1}^{k} x(i) - \bar{x} \tag{5.1}$$

2. The integrated time series y is then divided into N/n non-overlapping boxes of length n, where n is individual timescales at which we want to compute fluctuations. The box sizes have an impact on the DFA scaling exponent and are usually chosen between $n = [10, N/4]$ [131] to get good estimate of RMS fluctuations at each scale with $[N/10, 4]$ number of boxes. We used 25 box sizes between $n = [10, N/4]$ equidistant on log_2 scale as our number of samples was a power of 2.

3. At each scale n, for every non-overlapping segment of y of length n, trend is obtained by least square linear fit. The y_n is concatenation of trends at a scale n for all the N/n boxes and the RMS fluctuations are computed according to equation (5.2).

$$F(n) = \sqrt{\frac{1}{N}\sum_{i=1}^{N}(y(i) - y_n(i))^2} \qquad (5.2)$$

4. A log-log plot of fluctuations at each timescale n ($log_2 F(n)$ vs $log_2 n$) was plotted and DFA scaling exponent was obtained by calculating the slope of the linear fit to this plot.

Since N is not divisible by n for each box size, fluctuations were obtained from performing the above analysis from forward and backward direction [134] of each EEG window and then averaging them at each timescale. When the log-log DFA plot is linear, we obtain a DFA scaling exponent or Hurst exponent that indicates power-law in fluctuations at different timescales.

5.2.4 LRTC in broadband EEG and alpha oscillation amplitude fluctuations during movement intention

We studied the changes in LRTC in the broadband EEG and compared it with the LRTC in the alpha oscillation amplitude envelope during movement from the literature [38]. For clarity, throughout the paper, we use H_{BB} to indicate DFA scaling exponent or Hurst exponent in the broadband and H_{alpha} to indicate Hurst exponent in the amplitude envelope of the alpha oscillations.

5.2.4.1 DFA on single-trial broadband EEG

We performed DFA on each 2 s sliding broadband (0.5-45 Hz) EEG window shifted by 100 ms to obtain continuous changes in the LRTC (Hurst exponent H_{BB}) throughout the trial during movement. The Hanning window was applied to each 2 s window to avoid edge effects. 256 samples were available for performing DFA on 2 s window. Delignieres et al. [131] have shown that DFA method can accurately estimate Hurst exponent in short time series. Our range of timescales ($[10, N/4]$ samples i.e. [78ms 0.5s]) is within the range suggested by Li et al. [245] $[max(k+2, F_s/F_{max}), min(N/4, F_s/F_{min})]$ where $k = 1$ (linear detrending in DFA) for filtered data between F_{min}(0.5 Hz) and F_{max} (45 Hz). We used an exponential smoothing filter to smooth the H_{BB} in consecutive windows in single trials in order to avoid

noisy estimates of H_{BB}. We validated the scaling exponents H_{BB} using maximum likelihood
DFA [127].

5.2.4.2 Validation of LRTC

We validated our LRTC results to confirm that the obtained LRTCs were not artifactual. The
autocorrelation of a time series decays exponentially if it has short-range dependence and
slower than exponential if it has long-range dependence [120]. A specific case of long-range
dependence is LRTC where the autocorrelation decays according to the power-law which
is identified using Hurst exponent. Hence, to identify LRTC, we must validate the Hurst
exponent obtained using DFA. We systematically validated the LRTC in three stages as
follows.

Identification of significant correlations in broadband EEG using surrogate test   We
first identified whether significant temporal correlations are present in the broadband 2 s EEG
windows and their DFA exponents H_{BB} are significantly different from the DFA exponents
of white noise obtained by randomly shuffled samples from the same EEG windows using
surrogate test [131, 246].

Determination of long-range vs short-range dependence in the broadband EEG   Then
we identified whether these correlations are short-range or long-range dependence by com-
paring the fit of corresponding ARMA(p,q) and ARFIMA(p,d,q) models to each 2 s EEG
windows using Akaike's information criterion (AIC) [119, 32, 131]. We estimated the orders
p and q of ARFIMA and ARMA independently by comparing models of orders p=1...10 and
q=0 (this range was selected by observing the autocorrelation function and partial autocorre-
lation function of EEG) using AIC. The ARMA model was estimated using the functions pro-
vided by Econometrics toolbox in MATLAB (https://www.mathworks.com/help/econ/). For
estimating ARFIMA, we first fractionally differentiated our EEG window with $d = H_{BB} - 0.5$
and then fitted ARMA(p,q) to it.

**Identification of LRTC by validation of broadband DFA scaling exponent H_{BB} using
maximum likelihood DFA**   After establishing the long-range dependence, we then nar-
rowed down on the type of long-range dependence. If the fluctuations in log-log DFA plot at
different timescales follow a linear relationship, then this regularity can be captured by the
least squared fit and the slope of this linear fit represents a well-defined power-law scaling
exponent [126, 127]. We used maximum likelihood DFA (ML-DFA) [126, 127] method to
show that the linear fit is the best fitting model to the log-log DFA fluctuation plot.

The DFA scaling exponents are valid if the linear model fitted best to the log-log DFA fluctuation plot [128]. Firstly, we assessed the quality of the linear fit using R^2 measure [29]. Identifying the power-law is inherently difficult [119]. Frequently used R^2 measure is insensitive [127] because it may yield high values even for a non-linear relationship in the data [119]; therefore it is not sufficient to asses the quality of the linear fit. Hence, we used the ML-DFA [127, 126] to compare the fits of different models.

We fitted polynomials of order 1 to 5, an exponential function, a logarithmic function and a root function as suggested in Botcharova et al. [127] to the log-log DFA fluctuations and compared them using AIC and Bayesian information criterion (BIC). If the resulting best fitting model was linear, then we interpret it as an indicator of potential power-law and LRTC.

5.2.4.3 DFA of stitched broadband EEG and alpha envelope

Traditionally, the LRTCs are found in alpha amplitude fluctuations [29, 38, 36, 135]. Since the alpha amplitude has a very low frequency, LRTC cannot be computed reliably in short timescales within 2 s windows and require longer timescales. We bandpass filtered each EEG window between 8-13 Hz and then obtained its amplitude envelope by computing the analytic signal using Hilbert transform. We then stitched the corresponding EEG envelope windows from all the 40 trials for each participant to obtain longer EEG segments of approximately 80 s. Stitching of the data does not affect DFA scaling exponent [126, 247, 248]. We selected the timescales between [2 s, 20 s] corresponding to approximately box sizes of $[2^8, 2^{11}]$ samples. Then we applied the DFA analysis to obtain scaling exponents H_{alpha} and validated them using ML-DFA. To verify our single-trial broadband LRTCs, we computed DFA exponents on stitched broadband EEG.

5.2.5 Classification of H_{BB} to detect movement in single trials for BCI

The H_{BB} of each participant was classified into right tap vs resting state and left tap vs resting state independently using binary Linear Discriminant Analysis (LDA) classifier. The single-trial H_{BB} from C3, Cz and C4 were used as three features for LDA. A separate LDA classifier was trained for each sliding window with the feature vectors from corresponding windows in all the movement trials and the same number of features vectors randomly chosen from the resting state trials of that participant. Each LDA had 40 data samples with three features for each class. A 10x10 fold cross-validation was used to obtain the classification accuracies, sensitivities and specificities at the time points given by the 2 s sliding windows. The

95% confidence level for binary classification (tap or rest) was obtained from the binomial distribution with $n =$ number of EEG trials and $p = 0.05$.

5.2.5.1   Statistical analysis

We used parametric t-test and non-parametric Mann-Whitney U test for identifying statistical significance. We determined the normality of the data using one-sample Kolmogorov-Smirnov test available in MATLAB. We used t-test for normally distributed data, and Mann-Whitney U test for the data without normal distribution throughout this paper.

5.3   Results

We have identified the temporal dynamics of the long-range dependencies in the broadband EEG during movement intention and execution and compared them with the temporal dynamics of alpha oscillation amplitude envelope fluctuations in the following sections.

5.3.1   The changes in the broadband LRTCs (H_{BB}) during voluntary movement

The time evolution of the mean H_{BB} obtained on a single-trial basis for individual participants in C3, Cz and C4 are shown in Fig 5.2a. The H_{BB} increased during movement intention and execution of right and left index finger tapping and restored to its baseline level afterwards. There was no such increase in the H_{BB} during the resting state.

  The solid vertical line in Fig 5.2a marks the onset of the movement at 0 s and two vertical dotted grey lines show the period between which H_{BB} for right (red) and left (blue) finger tap is significantly different from resting state (black) ($p < 0.05$, Mann-Whitney U test, $n = 40$ (number of trials)). The non-parametric Mann-Whitney U test was performed at each time point during the trial with the H_{BB} values from the corresponding windows from all the trials of movement and resting state. The peaks of H_{BB} in the individual trials were not time-locked or aligned. Being able to compute the DFA exponent on a single-trial basis can allow its use as a feature for self-paced movement based BCI. Fig 5.2b shows the grand average of mean H_{BB} in all the participants. The H_{BB} during movement was significantly different from the resting state ($p < 0.05$, Mann-Whitney U test, $n = 14$ (number of participants)). The H_{BB} during movement and resting state was between 0.5 and 1 indicating the presence of power-law decay and LRTC in the autocorrelation of broadband EEG [238]. The LRTCs in EEG become stronger during voluntary movement.

5.3.1.1 Identification of significant correlations in broadband EEG using surrogate test

The surrogate test confirmed that H_{BB} in 2s EEG windows were significantly different from the DFA exponents of randomly shuffled samples from the same EEG windows ($p = 0$, Mann-Whitney U test, $n = 203688$ (individual windows in all the participants)). The scaling exponents of the shuffled data were close to 0.5 as shown in Fig 5.3, confirming the presence of white noise with no correlations. Thus, there were significant correlations present in the broadband 2s EEG.

5.3.1.2 Determination of long-range vs short-range dependence in the broadband EEG

The comparison of ARMA for short-range dependence and ARFIMA for long-range dependence using AIC resulted in the selection of the ARFIMA model by AIC most of the times. Hence, the ARFIMA model was a better fit to the broadband EEG windows confirming that the long-range dependence was indeed present.

5.3.1.3 Identification of LRTC by validation of broadband DFA scaling exponent H_{BB} using maximum likelihood DFA

The average R^2 measure for all EEG windows of all the participants in all the channels was 0.96 ± 0.02 (mean $\pm$ SD) indicating that the fitted line to the DFA fluctuation plot is a close fit. The ML-DFA method resulted in the selection of the linear model for 80% of the times in all the windows across all the trials, channels and participants during all the three conditions. In the remaining cases, a quadratic polynomial was chosen. We attribute this to the noise induced in computing the root mean square (RMS) DFA fluctuations at the larger timescales due to short EEG segments. The distribution of the coefficient of the linear term in the linear model and the quadratic model was the same when these respective models were the best fitting. In the case where the quadratic model was chosen, the ratio of the coefficient of the quadratic term to that of the linear term was small (0.02) showing significantly smaller contribution of quadratic term than the linear term ($p < 0.05$, two-tailed t-Test, $n = 203688$ (individual windows in all the participants)) and hence we did not discard these EEG windows. All these factors lead us to conclude that the log-log DFA fluctuation plot was linear and the H_{BB} was indeed valid.

5.3.2   Broadband LRTC and alpha oscillation amplitude envelope LRTC on stitched EEG

We obtained LRTC on longer stitched EEG segments in both broadband and alpha oscillation amplitude envelope. We then compared the broadband LRTC and alpha amplitude envelope LRTC in the following sections.

5.3.2.1   Verification of changes in broadband LRTC (H_{BB}) during movement using stitched EEG

The progression of the H_{BB} of stitched EEG in Fig 5.4a also shows that the scaling exponents increase significantly during intention and execution of the movement ($p < 0.05$, Mann-Whitney U test, $n = 14$ (number of participants)). The H_{BB} values are similar for both 2 s windows and stitched data and are in the range of 0.5 to 1. The scaling exponents of the stitched EEG were validated using ML-DFA. The linear model was selected by AIC and BCI individually for 96% times of all the stitched EEG segments in all the windows of all the three channels in all the participants and three conditions. This confirmed the validity of the H_{BB} estimates on single 2 s windows and the presence of LRTC in the broadband EEG. ML-DFA results showed that the quadratic model was previously incorrectly selected in the single-trial DFA because of the noise in the estimation of RMS fluctuations at higher timescales due to short EEG segments.

5.3.2.2   Alpha envelope LRTC (H_{alpha}) using stitched data

The H_{alpha} values decreased significantly during the movement as shown in Fig 5.4b ($p < 0.05$, Mann-Whitney U test, $n = 14$) consistently with the literature [38]. This decrease in H_{alpha} is more prominent in C3 and C4. We validated these exponents which ranged between 0.5 to 1 using ML-DFA and confirmed the presence of LRTCs in the fluctuations of the alpha amplitude envelope of stitched EEG.

5.3.2.3   Correlation between broadband LRTC H_{BB} and alpha oscillation envelope LRTC H_{alpha}

The broadband LRTC and alpha LRTC changed in opposite directions during movement. The broadband LRTCs increased Fig 5.4a, while the alpha envelope LRTCs decreased Fig 5.4b during movement. Fig 5.4c shows the scatter plot between H_{BB} and H_{alpha} using stitched data during the three conditions and their corresponding correlation coefficients. A clear

distinction is seen in the behaviour of the dynamics of H_{BB} and H_{alpha} during resting state when they are uncorrelated and during movement when they are inversely correlated.

5.3.2.4 Timescales of broadband LRTCs and alpha envelope LRTCs

Fig 5.5a shows the grand average broadband DFA plots and Fig 5.5b shows the grand average alpha envelope DFA plots. The broadband DFA fluctuations are linear (and scaling exponent is valid) in the log-log plot on the shorter timescales $< 2^7$, while the alpha envelope DFA fluctuations are linear only on the longer timescales $> 2^8$. This shows that broadband LRTCs are present on the shorter timescales capturing faster changes in the dynamics and alpha envelope LRTCs are present on the longer timescales representing slower changes in the dynamics. Though both the LRTCs show change in dynamics during the voluntary movements, broadband LRTCs could be used to identify this change almost instantly as opposed to the alpha envelope LRTCs which requires longer EEG segments for detection.

5.3.3 Classification accuracies of single-trial DFA scaling exponents for identification of movement

The average peak classification accuracy of $75.88 \pm 6.4\%$ was obtained around 1 s after the movement onset which corresponds to EEG window from -1 s to +1 s. The maximum difference between the movement and resting state H_{BB} was also approximately at 1 s (see Fig 5.2b). Table 5.1 shows the peak classification accuracies and the corresponding sensitivities and specificities for all the participants. The sensitivities and specificities are almost equal to the classification accuracies indicating that the classifier is reliable. The time of movement intention was recorded as the time when the classification accuracy crosses the significance threshold (see Table 5.1). We observed that indeed the movement can be predicted 0.5 s before its actual onset using the LRTCs in broadband EEG over shorter timescales for both right and left tap.
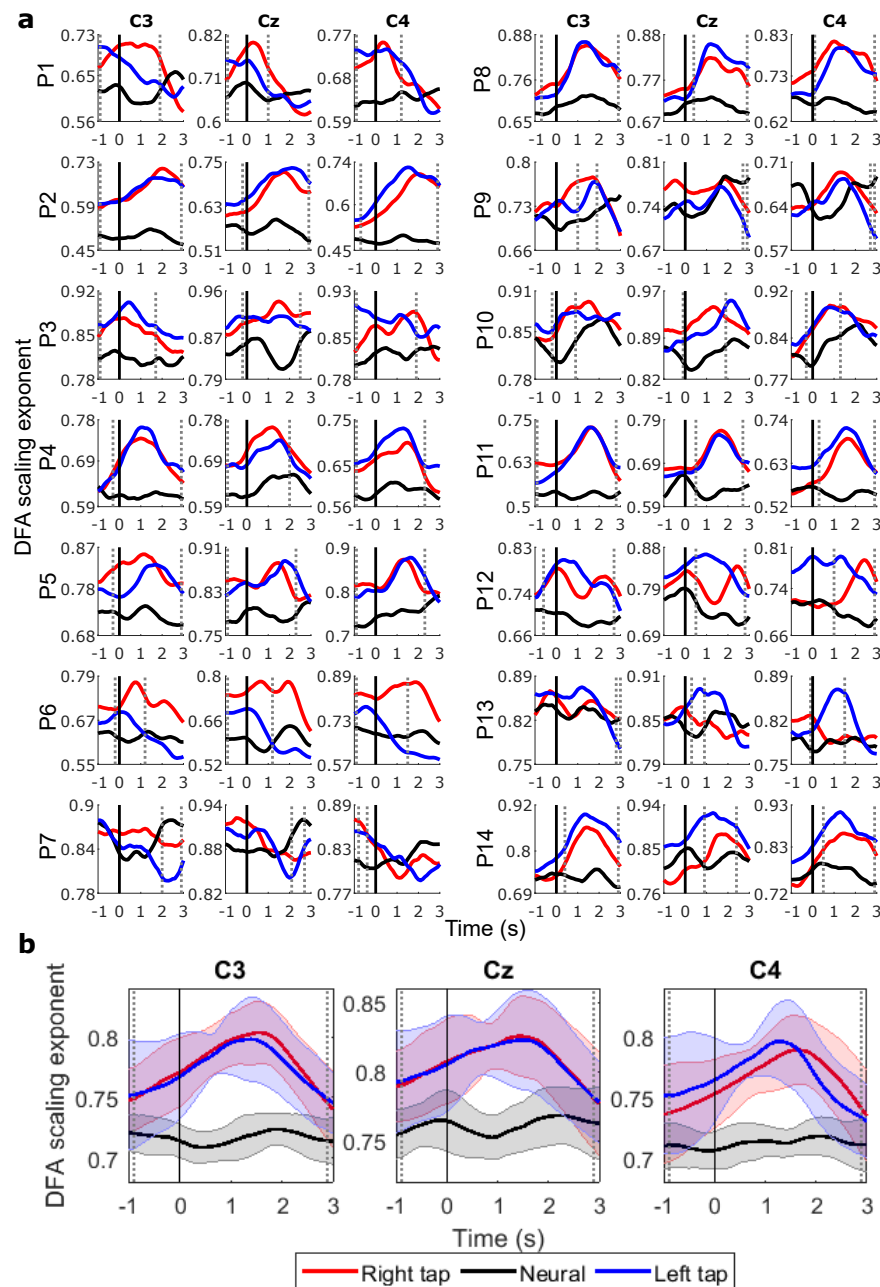
Fig. 5.2 The time evolution of DFA scaling exponents of broadband EEG (H_{BB}) in the individual participants and grand average of all the participants. (a) The progressions of mean H_{BB} in individual participants in channels C3, Cz and C4 during right finger tap (red), left finger tap (blue) and resting state (black). The H_{BB} increases during movement intention and execution. The movement onset is at 0 s marked by a solid vertical line. The H_{BB} of movement trials is significantly different from the H_{BB} of resting state trials in the time region between the dotted grey vertical lines. (b) The progression of the grand average of mean H_{BB} of all the participants. The shaded areas show the standard deviation. A clear increase in H_{BB} is seen during the movement.
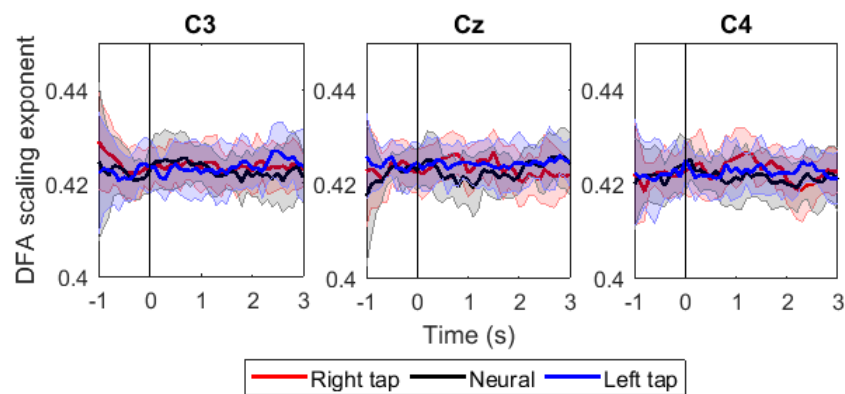
Fig. 5.3 **The time evolution of DFA scaling exponents in the randomly shuffled surrogate data.** The progressions of grand average of mean DFA scaling exponent of the randomly shuffled surrogate windows of all the participants in channels C3, Cz and C4 during right finger tap (red), left finger tap (blue) and resting state (black). LRTCs are not present in the shuffled data. The movement onset is at 0 s marked by a solid vertical line. The shaded areas show the standard deviation.
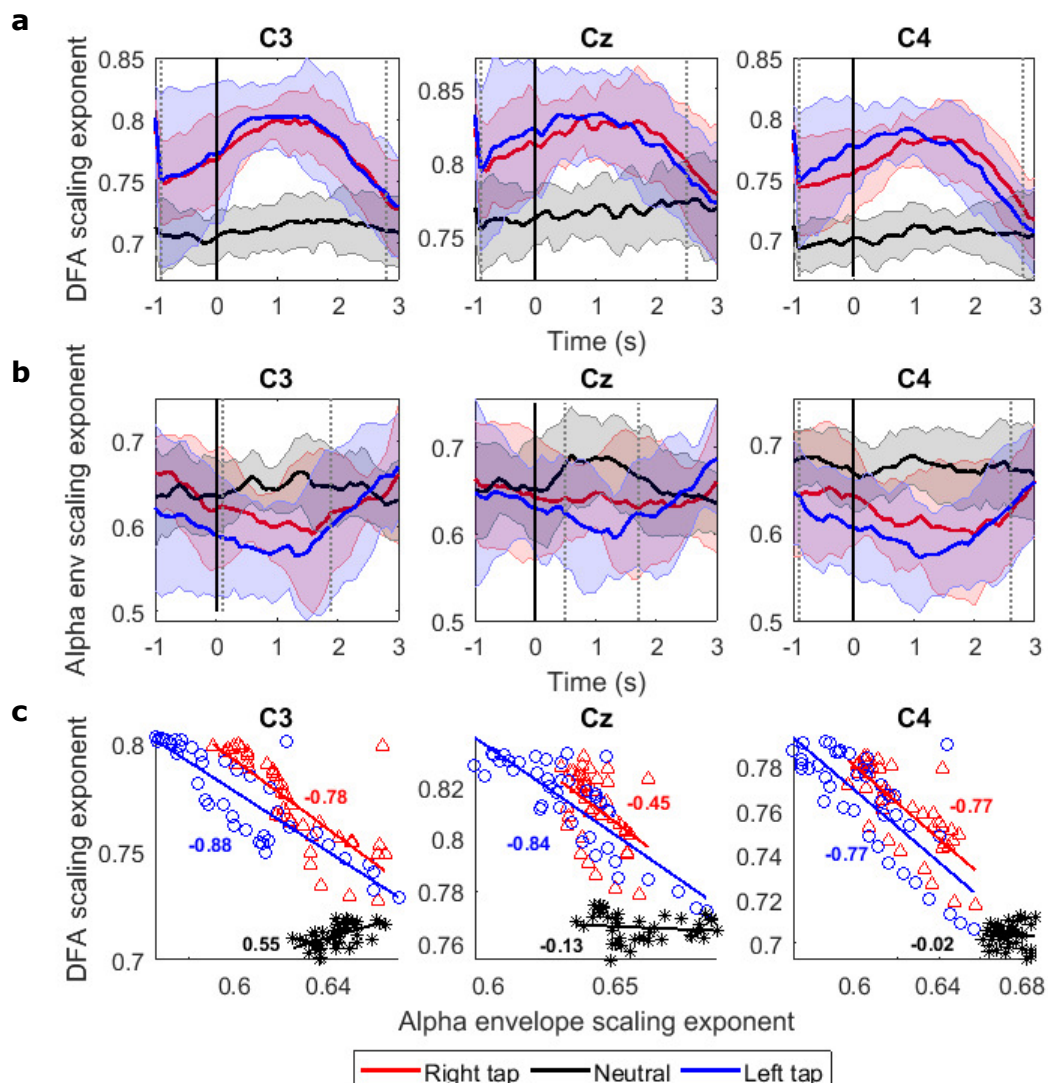
Fig. 5.4 **The progression of the grand average DFA scaling exponents in the stitched broadband EEG segments (H_{BB}) and the envelope of alpha oscillations (H_{alpha}).** (a) The progressions of grand average broadband H_{BB} of all participants in channels C3, Cz and C4 during right finger tap (red), left finger tap (blue) and resting state (black). The H_{BB} increases during movement intention and execution. The movement onset is at 0 s marked by a solid vertical line. The H_{BB} during the movement is significantly different from the H_{BB} during the resting state in the time region between the dotted grey vertical lines. The shaded area represents the standard deviation. (b) The progression of the grand average alpha oscillation amplitude envelope H_{alpha} of all the participants. The H_{alpha} decreases during the movement intention and execution. The H_{alpha} during movement is significantly different from the resting states in the times between the vertical dotted grey lines. (c) The scatter plot of the mean H_{BB} and H_{alpha} in all the three channels with their corresponding correlation coefficients. The correlation coefficients suggest an inverse correlation between H_{BB} and H_{alpha} during right tap (red) and left tap (blue), while there is no correlation during resting state (black).
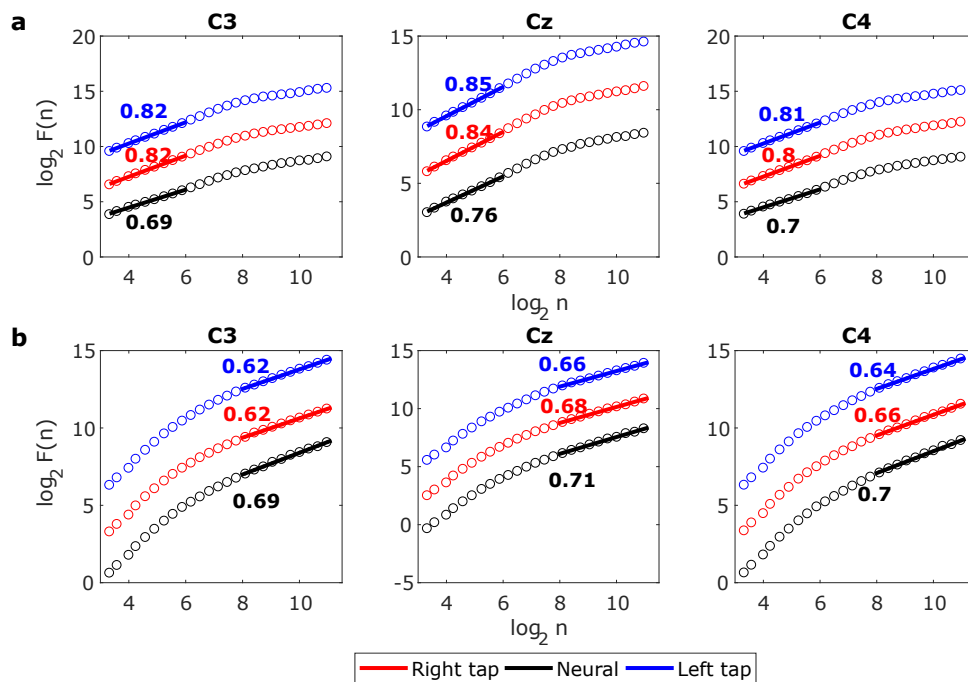
Fig. 5.5 **The grand average DFA plots for stitched broadband EEG and alpha amplitude fluctuations during movement.** (a) The grand average DFA plots for stitched broadband EEG in C3, Cz and C4 during right tap (red), left tap (blue) and resting state (black) for all the participants. This EEG segment is extracted from -1 s to +1 s of the movement onset. The Hurst exponents obtained from the slope of the fitted line to the DFA plots are shown. (b) The grand average DFA plots for stitched alpha amplitude fluctuations in the three channels. The broadband DFA exponents are valid over shorter scales and the alpha envelope DFA exponents are valid over longer timescales.

Sub. no.	Left finger tapping				Right finger tapping			
	Accuracy (%)	Sensitivity (%)	Specificity (%)	Time (s)	Accuracy (%)	Sensitivity (%)	Specificity (%)	Time (s)
1	73.00	73.25	72.75	-1.0	75.88	72.00	79.75	-0.5
2	87.55	91.02	84.08	-1.0	84.49	81.63	87.35	-1.0
3	73.75	74.25	73.25	-1.0	71.25	76.25	66.25	-0.7
4	81.88	82.00	81.75	-0.2	77.13	76.25	78.00	-0.1
5	74.88	83.00	66.75	-0.3	77.50	78.50	76.50	-0.35
6	71.63	77.14	66.12	-0.7	77.96	79.59	76.33	-1.0
7	65.00	61.75*	68.25	0.1	65.00	70.50	59.50*	-0.6
8	80.38	81.00	79.75	0.3	79.00	77.50	80.50	0.2
9	73.25	68.50	78.00	-0.6	78.50	75.25	81.75	-0.6
10	66.63	60.50*	72.75	0.9	74.63	74.75	74.50	-0.1
11	87.88	90.25	85.50	-1.0	89.25	92.50	86.00	-1
12	74.00	72.75	75.25	-0.9	74.63	76.00	73.25	-0.5
13	72.50	73.00	72.00	-1.0	65.38	66.50	64.25	-1.0
14	77.38	73.50	81.25	-0.6	74.38	72.25	76.50	0.2
Mean	75.69	75.85	75.53	-0.50	76.07	76.39	75.75	-0.50
SD	6.77	9.10	6.32	0.59	6.40	6.05	7.92	0.43
Median	73.88	73.88	74.25	-0.65	76.51	76.13	76.51	-0.55

Table 5.1 The peak accuracies and timings of significance crossing for right and left finger movement *vs* resting state classifications. All values except the ones marked by * are significantly above chance level ($p < 0.05$).

5.4   Discussion

The temporal dynamics of the broadband EEG during voluntary movement remains mostly unexplored in the literature as opposed to the commonly studied narrowband oscillatory ERD/ERS [90] or low frequency MRCP [53, 91]. We have found that LRTCs (H_{BB} between 0.5 to 1) are present in broadband EEG which increase during movement (Fig 5.2). This ubiquitous presence of LRTC suggests potential power-law dynamics in the temporal broadband brain activity.

The broadband activity which is arrhythmic and hence scale-free in nature coexists with oscillatory processes in the brain [23]. Our results suggest the presence of this scale-free property of the broadband EEG over small timescales (78 ms-1 s) (Fig 5.5). The arrhythmic broadband neuronal activity can be considered as a stochastic process due to the lack of a characteristic timescale, and hence we can obtain a good estimate of the Hurst exponent (H_{BB}) using short segment (2 s) of broadband EEG with 256 samples [131]. The single trial estimates of H_{BB} obtained from the 2 s EEG segments (Fig 5.1b) were validated using the longer stitched EEG segments of 80 s (Fig 5.3a).

We systematically identified and validated LRTCs in the short 2 s broadband EEG windows by establishing that there is a significant correlation in the data using surrogate test [246], then identifying the nature of these correlations as long-range dependence using ARFIMA modelling [32, 249] and finally showing that these long-range dependencies are in fact LRTCs (power-law decay of autocorrelation) using ML-DFA [127]. Clauset et al. [119] discuss that identifying power-law is a difficult problem and linearity on the log-log plot is a necessary but not sufficient condition for detecting the power-law. However, here we accept the assumption that the linear trend of the DFA fluctuations at different scales is an indicator of the power-law according to several studies in EEG [29, 36, 128].

Clauset et al. [119] also suggested that the best approach for identifying the power-law is by comparing different models and determining whether the power-law is the best fitting model. Our rigorous analysis scheme is in line with this suggested approach and thus our results indicate that the broadband EEG indeed contains LRTCs.

According to Kantelhardt et al. the power-law is valid if it exists for at least one order of magnitude [125] which we obtain in the stitched broadband EEG (78 ms to 1 s). The LRTC in the single trial 2 s broadband EEG was present over a short range of 78 ms to 0.5 s. The analysis of stitched broadband EEG of 80 s allows us to extrapolate that this LRTC dynamics holds up to 1 s (Fig 5.4a). The range of 78 ms to 0.5 s falls within the recommended range for DFA plot of the filtered data by Li et al. [245] to avoid effects of filtering on DFA. The study by Hu et al. [33] also found LRTCs in the neuronal firing in the similar range of timescales

as ours which helps in confirming that LRTCs exist in the shorter timescales in the neuronal activity.

In spite of the presence of broadband LRTC in short range of timescales irrespective of the length of the data, they do not extend over longer timescales. The stitched H_{BB} plots in Fig 5.5 show that there is a crossover at 2 s (2^8). This suggests that the broadband activity may be multi-fractal [124], in which a single power-law is valid in the range of 78 ms to 1 s. In the timescales beyond the crossover point, there is a different scale-free trend (manifested by the linear log-log behaviour) with different scaling exponent, the investigation of which is beyond the scope of this paper since we do not observe these timescales in single 2 s windows. Multi-fractal systems are often modelled by stochastic processes. Similarly, we also modelled our arrhythmic broadband EEG using ARFIMA by considering it as a stochastic process with LRTC.

The range of timescales over which H_{BB} is valid is especially interesting because it enabled monitoring of the instantaneous modulations in the broadband LRTC, facilitating the detection of voluntary movement intention in single trials. These LRTCs over small timescales characterise long-memory of the faster processes as opposed to larger timescales that contain the long-memory of slower brain processes. In the case of a motor task, the brain has to switch between different cortical areas and modulate the neuronal activity selectively to produce dynamic movement; stronger LRTCs may provide favourable conditions for this [243]. This might be one of the reasons for the increase in the broadband LRTCs. We infer that the broadband activity is multi-fractal and more dynamic with changes happening over shorter timescales. Multi-fractality was also observed by Hu et al. [33] in neuronal firing during movement task. Consistent with our results, they also observed that the LRTCs increased during the reaching movement in neuronal firings that correlated with the movement trajectory and the LRTC was reset at the beginning of next movement.

Becker et al. [250] reported that the increase in power of alpha oscillations in the spontaneous activity caused a decrease in the long-range dependence in the lower frequency (<5Hz) broadband EEG. Extending their finding to a wider range of broadband frequencies, we also obtained this inverse relationship between alpha power (which decreases leading to ERD [26]) and broadband activity which increased during voluntary movement. However, it must be noted that Becker et al. concluded the existence of causality simply be identifying the lag at which the maximum correlation between the alpha power and LRTCs in < 5 Hz band occurs, which may not be sufficient to establish causality. Moreover, such causal relationship may not exist in the case of wider broadband LRTC (0.5-45 Hz), determination of which is out of the scope of this paper.

The LRTCs in EEG are usually detected in the amplitude fluctuations of the narrowband oscillations [29, 36, 43]. Such LRTCs of alpha oscillations decrease due to a sensorimotor stimulus or task [38]. We have also observed the same effect on LRTCs in the amplitude fluctuations of the alpha oscillations obtained from the stitched EEG windows (see Fig 5.3b). Computing LRTCs in the alpha oscillation amplitude requires a longer EEG segment. Thus LRTC analysis of alpha amplitude faces limitations on observing fast LRTC changes and their continuous assessment in single trials during a short event such as movement, unlike broadband EEG. The continuous monitoring of the ongoing changes in broadband LRTC achieved using 2 s sliding windows gives an additional dimension of information related to movement.

The movement caused modulations in the broadband and oscillatory dynamics, but in opposite directions and over different timescales. The H_{BB} and H_{alpha} obtained from stitched EEG are uncorrelated during the resting state and there is a switch in their behaviour during movement, when they become coupled and inversely correlated (with a strong average correlation coefficient of -0.8) (see Fig 5.4c). In the resting state, H_{BB} has lower variance and H_{alpha} has a larger range of observed values. Hence, the alpha amplitude and broadband LRTCs reflect distinct processes occurring during voluntary movement, capturing the slow processes on the macroscopic level and complementary fast processes on the microscopic level, respectively.

There may be several different mechanisms giving rise to the power-law dynamics [251]. Bedard et al. [252] suggest that ionic diffusion is responsible for frequency dependent electric conductivity in cortical tissue leading to 1/f scaling in the spectrum of macroscopic neural activity measurements. The LRTC is often considered as the characteristic of criticality in the brain processes [144, 62, 29] that allows for efficient processing, optimising the information transfer, storage capacity and faster adaptation to varying processing demands [37]. However, it is at best a necessary but not sufficient condition for criticality. The LRTC may arise from processes that are not at criticality. We also observed yet another process with LRTC in the broadband EEG which adds to the LRTCs that are ubiquitously present in several neuronal processes [34, 35, 29, 36, 128, 126, 133]. Switching between different cortical areas to perform quick movement is facilitated by the balance between excitation and inhibition [243]. Achieving excitation/inhibition balance may lead to critical dynamics that are enhanced resulting in the increase in LRTCs [243, 135, 62]. By analogy, increase in the broadband LRTC during the movement may also be a result of the excitation/inhibition balance. Further investigation is needed for understanding the mechanisms of broadband LRTC dynamics.

We have shown that we can reliably detect voluntary movement using LRTC from 2 s single broadband EEG segments prior to its onset with the average classification accuracy of

$75.88 \pm 6.4\%$ (Table 5.1). This can have applications in motor-based BCIs. The classification accuracies using broadband LRTC are comparable to the accuracies obtained in the BCI literature [71, 112, 200, 114]. The broadband LRTC is a novel neural correlate of the movement that provides additional and complementary information about the movement with high accuracy. When combined with ERD and MRCP, broadband LRTC features may improve hybrid classification accuracy. Though we used an offline analysis in this paper, the DFA analysis is done on single trial basis with movement detected every 100 ms based on the 2 s EEG segment and can be easily adapted for online BCI. We can also predict the movement intention on an average 0.5 s prior to the movement onset (Table 5.1), which is a useful attribute for BCIs. The successful application of broadband LRTCs as features for offline BCI serves as a robust method of validation of their dynamical changes occurring during voluntary movement. Having broadband LRTC as an additional neural correlate with the capability of detecting movement independently may also be useful in the cases where individuals are unable to operate BCIs with common ERD and MRCP features.

5.5 Conclusions

We have characterised the ongoing changes in the LRTCs in broadband EEG on short timescales using Hurst exponent (H_{BB}) during voluntary movement and used it to identify movement intention and execution of single asynchronous finger tap. The LRTCs in the broadband EEG increased significantly during movement intention and execution. This is in contrast to the decrease in the LRTCs in alpha oscillation amplitude envelope obtained in the literature (which we could only observe by stitching EEG trials together). Thus, there are complementary fast processes from scale-free broadband arrhythmic neuronal activity and slow processes from oscillatory neuronal activity contributing to voluntary movement generation.

The broadband LRTC has proved to be a novel neural correlate that can detect whether a movement is present every 100 ms on a single-trial basis with the accuracy of $75.88 \pm 6.4\%$. It can also predict the movement 0.5 s prior to its onset. Hence, the broadband LRTC provides a new stream of movement related information for application in BCI. If combined with other complementary neural correlates of movement such as ERD/S and MRCP, broadband LRTCs may improve the classification accuracies of motor-based BCIs.

Chapter 6

Modelling the Short and Long-Range Temporal Correlations in Broadband EEG during Movement using ARFIMA

Maitreyee Wairagkar, Yoshikatsu Hayashi, Slawomir J Nasuto

This chapter has been prepared for submission to the journal Frontiers in Neuroscience. The previous chapter identified LRTC in the broadband. This chapter models LRTC along with the short-range dependencies in the broadband EEG using ARFIMA model. This chapter also establishes the complementarity between the arrhythmic LRTC process and rhythmic ERD and also suggests the suitability of LRTC and SRD features for application in BCI.

Abstract

Electroencephalography (EEG) undergoes complex temporal and spectral changes during voluntary movement intention. There is more focus on narrowband spectral processes such as event-related desynchronisation (ERD) in the sensorimotor rhythms, however, the changes in the temporal dynamics, especially in the broadband arrhythmic EEG are not widely studied. The long-range temporal correlations (LRTC) are ubiquitously present in several neuronal processes. In this paper, we study the ongoing changes in the dynamics of long and short-range temporal dependencies (SRD) in the broadband EEG during movement intention. We found LRTC in very short 2 s windows of broadband EEG and modelled it using autoregressive fractionally integrated moving average (ARFIMA) model. The ARFIMA(p, d, q) allowed simultaneous modelling of LRTC process through its fractional

differencing parameter d and SRD processes through AR and MA parameters. We found that the broadband LRTC increased significantly ($p < 0.05$) during movement intention and execution. There was also a significant ($p < 0.05$) change in the SRD parameters during movement. To assess the complementarity of the broadband arrhythmic LRTC and narrowband spectral ERD, we computed ERD on EEG with and without LRTC and found that the presence or absence of LRTC in the broadband EEG does not affect the ERD. The LRTC and ERD are independent processes providing complementary information about the movement. We used the linear discriminant analysis classifier with hybrid features with combinations of LRTC, ERD and ARFIMA to detect movement intention. The ERD gave lowest classification accuracy of $72 \pm 5.8\%$, LRTC gave a higher accuracy of $75.9 \pm 6.4\%$, hybrid LRTC and ERD gave an accuracy of $78.2 \pm 6.9\%$ and the highest accuracy of $88.3 \pm 4.2\%$ was obtained for ARFIMA and ERD features together. The ARFIMA parameters were also able to predict the movement 1 s prior to its onset and LRTC and ERD features combined predicted movement 0.6 s before its onset. The ongoing changes in the long and short-range temporal dependencies in broadband EEG contribute to motor command generation and can be used to detect movement successfully. These temporal dependencies provide different and additional information about movement and can be used in brain computer interface.

6.1   Introduction

Movement being the primary mode of interaction with the environment makes studying the neuronal processes involved in it more interesting. The temporal and spectral changes occur in the neuronal processes during voluntary movement. Detecting the movement intention from identifying these changes in the neuronal processes observed in electroencephalography (EEG) not only helps in understanding motor command generation but also have applications in brain computer interfaces (BCI). Traditionally, spectral power changes in the narrowband oscillations in EEG such as event-related (de)synchronisation (ERD/S) [26] are used to determine movement. Along with these narrowband spectral processes, changes also occur in the temporal processes in EEG. It is known that EEG shows long-range temporal correlation (LRTC) [29, 39] which occurs because of the power-law decay of its autocorrelation. The alpha band amplitude shows LRTCs which are known to decrease during movement [38]. Despite both the temporal and spectral changes, narrowband spectral features such as ERD are explored more commonly [44, 90], especially for movement detection and its applications in BCI. The LRTCs during movement also primarily are obtained on the narrowband alpha amplitude of the longer segments of EEG [29, 135]. Such LRTCs require a repeated movement and could not be used for detecting the movement in real time from the ongoing

EEG. There is a paucity of research studying the ongoing temporal changes in the broadband EEG to detect movement on the single trial basis. In our previous study, we found that the autocorrelation of the broadband EEG decayed slower during movement [237]. Hence, here we investigate the temporal dependencies in the broadband EEG in details and also study its relationship with the ERD.

The temporal dynamics in the brain processes can be assessed by studying the temporal dependencies in EEG. These temporal dependencies can be directly observed from the autocorrelation function (ACF) of EEG. If the autocorrelation becomes zero after finite time lags or it decays exponentially, then the time series is said to have a short-range dependence (SRD), otherwise, if the ACF decays slower than exponential, then it has a long-range dependence (LRD) [253, 249]. A specific case of LRD is LRTC which is characterised by the power-law decay of the ACF [120]. LRTCs are widely observed in neuronal processes recorded at different levels that show power-law scaling such as neuronal firings [33], neuronal avalanches [34, 35], local field potentials [34], electrocorticography, and non-invasive EEG and magnetoencephalography [34, 36]. The spontaneous EEG is known to have LRTC [132, 36]. The EEG spectrum is of the form $1/f$ which shows power-law scaling. The LRTCs have been ubiquitously observed in both periodic and aperiodic neuronal processes in EEG such as various narrowband oscillation amplitude fluctuations [29, 39], alpha oscillation phase [120], broadband phase synchrony [37] avalanches [34, 35] and energy profile of EEG [133, 34].

The LRTCs in EEG are typically obtained in the alpha band amplitude fluctuations [38, 135]. It has been observed that during movement, the LRTC in the sensorimotor oscillations decreases possibly due to the disruption caused in the long-memory process by movement [38, 128, 126]. However, these alpha amplitude LRTCs completely disregard the LRTCs in the broadband EEG. The brain rhythms are non-stationary and not strictly restricted to the selected narrow sinusoidal frequency bands [103] and hence the LRTCs computed on such rhythms can overlook important features present in the entire power spectrum. The arrhythmic broadband processes and oscillatory processes coexist in the neuronal activity [23]. The broadband arrhythmic brain activity was previously considered background noise, however, recent studies demonstrate that it is physiologically and functionally relevant [23], its dynamics change with task demand and cognitive state and it has been associated with the excitation/inhibition balance of the neuronal populations [61]. It is hence interesting to determine the unexplored changes in the temporal dynamics of the arrhythmic broadband EEG during voluntary movement. The traditional narrowband analysis requires long EEG segments [29] and considers LRTCs as an invariant property of brain dynamics over several scales. This approach does not facilitate observation of the ongoing

instantaneous changes in LRTC. The [238] characterised changes in LRTCs using Kalman filter, but their timescales were several seconds long. Here we compute instantaneous changes in the LRTC using 2 s broadband EEG windows over shorter timescales to detect movement intention.

The LRTC can be quantified by the exponent of the power-law decay (α) of the ACF (ρ) following the relation $\rho(t) = Ct^{-\alpha}$ where C is a constant, and equivalently by taking its Fourier transform as the exponent (β) power spectrum of EEG (S) by the relation $S(t) = Bf^{-\beta}$, B is a constant, where $\beta = 1 - \alpha$ [120]. More conveniently, the Hurst exponent (H) can be used to quantify LRTC reliably [244, 131] because using above methods are challenging in practice. The relation between H and β is $H = \frac{1-\beta}{2}$ [244]. Detrended fluctuation analysis (DFA) [122] is commonly used to estimate Hurst exponent because it is effective on non-stationary time series [131, 39, 134].

In this study, we not only identify the LRTCs in the ongoing dynamics of the broadband EEG during movement but also model these LRTCs. One of the models for modelling the LRD process is autoregressive fractionally integrated moving average (ARFIMA) model. The ARFIMA(p, d, q) contains three components: autoregressive (AR) process of order p, moving average (MA) process of order q and LRD parameter d ($d = H - 0.5$) [32]. The ARFIMA is a generalisation of autoregressive integrated moving average (ARIMA) model. To model a non-stationary time series, an integrated model such as ARIMA(p, d, q) can be used as differencing a time series d times could make it stationary, after which the remaining stationary ARMA(p, q) parameters can be estimated. In the case of LRD time series with the power spectrum of the form $1/f$, the time series must be fractionally differenced to make it stationary. Hence ARFIMA(p, d, q) model with a fractional difference parameter d is more suitable [32]. We chose the ARFIMA model because it allows modelling both SRD and LRD simultaneously which enabled us to investigate the changes in the ongoing dynamics of both the types of dependencies during voluntary movement intention and execution. The ARFIMA is useful for modelling broadband EEG because these types of parametric models can describe completely the second order statistics of time series [139]. To our knowledge, ongoing changes in the dynamics of LRTC and SRD in the broadband EEG on short windows were not investigated during motor command generation and applied for detection of movement on a single trial basis.

In the literature, parametric models for time series analysis such as autoregressive, adaptive autoregressive, multivariate adaptive autoregressive [254] models were used for movement detection from EEG. However, these attempted to model only selected frequency band amplitudes (alpha and beta). None of the studies modelled the broadband EEG along with its long and short-range components.

We also investigated the relationship between these temporal dependencies in the broadband EEG and ERD during movement which remains unexplored in the literature. We hypothesise that the ARFIMA parameters related to LRTC and SRD can provide additional information about the movement which is complementary to the commonly used ERD and provide deeper insights into the processes involved in the motor command generation. We used BCI style EEG analysis pipeline where the ERD and ARFIMA features were estimated on a single trial basis to detect movement intention with high accuracies. The aims of this paper are 1) to provide a complete characterisation of temporal dependencies (SRD/LRD) in broadband EEG during movement; 2) to accomplish this using ARFIMA model and observe the effect of movement on its parameters; 3) to investigate the relationships between ERD and the temporal dependencies LRD and SRD; 4) to use the three independent streams of information provided by LRTC, SRD and ERD to classify movement intention for applications in BCI.

6.2   Materials and Methods

6.2.1   Participants

EEG was recorded from fourteen healthy participants (8 female, age 26 ± 4 years, 12 right handed) with no prior EEG and BCI experience. This study was carried out in accordance with the recommendations of the human experimentation guidelines of the University of Reading. The ethical approval for EEG experiment was obtained from the ethics committee of the School of Systems Engineering, University of Reading, UK. Informed written consent was obtained from all the participants prior to EEG recording in accordance with the Deceleration of Helsinki.

6.2.2   Experimental paradigm

We chose a self-paced, asynchronous single index finger tapping task. Each EEG trial started with a fixation cross at the centre of the screen for 2 s followed by an instruction for right index finger tap, left index finger tap and resting state in a random order. The participants were asked to perform the task at any random time of their choice within a window of 10 s following the instruction. To avoid cue effects, we instructed participants not to tap immediately after the display of the instruction. There was a break of 1 to 1.5 s at the end of each trial. The experimental paradigm was developed in MATLAB Simulink R2014a (The MathWorks, Inc., Natick, Massachusetts, United States) using the BioSig toolbox [205].

We recorded 40 EEG trials per condition at the sampling rate of 1024 Hz. EEG was later downsampled to 128 Hz for further processing. The impedances of all the electrodes were kept below 7 $k\Omega$. We recorded EEG using a Deymed TruScan 32 EEG amplifier (Deymed Diagnostic s.r.o., Hronov, Czech Republic) and EASYCAP EEG cap (EASYCAP GmbH, Herrsching, Germany). In this study, we used channels C3, Cz and C4 according to the international 10-20 system out of the 19 EEG channels recorded with a referential montage with reference on FCz and ground on AFz.

We recorded the onset of a finger tap with a bespoke microcontroller tapping device developed using an 8-bit Microchip PICDEM2 Plus demo board (Microchip Technology Inc., Arizona, USA) at 1000 Hz. The participants placed both the index fingers in the corresponding finger caps of the tapping device. The two channels of binary tapping signals, capturing the onset and duration of each finger tap were co-registered with EEG using TOBI SignalServer 2.0 protocol [208]. The EEG data is available from http://dx.doi.org/10.17864/1947.117 [209]. The details of the experimental paradigm and artefacts removal are given in [237].

6.2.2.1   Pre-processing and artefacts removal

We performed all EEG analysis offline in MATLAB. We filtered EEG using a fourth order zero-phase non-causal Butterworth filter to avoid phase distortions. The power-line noise was removed with a notch filter at 50 Hz. We removed the DC offset and the high frequency noise from EEG by band-pass filtering between 0.5-45 Hz.

We performed artefacts removal using independent component analysis (ICA) [236] using the EEGLAB toolbox for MATLAB [211], which uses an automated version of infomax ICA [212]. We manually identified and removed the independent components with artefacts. We visually inspected the reconstructed uncontaminated EEG again and eliminated any undesirable trials containing residual large artefacts. EEG was segmented into time locked trials of 6 s (-3 s to +3 s from the onset of the finger tap). These trials were divided into 2 s sliding windows from time $t - 2$ s to t shifted by 100 ms. The indices obtained at time t for a single trial were computed independently on a 2 s broadband (0.5-45 Hz) EEG window from $t - 2$ s to t.

6.2.3   Identifying long-range temporal correlation (LRTC) in broadband EEG using detrended fluctuation analysis (DFA)

Whether a time series has a long-range dependence or short-range dependence can be identified from the decay of its autocorrelation function (ACF) and log-log plot of its power spectrum. If the ACF decays according to the power-law and the log-log power spectrum

shows a straight line then the time series has LRTC. If the ACF decays exponentially and the log-log power spectrum is not linear, then it has SRD. To identify the temporal dependencies in the 2 s broadband EEG, we computed the ACF and log-log power spectrum obtained by squaring the Fourier transform. We plotted the grand average ACF and power spectrum of all the windows in all the trials in all the participants.

The LRTCs can be quantified by Hurst exponent using DFA [122] which facilitates the detection of the LRTC embedded in a non-stationary time series such as EEG by avoiding the artefactual dependencies caused by non-stationarity and trends [122, 134]. We performed the DFA on each 2 s sliding window of the broadband EEG which gave an estimate of the Hurst exponent H every 100 ms. The Hanning window was applied to each 2 s EEG segment prior to the DFA to avoid edge effects. The DFA was performed as follows:

1. The 2 s EEG window X of length N (256 samples) was integrated according to equation 6.1 where $k = 1, ..., N$ and Y is the integrated time series.

$$Y_k = \sum_{i=1}^{k} X_i - \bar{X} \tag{6.1}$$

2. The integrated time series Y was divided into N/n non-overlapping boxes of length n, where n is an individual timescale at which we computed the root mean square (RMS) fluctuations. We chose the timescales of $n = [10, N/4]$ samples (i.e [78 ms 0.5 s]). The box sizes of $n = [10, N/4]$ are commonly used to get good estimate of RMS fluctuations at each timescale with $[N/10, 4]$ number of boxes [131, 127]. We used 25 box sizes between $n = [10, N/4]$ equidistant on log_2 scale as our number of samples was a power of 2. [131] have shown that we can obtain correct estimates of Hurst exponent using a short time series of length 256 with DFA. Our box sizes were within the range suggested by [245] $[max(k+2, \frac{F_s}{F_{max}}), min(\frac{N}{4}, \frac{F_s}{F_{min}})]$ where $k = 1$ (linear detrending in DFA) for filtered data between F_{min} (0.5 Hz) and F_{max} (45 Hz).

3. At each scale n, for every non-overlapping segment of Y of length n, a trend was obtained by the least square linear fit. Y_n is concatenation of trends at a scale n for all the N/n boxes and the RMS fluctuations were computed according to equation 6.2 for each $n = [10, N/4]$.

$$F_n = \sqrt{\frac{1}{N} \sum_{i=1}^{N} (Y_i - Y_{n,i})^2} \tag{6.2}$$

4. The N was not fully divisible by n for each box size. Hence, we obtained the final RMS fluctuations by averaging the F_n computed using the steps 1 to 3 from the forward and backward direction of each EEG window X [134].

5. We computed the Hurst exponent by obtaining the slope of the linear fit to the log-log plot of RMS fluctuations at each timescale n ($log_2F(n)$ vs log_2n).

After obtaining H for each EEG window, exponential smoothing filter was used to smooth H in the consecutive sliding windows in the single trials to avoid noisy estimates.

The Hurst exponent estimated using DFA is valid and suggests the presence of the power-law in the fluctuations at different timescales only if the log-log DFA plot is linear. We validated the Hurst exponents H by assessing the linearity of the log-log DFA plot by comparing the fit of the linear, polynomial, logarithmic and exponential models to it using the ML-DFA method detailed in [127]. The LRTC is present in the time series if the Hurst exponent is between 0.5 and 1 [134, 29].

6.2.4 Modelling the broadband EEG using autoregressive fractionally integrated moving average (ARFIMA) model

The AFRIMA allows simultaneous estimation of both LRTC and SRD in a time series [32]. The ARFIMA(p,d,q) incorporates SRD processes through the AR parameters p and the MA parameters q, and the LRTC process through the fractional differencing parameter d. The ARFIMA(p,d,q) model in which d can have a fractional value is a generalised form of the ARIMA(p,d,q) model in which d is an integer denoting the level of differencing. The ARIMA(p,d,q) model which incorporates the differenced process with parameter d is itself a generalisation of the ARMA(p,q) model of a stationary process [31]. The ARFIMA(p,d,q) model is given by Eq 6.3 [120].

$$\left(1 - \sum_{i=1}^{p} \phi_i B^i\right)(1-B)^d X_t = \left(1 + \sum_{i=1}^{q} \theta_i B^i\right)\varepsilon_t \tag{6.3}$$

B is the backshift operator, such that $BX_t = X_{t-1}$ and $B^n X_t = X_{t-n}$, ϕ_p are the AR coefficients of the order p, θ_q are the MA coefficients of the order q and ε_t is an innovation at time t drawn from a normal distribution. For ARFIMA, d can have a fractional value. We estimated the ARFIMA(p,d,q) for each 2 s sliding window of the single trial broadband EEG by firstly fractionally differencing the series with d and then estimating the parameters of ARMA(p,q) as described in the following sections.

6.2.4.1 Removing LRTC from EEG with fractional differencing

The parameter d accounts for the LRTC in the ARFIMA process. The AR and MA parameters can only be estimated accurately for a stationary SRD process. The first step of fitting ARFIMA was to fractionally difference each 2 s EEG window by its corresponding fractional differencing parameter d to remove LRTC and make it stationary. The parameter $d = H - 0.5$, where H was estimated by the DFA method described in the previous section 6.2.3. The fractional differencing can be performed using a binomial series expansion as given in the Eq 6.4 with a Gamma function [255–257]. We used the Matlab fast fractional difference algorithm provided in [258] for fractionally differencing each EEG window.

$$(1 - B)^d = \sum_{k=0}^{\infty} \begin{pmatrix} d \\ k \end{pmatrix} (-B)^k \tag{6.4}$$

6.2.4.2 Identification of the order of the ARMA(p,q)

The AR and MA parameters p and q of the ARFIMA were estimated by fitting the ARMA(p,q) model to the fractionally differenced EEG window. The stability of the model was assessed by confirming the stationarity of the time series using augmented Dicky-Fuller test for unit root [259]. We then identified the model order of ARMA for each 2 s EEG window using Akaike Information Criterion (AIC) [129] by comparing the models with p ranging from 1 to 10 and q ranging from 1 to $p - 1$. The order of the best fitting ARMA(p,q) model which gave the least AIC for the maximum number of EEG windows in all the participants was chosen as the order of the AR and MA parameters of ARFIMA.

6.2.4.3 Estimation of ARFIMA(p,d,q)

Having identified the order of the ARMA part of the ARFIMA, we then estimated the AR and MA parameters p and q respectively using the Matlab functions *arima( )* and *estimate( )* from Econometrics toolbox [260] for each 2 s sliding broadband EEG window. The residual analysis was performed on the estimated model using Ljung-Box Q test [261] to assess whether the residuals have any significant autocorrelation and one-sample Kolmogorov-Smirnov test [262] to evaluate if the residuals have a normal distribution. All the parameters d, p and q obtained for each window were then plotted to assess the ongoing change during the trial.

6.2.5   Event-related desynchronisation (ERD) on single trial EEG

The ERD analysis was also done on individual 2 s EEG sliding windows. We used the band power method for characterising the ERD [26]. Each EEG window was band-pass filtered between 8-13 Hz (alpha band). The mean of each window was subtracted from itself. The analytic signal obtained from the absolute value of the Hilbert transform of EEG was used to get the amplitude of the alpha band. The band power was computed by taking the mean of the squared alpha band amplitude. The ERD is the relative change in the alpha band power from the baseline during movement. We computed the baseline alpha band power R for the individual participant by averaging the band powers of all the 2 s windows in all the resting state trials. We then computed the percent ERD at each time t by subtracting the baseline R from the band power of 2 s sliding EEG window A_t using $ERD_t = \left(\dfrac{A_t - R}{R} \right) \times 100$.

We also evaluated ERD as above on the fractionally differenced EEG windows to observe the effect of removal of LRTC from EEG on the ERD in alpha band.

6.2.6   Hybrid classifier for movement intention detection

From the temporal and spectral EEG analysis described in the previous sections, we computed three types of features: LRTC obtained from DFA, SRD obtained from the parameters of ARFIMA and well known ERD which could be used for detecting movement from EEG. We performed the classification using various combinations of the LRTC, SRD and ERD features to identify right tap vs resting state and left tap vs resting state independently using binary linear discriminant analysis (LDA). Our goal was to compare the performance of the classifier for movement intention detection using these features independently and with hybrid combinations of these features.

The classification was done on each participant independently. We trained a separate LDA classifier for each sliding window with the feature vectors from corresponding windows in all the movement trials and the same number of features vectors randomly selected from the resting state trials of that participant. Each LDA had 40 data samples (equivalent to the number of trials) with the selected number of features for each class. We used 10x10 fold cross-validation to assess the performance of the classifier by obtaining the classification accuracies, sensitivities and specificities at each time point in the trial given by the 2 s sliding windows. The 95% confidence level for binary classification (movement vs rest) was obtained from the binomial distribution with $n =$ number of EEG trials and $p = 0.05$. We also noted the time at which classifier crossed this threshold as the time of significantly identifying the movement intention.

6.3   Results

6.3.1   Autocorrelation function and power spectrum of broadband EEG during voluntary movement

We plotted the ACF and the log-log power spectrum of a 2 s EEG window from -1 s to +1 s of movement onset such that it contained the information regarding movement intention and execution. We also plotted the ACF and the log-log power spectrum of the corresponding resting state EEG 2 s window. Figure 6.1A shows that the ACF decays slowly (slower than exponential) in all the conditions indicating the presence of LRD. The ACF decays slower for right and left finger tapping indicating an increase in LRD. Figure 6.1B shows the log-log power spectrum which is linear in all the three conditions with a peak at approximately 10 Hz as expected. The linear log-log power spectrum suggests that the dependence is in fact LRTC. If the slope of the power spectrum is between -0.5 to -1.5, then it indicates LRTC in the time series [32]. The slopes that we observe are in the valid range for LRTC with a slightly increased slope for right and left finger tapping. We explore the increase in LRTC during the voluntary movement further in the next sections. The 10 Hz peaks for right and left finger tapping have lower power than that of the resting state peak, especially in channels C3 and C4; this clearly represents the ERD during voluntary movement.

6.3.2   LRTC in the broadband EEG using DFA

We obtained valid Hurst exponents for the LRTCs in 2 s broadband EEG windows in the range of 0.5 to 1 using DFA. The ML-DFA validated the DFA scaling exponents by selecting the linear model as the best fitting model to the log-log DFA fluctuation plots confirming the presence of the LRTCs in the broadband EEG. The LRTC was present in EEG in the movement state as well as in the resting state. Figure 6.2 shows the grand average Hurst exponent throughout EEG trial of all the participants during movement and resting states. We can see a clear increase in the LRTC during movement intention and execution. The Hurst exponent H increased significantly from the resting state between the grey dotted bars ($p < 0.05$, Mann-Whitney U test, n=14 (number of participants)). The H was used to obtain the fractional differencing parameter d for ARFIMA by subtracting 0.5 from it.

(A)

(B)
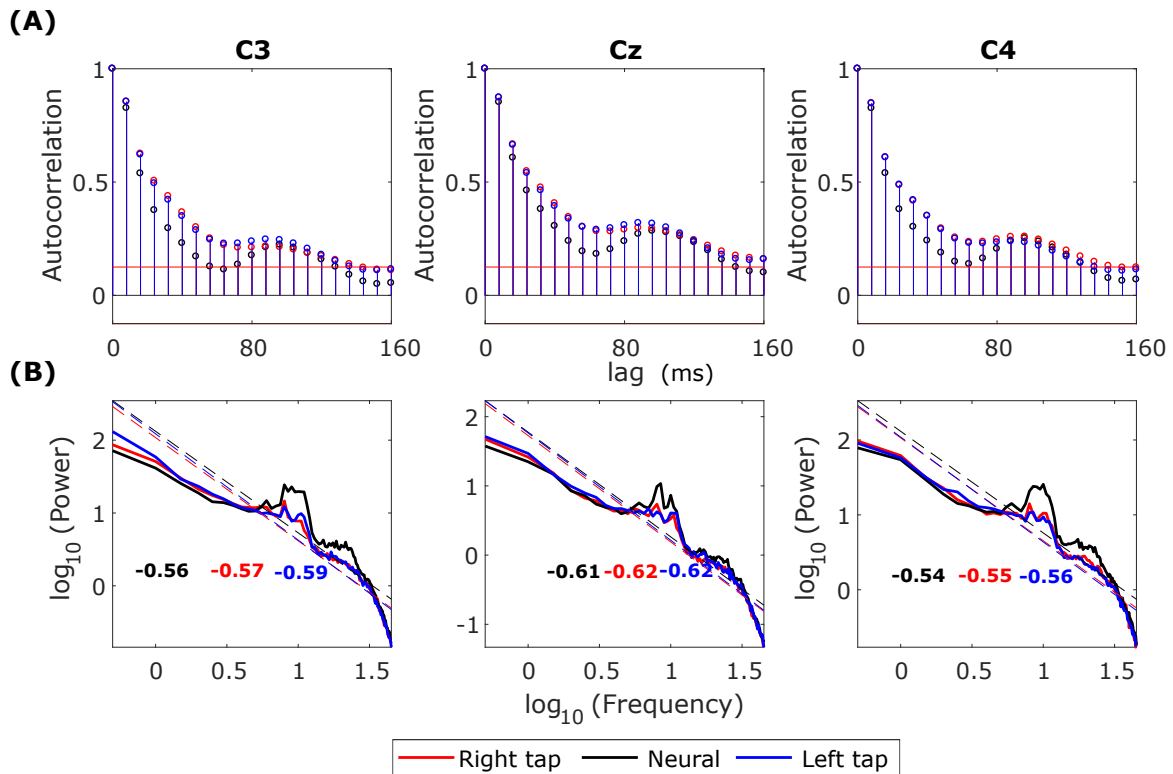
Fig. 6.1 **Grand average autocorrelation function (ACF) and power spectrum of EEG during movement.** (A) The grand average ACF of 2 s broadband EEG from -1 s to +1 s for all the participants for right finger tapping (red), left finger tapping (blue) and resting state (black) in channels C3, Cz and C4. The ACF decays slowly indicating the LRD. (B) The grand average log-log power spectrum in the channels C3, C4 and Cz for all the three conditions. The log-log power spectrum is linear in all the cases with slopes between -0.5 and -1.5 suggesting the presence of LRTC.

6.3.3   Modelling the broadband EEG using ARFIMA(p,d,q)

6.3.3.1   Removal of LRTC from EEG with fractional differencing

We examined the ACF and the log-log power spectrum of the fractionally differenced EEG windows with d to identify whether the LRTC has been removed so that the ARMA(p,q) model could be fitted. Figure 6.3 shows the grand average ACF, partial autocorrelation function (PACF) and log-log power spectrum of the fractionally differenced 2 s broadband EEG windows from -1 s to +1 s of movement onset in all the three conditions. Figure 6.3A shows that the ACF decays fast (after 4 lags) after fractional differencing and figure 6.3B shows that the partial ACF cuts off after 9 lags suggesting the presence of the SRD in the residual EEG.
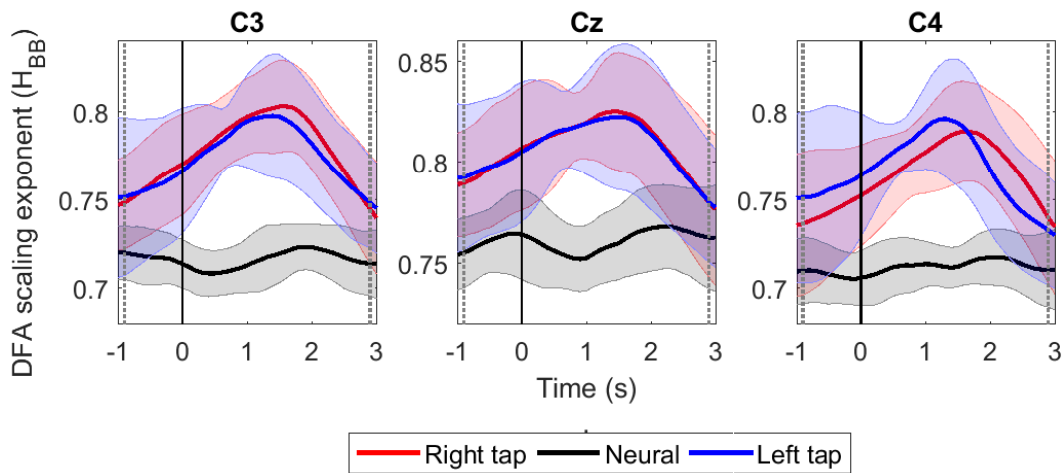
Fig. 6.2 **The grand average time evolution of Hurst exponents of broadband EEG (**H **quantifying LRTC)**. The progressions of grand average H in all the participants in channels C3, Cz and C4 during right finger tap (red), left finger tap (blue) and resting state (black). The LRTC increases during movement intention and execution. The movement onset is at 0s marked by a solid vertical line. The H of movement trials is significantly different from the H of resting state trials in the time region between the dotted grey vertical lines. The shaded areas shows the standard deviation.

The log-log power spectrum is also no longer linear. Figure 6.3C shows that the lower frequencies have been flattened creating a bend in the power spectrum which again confirms the removal of LRTC. The slopes of the power spectra are also outside the range of -0.5 and -1.5 for the LRTC. The decrease in alpha power in right and left movement conditions is still visible in the channels C3 and C4 as smaller 10 Hz peaks than that of the resting state which is consistent with the ERD.

6.3.3.2 Identification of the order of the ARMA(*p,q*) model

The fractionally differenced EEG was confirmed to be stationary by the augmented Dicky-Fuller test for unit roots ($p < 0.05$). EEG windows did not have unit roots indicating the stability of the ARMA model to be fitted to the SRD process.

Figure 6.3B shows that the partial ACF cuts off after 9 lags which can suggest the initial estimate of the AR order could be 9. According to the AIC, the order of the best fitting model was ARMA(10,0) for 85% of times of all the windows in all the trials in all the channels and all the participants. In some cases where the order of MA (q) was greater than zero, the roots were non-invertible and hence we set $q = 0$ since ARMA(p,q) can also be represented by AR(p) with higher order. The distribution of the selected orders of the models

(A)

(B)

(C)
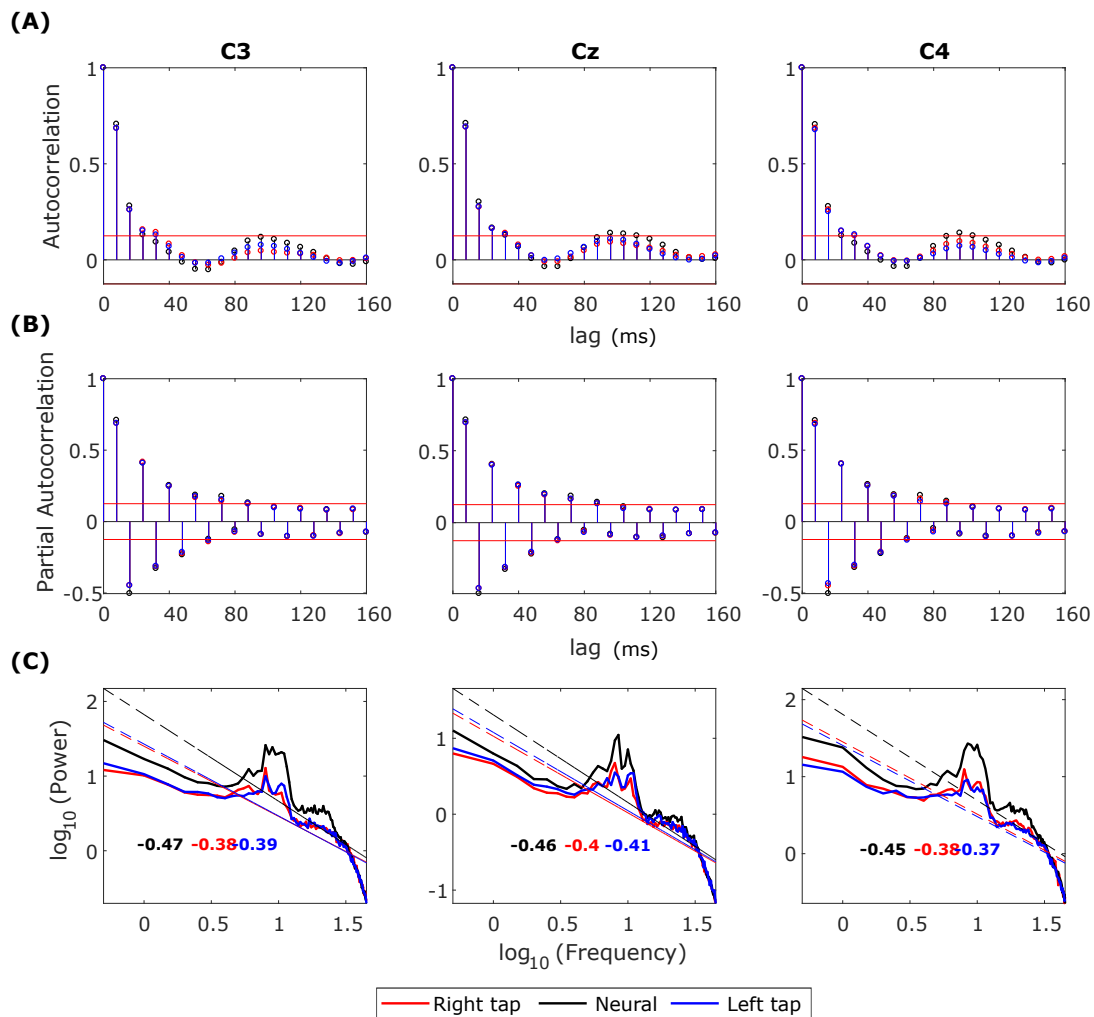
Fig. 6.3 **Grand average autocorrelation function (ACF), partial autocorrelation function (PACF) and power spectrum of the fractionally differenced EEG.** (A) The grand average ACF of 2 s broadband fractionally differenced EEG from -1 s to +1 s for all the participants for right finger tapping (red), left finger tapping (blue) and resting state (black) in channels C3, Cz and C4. The ACF decays fast indicating SRD. (B) The grand average of partial ACF in all the three channels in movement and resting state conditions which cuts off after 9 lags. (C) The grand average log-log power spectrum in the channels C3, C4 and Cz for all the three conditions. The log-log power spectrum is no more linear with slopes outside the range of LRTC (-0.5 and -1.5).

by AIC remained the same for all the channels, all the participants, all the conditions before movement, during movement and after the movement. Hence we selected ARMA(10,0) for modelling the SRD in fractionally differenced EEG.

6.3.3.3 Estimation of ARFIMA(*10,d,0*)

The AR parameters of the order 10 were estimated and the residual analysis was performed on the residue of the model ARMA(10,0). The residual analysis using Ljung-Box Q test showed that for 95% of all EEG windows, the estimated ARMA(10,0) fitted well ($p < 0.05$) to the SRD process in the fractionally differenced EEG and there was no more information in the residuals left to be modelled. The Kolmogorov-Smirnov test confirmed that the residuals of all EEG windows had a normal distribution ($p < 0.05$). Thus we modelled 2 s broadband EEG windows successfully using ARFIMA(10,*d*,0) and estimated the 11 model parameters (*d* and 10 parameters for AR).

6.3.4 Changes in the long-range and short-range temporal dependence identified from the ongoing ARFIMA(10,*d*,0) during movement

ARFIMA incorporated the LRTC through the parameter *d* and the SRD through ten AR parameters. Figure 6.4 shows the grand average time progressions of these ARFIMA parameters throughout the movement trial in all the participants. A clear increase in the parameter *d* was observed during movement intention and execution. The parameter *d* was significantly different in movement trials and resting state trials ($p < 0.05$, Mann-Whitney U test, $n = 203688$ (individual windows on which parameters were estimated in all the participants)). The first six of the ten AR parameters showed change during movement in all the three channels. Though there is a change during movement, there is no significant difference in the individual parameter in the movement trials vs resting state trial for all the participants together. Thus, on grand average, during movement there was a change in the SRD in the broadband EEG though not significant, whereas, the LRTC in the broadband EEG increased significantly.

Same results were obtained on individual participants for *d* on single trials. However, there was a lot of variability in the AR parameters in the individual participants. 10 out of 14 participants showed a significant change in the AR parameters between resting state trials and movement trials ($p < 0.05$, Mann-Whitney U test, $n = 40$ (number of trials, note that the p-value was obtained at each time point during the trial)). Out of the 10 participants that showed a significant change, 80% showed a change in all the three channels and 90% showed a significant change in at least the first 6 AR parameters. These parameters had a higher magnitude. None of the participants showed a significant change in AR parameters 8, 9 and 10 which had lower magnitude. The absolute values of the AR parameters decreased gradually in the higher order parameters. The consecutive order AR parameter values alternated between positive and negative as seen in the figure 6.4.
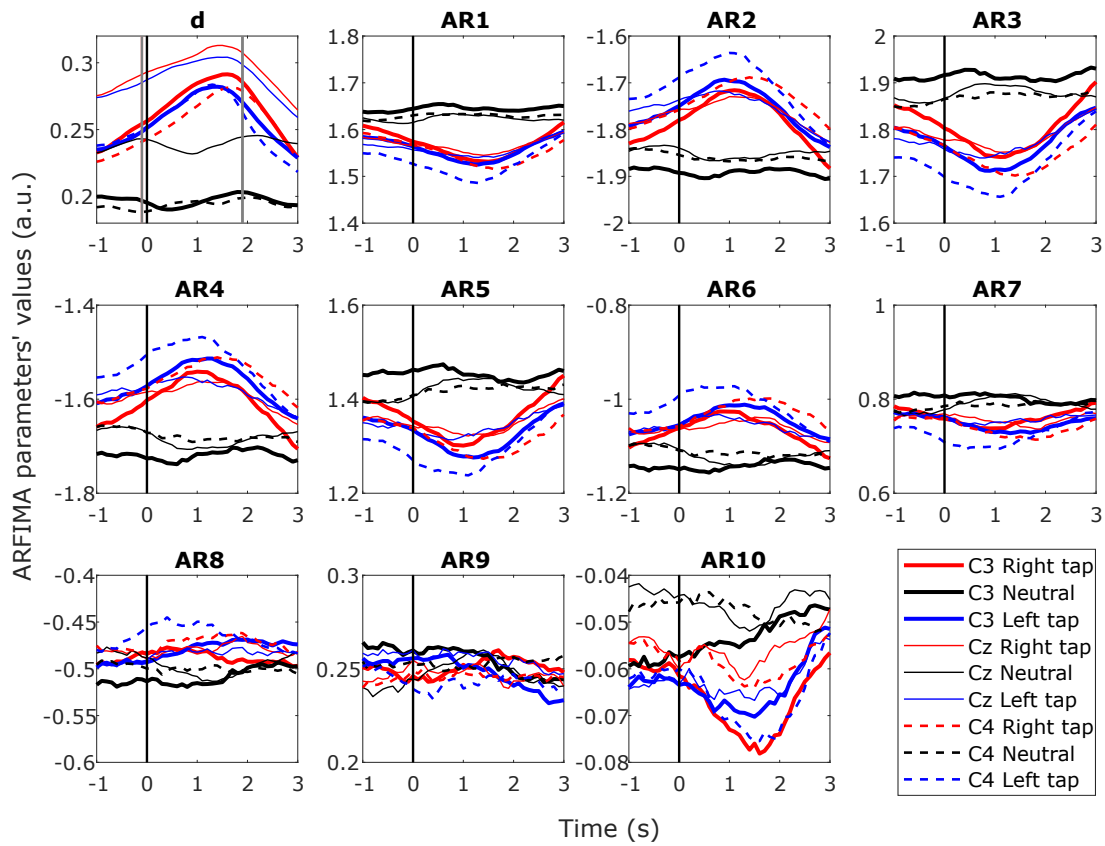
Fig. 6.4 **Time progression of the grand average ARFIMA(10,*d*,0) estimated parameters for the broadband EEG.** The time progression of ten grand average AR parameters reflecting the dynamics of short-range dependence and fractional differencing parameter *d* reflecting the dynamics of long-range dependence (LRTC) throughout the trial in C3, Cz and C4 for right finger tapping, left finger tapping and resting state. The movement onset is at 0 s marked by a solid vertical line. The grand average AR parameters for SRD did not change significantly during movement, whereas the parameter *d* increased significantly ($p < 0.05$) during the movement.

6.3.5 Relationship between short and long-range temporal correlation and ERD

We tested the effect of LRTC on ERD by comparing the ERD on raw EEG having LRTC and EEG having SRD after removing the LRTC using fractional differencing. Figure 6.5 shows the ERD with and without LRTC (solid line and dotted line respectively) in right finger tap, left finger tap and resting state. Both the ERDs follow similar traces and show a significant decrease in the alpha band power during movement as compared to the resting state ($p < 0.5$, Mann-Whitney U test, n=14 (number of participants)) as expected. However, the difference between ERD with and without LRTC was not significant as seen from the

difference between the dotted and solid line in the figure 6.5. The difference is negligible in the resting state (black) and right finger tapping (red). Same results were obtained for the individual participants' ERD on single trials. Thus, the ERD is unaffected by the presence of LRTC in EEG. This indicates that the LRTC and ERD are different and independent processes.
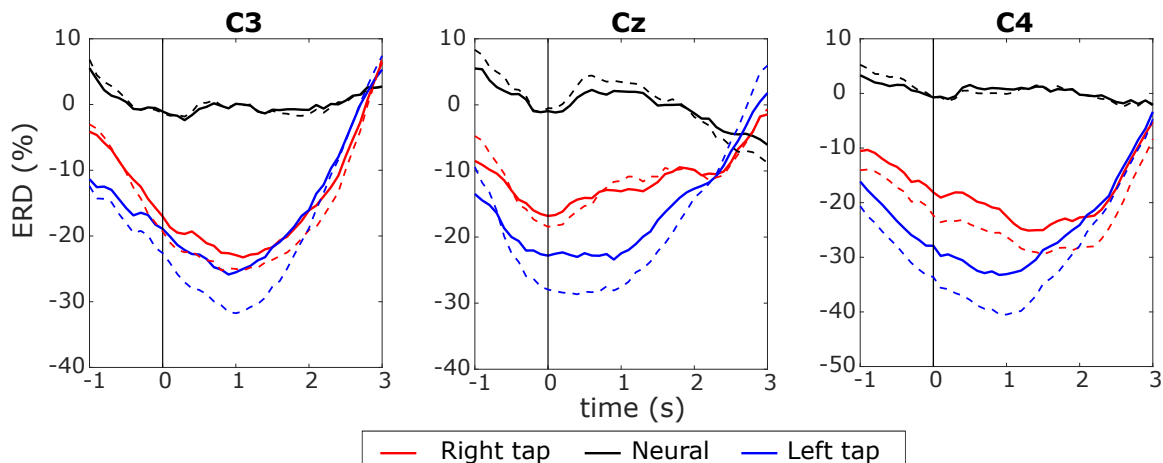
Fig. 6.5 **Time progression of the grand average ERD with and without long-range dependence.** The solid lines show the time progression of grand average ERD on raw EEG which contains LRTCs in the right finger tap (red), left finger tap (blue) and resting state (black) trials from all the participants. The dotted lines represent the ERD after removing LRTCs from the broadband EEG by fractionally differencing it by d. The movement onset is at 0 s shown by a solid vertical line. Both the ERDs during movement are significantly different from the resting state ($p < 0.05$). ERDs with and without LRTCs are not significantly different. Both the ERDs are very similar during resting state, and ERD without LRTC is slightly greater which is seen more clearly in the left tap condition.

We also studied the relationship between LRTC and ERD by comparing the Hurst exponents H with the ERD values. The ERD decreased whereas the LRTC increased during the movement. The scatter plot of the grand average ERD and LRTC in figure 6.6A shows a strong inverse correlation between them with the high correlation coefficients for right and left finger tap conditions. There was no correlation between ERD and LRTC during the resting state. During movement, there is a switch in the dynamics of ERD and LRTC and they become coupled from their uncorrelated state during the resting condition.

The figure 6.6B shows the distribution of lags at which there is a maximum correlation between LRTC and ERD in single trials in all the participants in all the three conditions. The correlation is maximum at lag 0, which indicates that LRTC or ERD processes do not precede one another and occur at the same time.
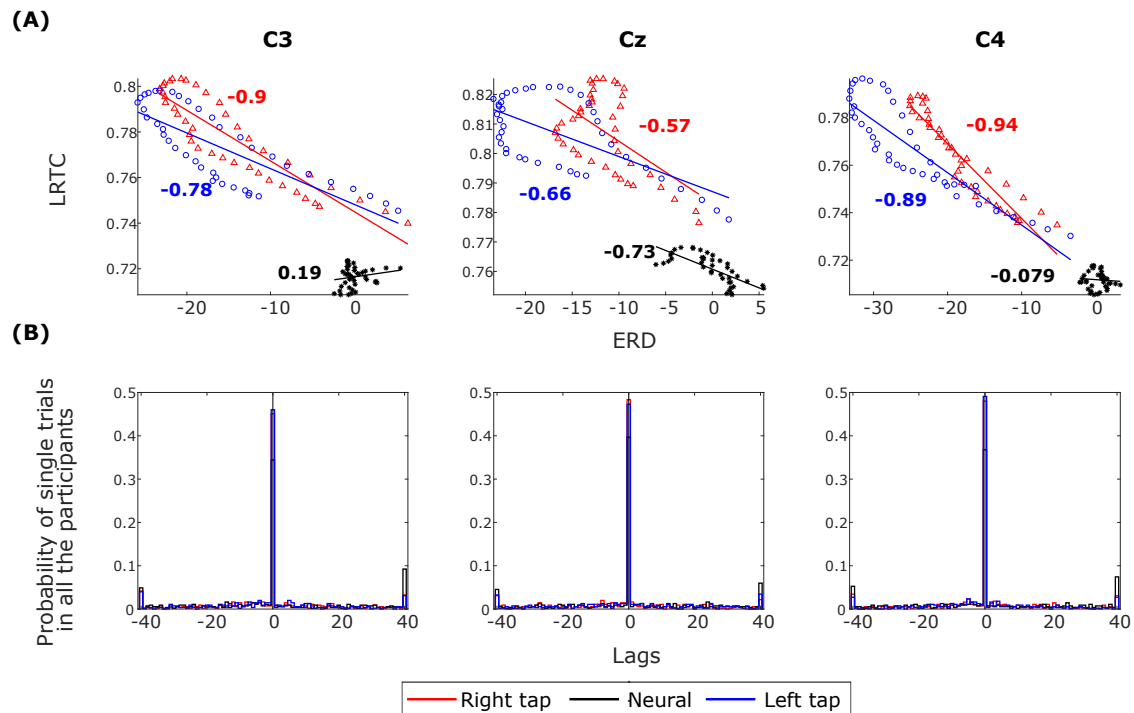
Fig. 6.6 **The correlation between ERD and LRTC.** (A) Scatter plot shows strong inverse correlation between ERD and LRTC during right (red) and left (blue) finger tapping in channels C3, Cz and C4. There is no correlation between ERD and LRTC during resting state (black). The correlation coefficients are shown beside the fitted straight lines. (B) The distribution of lags with maximum cross-correlation between LRTC and ERD in single trials of all the participants in all the three conditions. The LRTC and ERD have maximum correlation at lag 0.

6.3.6 Hybrid classifier for movement intention detection

We compared the LDA classification accuracies for movement intention detection using hybrid features of LRTC, ERD and ARFIMA. For the LRTC features, we used H from all the three channels C3, Cz and C4 as LRTCs were observed in all the three channels with equal strength (figure 6.2). For the ERD features, we used channel C3 and C4 as Cz showed relatively less distinction between movement and rest ERD (figure 6.5). For the ARFIMA features, we used parameters d and AR1 to AR6 from all the three channels since these AR parameters significantly changed in most participants during movement ($p < 0.05$) leading to 21 features. The classification accuracies, sensitivities and specificities for all the participants using all the classifiers are shown in table 6.1 and 6.2. The classification accuracies of ERD with and without LRTC (not shown in the table) were the same.

Left finger tapping

P no.	LRTC			ERD			LRTC+ERD			ARFIMA+ERD		
	Acc. (%)	Sen. (%)	Spe. (%)	Acc. (%)	Sen. (%)	Spe. (%)	Acc. (%)	Sen. (%)	Spec. (%)	Acc. (%)	Sen. (%)	Spe. (%)
1	73.00	73.25	72.75	69.13	88.75	49.50*	73.38	76.75	74.00	86.88	86.50	87.25
2	87.55	91.02	84.08	84.29	96.73	71.84	89.59	93.88	85.31	93.88	95.10	92.65
3	73.75	74.25	73.25	69.13	86.25	52.00*	73.50	71.00	76.00	90.00	88.25	91.75
4	81.88	82.00	81.75	76.25	82.50	70.00	79.38	78.00	80.75	90.75	91.50	90.00
5	74.88	83.00	66.75	74.13	95.50	52.75*	78.63	90.75	66.50	87.13	89.25	85.00
6	71.63	77.14	66.12	72.86	76.73	68.98	77.55	80.82	74.29	86.94	88.16	85.71
7	65.00	61.75*	68.25	72.75	65.25	80.25	70.63	62.00*	79.25	84.00	86.50	81.50
8	80.38	81.00	79.75	70.00	86.00	54.00*	80.63	79.25	82.00	89.00	89.00	89.00
9	73.25	68.50	78.00	69.88	74.00	65.75	67.25	66.25	6825	82.50	81.25	83.75
10	66.63	60.50*	72.75	63.88	71.25	56.50*	69.00	70.50	67.50	92.38	88.50	96.25
11	87.88	90.25	85.50	81.00	97.75	64.25	88.00	89.00	67.50	94.63	95.00	94.25
12	74.00	72.75	75.25	75.50	94.75	56.25*	77.00	82.50	71.50	88.75	93.25	84.25
13	72.50	73.00	72.00	69.25	59.25	79.25	74.88	70.50	79.25	86.00	81.75	90.25
14	77.38	73.50	81.25	73.63	87.25	60.00*	88.88	87.75	88.25	93.75	96.00	91.50
Mean	75.69	75.85	75.53	72.98	83.00	62.95	77.82	78.50	77.13	89.04	89.29	88.79
SD	6.77	9.10	6.32	5.23	12.12	10.08	6.97	9.66	7.17	3.74	4.57	4.35
Med.	73.88	73.88	74.25	72.81	86.13	62.13*	77.28	78.63	77.63	88.88	88.75	89.50

Table 6.1 The peak LDA classification accuracies for the left finger movement vs resting state for all the participants using LRTC, ERD and ARFIMA features. All values except the ones marked by * are significantly above chance level($p < 0.05$).

Right finger tapping

P no.	LRTC			ERD			LRTC+ERD			ARFIMA+ERD		
	Acc. (%)	Sen. (%)	Spe. (%)	Acc. (%)	Sen. (%)	Spe. (%)	Acc. (%)	Sen. (%)	Spec. (%)	Acc. (%)	Sen. (%)	Spe. (%)
1	75.88	72.00	79.75	67.25	81.50	53.00*	78.75	74.75	82.75	89.88	90.50	89.25
2	84.49	81.63	87.35	84.69	97.14	72.24	92.65	88.98	96.33	95.71	97.96	93.47
3	71.25	76.25	66.25	65.50	72.50	58.50*	71.25	72.00	70.50	81.25	78.00	84.50
4	77.13	76.25	78.00	72.75	81.25	64.25	82.63	84.00	81.25	88.25	88.00	88.50
5	77.50	78.50	76.50	75.00	95.25	54.75*	79.00	84.25	73.75	87.50	91.50	83.50
6	77.96	79.59	76.33	71.22	77.96	64.49	86.33	85.71	86.94	93.06	93.88	92.24
7	65.50	70.50	59.50*	69.50	61.25	77.75	68.38	59.25*	77.50	83.25	82.25	84.25
8	79.00	77.50	80.50	67.25	92.75	41.75*	80.50	84.25	76.75	89.25	87.50	91.00
9	78.50	75.25	81.75	74.88	87.25	62.50	71.63	73.50	69.75	80.63	83.50	77.75
10	74.63	74.75	74.50	62.50	55.50*	69.50	74.75	73.50	76.00	85.63	84.75	86.50
11	89.25	92.50	86.00	80.75	97.50	64.00	89.00	87.25	90.75	92.13	90.00	94.25
12	74.63	76.00	73.25	73.50	87.00	60.00*	75.25	78.25	72.25	89.13	87.25	91.00
13	65.38	66.50	64.25	65.75	72.00	59.50*	72.00	72.00	72.00	82.00	80.50	83.50
14	74.38	72.25	76.50	64.00	58.00*	70.00	78.50	79.50	77.50	88.50	90.25	86.75
Mean	76.07	76.39	75.75	71.04	79.78	62.30*	78.62	78.37	78.86	87.58	87.56	87.60
SD	6.40	6.05	7.92	6.40	14.30	9.00	7.14	8.11	7.94	4.56	5.40	4.64
Med.	76.51	76.13	76.51	70.36	81.38	63.25	78.63	78.88	77.13	88.38	87.75	87.63

Table 6.2 The peak LDA classification accuracies for the right finger movement vs resting state for all the participants using LRTC, ERD and ARFIMA features. All values except the ones marked by * are significantly above chance level($p < 0.05$).

The LRTC features showed higher classification accuracies than the ERD features. Combining the LRTC and ERD features improved the classification accuracies further. The hybrid classifier with ARFIMA and ERD gave the highest mean classification accuracy of $88.71 \pm 4.12\%$ and the accuracies. The classification accuracies using ARFIMA features alone was only marginally lower (by 1-2%) than hybrid ARFIMA and ERD classifier (not shown in the table). The ERD, LRTC and ARFIMA accuracies were also correlated i.e the participant with lower classification accuracy with LRTC and ARFIMA also showed lower classification accuracies with ERD.

Statistical tests on classification accuracies of LRTC, ERD, LRTC+ERD and ARFIMA+ ERD for all participants were performed by doing multiple comparisons using the non-parametric repeated measures Wilcoxon signed-rank test. Correction for six multiple comparisons between four types of features mentioned above was done using the Holm-Bonferroni method [224] at a significance level of 0.05. The Holm-Bonferroni method was chosen because it is uniformly more powerful and less conservative than Bonferroni correction for multiple comparisons. The classification accuracy with ARFIMA+ERD was significantly higher than all the other features ($p < 10^{-5}$). The next highest accuracy was of LRTC+ERD which was significantly higher than LRTC and ERD ($p < 0.004$). The accuracy of LRTC was significantly higher than that of ERD ($p < 0.0006$) with ERD having statistically the lowest accuracy of all the features.

The LRTC classification accuracies, sensitivities and specificities were all similar which shows that this classifier is robust and reliable. The hybrid classifier of LRTC and ERD and ARFIMA and ERD also showed the same robustness. Interestingly, the ERD classifier had high sensitivity but low specificity leading to lower accuracy. This indicates that by using ERD we are likely to identify movement with higher accuracy but also get more false positives during the resting state. Considering these results, including the LRTC and SRD temporal dependency features improves the movement intention detection instead of using only ERD. The LRTC and SRD provide complementary information to ERD about motor command generation.

The classification accuracies did not change after using the principal components obtained from PCA on the ARFIMA features for each participant. Around 8 principal components accounted for 95% variance in all the participants. Using these components gave an average accuracy of 79%. However, using the remaining principal components also gave a classification accuracy of about 79%. In fact, any subsection of the ARFIMA features gave similar classification accuracy. The classification accuracy was highest when all the ARFIMA features were used and dropped to the accuracy similar to hybrid LRTC and ERD features when the number of features was drastically reduced. This suggests that all the features

obtained from ARFIMA were symmetrical and equally important. The feature space became sparser as the number of features increased leading to higher classification accuracies.

6.3.6.1 Timing of movement intention detection

The figure 6.7 shows the time at which the classification accuracies crossed the significance threshold (chance level) in all the four classifiers. The LRTC, ERD and ARFIMA all were able to detect movement intention before its onset in most of the participants. On average, ERD detected movement -0.25 s of the actual movement onset, LRTC detected it at -0.5 s, hybrid classifier with LRTC and ERD detected it even earlier at -0.6 s and ARFIMA with ERD detected movement earliest at -1 s. All the classifiers with temporal features detected movement earlier than ERD. This shows the suitability of the hybrid classifier with temporal dependency features for application in the BCI.
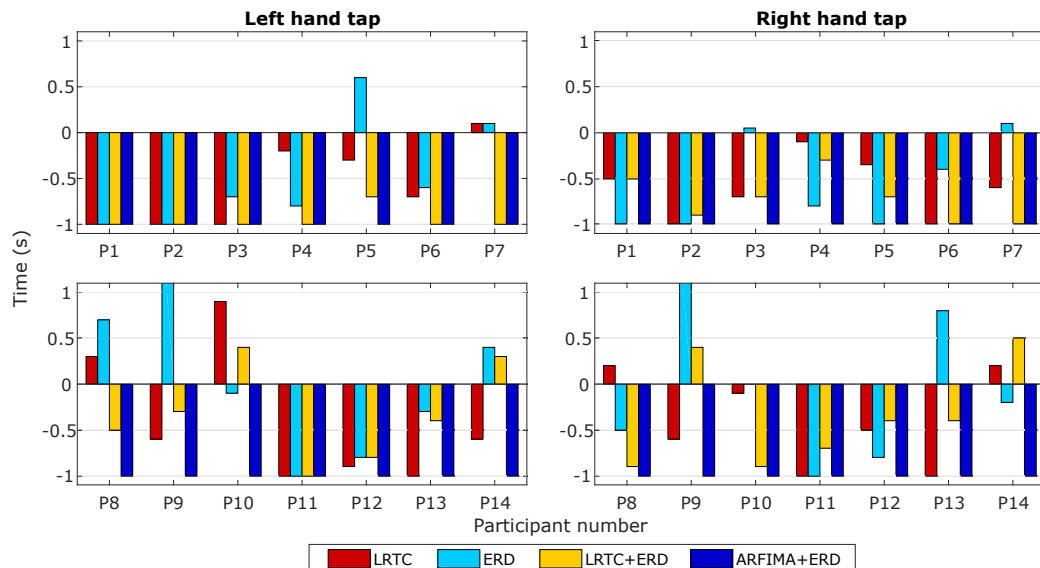
Fig. 6.7 **The timings of movement intention detection.** The timings of movement intention detection when the classification accuracy crossed the significance threshold for right finger tap and left finger tap are shown for all the 14 participants. Timings for participants 1 to 7 are in the first row and timings for participants 8 to 14 are in the second row. Timings obtained from four classifiers using LRTC, ERD, hybrid LRTC and ERD and hybrid ARFIMA and ERD features are shown with distinct colours.

Statistical tests on timings of movement intention detection of LRTC, ERD, LRTC+ERD and ARFIMA+ERD for all participants were performed using the non-parametric repeated measures Wilcoxon signed-rank test and corrected with Holm-Bonferroni method [224] for multiple comparisons at a significance level of 0.05. The ARFIMA+ERD features detected movement intention significantly earlier than all the other features ($p < 10^{-3}$). There was

no significant difference in the movement intention detection timings of LRTC, ERD and LRTC+ERD.

6.4   Discussion

We characterised the short and long-range temporal correlations during movement. We have not only identified the ongoing changes in the dynamics of these temporal dependencies in the broadband EEG but also modelled them successfully using ARFIMA(10,d,0). Several other studies model EEG with ARMA models [263–265, 86, 266], however, these models are suitable for processes with SRD. We have shown that the broadband EEG contains LRTCs and hence ARFIMA model is more suitable since it incorporates both LRTC and SRD simultaneously. After fractionally differencing the broadband EEG by ARFIMA parameter d, the residual EEG still contained SRD that were modelled by the *AR* parameters of ARFIMA. Modelling only LRTC or SRD would not have given a complete characterisation of all the temporal dependencies in the broadband EEG. We monitored the ongoing changes in both the LRTC and SRD in broadband EEG continuously to detect movement intention with high accuracy which has not been done before.

The order of AR parameters of ARFIMA that we identified using AIC is in the similar range as the orders used by studies modelling EEG with AR. The AR orders identified by other studies were between 9 and 13 by [137], 10 by [84], 8.67 by [138] and 16 by [136]. The AIC or Bayesian information criterion are common methods for finding the model order which we also used for model order identification.

We found that the LRTC increased significantly during the movement ($p < 0.5$) consistently in all the participants. This shows that the LRTCs play a role in movement generation. Even though there was a change in the SRD parameters, there was a lot of variability in different participants and hence was it less robust. The SRD parameters changed significantly ($p < 0.5$) in 10 out of 14 (71.4%) participants. The ARFIMA is a detailed mathematical model for time series but it does not give an explanation of the underlying physiological processes and interpretation of EEG [32]. However, it helped us to identify the LRTC and SRD processes in the broadband EEG and observe the ongoing changes in their parameters simultaneously during movement.

Most of the studies use AR and MA models simply for extracting the features from EEG, mostly from sensorimotor rhythms for BCI classification, however, these studies do not describe the nature of the ongoing changes in the model parameters during motor activity [263–265, 86]. The parametric ARMA models were used to characterise spectral features of specific bands, especially of the sensorimotor rhythms for movement [264, 84,

161, 266, 267]. The ongoing changes in the LRTCs were not studied previously and LRTCs have not been used for identification of movement intention. Here we show the average temporal evolution of individual parameter of ARFIMA containing both the LRTC and SRD during movement. These broadband temporal dynamics are more robust because they do not need a selection of participant specific frequency bands for better performance [26, 223].

We estimated the ARFIMA parameters offline on 2 s windows shifted by 100 ms with the online type of processing pipeline. We obtained new model parameters every 100 ms describing the ongoing changes in the LRTC and SRD that allowed us to detect the movement intention. The sliding window approach has been commonly used for estimating model parameters for non-stationary time series [266] where the model is estimated at each time window. However, the model estimation and residual analysis is computationally expensive and might need efficient execution for BCI classification, where delays in the command generation from EEG are not suitable. The LRTC quantification, on the other hand, is achievable within the available time window for EEG processing and will not induce delays in the BCI. This could be a suitable approach for movement detection which is informed on the actual ongoing temporal dynamics instead of simply using the model parameters without studying them.

Figures 6.1 and 6.2 show the LRTCs in short 2 s broadband EEG windows. We have confirmed that the LRTCs can be detected on short windows in broadband with rigorous analysis and ML-DFA [127] for validating the Hurst exponent. The removal of the LRTCs by fractionally differencing EEG destroyed these long-range dependencies leading to flattening of the power spectrum in lower frequencies as seen in Figure 6.3 which is an indicator of SRD. This showed that the broadband EEG contained both SRD and LRTC, the former was only observed after removing the latter.

The ERD is a well established narrowband process occurring during movement. We studied the relationship between the arrhythmic broadband LRTC and the narrowband rhythmic ERD, and how the LRTC affects ERD. The LRTC which increases during movement is strongly and inversely correlated with the ERD which decreases during movement. Removing the LRTC from the broadband EEG does not affect the ERD significantly. This can be seen from figure 6.5. The LRTC and ERD belong to the different degrees of freedom of movement generating neuronal process as the LRTC is represented by the broadband $1/f$ process and the ERD is represented by the alpha peak that resides over this $1/f$ spectrum. [250] suggested that the alpha power causes the change in LRTC which they observe from the negative lag of maximum correlation between alpha power and LRTC in the spontaneous EEG. However, this is not sufficient to conclude the causal effect between the alpha power and LRTC. We also plotted the lags of maximum correlation between ERD and LRTC and observed that

there was a maximum correlation between the two at lag zero (see figure 6.6). We did not observe the precedence of ERD. Thus, empirically we found that the broadband LRTC and ERD are independent processes and one does not cause the other. Though we found no causal relationship between the two, they both change during motor command generation which might suggest that there may be a common underlying process causing the changes in the independent processes of the ERD, LRTC as well as SRD.

Another independent neuronal process known to occur during movement intention is motor-related cortical potential (MRCP) or Bereitschafts potential [53, 51]. [268] used an AR model with exogenous input by incorporating the Bereitschafts potential as the exogenous input for movement detection. They also observed an increase in the classification accuracy by combining the features from complementary processes. We have previously shown that the changes in the temporal dependencies are also complementary to the MRCPs [231] because MRCP characterises the trend of EEG by eliminating the fluctuations and on the contrary, the LRTC characterises the dynamics in the fluctuations by eliminating the trends using DFA. Thus we have independent processes of LRTC, SRD, ERD and MRCP containing complementary information about motor command generation.

The hybrid classifier with ARFIMA parameters and ERD has a feature vector with high dimensionality and gives high classification accuracies. It was clear that increasing the feature vector dimensionality improved the classification accuracy significantly ($p < 10^{-5}$) than just ERD, LRTC or their combination which had maximum 5 features. We used 10×10 fold cross-validation scheme to mitigate for overfitting with ARFIMA parameters. The ARFIMA parameters reinforce the difference between the resting state and movement as multiple parameters show a clear distinction between the two conditions (see Fig 6.4) . Higher dimensionality made the feature space sparse, making it easier for LDA to find an optimum classification boundary. It is common in BCI to have feature vectors of high dimensionality as generally several features are extracted from several channels and used for classification [269]. For example, the study in [254] used 52 features. The training sets in BCI are often relatively small because of the time consuming EEG recording processes which is also exhausting for the participants [269]. Our hybrid classifier thus follows common practices in BCI giving high classification accuracies. However, it would be interesting to observe whether the classification accuracies using ARFIMA features remain the same after increasing the number of trials significantly.

Despite using the 10×10 fold cross-validation scheme with the ARFIMA features, we cannot exclude a possibility that the high classification accuracy obtained using large number of ARFIMA features might be a consequence of overfitting. The main limitation of this study is the small number of EEG trials per class which can possibly lead to overfitting of LDA

classifier using ARFIMA parameters as features. As a rule of thumb, there should be 10 times more training samples than the number of features [207]. Hence, the true classification accuracy using ARFIMA parameters can be assessed after using at least 10 times more EEG trials than the number of features.

The PCA on the 21 ARFIMA features revealed that the classification accuracies remained the same. The classification accuracies decreased when the principal components with the largest variance were chosen and it increased when more principal components were added to it. The accuracy was similarly high with any subgroup of the principal components but lower than that of all the components. Finding the optimum coordinate system by PCA on raw features did not improve the classification accuracy because the feature matrix was sparse and symmetric. The robustness of the ARFIMA features can be determined by studying the performance of the classifier with more number of trials for training.

The ERD has higher sensitivity and it is likely to give more false positives during the resting state leading to lower overall accuracy (Table 6.1 and 6.2). The LRTC based classifier has similar sensitivity and specificity indicating that the LRTCs are not biased towards movements and provide overall higher accuracy. The movement and resting state can be identified with equal accuracy using LRTC features. The ARFIMA features also showed similar sensitivity and specificity. The ARFIMA and ERD features together also show low standard deviation in the accuracies of different participants. The movement can be predicted earliest using all the hybrid features containing ARFIMA and ERD up to 1 s prior to its onset. LRTC alone can predict the movement 0.6 s prior to its onset and ERD can predict movement latest at 0.25 s prior to its onset. The ARFIMA and LRTC features facilitate the earliest detection of the movement intention which can be beneficial for the use in BCI.

6.5   Conclusion

We investigated the ongoing dynamics of all the temporal dependencies in the broadband EEG during movement intention. We showed that the broadband EEG have LRTC and we studied the ongoing changes in its dynamics using as short as 2 s sliding EEG windows. Removing the LRTC by fractional differencing revealed the underlying SRD in the broadband EEG. We modelled the LRTC simultaneously with the SRD using ARFIMA(10,d,0) model where the parameter d represents the LRTC process and the AR parameters represent the SRD process.

The broadband LRTC increased significantly ($p < 0.05$) during movement in all the three channels C3, Cz and C4 of all the participants. There was also a change in the SRD parameters, however, this change was not significant in all the participants. Only 10 out of

14 participants showed significant changes in the SRD. The presence or absence of LRTC in the broadband EEG did not affect the ERD. The ERD or LRTC also did not precede one another during movement. Hence, the LRTC and ERD are independent processes contributing to voluntary movement generation and provide complementary information about the movement.

We were able to predict the movement using the ongoing changes in the temporal dependencies with high accuracies. The LRTC gave better classification accuracy than the ERD and hybrid LRTC and ERD features gave better classification accuracy than the individual features. The best classification accuracy was obtained for hybrid ARFIMA and ERD features ($88.3 \pm 4.2\%$) which was significantly better than the rest of the classification features ($p < 0.05$). We could also predict movement 1 s before its onset using hybrid ARFIMA and ERD features and 0.6 s before its onset using hybrid LRTC and ERD features. Hence these temporal dependencies of LRTC and SRD could be used in the online BCI.

Chapter 7

General Discussion

7.1   Novel contributions

This thesis characterised the dynamics of the temporal dependencies in the broadband (0.5 - 45 Hz) EEG during voluntary movement intention using sliding windows of 2 s. This thesis has discovered a new arrhythmic broadband temporal process capturing the ongoing fast dynamics from very short segments of EEG. This ongoing arrhythmic process is distinct from the rhythmic processes (oscillations) and slow cortical potentials (ERP) and provides an additional information about an event. This arrhythmic process has been characterised by the short and long-range temporal dependencies that change significantly during movement. The temporal dynamics of the arrhythmic EEG have unmasked the novel properties of the ongoing changes in the long-range dependency neuronal process that has not been observed previously. This thesis has identified a novel correlate of movement. This novel phenomenon can be used to acquire a deeper insight into different cognitive events.

The following main findings are the novel contributions to the knowledge of the temporal dynamics of the broadband EEG, and motor command generation and movement intention detection from EEG:

1. The temporal dynamics of the broadband EEG change during movement intention and execution represented by the slower decay of its autocorrelation. During movement, the autocorrelation has larger relaxation time due to slow decay as opposed to resting state when the relaxation time is small due to faster decay.

2. The slowing of the autocorrelation decay is observed in any subset of the frequencies and is similar to that of the broadband EEG. This suggests similar dynamics across different spectral scales.

3. The autocorrelation decays according to the power-law which indicates LRTC in the broadband EEG. The LRTC in short 2 s windows represents fast scale-free dynamics over small timescales.

4. The LRTC quantified by the Hurst exponent using DFA increases significantly ($p <$ 0.05) during movement intention and execution.

5. The novel approach of evaluating ongoing LRTC, a property of temporal dynamics which is typically considered as invariant over longer periods has been discovered. This allowed for movement detection from the ongoing EEG.

6. The increase in the broadband LRTC is in contrast to the decrease in the LRTC in the alpha band fluctuations during movement. The broadband LRTCs were obtained on 2 s windows whereas to observe LRTCs on the alpha band, longer segments had to be created by stitching the corresponding EEG windows from all the trials and could not be used to detect movement from ongoing EEG.

7. The broadband EEG not only contain LRTC but also SRD which is observed after removing LRTC from EEG using fractional differencing. These long and short-range dependencies were simultaneously modelled using ARFIMA.

8. The SRD parameters also changed significantly ($p < 0.05$) during movement intention in the majority of the participants, but had larger inter-participant variability.

9. The ongoing changes in the LRTC and SRD were able to detect movement with higher accuracy than the ERD and MRCP. The hybrid combinations of these features that included temporal dynamics have higher classification than the ones without.

10. The movement can be predicted as early as 1 s prior to its onset using temporal dependencies.

11. The ERD showed bias towards movement and had higher sensitivity and lower specificity leading to false positives during resting state, lowering the performance of the movement detection. The LRTC did not show such bias and was more robust and accurate predictor of movement.

12. The temporal dynamics of the broadband EEG are independent and complementary to the ERD and MRCP and give different information about the movement intention.

13. The LRTC and SRD could be used in applications in BCI for robust movement detection.

14. The LRTC is very robust as it does not need a selection of participant specific frequency band or spatial location.

15. The new approach of studying the changes in the fast dynamics of short and long-range temporal dependencies in the broadband EEG on single trial basis serves as a novel neuroscience tool to study the persistent neuronal processes in the brain across all the frequency bands and several timescales.

7.2 Discussion

7.2.1 Complementarity of arrhythmic LRTC and rhythmic ERD

The ERD/S only represents the relative changes in the average amplitude of spectral power in different frequency bands, but the LRTC and SRD in broadband analyse the temporal changes in entire EEG spectrum by characterising the underlying much complex neuronal dynamics. The former describe spectral characteristics of the rhythmic processes and the latter describe the scale-free temporal dynamics with complex interactions in arrhythmic process. The broadband LRTC is represented by the $1/f$ spectrum and the ERD is the distinct peak in alpha frequencies that is present on the top of this $1/f$ spectrum as shown in Fig 7.1 and hence it can be discerned even visually that these two components of EEG provide different dimensions of information and are complementary.

7.2.2 Complementarity of fluctuation dynamics of LRTC and slow potentials of MRCP

The MRCP and LRTC processes characterise opposite properties of EEG. The MRCP is identified by extracting the trends or slow potentials which are considered to contain event-related information by eliminating the fluctuations in EEG. On the other hand, the LRTC is identified by extracting the temporal dynamics of the fluctuations over several timescales by removing the trends in EEG. In the MRCP, the ongoing fluctuations in EEG are considered as noise and are eliminated by averaging over several trials, whereas in the LRTC, EEG fluctuations are considered useful and their complex dynamics are characterised. This contrast is shown in Fig 7.2 [270]. These two processes are hence independent and complementary.

Thus, this thesis takes a very different approach towards the analysis of the broadband EEG dynamics and demonstrates that the fluctuations in EEG in fact contain important information about voluntary movement intention which otherwise would have been neglected
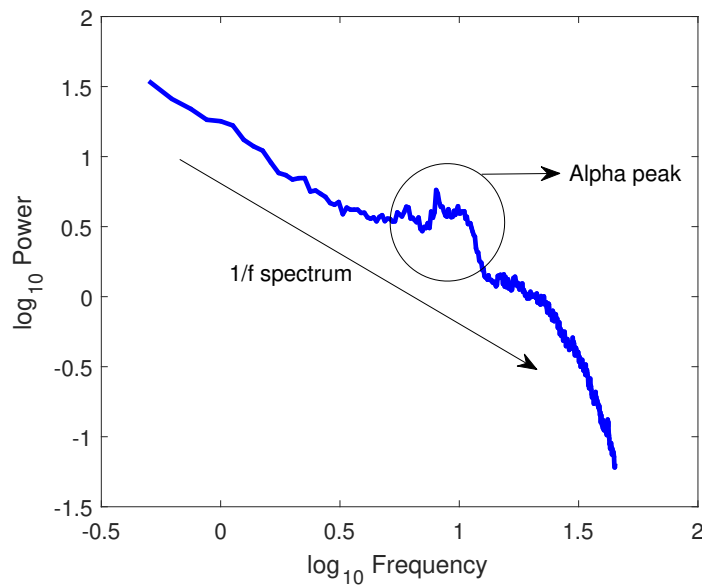
Fig. 7.1 **Power spectrum of EEG** The average power spectrum of EEG of all the participants in log-log scale which shows $1/f$ broadband spectrum and a distinct peak at the alpha power around 10 Hz.

in the MRCP. This has been shown in chapters 4, 5 and 6. Typically, in MRCP, the fluctuation noise in EEG is reduced by averaging over several trials and hence single trial extraction of MRCP which is required for online movement detection is difficult [271] but still implemented [272]. The LRTC and MRCP also mostly do not overlap in their frequency composition since MRCP is restricted to very low frequencies and the broadband LRTC contains all the frequencies. The Fig 7.3 shows the expanse of ERD, MRCP and LRTC in time around movement onset and frequencies.

7.2.3 Relationship between the broadband LRTC and alpha oscillation

The study done by Becker et al. [250] suggests that the alpha rhythm is the main component that drives all the functional processes and causes LRTC. However, chapter 6 investigates the relationship between the alpha band and the broadband LRTC and finds that even if the progression of these processes is inversely correlated during the movement, there is no evidence of causation. It was found that alpha band amplitude changes do not cause changes in the LRTC and neither does it precedes the changes in the LRTC.

The oscillations are prevalent features of EEG believed to play the main role in functioning of the brain. However, recently it has been shown that the oscillations, traditionally assumed to be sinusoidal can be non-sinusoidal [273]. Fourier approaches of analysing these
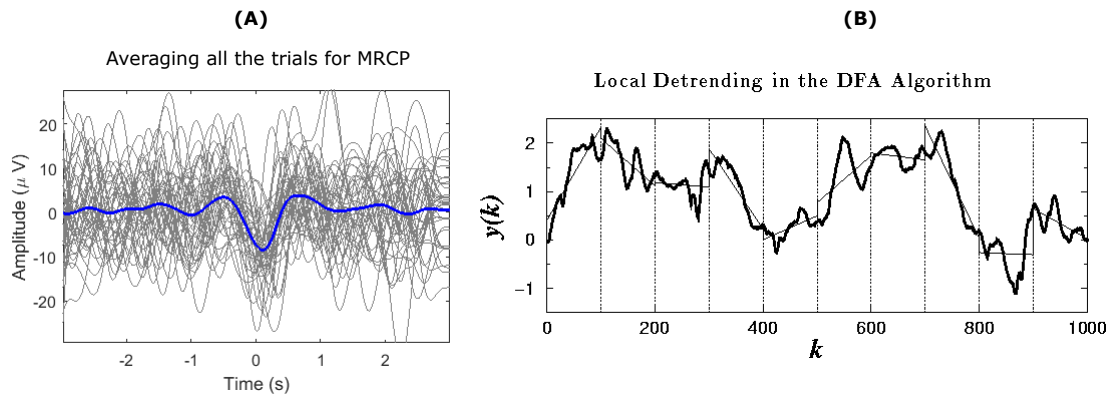
Fig. 7.2 **Comparison of MRCP and LRTC** (A) The MRCP obtained by averaging over all the trials is shown. Averaging eliminates the fluctuations in individual trials (grey) to reveal the slow negative potential of MRCP (blue) around movement. The movement onset is at 0 s. (B) The detrending step at a particular timescale in DFA to extract the fluctuations in single trial for determination of LRTC. This sub-figure is adapted from [270].

oscillations can disregard the non-sinusoidal features of these oscillations and overlook their crucial information content which needs new analysis methods [103]. Moreover, the oscillations are extracted using pre-defined frequency bands from EEG, which in reality are not well defined and may change in different individuals, so the frequency bands may not represent actual oscillations. The analysis of the oscillations is conducted without consideration of underlying arrhythmic processes. The arrhythmic processes are dynamic and change under different circumstances and these changes can affect the properties of oscillations such as central frequency, power and bandwidth [61]. Also, the broadband arrhythmic EEG contains fast dynamics which cannot be obtained from characterising the dynamics of individual oscillations. Hence, it is important to analyse rhythmic and arrhythmic components of EEG separately as they provide complementary information. This has been achieved in chapters 3, 5 and 6 of this thesis.

7.2.4   LRTC in broadband EEG and its application in BCI

The LRTC in the broadband EEG was found on short timescales between 0.78 ms to 1 s. The chapter 5 discusses that this might be because the broadband EEG could be multifractal having different scaling exponents at different timescales. The presence of multifractality is a valid assumption because the broadband arrhythmic EEG activity is very complex with multi-layered temporal dynamics. The LRTC found in these particular timescales is especially useful for detecting the ongoing changes in the temporal dependencies in the short events, such as movement. This is because these changes during the movement are fast and do
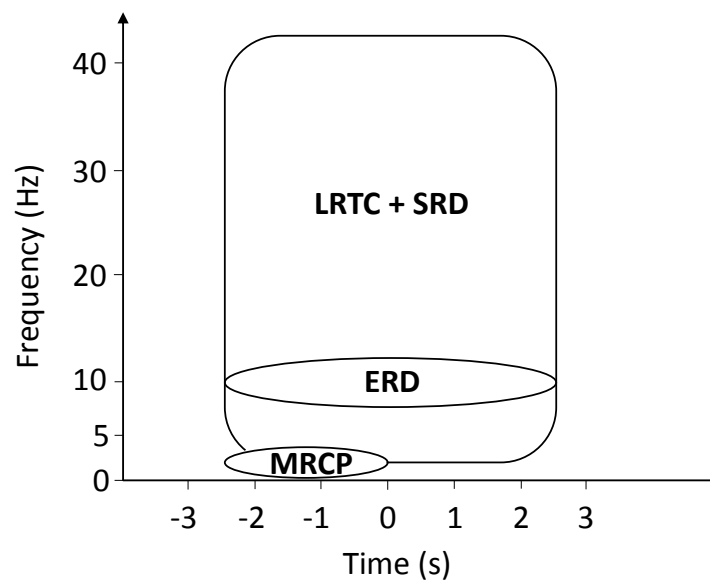
Fig. 7.3 **Time and frequency expanse of ERD, MRCP, LRTC and SRD processes** The figure shows the time relative to the movement and frequencies in which ERD, MRCP, LRTC and SRD processes occur during movement intention and execution.

not persist over long time and hence cannot be detected at the longer timescales. On the other hand, shorter timescale cannot be used to determine the scaling exponent of LRTC robustly because of insufficient number of samples available at these shorter timescales. Hence, the scale over which the LRTC is observed is optimal for the purpose of detecting ongoing dynamics during movement. The proof of principle of using the temporal dynamics for BCI to control virtual reality and soft robotics systems is demonstrated in the published work [174]. This work which is first authored by Maitreyee Wairagkar, the author of this thesis who developed the BCI, was done in collaboration with the colleagues who developed the virtual reality and soft robotic systems, is given in the Appendix A.

In chapter 3, the temporal dependencies in the broadband EEG were characterised using an exponential fit to the autocorrelation which gave an initial estimate of the nature of its decay. Later in the chapter 5, it was found that the decay of the broadband autocorrelation was in-fact power-law giving rise to LRTC. Nevertheless, the changes in the decay of autocorrelation from the baseline during movement could still be modelled accurately using both the exponential decay and power-law even though the exponential decay was not the most accurate model.

The LRTC was found with equal strength in all the three channels C3, Cz and C4. There was no lateralisation for right hand vs left hand movement. This may be due to the spread of LRTC over the motor cortex due to volume conduction. The other reason might be that

the changes in the broadband LRTC are neural correlates of movement intention and other general properties but does not encode information of handedness and hence is not localised.

The study by Robinson et al. [232] that used our method of broadband autocorrelation decay showed that the temporal dependencies also encode information about the speed of the movement. This validated the broadband temporal dependencies approach proposed in this and also showed its repeatability. This work indicated that the ongoing changes in LRTC during different types of movement can also reveal other properties of movement such as speed.

The thesis used DFA for quantifying the broadband LRTC. The DFA technique was chosen because it is known to give correct estimates of LRTC over short timescales and it is effective for non-stationary data such as broadband EEG due to the detrending step. However, Bryce et al. [274] claims that linear or polynomial detrending in DFA is not an effective approach for eliminating non-stationarity and in fact can introduce artefacts into the results because the non-stationary times series consists of more complex trends. In this thesis, these complex trends were removed by subtracting the mean of the upper and lower envelopes of broadband EEG, however, this took away information from the fluctuations instead of just trends and hence was not useful to get accurate estimate of the LRTC. This thesis studies the LRTCs over very short timescales, over which the linear approximation of trends for detrending in DFA is more appropriate.

Chapter 6 shows that the ARFIMA is more accurate for modelling the broadband EEG containing LRTC. In the literature however, AR, MA or ARMA models for SRD processes were commonly used [136, 137, 84, 138]. These studies did not model the broadband EEG, but instead, again focused on modelling individual oscillations, especially the alpha band with ARMA models to extract their spectral properties during movement and thus despite doing analysis in the temporal domain, restricted to the canonical spectral properties. The ARFIMA modelled SRD and LRTC simultaneously, however, there was more variability in the SRD parameters among participants. Therefore LRTC is more robust indicator of movement. The modelling can also be computationally expensive and must be executed efficiently for movement intention detection for BCI. Moreover, the high classification accuracy of ARFIMA features should be tested for overfitting using higher number of EEG trials in the future to develop a robust BCI.

7.2.5   Mechanisms of LRTC

There are several mechanisms in the brain that may give rise to LRTC. The possible mechanisms of LRTC are discussed in chapter 5. The brain is said to have evolved to criticality without any external driving force and hence displays SOC, a state of imbalance in which

it is ready to respond to changing cognitive demands efficiently. The criticality of the brain is merely a hypothesis based on the observation of power-law statistics in several different neuronal processes. The LRTC, which represents power-law dynamics of the fluctuations of neurophysiological signals is often considered as the hallmark of criticality in the brain [29, 120, 62]. However, the presence of power-law dynamics in the form of LRTC is not sufficient to conclude the presence of criticality [275, 276]. Nevertheless, the SOC hypothesis is widely accepted because the brain shares common features with SOC systems, such as large numbers of components (neurons), non-linear interactions between them, presence of perturbations caused by stimuli, stochastic behaviour and information processing via spatiotemporal correlations [29]. In the literature, the criticality is suggested to be present in the different EEG oscillations [29, 43].

Two instances of LRTCs, broadband LRTC and alpha oscillation LRTC with different scaling exponents were observed in EEG. The different scaling exponents suggest that the underlying neuronal mechanisms of these two processes are distinct [29]. During movement, the changes in the LRTCs happen in the opposite directions, the broadband LRTC increases while the alpha oscillation LRTC decreases. In the critical state, the perturbations such as movement intention can disrupt the ongoing activity, leading to ERD which is suppressed alpha oscillation and consequently reduction in the alpha LRTC which has been observed in chapter 5. However, since this is the case of LRTCs of oscillations which take place on longer timescales, the processes leading to simultaneous increase in the broadband LRTC on short timescales may be different and may not be critical. It is hence difficult to assume any underlying mechanisms of the broadband LRTC and to find the the evidence of criticality in the broadband LRTC is difficult.

One of the physiological interpretation of brain being poised at criticality is that there is balance between excitation and inhibition [62, 243]. Poil et al. [62] showed that the LRTC in oscillations and critical dynamics arise simultaneously in networks in which excitation and inhibition are balanced causing steady oscillations leading to optimum signal propagation. Samek et al. [243] also found that the oscillatory LRTCs were individual-specific. Switching between different cortical areas to perform quick movement is facilitated by the balance between excitation and inhibition [243] which may lead to increase in criticality during movement. The increased broadband LRTC may be the manifestation of this phenomenon. However, all the research in the literature in the related areas study the criticality in oscillations and hence it is difficult to identify whether the broadband LRTCs are consequence of criticality or excitation/inhibition balance.

This thesis would like to propose another hypothesis for the change in LRTC and SRD during movement. Zhigalov et al. [43] showed that the closed-loop stimuli can change the

LRTCs. By analogy, there is a possibility that the change in LRTC during movement is caused because of the feedback loop between thalamus and cortex. The systematic change in both LRTC and SRD during movement may have been caused by an underlying driving signal. This driving signal sets a thalamocortial feedback loop causing increase in the broadband LRTC and also change the excitability in the local neuronal populations leading to changes in the SRD. The same driving signal may also cause ERD by changing the recruitment of the neuronal population that fire in sync. However, further investigation will be needed to assess this hypothesis of driving signal and thalamocortical feedback loop.

7.3 Conclusion

This thesis has shown that the complex temporal dynamics of the broadband EEG contribute to the neuronal processes involved in voluntary movement generation. Particularly, the LRTC in the ongoing single trial broadband EEG over short timescales increases significantly ($p < 0.05$) and the parameters representing SRD also show significant changes during the movement intention and execution. This thesis confirms that the broadband EEG which contains scale-free dynamics in the form of LRTC even on shorter timescales is functionally relevant and is not a background noise as it was considered in the past. The LRTC and SRD give additional information about the movement intention which is independent and complementary to the ERD/S and MRCP. This is observed from the improvement in the classification accuracies using hybrid features that included LRTC and SRD and earlier prediction of movement up to 1 s prior to movement onset as compared to the ERD and MRCP. The complete information about movement intention cannot be obtained if the temporal dependencies in the broadband EEG are disregarded.

Thus, this thesis proposes that there are three independent and complementary fundamental neural correlates of voluntary movement 1) changes in the temporal dependencies in broadband EEG (LRTC and SRD); 2) changes in the sensorimotor rhythms (ERD and ERS); and 3) changes in the slow negative cortical potentials (MRCP and BP). The changes in the broadband LRTCs were robust, selection of most responsive frequency band or spatial location was not required, LRTCs were quantified from short 2 s EEG segments on single trial basis, they give high classification accuracies and early prediction of movement before its onset. All these properties make LRTC suitable for application in motor-based BCI and improve its performance.

7.4 Impact

This thesis will have a broader impact on the fields of neuroscience of movement, neuronal processes in sensorimotor cortex, EEG analysis, scale-free dynamics and BCI. This will especially contribute to the improvement in the understanding of motor command generation and movement intention detection. The dynamics of the long-range temporal dependencies have not been previously employed to detect the movement from the ongoing broadband EEG. This not only provides a novel method of movement intention detection but also gives a deeper insight into the neuronal mechanisms for motor command generation. This research has helped in obtaining overall information about movement from single channels in real time adding to the previous knowledge which was limited to the phenomena of ERD/S and MRCP. This has led to three separate streams of movement related information from EEG.

This thesis has also contributed in identifying a novel approach of analysing EEG using broadband activity and LRTC on single trials. This has an impact on the overall treatment of the broadband EEG which used to be considered as a background noise. This thesis has emphasised the importance of the complex dynamics of the broadband EEG which has large amount of information about an event. The approach of using broadband EEG can give insight into the additional global properties of EEG instead of restricting the analysis to individual frequency bands and provide information that persists over several frequency scales at once. The broadband EEG allows the study of arrhythmic neuronal processes which cannot be observed from individual oscillations. This thesis also proved that the ARFIMA model estimated on sliding windows that can incorporate LRTC and SRD together is more suitable for modelling broadband EEG and the parameters of this model change on the ongoing basis reflecting the event. Such models estimated on sliding windows can have broader applications in the assessment of the dependencies in different neuronal processes.

This thesis has shown that the broadband EEG contains LRTC on short timescales and these LRTCs change during an event and contain information related to movement. The fast changes in the temporal dynamics captured by LRTC on short timescales have not been obtained before. This thesis has provided a motivation to identify such changes in LRTC during different events. Traditionally, the temporal dynamics of LRTC were considered invariant in a particular state and hence were obtained for the entire duration of EEG during that state. However, this thesis has shown that these dynamics of LRTC may change on the short ongoing basis and analysis of these fast dynamics may prove to be useful and can have functional relevance. This thesis has also demonstrated the importance of obtaining temporal dynamics on the single trial basis. Single trial analysis of EEG has been increasingly considered in various areas of neuroscience and hence the approach proposed in this thesis can be useful. The approach of determination of ongoing changes in LRTC on short scales

may prove to be useful for different broadband neuronal recordings such neural firings, LFP, MEG, EMG etc. since these recordings show the traditional invariant LRTC on longer timescales.

Finally, the research in this thesis can also have an impact on BCIs. The broadband EEG temporal dynamics on single trials provide additional information about movement improving its classification accuracy and is overall a robust marker of movement which does not need any fine tuning of spectral and spatial parameters. This novel signal processing for BCI have a potential of improving its accuracy and movement prediction time.

7.5   Future directions

The novel approach of extracting information from single trial broadband EEG by evaluating the ongoing dynamics of the short and long-range temporal dependencies could be used as a new research tool in neuroscience and it will be interesting to find its applications outside motor-related events. It will be interesting to study whether these fast changes in the LRTC are restricted to the motor-related tasks or can be observed in other cognitive processes such as mental calculations, memory tasks, speech tasks, mental states such as relaxation, attention, excitation, different emotional states and visual processes as well. Estimating the LRTC and SRD changes in the broadband recordings can give additional information about these cognitive processes and may contribute to the advancement of their understanding.

For studying motor command generation further, it would also be interesting to look at what other type of information can be obtained from ongoing changes in the temporal dependencies such as speed of movement, direction of movement, its force and the gesture or type of movement. The work done by [232] have already used our method of autocorrelation decay analysis to demonstrate that the speed of the movement can be decoded from the changes in the autocorrelation relaxation time. It would be interesting to study the changes in the temporal dynamics of the EEG during motor imagery of continuous movement with neurofeedback.

The broadband LRTC dynamics were similar in all the channels over sensorimotor region and there was no lateralisation. It will be useful to investigate LRTC's spatial localisation and spatial progression throughout the course of the event by using dense array of EEG electrodes to obtain higher spatial resolution. It will also be useful to study the differences in the broadband LRTCs on the source level (obtained using source localisation) compared to the surface electrode level during movement.

The understanding of the ongoing fast dynamics of the LRTC can be advanced by studying the spatial broadband long-range dependencies in neural networks and the spatial

impact of the broadband LRTC can be assessed. Studying the long-range dependencies in the temporal processes as well as the spatial neural networks can give further insight into the brain functioning and the impact of functional connectivity on the LRTC.

The next step in the research presented in this thesis would be studying the neuronal mechanisms giving rise to the fast dynamics of SRD and LRD and getting an insight on the physiological processes underneath. The mechanisms causing changes in LRTC and SRD would have to be investigated by considering the possibility of an external (extra-cortical) driving signal giving rise to changes in LRTC, for example by activating thalamocortical feedback loops. The causes of this increase in the broadband LRTC could be then explored using theoretical models containing external driving signals such as variants of ARIMAX and simulations. It will be interesting to identify other causes of the changes in the broadband LRTC on the short timescale and study the impact of neurofeedback, transcranial magnetic stimulation (TMS) and functional electrical stimulation (FES) and whether these lead to the enhancement or destruction of the broadband LRTC and the mechanisms leading to it.

The occurrence of LRTC in the neuronal processes has been attributed to the criticality in the brain [29, 144, 62], however there could be several different mechanisms leading to LRTC. It will be interesting to study this hypothesis of criticality as a possible mechanism of broadband LRTC. This thesis has also shown the possibility of the broadband processes being multifractal, the investigation of which can help in interpretation of such processes.

The ARFIMA model has been used in this thesis to model the LRTC, however, it does not explain the underlying physiological processes associated with LRTC [32]. Hence, it can be useful to find if LRTC can be modelled using dynamical models such as variants of the neural-mass models [277, 278] that can account for the physiological processes in the brain. The dynamical models have been commonly employed to model individual brain rhythms [277, 278] and it will be interesting to assess the potential of such models to incorporate the temporal dynamics in the broadband EEG.

Finally, it will be interesting to apply the novel broadband LRTC and SRD based movement intention detection in online BCI and compare its performance with the traditional ERD/MRCP based BCIs. Further analysis will be required to evaluate how these LRTCs change from session to session and on different days, the impact of the noise in EEG on the LRTC and to identify the cause of variability in SRD in different participants for assessing the suitability of these novel broadband temporal approaches to BCIs. This thesis has suggested that LRTC and SRD can have a great potential for use in non-invasive movement-based BCI.

7.6 Individual contribution to papers

The chapters 3 to 6 of this thesis are written in the form of research articles. The papers in chapters 3 and 4 are already published and paper in chapter 5 has been submitted to the journal and chapter 6 is ready for submission. Maitreyee Wairagkar (MW), the author of this thesis is the first author of all the four papers. MW was supervised by Slawomir J Nasuto (SJN) and Yoshikatsu Hayashi (YH), the other authors of these papers. All the research included in the four papers and this thesis has been conducted solely by MW. There were no other collaborators on the project. MW identified the research questions, performed the literature review, designed and conducted EEG experiments, developed the methodology of EEG analysis, implemented EEG analysis by writing the programs and MATLAB scripts, analysed and validated the results, created figures, graphs and tables from the results, interpreted the results and wrote all the four manuscripts (and the one in the appendix) and revised them. MW was also the corresponding author on these papers. MW not only wrote the papers but also presented the research included in the papers in various conferences and symposiums as listed in Appendix C in the form of oral presentations and posters.

The supervisors SJN and YH provided the guidance for the research in all the papers through extensive discussions of the research direction, methodological approaches, results and their interpretation. SJN and YH also reviewed the manuscripts.

References

[1] A. L. Hodgkin and A. F. Huxley. A quantitative description of membrane current and its application to conduction and excitation in nerve. *The Journal of Physiology*, 117(4):500–544, 8 1952.

[2] Emery N Brown, Robert E Kass, and Partha P Mitra. Multiple neural spike train data analysis: state-of-the-art and future challenges. *Nature Neuroscience*, 7(5):456–461, 5 2004.

[3] K O Johnson. Neural coding. *Neuron*, 26(3):563–6, 6 2000.

[4] Karen C. Cheung. Implantable microscale neural interfaces. *Biomedical Microdevices*, 9(6):923–938, 10 2007.

[5] Marie Engelene J. Obien, Kosmas Deligkaris, Torsten Bullmann, Douglas J. Bakkum, and Urs Frey. Revealing neuronal function through microelectrode array recordings. *Frontiers in Neuroscience*, 8:423, 1 2015.

[6] Alan D. Legatt, Joseph Arezzo, and Herbert G. Vaughan. Averaged multiple unit activity as an estimate of phasic changes in local neuronal activity: effects of volume-conducted potentials. *Journal of Neuroscience Methods*, 2(2):203–217, 4 1980.

[7] Andre Palmini. The concept of the epileptogenic zone: a modern look at Penfield and Jasper's views on the role of interictal spikes. *Epileptic disorders : international epilepsy journal with videotape*, 8 Suppl 2:10–5, 8 2006.

[8] Abraham Kuruvilla and Roland Flink. Intraoperative electrocorticography in epilepsy surgery: useful or not? *Seizure*, 12(8):577–84, 12 2003.

[9] Ernst Niedermeyer and F. H. Lopes da Silva. *Electroencephalography : basic principles, clinical applications, and related fields*. Lippincott Williams & Wilkins, 2005.

[10] G H Klem, H O Lüders, H H Jasper, and C Elger. The ten-twenty electrode system of the International Federation. *Electroencephalogr Clin Neurophysiol*, 52(3):3–6, 1999.

[11] William O. Tatum. *Handbook of EEG interpretation*. Demos Medical Publishing, 2014.

[12] Matti Hämäläinen, Riitta Hari, Risto J. Ilmoniemi, Jukka Knuutila, and Olli V. Lounasmaa. Magnetoencephalography—theory, instrumentation, and applications to noninvasive studies of the working human brain. *Reviews of Modern Physics*, 65(2):413–497, 4 1993.

[13] P. Rinck. Magnetic resonance: a critical peer-reviewed introduction. In *Magnetic resonance in medicine. The basic textbook of the European magnetic resonance forum*, pages 21–01, 2014.

[14] Nikos K. Logothetis, Jon Pauls, Mark Augath, Torsten Trinath, and Axel Oeltermann. Neurophysiological investigation of the basis of the fMRI signal. *Nature*, 412(6843):150–157, 7 2001.

[15] Alfons Schnitzler and Joachim Gross. Normal and pathological oscillatory communication in the brain. *Nature Reviews Neuroscience*, 6(4):285–296, 4 2005.

[16] Rodolfo R. Llinas. Intrinsic electrical properties of mammalian neurons and CNS function: a historical perspective. *Frontiers in Cellular Neuroscience*, 8:320, 11 2014.

[17] Xiao-Jing Wang. Neurophysiological and Computational Principles of Cortical Rhythms in Cognition. *Physiological Reviews*, 90(3):1195–1268, 7 2010.

[18] Wolfgang Klimesch. Memory processes, brain oscillations and EEG synchronization. *International Journal of Psychophysiology*, 24(1-2):61–100, 11 1996.

[19] Gennady G. Knyazev. EEG delta oscillations as a correlate of basic homeostatic and motivational processes. *Neuroscience & Biobehavioral Reviews*, 36(1):677–695, 1 2012.

[20] Erol Başar, Canan Başar-Eroglu, Sirel Karakaş, and Martin Schürmann. Gamma, alpha, delta, and theta oscillations govern cognitive processes. *International Journal of Psychophysiology*, 39(2-3):241–248, 1 2001.

[21] F. Amzica and M. Steriade. Electrophysiological correlates of sleep delta waves. *Electroencephalography and Clinical Neurophysiology*, 107(2):69–83, 4 1998.

[22] Wolfgang Klimesch. EEG alpha and theta oscillations reflect cognitive and memory performance: a review and analysis. *Brain Research Reviews*, 29(2-3):169–195, 4 1999.

[23] Biyu J. He. Scale-free brain activity: Past, present, and future. *Trends in Cognitive Sciences*, 18(9):480–487, 9 2014.

[24] Jaime A. Pineda. The functional significance of mu rhythms: Translating "seeing" and "hearing" into "doing". *Brain Research Reviews*, 50(1):57–68, 12 2005.

[25] Steven J. Luck. *An introduction to the event-related potential technique*. 2014.

[26] Gert Pfurtscheller and Fernando H. Lopes Da Silva. Event-related EEG/MEG synchronization and desynchronization: Basic principles. *Clinical Neurophysiology*, 110(11):1842–1857, 11 1999.

[27] Steven J. (Steven John) Luck and Emily S.. Kappenman. *Oxford handbook of event-related potential components*. Oxford University Press, 2012.

[28] MGH Coles and MD Rugg. *Event-related brain potentials: An introduction.* Oxford University Press, 1995.

[29] Klaus Linkenkaer-Hansen, Vadim V Nikouline, J Matias Palva, Risto J Ilmoniemi, Vadim V. Nikulin, J Matias Palva, and Risto J Ilmoniemi. Long-range temporal correlations and scaling behavior in human brain oscillations. *The Journal of neuroscience*, 21(4):1370–7, 2001.

[30] John S. Barlow. Autocorrelation and Crosscorrelation Analysis in Electroencephalography. *IRE Transactions on Medical Electronics*, ME-6(3):179–183, 9 1959.

[31] George E. P. Box and Gwilym M. Jenkins. *Time Series Analysis: Forecasting and Control. 2d ed.* John Wiley & Sons, Hoboken, NJ, USA, 2015.

[32] Eric-Jan Wagenmakers, Simon Farrell, and Roger Ratcliff. Estimation and interpretation of $1/f\alpha$ noise in human cognition. *Psychonomic Bulletin & Review*, 11(4):579–615, 2004.

[33] Jing Hu, Yi Zheng, and Jianbo Gao. Long-Range Temporal Correlations, Multifractality, and the Causal Relation between Neural Inputs and Movements. *Frontiers in Neurology*, 4:158, 10 2013.

[34] Marc Benayoun, Michael Kohrman, Jack Cowan, and Wim van Drongelen. EEG, temporal correlations, and avalanches. *Journal of Clinical Neurophysiology*, 27(6):458–464, 12 2010.

[35] J Matias Palva, Alexander Zhigalov, Jonni Hirvonen, Onerva Korhonen, Klaus Linkenkaer-Hansen, and Satu Palva. Neuronal long-range temporal correlations and avalanche dynamics are correlated with behavioral scaling laws. *Proceedings of the National Academy of Sciences of the United States of America*, 110(9):3585–90, 2 2013.

[36] Vadim V. Nikulin and T. Brismar. Long-range temporal correlations in electroencephalographic oscillations: Relation to topography, frequency band, age and gender. *Neuroscience*, 130(2):549–558, 1 2005.

[37] Manfred G. Kitzbichler, Marie L. Smith, Søren R. Christensen, and Ed Bullmore. Broadband Criticality of Human Brain Network Synchronization. *PLoS Comput Biol*, 5(3):e1000314, 3 2009.

[38] Klaus Linkenkaer-Hansen, Vadim V. Nikulin, J Matias Palva, Kai Kaila, and Risto J Ilmoniemi. Stimulus-induced change in long-range temporal correlations and scaling behaviour of sensorimotor oscillations. *European Journal of Neuroscience*, 19(1):203–211, 1 2004.

[39] Richard Hardstone, Simon-Shlomo Shlomo Poil, Giuseppina Schiavone, Rick Jansen, Vadim V. Nikulin, Huibert D Mansvelder, and Klaus Linkenkaer-Hansen. Detrended Fluctuation Analysis: A Scale-Free View on Neuronal Oscillations. *Frontiers in Physiology*, 3:450, 2012.

[40] Vadim V. Nikulin, Erik G. Jönsson, and Tom Brismar. Attenuation of long-range temporal correlations in the amplitude dynamics of alpha and beta neuronal oscillations in patients with schizophrenia. *NeuroImage*, 61(1):162–169, 5 2012.

[41] F. U. Hohlefeld, J. Huebl, C. Huchzermeyer, G. H. Schneider, T. Schönecker, A. A. Kühn, G. Curio, and Vadim V. Nikulin. Long-range temporal correlations in the subthalamic nucleus of patients with Parkinson's disease. *European Journal of Neuroscience*, 36(6):2812–2821, 9 2012.

[42] Chunfang Wang, Jingang Du, Ying Zhang, Peng Zhou, and Dong Ming. The long-range temporal correlations of broadband EEG oscillations in poststroke depression subjects with basal ganglia infarction. In *Proceedings of the Annual International Conference of the IEEE Engineering in Medicine and Biology Society, EMBS*, volume 2016-Octob, pages 1830–1833. IEEE, 8 2016.

[43] Alexander Zhigalov, Gabriele Arnulfo, Lino Nobili, Satu Palva, and J Matias Palva. Relationship of Fast- and Slow-Timescale Neuronal Dynamics in Human MEG and SEEG. *Journal of Neuroscience*, 35(13):5385–5396, 4 2015.

[44] Bin He, Bryan Baxter, Bradley J. Edelman, Christopher C. Cline, and Wenjing W. Ye. Noninvasive Brain-Computer Interfaces Based on Sensorimotor Rhythms. *Proceedings of the IEEE*, 103(6):907–925, 2015.

[45] James S. Albus. A theory of cerebellar function. *Mathematical Biosciences*, 10(1-2):25–61, 2 1971.

[46] J. P. Scholz and Gregor Schöner. The uncontrolled manifold concept: identifying control variables for a functional task. *Experimental Brain Research*, 126(3):289–306, 5 1999.

[47] Edward J. Fine, Catalina C. Ionita, and Linda Lohr. The History of the Development of the Cerebellar Examination. *Seminars in Neurology*, 22(4):375–384, 1 2002.

[48] WILDER Penfield and EDWIN Boldrey. Somatic Motor and Ssensory Representation in the Cerebral Cortex of Man as Studied by Electrical Stimulation. *Brain*, 60(4):389–443, 12 1937.

[49] Elaine Nicpon Marieb and Katja Hoehn. *Human anatomy & physiology*. Pearson Benjamin Cummings, 2007.

[50] Barb Abelhauser. Homunculus II – The View from a Drawbridge, 2016.

[51] Hiroshi Shibasaki and Mark Hallett. What is the Bereitschaftspotential? *Clinical Neurophysiology*, 117(11):2341–2356, 2006.

[52] Gert Pfurtscheller. Event-related synchronization (ERS): an electrophysiological correlate of cortical areas at rest. *Electroencephalography and Clinical Neurophysiology*, 83(1):62–69, 7 1992.

[53] Ou Bai, Varun Rathi, Peter Lin, Dandan Huang, Harsha Battapady, Ding-Yu Yu Fei, Logan Schneider, Elise Houdayer, Xuedong Chen, and Mark Hallett. Prediction of human voluntary movement before it occurs. *Clinical Neurophysiology*, 122(2):364–372, 2011.

[54] Szilárd Bulárka and Aurel Gontean. Brain-Computer Interface review. In *Electronics and Telecommunications (ISETC), 2016 12th IEEE International Symposium on*, pages 219–222. IEEE, 2016.

[55] Setare Amiri, Reza Fazel-Rezai, and Vahid Asadpour. A review of hybrid brain-computer interface systems. *Advances in Human-Computer Interaction*, 2013:1, 2013.

[56] Kai Keng Ang and Cuntai Guan. Brain-computer interface in stroke rehabilitation. *Journal of Computing Science and Engineering*, 7(2):139–146, 2013.

[57] Kai Keng Ang, Cuntai Guan, Karen Sui Geok Chua, Beng Ti Ang, Christopher Kuah, Chuanchu Wang, Kok Soon Phua, Zheng Yang Chin, and Haihong Zhang. Clinical study of neurorehabilitation in stroke using EEG-based motor imagery brain-computer interface with robotic feedback. In *Engineering in Medicine and Biology Society (EMBC), 2010 Annual International Conference of the IEEE*, pages 5549–5552. IEEE, 2010.

[58] Jing Jin, Hanhan Zhang, Ian Daly, Xingyu Wang, and Andrzej Cichocki. An improved P300 pattern in BCI to catch user's attention. *Journal of Neural Engineering*, 14(3):36001, 2017.

[59] Kai Keng Ang and Cuntai Guan. EEG-Based Strategies to Detect Motor Imagery for Control and Rehabilitation. *IEEE Transactions on Neural Systems and Rehabilitation Engineering*, 25(4):392–401, 4 2017.

[60] Han-Jeong Hwang, Soyoun Kim, Soobeom Choi, and Chang-Hwan Im. EEG-Based Brain-Computer Interfaces: A Thorough Literature Survey. *International Journal of Human-Computer Interaction*, 29(12):814–826, 12 2013.

[61] Matar Haller, Thomas Donoghue, Erik Peterson, Paroma Varma, Priyadarshini Sebastian, Richard Gao, Torben Noto, Robert T Knight, Avgusta Shestyuk, and Bradley Voytek. Parameterizing neural power spectra. *bioRxiv*, page 299859, 2018.

[62] Simon-Shlomo Shlomo Poil, Richard Hardstone, Huibert D Mansvelder, and Klaus Linkenkaer-Hansen. Critical-State Dynamics of Avalanches and Oscillations Jointly Emerge from Balanced Excitation/Inhibition in Neuronal Networks. *Journal of Neuroscience*, 32(29):9817–9823, 2012.

[63] Gert Pfurtscheller and A Aranibar. Event-related cortical desynchronization detected by power measurements of scalp EEG. *Electroencephalography and Clinical Neurophysiology*, 42(6):817–826, 6 1977.

[64] Gert Pfurtscheller. Graphical display and statistical evaluation of event-related desynchronization (ERD). *Electroencephalography and Clinical Neurophysiology*, 43(5):757–760, 11 1977.

[65] Gert Pfurtscheller and Christa Neuper. Chapter 28 Future prospects of ERD/ERS in the context of brain-computer interface (BCI) developments. *Progress in Brain Research*, 159:433–437, 1 2006.

[66] Gert Pfurtscheller and F. H. Lopes da Silva. *Event-related desynchronization*. Elsevier Science, 1st edition, 1999.

[67] C. Guger, G. Edlinger, W. Harkam, I. Niedermayer, and Gert Pfurtscheller. How many people are able to operate an EEG-based brain-computer interface (BCI)? *IEEE Transactions on Neural Systems and Rehabilitation Engineering*, 11(2):145–147, 2003.

[68] Benjamin Blankertz, Florian Losch, Matthias Krauledat, Guido Dornhege, Gabriel Curio, and K-R K.-R. Muller. The Berlin Brain–Computer Interface: Accurate Performance From First-Session in BCI-Naive Subjects. *IEEE Transactions on Biomedical Engineering*, 55(10):2452–2462, 2008.

[69] Wolf Singer. Synchronization of cortical activity and its putative role in information processing and learning. *Annual Review of Physiology*, 55(1):349–374, 10 1993.

[70] Fernando Lopes da Silva. Neural mechanisms underlying brain waves: from neural membranes to networks, 8 1991.

[71] J Ibáñez, J I Serrano, M. D. Del Castillo, E Monge-Pereira, F Molina-Rueda, I Alguacil-Diego, and J L Pons. Detection of the onset of upper-limb movements based on the combined analysis of changes in the sensorimotor rhythms and slow cortical potentials. *Journal of Neural Engineering*, 11(5):056009, 10 2014.

[72] Evariste Demandt, Carsten Mehring, Klaus Vogt, Andreas Schulze-Bonhage, Ad Aertsen, and Tonio Ball. Reaching movement onset- and end-related characteristics of EEG spectral power modulations. *Frontiers in Neuroscience*, 6(MAY):1–11, 2012.

[73] Tomonari Omura and Shin'ichiro Kanoh. A basic study on neuro-feedback training to enhance a change of sensory-motor rhythm during motor imagery tasks. In *2017 10th Biomedical Engineering International Conference (BMEiCON)*, pages 1–5. IEEE, 8 2017.

[74] J. Kalcher and Gert Pfurtscheller. Discrimination between phase-locked and non-phase-locked event-related EEG activity. *Electroencephalography and Clinical Neurophysiology*, 94(5):381–384, 5 1995.

[75] Fatemeh Shahlaei, Niraj Bagh, M. Ramasubba Reddy, and A. D. Shaligram. Classification of Motor Imagery Tasks Using Inter Trial Variance in. *2018 IEEE International Symposium on Medical Measurements and Applications (MeMeA)*, 3528725544(Iv):4–9, 6 2018.

[76] Scott Makeig. Auditory event-related dynamics of the EEG spectrum and effects of exposure to tones. *Electroencephalography and Clinical Neurophysiology*, 86(4):283–293, 4 1993.

[77] Matteo Fecchio, Andrea Pigorini, Angela Comanducci, Simone Sarasso, Silvia Casarotto, Isabella Premoli, Chiara Camilla Derchi, Alice Mazza, Simone Russo, Federico Resta, Fabio Ferrarelli, Maurizio Mariotti, Ulf Ziemann, Marcello Massimini, and Mario Rosanova. The spectral features of EEG responses to transcranial magnetic stimulation of the primary motor cortex depend on the amplitude of the motor evoked potentials. *PLoS ONE*, 12(9):e0184910, 9 2017.

[78] Kenji Kato, Kensho Takahashi, Nobuaki Mizuguchi, and Junichi Ushiba. Online detection of amplitude modulation of motor-related EEG desynchronization using a lock-in amplifier: Comparison with a fast Fourier transform, a continuous wavelet transform, and an autoregressive algorithm. *Journal of Neuroscience Methods*, 293:289–298, 1 2018.

[79] Shuhei Nagamori and Hisaya Tanaka. Analysis method for ERD in mu-rhythm detection in motor imagery brain-computer interface. In *2016 IEEE International Conference on Systems, Man, and Cybernetics, SMC 2016 - Conference Proceedings*, pages 867–870. IEEE, 10 2017.

[80] Shuhei Nagamori and Hisaya Tanaka. ERD analysis method in motor imagery brain–computer interfaces for accurate switch input. *Artificial Life and Robotics*, 22(1):83–89, 3 2017.

[81] R. Salmelin, M. Hämäläinen, M. Kajola, and R. Hari. Functional segregation of movement-related rhythmic activity in the human brain. *NeuroImage*, 2(4):237–243, 12 1995.

[82] Lei Wang, Guizhi Xu, JiangWang, Shuo Yang, and Weili Yan. Application of Hilbert-Huang transform for the study of motor imagery tasks. In *2008 30th Annual International Conference of the IEEE Engineering in Medicine and Biology Society*, pages 3848–3851, 2008.

[83] M. Ortiz, E. Ianez, M. Rodriguez-Ugarte, and J. M. Azorin. Empirical mode decomposition use in electroencephalography signal analysis for detection of starting and stopping intentions during gait cycle. In *RO-MAN 2017 - 26th IEEE International Symposium on Robot and Human Interactive Communication*, volume 2017-Janua, pages 94–100. IEEE, 8 2017.

[84] Georg E. Fabiani, Dennis J McFarland, Jonathan R Wolpaw, and Gert Pfurtscheller. Conversion of EEG activity into cursor movement by a brain-computer interface (BCI). *IEEE Transactions on Neural Systems and Rehabilitation Engineering*, 12(3):331–338, 2004.

[85] Gernot R Müller-Putz, A. Schwarz, J. Pereira, and P. Ofner. From classic motor imagery to complex movement intention decoding: The noninvasive Graz-BCI approach. In *Progress in Brain Research*, volume 228, pages 39–70. Elsevier, 1 2016.

[86] Gert Pfurtscheller, Gernot R Müller-Putz, Alois Schlögl, B Graimann, Reinhold Scherer, Robert Leeb, C Brunner, C Keinrath, F. Lee, G. Townsend, Carmen Vidaurre, and Christa Neuper. 15 Years of BCI research at Graz University of Technology: Current projects. In *IEEE Transactions on Neural Systems and Rehabilitation Engineering*, volume 14, pages 205–210, 2006.

[87] Fabien Lotte, Marco Congedo, Anatole Lécuyer, Fabrice Lamarche, and Bruno Arnaldi. A review of classification algorithms for EEG-based brain–computer interfaces. *Journal of neural engineering*, 4(2):R1, 2007.

[88] Fei Meng, Kai-yu Tong, Suk-tak Chan, Wan-wa Wong, Ka-him Lui, Kwok-wing Tang, Xiaorong Gao, and Shangkai Gao. BCI-FES training system design and implementation for rehabilitation of stroke patients. In *Neural Networks, 2008. IJCNN 2008.(IEEE World Congress on Computational Intelligence). IEEE International Joint Conference on*, pages 4103–4106. IEEE, 2008.

[89] J Ibáñez, E López-Larraz, E Monge, F Molina-Rueda, Luis Montesano, and J L Pons. On Recalibration Strategies for Brain-Computer Interfaces Based on the Detection of Motor Intentions. In *Converging Clinical and Engineering Research on Neurorehabilitation II*, pages 775–779. Springer International Publishing, 2017.

[90] Han Yuan and Bin He. Brain-computer interfaces using sensorimotor rhythms: Current state and future perspectives. *IEEE Transactions on Biomedical Engineering*, 61(5):1425–1435, 5 2014.

[91] J Ibáñez, J I Serrano, M D Del Castillo, E Monge-Pereira, F Molina-Rueda, I Alguacil-Diego, and J L Pons. Detection of the onset of upper-limb movements based on the combined analysis of changes in the sensorimotor rhythms and slow cortical potentials. *Journal of neural engineering*, 11(5):56009, 2014.

[92] Eduardo Lopez-Larraz, Luis Montesano, Angel Gil-Agudo, and Javier Minguez. Continuous Decoding of Upper Limb Movement Intention from EEG Measurements on the. *Journal of NeuroEngineering and Rehabilitation*, 11(1):153, 2014.

[93] Trent J Bradberry, Rodolphe J Gentili, and José L Contreras-Vidal. Reconstructing Three-Dimensional Hand Movements from Noninvasive Electroencephalographic Signals. *Journal of Neuroscience*, 30(9):3432–3437, 3 2010.

[94] Alessandro Presacco, Ronald Goodman, Larry Forrester, and Jose Luis Contreras-Vidal. Neural decoding of treadmill walking from noninvasive electroencephalographic signals. *Journal of Neurophysiology*, 106(4):1875–1887, 10 2011.

[95] Alessandro Presacco, Larry W. Forrester, and Jose L. Contreras-Vidal. Decoding intra-limb and inter-limb kinematics during treadmill walking from scalp electroencephalographic (EEG) signals. *IEEE Transactions on Neural Systems and Rehabilitation Engineering*, 20(2):212–219, 3 2012.

[96] Han Yuan, Christopher Perdoni, and Bin He. Relationship between speed and EEG activity during imagined and executed hand movements. *Journal of Neural Engineering*, 7(2):026001, 4 2010.

[97] Han Yuan, Christopher Perdoni, and Bin He. Decoding speed of imagined hand movement from EEG. In *2010 Annual International Conference of the IEEE Engineering in Medicine and Biology Society, EMBC'10*, pages 142–145. IEEE, 8 2010.

[98] Xinyi Yong and Carlo Menon. EEG classification of different imaginary movements within the same limb. *PLoS ONE*, 10(4):e0121896, 4 2015.

[99] Teodoro Solis-Escalante, Gernot R Müller-Putz, Gert Pfurtscheller, and Christa Neuper. Cue-induced beta rebound during withholding of overt and covert foot movement. *Clinical Neurophysiology*, 123(6):1182–1190, 2012.

[100] Eileen Y.L. Lew, Ricardo Chavarriaga, Stefano Silvoni, and José Del R Millán. De-
tection of self-paced reaching movement intention from EEG signals. *Frontiers in
neuroengineering*, 5(July):13, 2012.

[101] Madiha Tariq, Pavel M. Trivailo, and Milan Simic. EEG-Based BCI Control Schemes
for Lower-Limb Assistive-Robots. *Frontiers in Human Neuroscience*, 12:312, 8 2018.

[102] Ke Liao, Ran Xiao, Jania Gonzalez, and Lei Ding. Decoding individual finger
movements from one hand using human EEG signals. *PloS one*, 9(1):e85192, 1 2014.

[103] Scott R Cole and Bradley Voytek. Cycle-by-cycle analysis of neural oscillations.
bioRxiv, page 302000, 2018.

[104] Jonathan R Wolpaw, Niels Birbaumer, Dennis J McFarland, Gert Pfurtscheller, and
Theresa M Vaughan. Brain–computer interfaces for communication and control.
Clinical neurophysiology, 113(6):767–791, 2002.

[105] Benjamin Blankertz, Florian Losch, Matthias Krauledat, Guido Dornhege, Gabriel
Curio, and K-R Muller. The Berlin Brain–Computer Interface: accurate performance
from first-session in BCI-naive subjects. *Biomedical Engineering, IEEE Transactions
on*, 55(10):2452–2462, 2008.

[106] Yan Bian, Hongzhi Qi, Li Zhao, Dong Ming, Tong Guo, and Xing Fu. Improvements
in event-related desynchronization and classification performance of motor imagery
using instructive dynamic guidance and complex tasks. *Computers in Biology and
Medicine*, 96:266–273, 5 2018.

[107] Wei-Yen Hsu. Assembling A Multi-Feature EEG Classifier for Left–Right Motor Im-
agery Data Using Wavelet-Based Fuzzy Approximate Entropy for Improved Accuracy.
International Journal of Neural Systems, 25(08):1550037, 12 2015.

[108] Isao Sakamaki, Mahdi Tavakoli, and Kim Adams. Generating forbidden region virtual
fixtures by classification of movement intention based on event-related desynchro-
nization. In *2017 IEEE Global Conference on Signal and Information Processing,
GlobalSIP 2017 - Proceedings*, volume 2018-Janua, pages 418–422, 2018.

[109] Isao Sakamaki, Camilo Perafan, Sandra Wiebe, Mahdi Tavakoli, and Kim Adams.
Assistive Technology Design and Preliminary Testing of a Robot Platform Based on
Movement Intention using Low-Cost Brain Computer Interface. *Submitted to the 2017
IEEE International Conference on Systems, Man, and Cybernetics.*, pages 2243–2248,
10 2017.

[110] Kyuhwa Lee, Dong Liu, Laetitia Perroud, Ricardo Chavarriaga, and José del R.
Millán. A brain-controlled exoskeleton with cascaded event-related desynchronization
classifiers. *Robotics and Autonomous Systems*, 90:15–23, 4 2017.

[111] Natalie Mrachacz-Kersting, Signe Rom Kristensen, Imran Khan Niazi, and Dario
Farina. Precise temporal association between cortical potentials evoked by motor
imagination and afference induces cortical plasticity. *The Journal of physiology*,
590(Pt 7):1669–82, 2012.

[112] Eileen Y.L. L Lew, Ricardo Chavarriaga, Stefano Silvoni, and José Del R Millán. Single trial prediction of self-paced reaching directions from EEG signals. *Frontiers in Neuroscience*, 8(AUG):222, 2014.

[113] Aqsa Shakeel, Muhammad Samran Navid, Muhammad Nabeel Anwar, Suleman Mazhar, Mads Jochumsen, and Imran Khan Niazi. A review of techniques for detection of movement intention using movement-related cortical potentials. *Computational and Mathematical Methods in Medicine*, 2015:1–13, 12 2015.

[114] Ren Xu, Ning Jiang, Chuang Lin, Natalie Mrachacz-Kersting, Kim Dremstrup, and Dario Farina. Enhanced low-latency detection of motor intention from EEG for closed-loop brain-computer interface applications. *IEEE Transactions on Biomedical Engineering*, 61(2):288–296, 2014.

[115] Michael G H Coles, Gabriele Gratton, and Emanuel Donchin. Detecting early communication: Using measures of movement-related potentials to illuminate human information processing. *Biological Psychology*, 26(1-3):69–89, 6 1988.

[116] Richard A. Andersen and Christopher A. Buneo. Intentional Maps in Posterior Parietal Cortex. *Annual Review of Neuroscience*, 25(1):189–220, 3 2002.

[117] Imran Khan Niazi, Ning Jiang, and Olivier Tiberghien. Detection of movement intention from single-trial movement-related cortical. *JOURNAL OF NEURAL ENGINEERING*, 066009(8):1–10, 10 2011.

[118] Bao-guo Xu and Ai-guo Song. Pattern Recognition of Motor Imagery EEG using Wavelet Transform. *Journal of Biomedical Science and Engineering*, 01(01):64–67, 2008.

[119] Aaron Clauset, Cosma Rohilla Shalizi, and M. E. J. Newman. Power-Law Distributions in Empirical Data. *SIAM Review*, 51(4):661–703, 2009.

[120] Maria Botcharova. *Modelling and analysis of amplitude, phase and synchrony in human brain activity patterns*. PhD thesis, University College London, 2014.

[121] James B. Bassingthwaighte and Gary M. Raymond. Evaluating rescaled range analysis for time series. *Annals of Biomedical Engineering*, 22(4):432–444, 7 1994.

[122] C-K K. Peng, Shlomo Havlin, H Eugene Stanley, and Ary L Goldberger. Quantification of scaling exponents and crossover phenomena in nonstationary heartbeat time series. *Chaos*, 5(1):82–87, 1995.

[123] Frédéric Crevecoeur, Benjamin Bollens, Christine Detrembleur, and T. M. Lejeune. Towards a "gold-standard" approach to address the presence of long-range auto-correlation in physiological time series. *Journal of Neuroscience Methods*, 192(1):163–172, 2010.

[124] Jan W Kantelhardt, Stephan A. Zschiegner, Eva Koscielny-Bunde, Shlomo Havlin, Armin Bunde, and H Eugene Stanley. Multifractal detrended fluctuation analysis of nonstationary time series. *Physica A*, 316(1-4):87–114, 12 2002.

[125] Jan W Kantelhardt. Fractal and Multifractal Time Series. In *Encyclopedia of Complexity and Systems Science*, chapter Fractal an, pages 3754–3779. Springer New York, 2009.

[126] Maria Botcharova, Luc Berthouze, Matthew J Brookes, Gareth R Barnes, and Simon F Farmer. Resting state MEG oscillations show long-range temporal correlations of phase synchrony that break down during finger movement. *Frontiers in Physiology*, 6(JUN):183, 2015.

[127] Maria Botcharova, Simon F Farmer, and Luc Berthouze. A maximum likelihood based technique for validating detrended fluctuation analysis (ML-DFA). *arXiv preprint arXiv:1306.5075*, q-bio.QM:1–22, 6 2013.

[128] Maria Botcharova, Simon F Farmer, and Luc Berthouze. Markers of criticality in phase synchronisation. *Frontiers in Systems Neuroscience*, 8:176, 2014.

[129] Hirotugu Akaike. A New Look at the Statistical Model Identification. *IEEE Transactions on Automatic Control*, 19(6):716–723, 12 1974.

[130] Gideon Schwarz. Estimating the Dimension of a Model. *The Annals of Statistics*, 6(2):461–464, 3 1978.

[131] Didier Delignieres, Sofiane Ramdani, Loïc Lemoine, Kjerstin Torre, Marina Fortes, and Grégory Ninot. Fractal analyses for 'short' time series: A re-assessment of classical methods. *Journal of Mathematical Psychology*, 50(6):525–544, 12 2006.

[132] Luc Berthouze, Leon M. James, and Simon F Farmer. Human EEG shows long-range temporal correlations of oscillation amplitude in Theta, Alpha and Beta bands across a wide age range. *Clinical Neurophysiology*, 121(8):1187–1197, 2010.

[133] L. M. Parish, G. A. Worrell, S. D. Cranstoun, S. M. Stead, P. Pennell, and B. Litt. Long-range temporal correlations in epileptogenic and non-epileptogenic human hippocampus. *Neuroscience*, 125(4):1069–1076, 1 2004.

[134] Jan W Kantelhardt, Eva Koscielny-Bunde, Henio H.A Rego, Shlomo Havlin, and Armin Bunde. Detecting long-range correlations with detrended fluctuation analysis. *Physica A: Statistical Mechanics and its Applications*, 295(3-4):441–454, 6 2001.

[135] Alexander Zhigalov, Alexander Ya Kaplan, and J Matias Palva. Modulation of critical brain dynamics using closed-loop neurofeedback stimulation. *Clinical Neurophysiology*, 127(8):2882–2889, 2016.

[136] Dennis J McFarland and Jonathan R Wolpaw. Sensorimotor rhythm-based brain-computer interface (BCI): Model order selection for autoregressive spectral analysis. *Journal of Neural Engineering*, 5(2):155–162, 6 2008.

[137] Gernot Florian and Gert Pfurtscheller. Dynamic spectral analysis of event-related EEG data. *Electroencephalography and Clinical Neurophysiology*, 95(5):393–396, 11 1995.

[138] Shim-Yih Shinn-Yih Tseng, Rong-Chi Chen, Fok-Ching Chong, and Te-Son Kuo. Evaluation of parametric methods in EEG signal analysis. *Med. Eng. Phyxs*, 17(1):71–78, 1 1995.

[139] Alois Schlögl, Technischen Universit, Technischen Wissenschaften, and Biomedizinische Technik. the Electroencephalogram and the Adaptive Autoregressive Model : Theory and Applications. *technical university of Graz*, Dissertati(April):68, 2000.

[140] Alois Schlögl, Felix Lee, Horst Bischof, and Gert Pfurtscheller. Characterization of four-class motor imagery EEG data for the BCI-competition 2005. *Journal of neural engineering*, 2(4):14–22, 12 2005.

[141] Per Bak, Chao Tang, and Kurt Wiesenfeld. Self-Organized Criticality: An Explanation of 1/f Noise. *Physical Review Letters*, 59(4):381–384, 1987.

[142] P Bak and M Paczuski. Complexity, contingency, and criticality. *Proceedings of the National Academy of Sciences of the United States of America*, 92(15):6689–96, 7 1995.

[143] C J Honey, C J Honey, O Sporns, O Sporns, L Cammoun, L Cammoun, X Gigandet, X Gigandet, J P Thiran, J P Thiran, R Meuli, R Meuli, P Hagmann, and P Hagmann. Predicting human resting-state functional connectivity from structural connectivity. *Proceedings of the National Academy of Sciences of the United States of America*, 106(6):2035–40, 2 2009.

[144] Paolo Massobrio, Lucilla de Arcangelis, Valentina Pasquale, Henrik J. Jensen, and Dietmar Plenz. Criticality as a signature of healthy neural systems. *Frontiers in Systems Neuroscience*, 9:22, 2 2015.

[145] Andreas Daffertshofer, Robert Ton, Morten L Kringelbach, Mark Woolrich, and Gustavo Deco. Distinct criticality of phase and amplitude dynamics in the resting brain, 2018.

[146] Woodrow L. Shew, Hongdian Yang, Thomas Petermann, Rajarshi Roy, and Dietmar Plenz. Neuronal avalanches imply maximum dynamic range in cortical networks at criticality. *The Journal of neuroscience : the official journal of the Society for Neuroscience*, 23(35):11167–77, 12 2009.

[147] Stavros I Dimitriadis and David Linden. Modulation of brain criticality via suppression of EEG long-range temporal correlations (LRTCs) in a closed-loop neurofeedback stimulation. *Clinical Neurophysiology*, 127(8):2878–2881, 2016.

[148] Peter Anderer, Stephen Roberts, Alois Schlögl, Georg Gruber, Gerhard Klösch, Werner Herrmann, Peter Rappelsberger, Oliver Filz, Manel J Barbanoj, Georg Dorffner, and Bernd Saletu. Artifact processing in computerized analysis of sleep EEG - A review. *Neuropsychobiology*, 40(3):150–157, 9 1999.

[149] Tzyy-Ping Ping Jung, Scott Makeig, Colin Humphries, Te-Won W Lee, M J McKeown, V Iragui, and T J Sejnowski. Removing electroencephalographic artifacts by blind source separation. *Psychophysiology*, 37(2):163–78, 3 2000.

[150] Alois Schlögl, C. Keinrath, D. Zimmermann, Reinhold Scherer, Robert Leeb, and Gert Pfurtscheller. A fully automated correction method of EOG artifacts in EEG recordings. *Clinical Neurophysiology*, 118(1):98–104, 1 2007.

[151] Georg Bartels, Li-Chen Shi, Bao-Liang Lu, Li-Chen Shi, and Bao-Liang Lu. Automatic artifact removal from EEG - a mixed approach based on double blind source separation and support vector machine. *2010 Annual International Conference of the IEEE Engineering in Medicine and Biology*, 2010:5383–5386, 8 2010.

[152] P Berg and M Scherg. Dipole modelling of eye activity and its application to the removal of eye artefacts from the eeg and meg. *Clinical Physics and Physiological Measurement*, 12(A):49–54, 1 1991.

[153] V Krishnaveni, S Jayaraman, L. Anitha, and K Ramadoss. Removal of ocular artifacts from EEG using adaptive thresholding of wavelet coefficients. *Journal of Neural Engineering*, 3(4):45–57, 2006.

[154] A Schloegl, K Lugger, and Gert Pfurtscheller. Using Adaptive Autoregressive Parameters for a Brain-Computer Interface Experiment. In *Proceedings of 19th IEEE/EMBS, Chicago, USA*, pages 2–4, 1998.

[155] Ian Daly, Reinhold Scherer, Martin Billinger, and Gernot Müller-Putz. FORCe: Fully online and automated artifact removal for brain-computer interfacing. *IEEE Transactions on Neural Systems and Rehabilitation Engineering*, 23(5):725–736, 9 2015.

[156] Swati Bhardwaj, Pranit Jadhav, Bhagyaraja Adapa, Amit Acharyya, and Ganesh R. Naik. Online and automated reliable system design to remove blink and muscle artefact in EEG. In *Proceedings of the Annual International Conference of the IEEE Engineering in Medicine and Biology Society, EMBS*, volume 2015-Novem, pages 6784–6787, 2015.

[157] Dennis J McFarland, Charles W Anderson, Klaus Robert Müller, Alois Schlögl, and Dean J Krusienski. BCI Meeting 2005 - Workshop on BCI signal processing: Feature extraction and translation. *IEEE Transactions on Neural Systems and Rehabilitation Engineering*, 14(2):135–138, 2006.

[158] Dennis J McFarland, Lynn M McCane, Stephen V David, and Jonathan R Wolpaw. Spatial filter selection for EEG-based communication. *Electroencephalography and clinical Neurophysiology*, 103(3):386–394, 9 1997.

[159] Benjamin Blankertz, Ryota Tomioka, Steven Lemm, Motoaki Kawanabe, and Klaus Robert Müller. Optimizing spatial filters for robust EEG single-trial analysis. *IEEE Signal Processing Magazine*, 25(1):41–56, 2008.

[160] Gernot R Müller-Putz, Ian Daly, and Vera Kaiser. Motor imagery-induced EEG patterns in individuals with spinal cord injury and their impact on brain-computer interface accuracy. *Journal of neural engineering*, 11(3):035011, 2014.

[161] Gert Pfurtscheller, Christa Neuper, C. Guger, W. Harkam, H Ramoser, Alois Schlögl, B. Obermaier, and M. Pregenzer. Current trends in Graz Brain-Computer Interface (BCI) research. *IEEE Transactions on Rehabilitation Engineering*, 8(2):216–219, 2000.

[162] C R Hema, M P Paulraj, Sazali Yaacob, A H Adom, and Ramachandran Nagarajan. An Analysis of the Effect of EEG Frequency Bands on the Classification of Motor Imagery Signals. *IJBSCHS Biomedical Soft Computing and Human Sciences*, 161226(1):121–126, 2010.

[163] Irena Koprinska. Feature Selection for Brain-Computer Interfaces. In *Pacific-Asia conference on knowledge discovery and data mining*, pages 100–111, 2010.

[164] Bethel C A Osuagwu, Leslie Wallace, Mathew Fraser, and Aleksandra Vuckovic. Rehabilitation of hand in subacute tetraplegic patients based on brain computer interface and functional electrical stimulation: a randomised pilot study. *Journal of neural engineering*, 13(6):65002, 2016.

[165] Ye Liu, Mingfen Li, Hao Zhang, Hang Wang, Junhua Li, Jie Jia, Yi Wu, and Liqing Zhang. A tensor-based scheme for stroke patients' motor imagery EEG analysis in BCI-FES rehabilitation training. *Journal of neuroscience methods*, 222:238–249, 2014.

[166] Mitsuru Takahashi, Kotaro Takeda, Yohei Otaka, Rieko Osu, Takashi Hanakawa, Manabu Gouko, and Koji Ito. Event related desynchronization-modulated functional electrical stimulation system for stroke rehabilitation: a feasibility study. *Journal of neuroengineering and rehabilitation*, 9(1):1, 2012.

[167] Dingguo Zhang, Guangquan Liu, Gan Huan, Jianrong Liu, and Xiangyang Zhu. A hybrid fes rehabilitation system based on CPG and BCI technology for locomotion: a preliminary study. In *Intelligent Robotics and Applications*, pages 1073–1084. Springer, 2009.

[168] Mitsuru Takahashi, Manabu Gouko, and Koji Ito. Fundamental research about electroencephalogram (EEG)-functional electrical stimulation (FES) rehabilitation system. In *Rehabilitation Robotics, 2009. ICORR 2009. IEEE International Conference on*, pages 316–321. IEEE, 2009.

[169] F Cincotti, F Pichiorri, P Aricò, F Aloise, F Leotta, F de Vico Fallani, Del R Millan, Marco Molinari, D Mattia, and others. EEG-based Brain-Computer Interface to support post-stroke motor rehabilitation of the upper limb. In *Engineering in Medicine and Biology Society (EMBC), 2012 Annual International Conference of the IEEE*, pages 4112–4115. IEEE, 2012.

[170] Gert Pfurtscheller, Gernot R Müller-Putz, Jörg Pfurtscheller, and Rüdiger Rupp. EEG-based asynchronous BCI controls functional electrical stimulation in a tetraplegic patient. *EURASIP Journal on Applied Signal Processing*, 2005:3152–3155, 2005.

[171] Chuanchu Wang, Kok Soon Phua, Kai Keng Ang, Cuntai Guan, Haihong Zhang, Rongsheng Lin, Karen Sui Geok Chua, Beng Ti Ang, and Christopher Wee Keong Kuah. A feasibility study of non-invasive motor-imagery BCI-based robotic rehabilitation for

Stroke patients. In *Neural Engineering, 2009. NER'09. 4th International IEEE/EMBS Conference on*, pages 271–274. IEEE, 2009.

[172] Kai Keng Ang, Cuntai Guan, Karen Sui Geok Chua, Beng Ti Ang, Christopher Kuah, Chuanchu Wang, Kok Soon Phua, Zheng Yang Chin, and Haihong Zhang. A clinical study of motor imagery-based brain-computer interface for upper limb robotic rehabilitation. In *Engineering in Medicine and Biology Society, 2009. EMBC 2009. Annual International Conference of the IEEE*, pages 5981–5984. IEEE, 2009.

[173] Balint Varkuti, Cuntai Guan, Yaozhang Pan, Kok Soon Phua, Kai Keng Ang, Christopher Wee Keong Kuah, Karen Chua, Beng Ti Ang, Niels Birbaumer, and Ranganathan Sitaram. Resting state changes in functional connectivity correlate with movement recovery for BCI and robot-assisted upper-extremity training after stroke. *Neurorehabilitation and Neural Repair*, 27(1):53–62, 2013.

[174] Maitreyee Wairagkar, Ioannis Zoulias, Victoria Oguntosin, Yoshikatsu Hayashi, and Slawomir J. Nasuto. Movement intention based Brain Computer Interface for Virtual Reality and Soft Robotics rehabilitation using novel autocorrelation analysis of EEG. In *Proceedings of the IEEE RAS and EMBS International Conference on Biomedical Robotics and Biomechatronics*, volume 2016-July, page 685, 2016.

[175] Guy Chéron, M Duvinage, C De Saedeleer, T Castermans, A Bengoetxea, M Petieau, K Seetharaman, T Hoellinger, B Dan, T Dutoit, and others. From spinal central pattern generators to cortical network: integrated BCI for walking rehabilitation. *Neural plasticity*, 2012, 2012.

[176] Po T Wang, Christine King, Luis A Chui, Zoran Nenadic, and An Do. BCI controlled walking simulator for a BCI driven FES device. In *Proc of RESNA Ann Conf*, 2010.

[177] Brendan Z Allison and Christa Neuper. Could anyone use a BCI? In *Brain-computer interfaces*, pages 35–54. Springer, 2010.

[178] C Guger, G Edlinger, W Harkam, I Niedermayer, and G Pfurtscheller. How many people are able to operate an EEG-based brain-computer interface (BCI)? *Neural Systems and Rehabilitation Engineering, IEEE Transactions on*, 11(2):145–147, 2003.

[179] Benjamin Blankertz, Guido Dornhege, Klaus-Robert Müller, Gerwin Schalk, Dean Krusienski, Jonathan R Wolpaw, A Schlogl, Bernhard Graimann, Gert Pfurtscheller, Silvia Chiappa, and others. Results of the BCI Competition III. In *BCI Meeting*, 2005.

[180] Gert Pfurtscheller, Brendan Z Allison, Günther Bauernfeind, Clemens Brunner, Teodoro Solis Escalante, Reinhold Scherer, Thorsten O Zander, Gernot Mueller-Putz, Christa Neuper, and Niels Birbaumer. The hybrid BCI. *Frontiers in neuroscience*, 4:3, 2010.

[181] Benjamin Blankertz, Klaus-Robert Müller, Dean J Krusienski, Gerwin Schalk, Jonathan R Wolpaw, Alois Schlögl, Gert Pfurtscheller, Jd R Millan, Michael Schröder, and Niels Birbaumer. The BCI competition III: Validating alternative approaches to actual BCI problems. *Neural Systems and Rehabilitation Engineering, IEEE Transactions on*, 14(2):153–159, 2006.

[182] Yohei Tomita, Francois-Benoit Vialatte, Gérard Dreyfus, Yasue Mitsukura, Hovagim Bakardjian, and Andrzej Cichocki. Bimodal BCI using simultaneously NIRS and EEG. *Biomedical Engineering, IEEE Transactions on*, 61(4):1274–1284, 2014.

[183] Gernot Müller-Putz, Reinhold Scherer, Clemens Brunner, Robert Leeb, and Gert Pfurtscheller. Better than random: A closer look on BCI results. *International Journal of Bioelectromagnetism*, 10(EPFL-ARTICLE-164768):52–55, 2008.

[184] Josef Faller, Carmen Vidaurre, Teodoro Solis-Escalante, Christa Neuper, and Reinhold Scherer. Autocalibration and recurrent adaptation: towards a plug and play online ERD-BCI. *Neural Systems and Rehabilitation Engineering, IEEE Transactions on*, 20(3):313–319, 2012.

[185] David Gutiérrez. Designing a spatial filter to improve SNR in two-class discrimination problems for BCI applications. In *Signals, Systems and Computers, 2008 42nd Asilomar Conference on*, pages 372–377. IEEE, 2008.

[186] Laurent; Lotte Fabien Clerc, Maureen ; Bougrain. *Brain Computer Interfaces : Methods, Applications and PerspectivesNo Title*. John Wiley & Sons, Incorporated, 1 edition, 2016.

[187] Xia Hong. Linear discriminant analysis. Technical report, University of Reading, Reading, 2011.

[188] Tzu-Tsung Wong. Performance evaluation of classification algorithms by k-fold and leave-one-out cross validation. *Pattern Recognition*, 48(9):2839–2846, 9 2015.

[189] Ron Kohavi. A Study of Cross-Validation and Bootstrap for Accuracy Estimation and Model Selection. In *International Joint Conference on Artificial Intelligence (IJCAI)*, 1995.

[190] Gaoxia Jiang and Wenjian Wang. Error estimation based on variance analysis of k-fold cross-validation. *Pattern Recognition*, 69:94–106, 9 2017.

[191] Ian T. Jolliffe and Jorge Cadima. Principal component analysis: a review and recent developments. *Philosophical Transactions of the Royal Society A: Mathematical, Physical and Engineering Sciences*, 374(2065):20150202, 4 2016.

[192] Lindsay I Smith. A tutorial on Principal Components Analysis. Technical report, 2002.

[193] James E. Arruda, Michael D. Weiler, Dominic Valentino, W.Grant Willis, Joseph S. Rossi, Robert A. Stern, Sherri M. Gold, and Laura Costa. A guide for applying principal-components analysis and confirmatory factor analysis to quantitative electroencephalogram data. *International Journal of Psychophysiology*, 23(1-2):63–81, 8 1996.

[194] Farid Ali Mousa, Reda A. El-Khoribi, and Mahmoud E. Shoman. A Novel Brain Computer Interface Based on Principle Component Analysis. *Procedia Computer Science*, 82:49–56, 1 2016.

[195] RGD Steel and JH Torrie. *Principles and procedures of statistics: with special reference to the biological sciences.* McGraw-Hill, 1965.

[196] Norman R. Draper and Harry. Smith. *Applied Regression Analysis.* John Wiley & Sons, 2014.

[197] Christoph Guger, Damien Coyle, Donatella Mattia, Marzia De Lucia, Leigh Hochberg, Brian L Edlow, Betts Peters, Brandon Eddy, Chang S Nam, Quentin Noirhomme, and others. Trends in BCI Research I: Brain-Computer Interfaces for Assessment of Patients with Locked-in Syndrome or Disorders of Consciousness. In *Brain-Computer Interface Research*, pages 105–125. Springer, 2017.

[198] Jing Jin, Ian Daly, Yu Zhang, Brendan Z Allison, and Eric W Sellers. Related content An optimized ERP brain–computer interface based on facial expression Adaptive P300-based control system. *Journal of Neural Engineering*, 14(3):036001, 6 2017.

[199] Herbert Ramoser, Johannes Muller-Gerking, Gert Pfurtscheller, Johannes Müller-Gerking, and Gert Pfurtscheller. Optimal spatial filtering of single trial EEG during imagined hand movement. *IEEE transactions on rehabilitation engineering : a publication of the IEEE Engineering in Medicine and Biology Society*, 8(4):441–6, 12 2000.

[200] Eduardo López-Larraz, Luis Montesano, Ángel Gil-Agudo, and Javier Minguez. Continuous decoding of movement intention of upper limb self-initiated analytic movements from pre-movement EEG correlates. *Journal of neuroengineering and rehabilitation*, 11(1):153, 2014.

[201] Bruce H Dobkin. Brain–computer interface technology as a tool to augment plasticity and outcomes for neurological rehabilitation. *The Journal of physiology*, 579(3):637–642, 2007.

[202] Natalie Mrachacz-Kersting, Signe Rom Kristensen, Imran Khan Niazi, and Dario Farina. Precise temporal association between cortical potentials evoked by motor imagination and afference induces cortical plasticity. *The Journal of physiology*, 590(7):1669–1682, 2012.

[203] Ali Bashashati, Mehrdad Fatourechi, Rabab K Ward, and Gary E Birch. A survey of signal processing algorithms in brain-computer interfaces based on electrical brain signals. *Journal of neural engineering*, 4(2):R32–R57, 6 2007.

[204] Yoshikatsu Hayashi, Kiyoshi Nagai, Koji Ito, Slawomir J Nasuto, Rui C V Loureiro, and William S Harwin. Analysis of EEG Signal to Detect Motor Command Generation towards Stroke Rehabilitation. In *Converging Clinical and Engineering Research on Neurorehabilitation*, pages 569–573. Springer, 2013.

[205] Carmen Vidaurre, Tilmann H Sander, and Alois Schlögl. BioSig: The Free and Open Source Software Library for Biomedical Signal Processing. *Computational Intelligence and Neuroscience*, 2011:1–12, 3 2011.

[206] David C Howell. *Statistical Methods for Psychology.* Wadsworth Cengage Learning, 7 edition, 2010.

[207] Yaser Abu-Mostafa. Machine Learning: The VC Dimension. Technical report, Caltech, 2012.

[208] Christian Breitwieser, Ian Daly, Christa Neuper, and Gernot R Müller-Putz. Proposing a standardized protocol for raw biosignal transmission. *IEEE Transactions on Biomedical Engineering*, 59(3):852–859, 3 2012.

[209] Maitreyee Wairagkar. EEG Data for Voluntary Finger Tapping Movement. *University of Reading Dataset*, 2017.

[210] Pedro M R Reis, Felix Hebenstreit, Florian Gabsteiger, Vinzenz von Tscharner, and Matthias Lochmann. Methodological aspects of EEG and body dynamics measurements during motion. *Frontiers in human neuroscience*, 8, 2014.

[211] Arnaud Delorme and Scott Makeig. EEGLAB: An open source toolbox for analysis of single-trial EEG dynamics including independent component analysis. *Journal of Neuroscience Methods*, 134(1):9–21, 3 2004.

[212] Scott Makeig, Tzyy-Ping Ping Jung, Anthony J Bell, Dara Ghahremani, and Terrence J Sejnowski. Blind separation of auditory event-related brain responses into independent components. *Proceedings of the National Academy of Sciences*, 94(20):10979–10984, 9 1997.

[213] Bin Lou, Bo Hong, Xiaorong Gao, and Shangkai Gao. Bipolar electrode selection for a motor imagery based brain? computer interface. *Journal of Neural Engineering*, 5(3):342, 2008.

[214] Carmen Vidaurre, Nicole Krämer, Benjamin Blankertz, and Alois Schlögl. Time domain parameters as a feature for EEG-based brain–computer interfaces. *Neural Networks*, 22(9):1313–1319, 2009.

[215] Reinhold Scherer, Felix Lee, Alois Schlogl, Robert Leeb, Horst Bischof, and Gert Pfurtscheller. Toward self-paced brain–computer communication: navigation through virtual worlds. *IEEE Transactions on Biomedical Engineering*, 55(2):675–682, 2008.

[216] Gert Pfurtscheller and Christa Neuper. Motor imagery and direct brain-computer communication. *Proceedings of the IEEE*, 89(7):1123–1134, 2001.

[217] Fabien Lotte. A tutorial on EEG signal-processing techniques for mental-state recognition in brain–computer interfaces. In *Guide to Brain-Computer Music Interfacing*, pages 133–161. Springer, 2014.

[218] Carmen Vidaurre, Alois Schlögl, R. Cabeza, Reinhold Scherer, and Gert Pfurtscheller. A fully on-line adaptive BCI. *IEEE Transactions on Biomedical Engineering*, 53(6):1214–1219, 6 2006.

[219] Scott Makeig, Stefan Debener, Julie Onton, and Arnaud Delorme. Mining event-related brain dynamics. *Trends in cognitive sciences*, 8(5):204–210, 2004.

[220] Patrice Clochon, Jean-Marc Fontbonne, Nathalie Lebrun, and Pierre Etévenon. A new method for quantifying eeg event-related desynchronization: amplitude evvelope analysis. *Electroencephalography and clinical neurophysiology*, 98(2):126–129, 1996.

[221] Marcel C M Bastiaansen, Jos J A Van Berkum, and Peter Hagoort. Event-related theta power increases in the human EEG during online sentence processing. *Neuroscience letters*, 323(1):13–16, 2002.

[222] M Wairagkar, Ian Daly, Yoshikatsu Hayashi, Slawomir Nasuto, and Interface Conference. Novel single trial movement classification based on temporal dynamics of EEG. In *International Conference on Brain Computer Interfaces, Graz, Austria*, 2014.

[223] P. J. Durka, D. Ircha, Christa Neuper, and Gert Pfurtscheller. Time-frequency microstructure of event-related electro-encephalogram desynchronisation and synchronisation. *Medical and Biological Engineering and Computing*, 39(3):315–321, 5 2001.

[224] Sture Holm. A simple sequentially rejective multiple test procedure. *Scandinavian journal of statistics*, pages 65–70, 1979.

[225] Chang S Nam, Yongwoong Jeon, Young-Joo Kim, Insuk Lee, and Kyungkyu Park. Movement imagery-related lateralization of event-related (de) synchronization (ERD/ERS): motor-imagery duration effects. *Clinical Neurophysiology*, 122(3):567–577, 2011.

[226] Wolfgang Klimesch, H Schimke, and J Schwaiger. Episodic and semantic memory: an analysis in the EEG theta and alpha band. *Electroencephalography and clinical Neurophysiology*, 91(6):428–441, 1994.

[227] W Klimesch and M Doppelmayr. encoding of new. *Neuroreport*, 7:1235–1240, 1996.

[228] Norbert Jaušovec, Ksenija Jaušovec, and Ivan Gerlič. Differences in event-related and induced EEG patterns in the theta and alpha frequency bands related to human emotional intelligence. *Neuroscience Letters*, 311(2):93–96, 2001.

[229] J Ibanez, J I Serrano, M D Del Castillo, E Monge, F Molina, F M Rivas, I Alguacil, J C Miangolarra, and J L Pons. Upper-limb muscular electrical stimulation driven by EEG-based detections of the intentions to move: A proposed intervention for patients with stroke. In *Engineering in Medicine and Biology Society (EMBC), 2014 36th Annual International Conference of the IEEE*, pages 1646–1649. IEEE, 2014.

[230] Mahyar Hamedi, Sh-Hussain Salleh, and Alias Mohd Noor. Electroencephalographic motor imagery brain connectivity analysis for BCI: a review. *Neural computation*, 2016.

[231] Maitreyee Wairagkar, Yoshikatsu Hayashi, and Slawomir J. Nasuto. Movement intention detection from autocorrelation of EEG for BCI. In *Lecture Notes in Computer Science (including subseries Lecture Notes in Artificial Intelligence and Lecture Notes in Bioinformatics)*, volume 9250, pages 212–221, 2015.

[232] Neethu Robinson and A. P. Vinod. Decoding speed of hand movement execution using temporal features of EEG. In *Neural Engineering (NER), 2017 8th International IEEE/EMBS Conference on*, pages 572–575. IEEE, IEEE, 5 2017.

[233] Han-Jeong Hwang, Kiwoon Kwon, and Chang-Hwang Im. Neurofeedback-based motor imagery training for brain-computer interface (BCI). *Journal of neuroscience methods*, 179(1):150–6, 4 2009.

[234] C P Pan, B Zheng, Y Z Wu, Y Wang, and X W Tang. Detrended fluctuation analysis of human brain electroencephalogram. *Physics Letters A*, 329(1):130–135, 2004.

[235] Boris Podobnik, Deng Duan Wang, Davor Horvatic, Ivo Grosse, and H Eugene Stanley. Time-lag cross-correlations in collective phenomena. *EPL*, 90(6):68001, 2010.

[236] Tzyy Ping Jung, Scott Makeig, C Humphries, T W Lee, M J McKeown, V Iragui, and T J Sejnowski. Removing electroencephalographic artifacts by blind source separation. *Psychophysiology*, 37(2):163–78, 3 2000.

[237] Maitreyee Wairagkar, Yoshikatsu Hayashi, and Slawomir J. Nasuto. Exploration of neural correlates of movement intention based on characterisation of temporal dependencies in electroencephalography. *PLoS ONE*, 13(3), 2018.

[238] Luc Berthouze and Simon F Farmer. Adaptive time-varying detrended fluctuation analysis. *Journal of Neuroscience Methods*, 209(1):178–188, 2012.

[239] Christopher T. Kello, Gordon D.A. Brown, Ramon Ferrer-i Cancho, John G. Holden, Klaus Linkenkaer-Hansen, Theo Rhodes, and Guy C. Van Orden. Scaling laws in cognitive sciences, 5 2010.

[240] Tomas Ros, P. Frewen, J. Théberge, A. Michela, R. Kluetsch, A. Mueller, G. Candrian, R. Jetly, Patrik Vuilleumier, and R. A. Lanius. Neurofeedback Tunes Scale-Free Dynamics in Spontaneous Brain Activity. *Cerebral Cortex*, 27(10):4911–4922, 9 2016.

[241] Tomas Ros, Bernard J. Baars, Ruth A. Lanius, and Patrik Vuilleumier. Tuning pathological brain oscillations with neurofeedback: a systems neuroscience framework. *Frontiers in Human Neuroscience*, 8:1008, 12 2014.

[242] Kun Hu, Plamen Ch Ivanov, Zhi Chen, Michael F. Hilton, H Eugene Stanley, and Steven A. Shea. Non-random fluctuations and multi-scale dynamics regulation of human activity. *Physica A: Statistical Mechanics and its Applications*, 337(1-2):307–318, 6 2004.

[243] Wojciech Samek, Duncan A.J. Blythe, Gabriel Curio, Klaus Robert Müller, Benjamin Blankertz, and Vadim V. Nikulin. Multiscale temporal neural dynamics predict performance in a complex sensorimotor task. *NeuroImage*, 141:291–303, 11 2016.

[244] Govindan Rangarajan and Mingzhou Ding. Integrated approach to the assessment of long range correlation in time series data. *Phys Rev E Stat Phys Plasmas Fluids Relat Interdiscip Topics*, 61(5A):4991–5001, 2000.

[245] Ruixue Li, Jiang Wang, and Yingyuan Chen. Effect of the signal filtering on detrended fluctuation analysis. *Physica A: Statistical Mechanics and its Applications*, 494:446–453, 2018.

[246] J M Hausdorff, C. K. Peng, Z. Ladin, J. Y. Wei, and Ary L Goldberger. Is walking a random walk? Evidence for long-range correlations in stride interval of human gait. *Journal of Applied Physiology*, 78(1):349–358, 1 1995.

[247] Kun Hu, Plamen Ch Ivanov, Zhi Chen, Pedro Carpena, and H Eugene Stanley. Effect of trends on detrended fluctuation analysis. *Physical Review E - Statistical Physics, Plasmas, Fluids, and Related Interdisciplinary Topics*, 64(1):19, 2001.

[248] Zhi Chen, Plamen Ch. Ivanov, Kun Hu, and H. Eugene Stanley. Effect of nonstationarities on detrended fluctuation analysis. *Physical Review E - Statistical Physics, Plasmas, Fluids, and Related Interdisciplinary Topics*, 65(4):15, 4 2002.

[249] Kjerstin Torre, Didier Delignieres, and Loïc Lemoine. Detection of long-range dependence and estimation of fractal exponents through ARFIMA modelling. *British Journal of Mathematical and Statistical Psychology*, 60(1):85–106, 5 2007.

[250] Robert Becker, Dimitri Van De Ville, and Andreas Kleinschmidt. Alpha oscillations reduce temporal long-range dependence in spontaneous human brain activity. *The Journal of Neuroscience*, 38(3):755–764, 2018.

[251] Michael P.H. Stumpf and Mason A. Porter. Critical truths about power laws, 2 2012.

[252] Claude Bédard and Alain Destexhe. Macroscopic models of local field potentials and the apparent 1/f noise in brain activity. *Biophysical Journal*, 96(7):2589–2603, 2009.

[253] Holger Dette, Philip Preuss, and Kemal Sen. Detecting long-range dependence in non-stationary time series. *Electronic Journal of Statistics*, 11(1):1600–1659, 2017.

[254] Imali T. Hettiarachchi, Thanh Thi Nguyen, and Saeid Nahavandi. Multivariate Adaptive Autoregressive Modeling and Kalman Filtering for Motor Imagery BCI. In *Proceedings - 2015 IEEE International Conference on Systems, Man, and Cybernetics, SMC 2015*, pages 3164–3168, 2015.

[255] Kai Liu, YangQuan Chen, and Xi Zhang. An Evaluation of ARFIMA (Autoregressive Fractional Integral Moving Average) Programs. *Axioms*, 6(4):16, 2017.

[256] Richard T. Baillie. Long memory processes and fractional integration in econometrics. *Journal of Econometrics*, 73(1):5–59, 1996.

[257] C. W.J. Granger and Roselyne Joyeux. An Introduction to Long-memory Time Series Models and Fractional Differencing. *Journal of Time Series Analysis*, 1(1):15–29, 1 1980.

[258] Andreas Noack Jensen and Morten Øregaard Nielsen. A fast fractional difference algorithm. *Journal of Time Series Analysis*, 35(5):428–436, 8 2014.

[259] Kyung So Im, M. Hashem Pesaran, and Yongcheol Shin. Testing for unit roots in heterogeneous panels. *Journal of Econometrics*, 115(1):53–74, 7 2003.

[260] The MathWorks Inc. Econometrics Toolbox Documentation - MathWorks United Kingdom (R2018a), 2018.

[261] G. M. Ljung and George E. P. Box. On a measure of lack of fit in time series models. *Biometrika*, 65(2):297–303, 8 1978.

[262] Frank J. Massey. The Kolmogorov-Smirnov Test for Goodness of Fit. *Journal of the American Statistical Association*, 46(253):68–78, 3 1951.

[263] Seyed Navid Resalat and Valiallah Saba. A Study of Various Feature Extraction Methods on a Motor Imagery Based Brain Computer Interface System. *Basic and Clinical Neuroscience Journal*, 7(1):13–20, 1 2016.

[264] Yongwook Chae, Jaeseung Jeong, and Sungho Jo. Toward brain-actuated humanoid robots: Asynchronous direct control using an EEG-Based BCI. *IEEE Transactions on Robotics*, 28(5):1131–1144, 2012.

[265] Jian Feng Hu. New biometric approach based on motor imagery EEG signals. In *FBIE 2009 - 2009 International Conference on Future BioMedical Information Engineering*, pages 94–97, 2009.

[266] Javier M. Antelis, Luis Montesano, Ander Ramos-Murguialday, Niels P Birbaumer, and Javier Minguez. Decoding Upper Limb Movement Attempt from EEG Measurements of the Contralesional Motor Cortex in Chronic Stroke Patients. *IEEE Transactions on Biomedical Engineering*, 64(1):99–111, 2017.

[267] Dennis J McFarland, William A Sarnacki, and Jonathan R Wolpaw. Effects of training pre-movement sensorimotor rhythms on behavioral performance. *Journal of Neural Engineering*, 12(6):066021, 12 2015.

[268] Dave P. Burke, Simon P. Kelly, Philip De Chazal, Richard B. Reilly, and Ciarán Finucane. A parametric feature extraction and classification strategy for brain-computer interfacing. *IEEE Transactions on Neural Systems and Rehabilitation Engineering*, 13(1):12–17, 2005.

[269] Fabien Lotte, Marco Congedo, Anatole Lécuyer, Fabrice Lamarche, and Bruno Arnaldi. A review of classification algorithms for EEG-based brain-computer interfaces. *Journal of Neural Engineering*, 4(2):R1–R13, 6 2007.

[270] Physionet.org. Detrended Fluctuation Analysis (DFA) [Internet]. *Available at: https://www.physionet.org/tutorials/fmnc/node5.html*, [Accessed.

[271] Imran Khan Niazi, Ning Jiang, Mads Jochumsen, Jørgen Feldbæk Nielsen, Kim Dremstrup, and Dario Farina. Detection of movement-related cortical potentials based on subject-independent training. *Medical and Biological Engineering and Computing*, 51(5):507–512, 5 2013.

[272] Ying Gu, Kim Dremstrup, and Dario Farina. Single-trial discrimination of type and speed of wrist movements from EEG recordings. *Clinical Neurophysiology*, 120(8):1596–1600, 2009.

[273] Scott R Cole and Bradley Voytek. Brain oscillations and the importance of waveform shape. *Trends in Cognitive Sciences*, 21(2):137–149, 2017.

[274] R. M. Bryce and K. B. Sprague. Revisiting detrended fluctuation analysis. *Scientific Reports*, 2(1):315, 12 2012.

[275] John M Beggs and Dietmar Plenz. Neuronal Avalanches in Neocortical Circuits. *The Journal of Neuroscience*, 23(35):11167–11177, 12 2003.

[276] Viola Priesemann, Matthias HJ Munk, Michael Wibral, and CG Wasterlain. Subsampling effects in neuronal avalanche distributions recorded in vivo. *BMC Neuroscience*, 10(1):40, 4 2009.

[277] Olivier David and Karl J Friston. A neural mass model for meg/eeg:: coupling and neuronal dynamics. *NeuroImage*, 20(3):1743–1755, 2003.

[278] Melissa Zavaglia, Laura Astolfi, Fabio Babiloni, and Mauro Ursino. A neural mass model for the simulation of cortical activity estimated from high resolution EEG during cognitive or motor tasks. *Journal of Neuroscience Methods*, 157(2):317–329, 2006.

Appendix A

Movement Intention based Brain Computer Interface for Virtual Reality and Soft Robotics Rehabilitation using novel Autocorrelation analysis of EEG

Maitreyee Wairagkar, Ioannis Zoulias, Victoria Oguntosin, Yoshikatsu Hayashi and Slawomir Nasuto

Abstract

Brain Computer Interface (BCI) could be used as an effective tool for active engagement of patients in motor rehabilitation by enabling them to initiate the movement by sending the command to BCI directly via their brain. In this paper, we have developed a BCI using novel EEG analysis to control a Virtual Reality avatar and a Soft Robotics rehabilitation device. This BCI is able identify and predict the upper limb movement. Autocorrelation analysis was done on EEG to study the complex oscillatory processes involved in motor

command generation. Autocorrelation represented the interplay between oscillatory and decaying processes in EEG which change during voluntary movement. To investigate these changes, the exponential decay curve was fitted to the autocorrelation of EEG windows which captured the autocorrelation decay. It was observed that autocorrelation decays slower during voluntary movement and fast otherwise, thus, movement intention could be identified. This new method was translated into online signal processing for BCI to control the virtual avatar hand and soft robotic rehabilitation device by intending to move an upper limb. The soft robotic device placed on the joint between upper and the lower arm inflated and deflated resulting to extension and flexion of the arm providing proprioceptive feedback. Avatar arm viewed in virtual 3D environment with Oculus Rift also moved simultaneously providing a strong visual feedback.

A.1   Introduction

Brain Computer Interface (BCI) provides a new mode of interaction with external devices directly via brain. BCI for rehabilitation is increasingly researched since it can enable a patient to be actively involved in rehabilitation instead of performing passive exercises. In this paper a novel movement intention BCI using autocorrelation analysis is described with its applications in Virtual Reality and Soft Robotics based rehabilitation. Common methods of detecting movement for EEG like Event Related Synchronization [26] and Movement Related Cortical Potentials [51] are limited to a narrow frequency bands and do not give other information. Hence, autocorrelation based wide band analysis was done to explore temporal dynamics of EEG during movement.

A.2   Method

EEG was recorded from 14 healthy participants for offline analysis which was later translated to online BCI (Fig A.1). and tested in pilot experiments. Firstly autocorrelation was computed on 1 s windows of EEG (0.5 – 30 Hz) every 100 ms from channels obtained by Laplacian filtering C3 and C4 with four surrounding channels. Exponential decay curve $Ae^{t\tau}$ was fitted to autocorrelation and decay constant τ was used as a feature to identify the movement. Virtual avatar arm moved upon receiving the command from BCI. BCI also simultaneously sent command to silicon soft module placed on elbow which inflated and deflated accordingly to perform extension and flexion of the arm.

Fig. A.1 Movement Intention based online BCI for Virtual Reality and Soft Robotics rehabilitation system

Results

Autocorrelation decayed slower before and during the movement and fast otherwise. This was determined by increase and decrease in the decay constant which was used to identify the movement intention. Sensitivity of 78.48 ± 8.36 was achieved for right hand and 78.25 ± 9.58 for left hand.

A.3 Disclussion and conclusion

Slow autocorrelation decay during movement indicated that EEG becomes more self-similar during movement and the processes are more random when there is no movement. This online BCI was able to identify the movement and send the appropriate command to virtual arm and soft robotic device. Virtual environment with Oculus helped in seamless production of stronger movement intention. Thus, an upper limb rehabilitation BCI was developed which provided proprioceptive and visual feedback simultaneously.

Appendix B

Long-Range Temporal Correlation using Bipolar Montage

B.1 LRTC on EEG channels with bipolar montage

Six longitudinal bipolar montage channels were created by subtracting F3-C3, Fz-Cz, F4-C4, C3-P3, Cz-Pz and C4-P4. The LRTC was computed on these six channels using the exactly the same method that is described in chapter 5. The objective of using bipolar montage was to identify whether it gives better classification accuracies for movement intention than using three monopolar channels C3, Cz and C4. The grand average LRTC on six bipolar channels is shown in Fig B.1. All the six channels show significant increase in the LRTC during movement intention and execution. LRTCs in bipolar channels F3-C3, Fz-Cz and F4-C4 are similar to those of monopolar channels from chapter 5. The LRTCs in bipolar channels C3-P3, Cz-Pz and C4-P4 have higher standard deviation than the previous three channels.

Table B.1 shows the LDA classification accuracies, sensitivities and specificities using LRTC from channels Fz-Cz, F4-C4, C3-P3, and channels C3-P3, Cz-Pz and C4-P4 as features. The classification accuracies are significantly lower (Wilcoxon signed-rank test, $p < 0.05$) than the accuracies of the monopolar montage described in chapter 5. Hence, the monopolar montage was used in chapter 5 and 6 for LRTC.
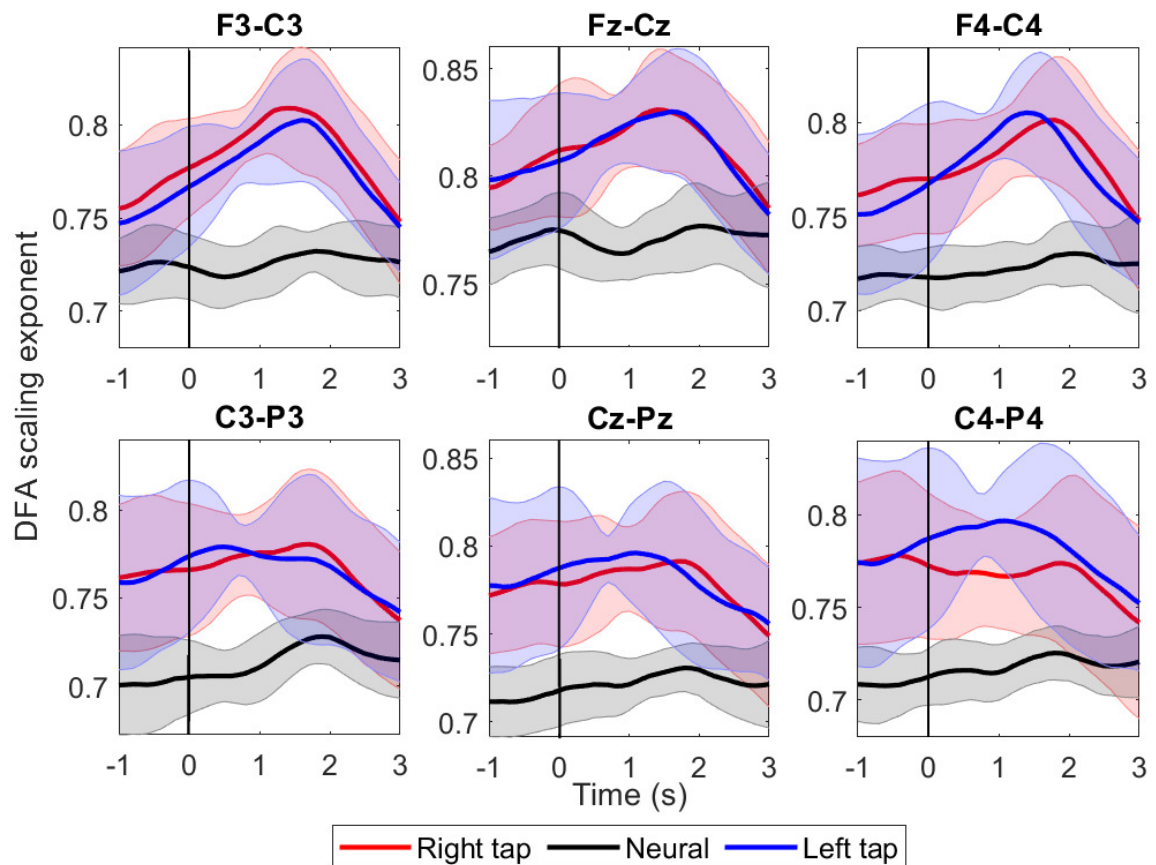
Fig. B.1 **Grand average long-range temporal correlation (LRTC) in bipolar channels.**
LRTCs on six longitudinal bipolar EEG channels F3-C3, Fz-Cz, F4-C4, C3-P3, Cz-Pz and
C4-P4 are shown. The vertical solid line marks the onset of movement at 0 s. The shaded
region represents the standard deviation.

Sub. no.	Left finger tapping (%)						Right finger tapping (%)					
	(F3-C3, Fz-Cz, F4-C4)			(C3-P3, Cz-Pz, C4-P4)			(F3-C3, Fz-Cz, F4-C4)			(C3-P3, Cz-Pz, C4-P4)		
	Acc.	Sen.	Spe.	Acc.	Sen.	Spe.	Acc.	Sen.	Spe.	Acc.	Sen.	Spe.
1	72.50	74.75	70.25	79.25	81.25	77.25	72.50	74.75	70.25	76.25	79.50	73.00
2	90.41	91.43	89.39	89.18	87.76	90.61	90.41	91.43	89.39	80.00	71.84	88.16
3	74.38	76.50	72.25	75.00	74.75	75.25	74.38	76.50	72.25	74.50	84.25	64.75
4	77.50	72.00	83.00	69.13	64.50	73.75	77.50	72.00	83.00	71.00	67.75	74.25
5	79.13	82.50	75.75	72.50	74.25	70.75	79.13	82.50	75.75	70.88	72.25	69.50
6	70.61	69.39	71.84	76.94	79.59	74.29	70.61	69.39	71.84	81.63	88.98	74.29
7	64.75	66.25	63.25	72.88	76.50	69.25	64.75	66.25	63.25	65.38	63.00	67.75
8	75.50	71.00	80.00	82.75	82.00	83.50	75.50	71.00	80.00	81.38	81.00	81.75
9	59.50	61.75*	57.25	64.00	63.50	64.50	59.50	61.75	57.25	66.75	64.00	69.50
10	68.38	67.25	69.50	71.25	74.50	68.00	68.38	67.25	69.50	70.13	70.75	69.50
11	90.75	87.50	94.00	87.13	88.75	85.50	90.75	87.50	94.00	88.38	96.25	80.50
12	72.38	74.25	70.50	70.75	80.25	61.25	72.38	74.25	70.50	75.25	78.75	71.75
13	65.38	66.75	64.00	73.88	79.25	68.50	65.38	66.75	64.00	65.88	64.50	67.25
14	80.38	76.50	84.25	80.25	81.50	79.00	80.38	76.50	84.25	71.88	65.25	78.50
Mean	74.39	74.13	74.66	76.06	77.74	74.39	74.39	74.13	74.66	74.23	74.86	73.60
SD	8.98	8.38	10.40	7.02	7.28	8.25	8.98	8.38	10.40	6.75	10.23	6.55
Median	73.44	73.13	72.04	74.44	79.42	74.02	73.44	73.13	72.04	73.19	72.04	72.38

Table B.1 The peak accuracies, sensitivities and specificities for right and left finger movement vs resting state classifications using bipolar channels. All values except the ones marked by * are significantly above chance level ($p < 0.05$).

Appendix C

Publications

C.1   Journal publications

M. Wairagkar, Y. Hayashi, S. J. Nasuto. "Exploration of Neural Correlates of Movement Intention based on Characterisation of Temporal Dependencies in Electroencephalography", PLOS ONE, Vol. 13, No. 3, pp e0193722, 2018.
https://dx.doi.org/10.1371/journal.pone.0193722

M. Wairagkar, Y. Hayashi, S. J. Nasuto. "Dynamics of Long-Range Temporal Correlations in Broadband EEG for Movement Prediction", Scientific Reports, 2018. (Submitted)

M. Wairagkar, Y. Hayashi, S. J. Nasuto. "Modelling the Short and Long-Range Temporal Correlations in Broadband EEG during Movement using ARFIMA", Frontiers in Neuroscience, 2018. (Ready for submission)

C.2   Datasets

M. Wairagkar, "EEG Data for Voluntary Finger Tapping Movement", University of Reading Dataset, 2017.
http://dx.doi.org/10.17864/1947.117

C.3   International peer-reviewed conferences

M. Wairagkar, I. Zoulias, et. al. "Movement Intention based BCI for Virtual Reality and Soft Robotics Rehabilitation using novel Autocorrelation analysis of EEG", IEEE RAS/EMBS

BioRob, Singapore, June 2016.
http://dx.doi.org/10.1109/BIOROB.2016.7523705

M. Wairagkar, I. Daly, Y. Hayashi, S. Nasuto. "Autocorrelation based EEG Dynamics depicting Motor Intention", International BCI Meeting 2016, CA, May 2016.
http://dx.doi.org/10.3217/978-3-85125-467-9-166

M. Wairagkar, Y. Hayashi, S. Nasuto. "Movement Intention detection from Autocorrelation of EEG for BCI", Brain Informatics and Health, Springer, Vol. 9250, pp. 212-221, 2015.
http://dx.doi.org/10.1007/978-3-319-23344-4_21

M. Wairagkar, I. Daly, Y. Hayashi, S. Nasuto. "Novel single trial movement classification based on temporal dynamics of EEG", Proceedings of Graz International BCI conference, Graz, Sept 2014.
http://dx.doi.org/10.3217/978-3-85125-378-8-81

M. Wairagkar, "Motor Imagery based Brain Computer Interface (BCI) using Artificial Neural Network Classifiers", Proceedings of the British Conference of Undergraduate Research, 2014.
https://bcur.org/journals/index.php/BCURProc/article/view/6

C.4 Presentations and conference abstracts

M. Wairagkar, "Detecting Movement Intention from Temporal Dependencies in Broadband EEG for BCI", Physiological Society Symposium- From lab to clinic: Pathways to translational brain machine interfaces for rehabilitation, Reading, September 2018. (**Oral presentation**)

M. Wairagkar, "Changes in long-range temporal correlations in broadband EEG during voluntary movement preparation – towards application in BCI", Biodynamics Conference, London, April 2018. (**Poster presentation**)

M. Wairagkar, "Temporal dynamics of EEG for movement intention detection using machine learning", Machine Learning Summer School, Tuebingen, July 2017. (**Poster presentation**)

M. Wairagkar, "Temporal analysis of EEG for brain computer interface", School of Biological Sciences, University of Reading Symposium, Reading, June 2017. (**Oral presentation**)

M. Wairagkar, Hybrid neuro-rehabilitation system using Brain Computer Interface, Virtual Reality and Soft Robotics, Euorohaptics, London, July 2016. (**Demonstration**)

M. Wairagkar, I. Zoulias, et. al. "Movement Intention based BCI for Virtual Reality and Soft Robotics Rehabilitation using novel Autocorrelation analysis of EEG", IEEE RAS/EMBS BioRob, Singapore, June 2016.(**Poster presentation**)

M. Wairagkar, I. Daly, Y. Hayashi, S. Nasuto. "Autocorrelation based EEG Dynamics depicting Motor Intention", International BCI Meeting 2016, CA, May 2016. (**Poster presentation**)

M. Wairagkar, "Movement Intention detection from Autocorrelation of EEG for BCI", Brain Informatics and Health, London, 2015. (**Oral presentation**)

M. Wairagkar, "Motor Imagery based Brain Computer Interface (BCI) using Artificial Neural Network Classifiers", British Conference of Undergraduate Research, 2014. (**Oral presentation**)